ELECTROCHEMICAL EVALUATION OF API-X100 PIPELINE STEEL IN SIMULATED CARBON DIOXIDE CORROSION ENVIRONMENTS

by

Faysal Fayez Eliyan

B.Sc. Mechanical Engineering, Qatar University, Doha, Qatar, 2009

A THESIS SUBMITTED IN PARTIAL FULFILLMENT OF THE
REQUIREMENTS FOR THE DEGREE OF
MASTER OF APPLIED SCIENCE

in

The Faculty of Graduate Studies

(Materials Engineering)

THE UNIVERSITY OF BRITISH COLUMBIA
(Vancouver)
June, 2011

Abstract

Corrosion evaluation of API-X100 pipeline steel was performed in simulated carbon dioxide corrosion conditions from selected electrochemical perspectives. Preliminary studies were devoted for studying the effect of the content of bicarbonate species; in aerated and in argon-purged deoxygenated conditions. On a separate scheme, the investigations were then pursued in 1-bar-CO_2-saturated media. The effect of temperature, salinity, acetic acid, and oil content were considered at specific ranges to reveal fairly the environmental effects on corrosion kinetics, passivation, and interfacial mechanisms. Chronological Open Circuit Potential (OCP) variations, polarization potentiodynamics, Electrochemical Impedance Spectroscopy (EIS) were utilized for the electrochemical studies. The corrosion rates increased with the bicarbonate content, higher temperature, upon aeration, upon anodically sensitive chloride addition, and with increased acetic acid content. In bicarbonate solutions, effective passivation was established with broad potential ranges, more facilitated with lower temperature, and in chloride free deoxygenated conditions. Low crude oil amounts were introduced, suppressing corrosion rates, acting dependently on temperature as an anodic and cathodic inhibitor, and influencing passivity with a better efficiency at lower temperatures and with less chloride content. A proposed model for electrochemically driven passivity in oil containing deoxygenated bicarbonate is discussed and selected thermodynamic characteristics for oil adsorption in CO_2-saturated media are presented. At the end of this study, weight loss measurements in autoclave-based 50-psi-CO_2-saturated media at 100 ^oC simulating stratified flows are discussed in brief.

Table of Contents

List of Tables

List of Figures

List of Symbols, Abbreviations, and Nomenclature

P_{CO2}	Partial pressure of carbon dioxide (CO_2)
T	Temperature
R	Universal gas constant (8.314 J/mol.K)
K_H	Solubility constant of carbon dioxide
K_W	Dissociation constant of water
K_1	First dissociation constant of (H_2CO_3)
K_2	Second dissociation constant of (H_2CO_3)
C	Concentration
K_{sp}	Solubility product
SS	Supersaturation
i_{corr}	Corrosion current density
E_{corr}	Corrosion potential
i_c	Critical current density
E_{pp}	Passivation potential
i_p	Passive current density
$E_{transpass}$	Transpassivation potential
CR	Corrosion rate
EIS	Electrochemical Impedance Spectroscopy
Z_{re}, Z’	Real impedance component
$Z_{im,}$ Z”	Imaginary impedance component
$\|Z\|$	Impedance modulus

θ	Fractional surface coverage
B	Energetic coefficient of proportionality
ΔG_{ads}	Free energy of adsorption
R	Universal gas constant
ΔH	Enthalpy
ΔS	Entropy

Acknowledgments

I would like to express my sincere, grateful feelings to my dearest supervisor Prof. Akram Alfantazi, for providing the persistent support and continuous guidance at all levels throughout the time of performing this research project. Without the patience, understanding, motivation, and encouragement, he maintained; this work would never be recognizably acceptable to the elite UBC-class standards we all are inspired by.

In addition, I would like to express my honest thanking to my colleagues who guided my first steps in the corrosion laboratory; Ahmad Ghahremaninezhad, Tirdad Nickchi, Ehsan Zahrani, Shima Karimi, Mathew Tunnicliffe, and Mohammed Al-Otaibi,.

I would like to thank also all the professors and staff at the materials engineering department in the University of British Columbia who contributed in succeeding this work.

Special thanks are for Qatar National Research Fund (QNRF) and Natural Sciences and Engineering Research Council of Canada (NSERC) for providing the financial momentum needed for this research effort.

Dedication

To the loving hearts in Qatar..
To my greatly beloved parents:

Dr. Fayez M. Eliyan & Reema Asfour
Who first told me:
"Do not leave your bike outdoors when it's rainy or it will rust!"

To my beloved brothers and sisters..
They are the five stars my eyes are always starred by whenever I look at the colorful Vancouverian horizons

Mohammed
Lubna *Afnan*

Areej *Edrees*

Chapter 1: General introduction and objectives

Transportation pipelines are the vital industrial facilities by which the continuous demand for oil and gas is achieved reliably over long distances. They are manufactured with variant diameters and wall thicknesses laid down to transport hydrocarbons at high flow rates and high operation pressures. They, in fact, introduce an important economic feasibility for oil and gas transportation, limiting the dependence on other costly means such as land or sea tankers.

In nowadays energy markets, there is an increased trend for higher hydrocarbon consumption rates making the oil plants to adopt upgraded strategies in operation and design. In that context, the necessity for high strength steels becomes more important especially, if possible, reduced material amounts are preferably considered for high pressures. New generations of High Strength Low Alloy (HSLA) steels are being developed for better structural integrity and enhanced long-term reliability. The greater strength is achieved by adding controlled alloying contents to the base steels, but however, corrosion becomes more susceptible and yet not easily predicted or controlled. In addition, factors induced from the materials selection add to the already complex interrelational factors that control the corrosion behavior with respect to the environmental variations.

The interest in this study is exclusively devoted for investigating the corrosion behavior of a new generation pipeline steel; API-X100 in conditions where the dissolved carbon dioxide necessarily governs the corrosion reactions.

From the failure susceptibility perspective, carbon dioxide corrosion is one of the most common degradations that pipelines are nowadays prone to [Nesic, 2007]. It was reported

that almost 60 % of oil pipeline corrosion failures in USA are sufficiently attributable to an inadequate understanding of the corrosive capabilities that the dissolved carbon carrying species have against pipeline steels [Kermani, 1997]. Many pipeline failures and disastrous fire explosions were mainly explained by the inner localized thinning of pipeline sections, controlled, especially at low flow rates, by the electrochemical dissolution [Xia, 1989].

Carbon dioxide gas dissolves in the multiphase pipeline flows at different extents, depending on temperature and pressure, producing the corrosive carbon carrying species. These species, besides the conventional salinity, include the weak carbonic acid (H_2CO_3), bicarbonate (HCO_3^-), and carbonate (CO_3^{2-}) driving the corrosion reactions in different fashions depending on their concentrations and on pH levels [Kermani, 2003]. The problem is basically associated with the increasing water content with time in the multiphase flows transported from aging oil wells. In these conditions, carbon dioxide gas has a greater potential to dissolve in the water phase wetting the pipeline walls. As the wetting surface increases and gets more stable, corrosion rates consequently are accelerated resulting in significant damages. Therefore, in simultaneous multiphase flows comprising oil, water, and miscellaneous gases, corrosion is restricted as far as the amount of water is low. Water cuts in these conditions become usually entrained in the oil continuum as small droplets or as dispersed slugs in the pipeline flows and oil then acts as a natural barrier against corrosion [Lotz, 1990]. However, when the amount of oil decreases, the stability of the emulsified oil-water interfaces becomes a critical factor especially if the flow rate is low [Smart, 1993]. Paraffin containing crude oils were evaluated in carbon dioxide corrosion environments and they were found to act as

effective inhibitors [Morales, 2000]. The corrosion rates decreased significantly with the increased oil amounts in a range from 70 to 90 wt% depending on the flow rates. In a detailed work, phase wetting maps for three crude oils were constructed to evaluate the corrosion inhibition in flow emulsions containing water cuts from 2 to 99 % [Tang, 2007]. In conditions where stable oil wetting was achieved, no corrosion attack occurred but in the intermittent water/oil wetting or comprehensive water wetting, the corrosion rates were high. Specific oil constituents were studied with respect to the corrosion behavior as performed by Hemandez et al. when statistical approaches were adopted to evaluate the corrosion inhibition capabilities for specific constituents in six Venezuelan crude oils [Hernandez, 2002].

There were many experimental works devoted for corrosion evaluation in low-oil containing emulsions in autoclaves and flow loops such as in [Masamura, 1984], [Villarreal, 2006], and [Efird, 1989], but however; the corrosion behaviors in similar conditions dominated exclusively by bicarbonate were not studied. Therefore, the interest in this study is to provide a fairly comprehensive view on the corrosion behavior in two separate cases encountered in oil pipelines simulated in glass test cells. The objectives from performing the electrochemical evaluations in the mildly alkaline bicarbonate-dominated and in the acidic carbonic acid-dominated media can be summarized as follows:

1. To evaluate corrosion kinetics in naturally aerated and deoxygenated bicarbonate solutions, as well as in CO_2-saturated solutions considering bicarbonate concentration, temperature, as well as salinity variations.

2. To evaluate the passivation behavior with respect to the potential ranges and the associated current densities in the aerated chloride free, and low chloride containing deoxygenated bicarbonate solutions.
3. To investigate the inhibitive capabilities of crude oil existing with low amounts on the anodic and cathodic reactions as well as possible roles acted during passivation in deoxygenated bicarbonate and CO_2-saturated solutions.

Chapter 2: Literature review

2.1. Chemistry of carbon dioxide saturated media

Carbon dioxide gas corrosion significance in the aqueous media is associated to its solubility where the aggressive species are produced with different concentrations. Carbon dioxide solubility is basically dependant on temperature (T) and on the partial pressure (P_{CO2}). In conditions where the partial pressure of carbon dioxide is 1 bar, the solubility, expressed with mole fraction (y) in a range of temperature from 273 to 353 K [Palmer, 1983] as:

$$R \ln(y) = a + b\, T^{-1} + c \ln(T) + d\, T \qquad (1.1)$$

The factors a, b, c, and d are assigned to specific pressures but for 1-bar-CO_2-saturated media, they are expressed as: a = -1327.8 J/K.mol, b = 72611.6 J/mol, c = 180 J/K.mol and d = -0.009 J/K^2.mol. R is the universal gas constant and equals 8.314 J/mol.K. The above relation is plotted in Figure 2.1 showing the decreasing mole fractions of the dissolved carbon dioxide with the higher temperature.

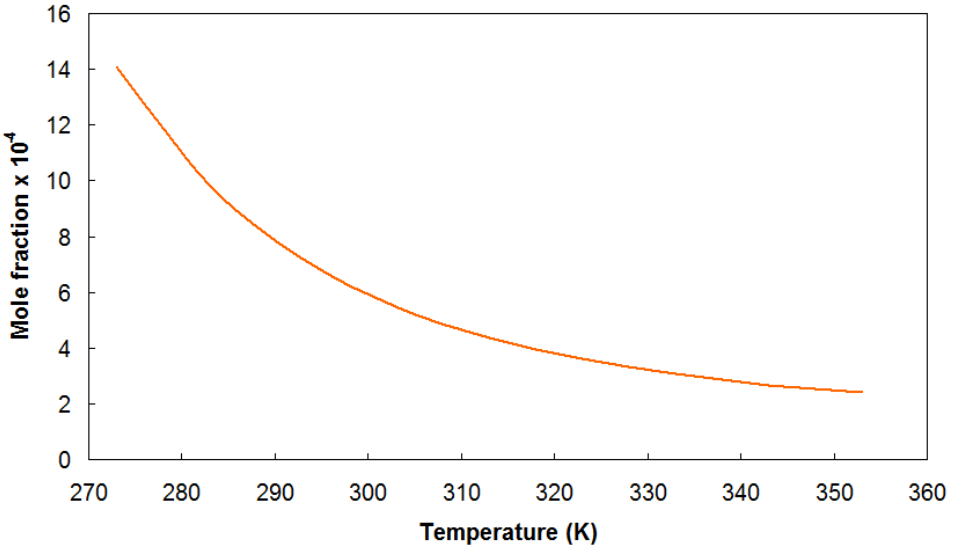

Figure 2.1. Mole fraction variations of carbon dioxide from 273 to 353 K in 1 bar CO_2 saturated aqueous media

2.2. Mechanisms of carbon dioxide corrosion

Corrosion of pipeline steels in CO_2-saturated media was reported in many studies as a complex phenomenon requiring great research efforts to investigate its mechanisms and the associated determining steps. Many views were proposed, but however, they were for describing the corrosion reactions in specific cases and they were not also widely recognized [Kermani, 2003]. Basically, CO_2 corrosion is an electrochemical process of a multistep nature between the corrosive species resulting from CO_2 dissolution and the dissolvable phases in the steel. A great effort has been devoted to determine the governing anodic and cathodic reactions and to determine the key species involved.

In literature, there is an agreement on three simultaneously occurring processes which are the anodic dissolution of iron to ferrous ions, cathodic reduction of carbon carrying species producing hydrogen, and the formation of effectively stable solid corrosion products; summarized as:

$$Fe + CO_2 + H_2O \rightarrow FeCO_3 + H_2 \qquad (1.2)$$

These processes were employed to provide an understanding on the possible governing mechanism(s) as performed in [Nesic, 2007], [Zhang, 2006], [Paolinelli, 2008], [Heuer, 1999], and [Lopez, 2003].

Most models proposed take primarily into account the chemical equilibrium among the reducible species resulting from carbon dioxide dissolution as:

$$CO_{2(g)} \leftrightarrow CO_{2(aq)} \qquad K_H = \frac{C_{CO_2}}{P_{CO_2}} \qquad (1.3)$$

$$CO_{2(aq)} + H_2O \leftrightarrow H_2CO_3 \qquad K_o = \frac{C_{H_2CO_2}}{C_{CO_2}} \qquad (1.4)$$

$$H_2CO_3 \leftrightarrow H^+ + HCO_3^- \qquad K_1 = \frac{C_{HCO_3^-} C_{H^+}}{C_{H_2CO_3}} \qquad (1.5)$$

$$HCO_3^- \leftrightarrow H^+ + CO_3^{2-} \qquad K_2 = \frac{C_{CO_3^{2-}} C_{H^+}}{C_{HCO_3^-}} \qquad (1.6)$$

$$H_2O \leftrightarrow H^+ + OH^- \qquad Kw = C_{H^+} C_{OH^-} \qquad (1.7)$$

Except with slight differences on reporting the importance of these species with respect to their ability to drive the corrosion reactions upon temperature or pressure variations, it was almost widely agreed that the cathodic reactions govern the overall process.

In a compiled synopsis by Burke, it was indicated that hydrogen evolution in the deoxygenated CO_2-saturated environments is the controlling process in the corrosion reactions [Burke, 1984]. In that early effort published, it was also reported from other 3 works that the limiting cathodic currents were higher in CO_2-saturated solutions of adjusted pH levels of 4, than those in CO_2-free solutions of the same pH level.

Schmitt confirmed the dependence of the uniform corrosion kinetics on hydrogen evolution where the process involves the heterogeneous hydration of chemisorbed CO_2 as the rate determining step [Schmitt, 1984]. However, this process was found to be necessarily temperature dependent in conditions where adherent corrosion product formations are not facilitated; at temperatures above 60 ^oC the permeability and/or solubility of iron carbonate ($FeCO_3$) formed more effectively controlled the corrosion reactions.

Hydrogen evolution is preceded by multistep reduction reactions of carbonic acid, bicarbonate, and hydrogen protons at extents depending fundamentally on pH levels making the reactions to occur near to interface or upon adsorption.

In one electrochemical chain, hydrogen protons resulting from carbonic acid dissociation diffuse to the steel surface where they get reduced [Schmitt, 1984] as:

$$CO_{2(sol)} + H_2O \leftrightarrow H_2CO_3 \quad (1.8)$$

$$H_2CO_{3(sol)} + H_2O \leftrightarrow H_3O^+_{(sol)} + HCO^-_{3(sol)} \quad (1.9)$$

$$H_3O^+_{(sol)} \leftrightarrow H_3O^+ \quad (1.10)$$

$$H_3O^+ + e^- \rightarrow H_{(ads)} + H_2O \quad (1.11)$$

Alternatively, carbon dioxide was proposed to get adsorbed and then hydrated producing adsorbed carbonic acid molecules where they get reduced directly, as proposed in [De Waard, 1975], or serving as sources for hydrogen protons as:

$$CO_{2(sol)} \leftrightarrow CO_{2(ads)} \quad (1.12)$$

$$CO_{2(ads)} + H_2O \leftrightarrow H_2CO_{3(ads)} \quad (1.13)$$

$$H_2CO_{3(ads)} + e^- \rightarrow H(ad) + HCO^-_3 \quad (1.14)$$

$$H_2CO_{3(ads)} + H_2O \leftrightarrow H_3O^+ + HCO^-_3 \quad (1.15)$$

$$H_3O^+ + e^- \rightarrow H_2CO_{3(ads)} + H_2O \quad (1.16)$$

At higher pH levels, carbonic acid can dissociate further producing bicarbonate species driving the cathodic reactions as proposed by Ogundle and White [Ogundle, 1987] as:

$$HCO^-_3 + e^- \rightarrow H_{(ads)} + CO^{2-}_3 \quad (1.17)$$

$$HCO^-_3 + H_{(ads)} + e^- \rightarrow H_2 + CO^{2-}_3 \quad (1.18)$$

The anodic reaction is widely represented by the direct dissolution of iron to ferrous ions as:

$$Fe \rightarrow Fe^{2+} + 2e^{-} \quad (1.19)$$

The corrosion products involving for example iron carbonate (pKsp = 10.54 at 25 ^{o}C [Tong, 2008]) form by the direct combination with carbonate or via reaction intermediates as [Heuer, 1999]:

$$Fe^{2+} + CO_3^{2-} \rightarrow FeCO_3 \quad (1.20)$$

$$Fe^{2+} + 2\ HCO_3^{-} \rightarrow Fe(HCO_3)_2 \quad (1.21)$$

$$Fe(HCO_3)_2 \rightarrow FeCO_3 + CO_2 + H_2O \quad (1.22)$$

The possible reactions governing the formation of iron carbonate and other iron oxides such as (Fe_2O_3) and (Fe_3O_4) are discussed in detail with respect to the anodic peaks and passivation regimes discussed in Chapters III and IV.

2.3. Environmental factors influencing CO_2 corrosion

2.3.1. Effect of temperature

It is widely recognized that the uniform CO_2 corrosion rates are accelerated with the higher temperature where the governing kinetics are enhanced and the associated transport processes are accelerated. In addition, the tendency and rate of formation of the corrosion products, whose characteristics can control the corrosion reactions, are also temperature dependent [Kermani, 2003].

In that respect of corrosion kinetics and products, it was reported that the corrosion rate was proportional with temperature in a range from 25 to 60°C, but it

stabilized within the higher temperature range from 90 to 125°C attributing that to the physical factors induced by the corrosion products [Gray, 1990]. Similarly, the temperature dependence of the corrosion rates was preserved in CO_2-saturated media containing 1 mass% chloride as the corrosion rates increased from 1 to 3 mm/yr, when the temperature increased from 20 to 80 ^oC respectively [Nesic, 1996]. In bicarbonate solutions, the electrochemical studies revealed that both anodic and cathodic reactions get accelerated with the higher temperature [Li, 2008]. Additionally, corrosion reactions at the low temperature 22 ^oC were under charge transfer controlled while they were mass transfer limit controlled at the higher temperatures, 40 and 80 ^oC. Electrochemical Impedance Spectroscopy (EIS) was utilized to investigate the protective capabilities of the corrosion products with respect to temperature variations [Kinsella, 1998]. The greater Nyquist semicircles depicted the increased corrosion resistance over time but the corrosion mechanisms did not show significant changes. Effect of temperature and the localized corrosion susceptibility were studied in saline deoxygenated bicarbonate solutions [Jelinek, 1980]. In that experimental work, it was found that raising the temperature to 90 ^oC restricted passivation breakdown in solutions containing less than 130 ppm. However, raising the temperature further made the breakdown more facilitated when the chloride concentration was above that threshold amount. Similarly, critical pH levels and chloride contents showed a dependence on temperature by which the susceptibility for corrosion attack changed from being localized to be a general type [Brossia, 2000].

2.3.2. Effect of carbon dioxide partial pressure

CO_2 partial pressure is the key factor that controls the concentrations of the corrosive species, pH levels, the corrosive significance of many physical and chemical factors, and consequently the corrosion rates [Kermani, 2003] and [Wang, 2004].

In conditions where the formation of corrosion products is not favored; for example at localized low-pH gradients, the corrosion rates were expectedly proportional with the partial pressure. Electrochemically, the accelerated cathodic reductions, which are described in section 2.2., were responsible for the greater metal dissolution [Nesic, 2004].

De Waard et al. and others reported the power dependence of the corrosion rates on P_{CO2} where the increased corrosion rates were correlated in relations with exponential powers ranging from 0.5 to 0.8 [De Waard, 1993] and [Dugstad, 1994].

McIntire et al. studied the corrosion behavior with respect to the partial pressure of carbon dioxide in the presence of oxygen. It was found that the significance of the protective corrosion products decreased, where the corrosion products dissolved attributing that to the catalytic action of carbonic acid [McIntire, 1990]. In addition, with respect to the corrosion types or surfaces, it was reported that corrosion was more susceptible to be of pitting type with greater carbon dioxide partial pressures [Crolet, 1994].

2.3.3. Effect of dissolved oxygen

Although that most CO_2 corrosion investigations are performed in deoxygenated media, the presence of trace amounts of oxygen getting leaked into the pipeline flows in the early stages of transportation represents a considerable corrosion significance [Lyons,

2005]. Oxygen or even appreciable aeration adds to the oxidizing power that carbon dioxide corrosion environment already has against pipeline steels even upon existence with a few amount of 0.006 M at 25 ^{o}C reported in [Tomashov, 1966]. Oxygen induces noticeable changes on the passivation and corrosion products whose properties depend on P_{CO2} where different oxide phases could exist with variant proportions [Butler, 1966]. For example, dissolved oxygen can contribute in forming a multi-layer type of passive films incorporating stable and/or transformable hydrous oxides such as ($FeO.nH_2O$), ($Fe(OH)_2$), and ($Fe(OH)_3$) [Ahmed, 2006] and as going to be discussed in Chapter III.

2.3.4. Effect of pH level

pH level is an important environmental factor considered in the corrosion mechanisms and other associated physical processes controlling CO_2 corrosion reactions. At low pH levels less than 4, corrosion mechanisms in the completely CO_2-saturated media are temperature-independent and controlled dominantly by the direct reduction of hydrogen protons [Nesic, 1996]. In addition, at low pH levels, the corrosion rates are expectedly high and the pipeline corrosion surfaces tend not to contain localized damages [Dugstad, 2000]. However, in conditions at higher pH levels greater than 5, the corrosive environment becomes, by pH-changing speciation, dominated by carbonic acid where it can contribute in the electrochemical reactions [Lopez, 2003]. Furthermore, the disassociation of carbonic acid occurs more readily to produce bicarbonate species at mildly alkaline pH levels, where as discussed previously, they can get involved in both anodic and cathodic reactions. From corrosion product adherence and stability

perspectives, it was reported that the formation of effective compact corrosion products was necessarily associated with higher pH levels [Kermani, 1994].

2.3.5. Effect of bicarbonate concentration

The corrosion rates were found proportional with the greater bicarbonate content [Xu, 1996] and the shapes of polarization curves showed changes accordingly [Mao, 1994]. In 0.5 and 1 M deoxygenated bicarbonate solutions, a unique anodic peak appeared at -600 mV_{SCE}. The passivation ranges were shorter as the bicarbonate content was as low as 0.05 and 0.1 M, and a second anodic peak appeared at -300 mV_{SCE} in these low bicarbonate containing solutions. Passivation was also studied by potentiodynamic polarization means in quite dilute bicarbonate solutions of 0.005 and 0.01 M in [Torres-Islas, 2008]. It was found that the potential at which the passivation starts (E_{pass}) was nobler as the bicarbonate content was less. The other associated electrochemical passivation characteristics showed a dependence on the heat treatment applied to the pipeline steels investigated.

In a similar scope, the current densities in the active anodic regions were noticeably accelerated with the bicarbonate content and anodic peaks appeared in 0.1 and 0.5 M solutions [Videm, 1993]. In addition, it was indicated that the passivation process comprising the multilayer oxide mixtures formed, upon the gradual decrease of the passive current density with the higher overpotenatial within a range exceeding 200 mV.

Zhang et al. studied the corrosion performance in simulated formation waters containing different bicarbonate contents at high temperatures utilizing polarization means. After analyzing the corrosion products, it was found that the better compactness and the consequent enhanced protectiveness were associated with the greater bicarbonate

content [Zhang, 2006]. In addition, the pH levels were monitored and their variations with respect to the bicarbonate content indicating the protectiveness of the corrosion products lowering corrosion rates. In a separates scheme, investigating the significance of miscellaneous anionic specie, the greater susceptibility for pitting in CO_2-saturated media was greatly associated with the presence of bicarbonate [Schmitt, 2000].

2.3.6. Effect of flow regimes

Oil and gas pipeline flows are transported with different regimes where upon the variations in the partial velocities and the corresponding phase amounts, oil, water, and gases interact to produce slugs, bubbles, and other hydrodynamic continuums. These regimes induce significant changes on the corrosion reactions especially with the velocity variations where the transfer of corrosive species or dissolution of protective corrosion scales get necessarily accelerated [Nesic, 2001]. Most of the corrosion evaluation studies performed in different flow regimes were comparatively reported on the variations of the partial velocities of liquid and gases as shown below in Figure 2.2 representing the common pipeline flow regimes.

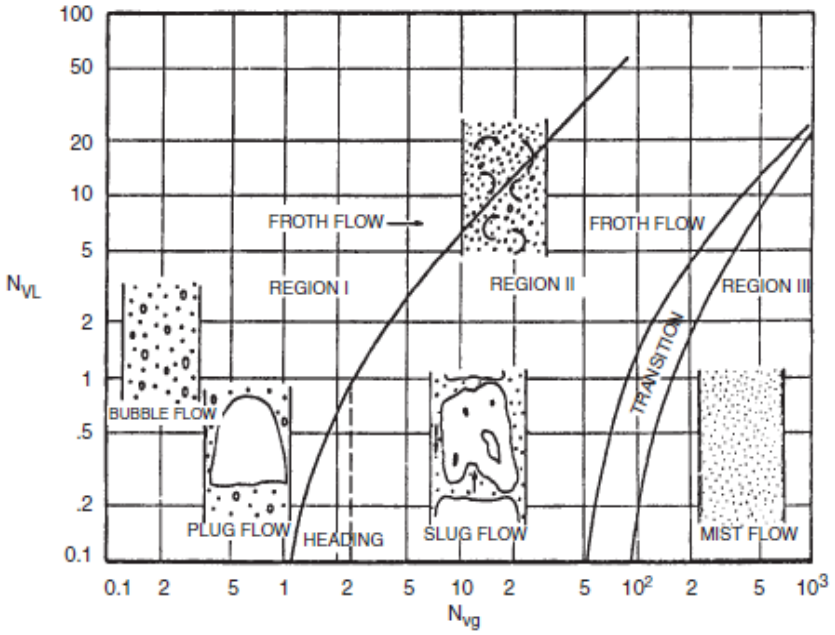

Figure 2.2. Flow regimes in oil pipelines at different liquid and gas velocities [Lyons, 2005].

From the field observations on the failure susceptibility perspectives with respect to the flow regime variations, topline pipeline sections are generally vulnerable to localized corrosion attacks while the lower sections readily suffer from general dissolution especially during slug flow modes [Jepson, 1996]. Palacios et al. reported an experimental work considering the effect of multiphase flow regimes on the corrosion behavior [Palacios, 1993]. In addition, the changes of morphological characteristics of the corrosion products with the same respect were also discussed indicating the enhanced protectiveness achieved at lower velocities. When the flow velocities are low and/or comprised of single phases, the corrosion susceptibility is significantly less than that in multiphase flows. Hydrodynamically, the vertical component of velocity of the single phase flows approaches zero near pipe walls while in multiphase flows; significant forces are induced on the steel surfaces and/or on the corrosion products leading to greater corrosion rates. The mass transfer of corrosive species and the dissolution of corrosion products become critical factors in evaluating the corrosion behaviors especially when the liquid phase exist in form of small droplets or extended slugs [Heuer, 1998]. Sun et al. studied the corrosion performance of X65 and C1018 in stratified flow conditions of superficial liquid velocity of 0.1 m/s and superficial gas velocity of 10 m/s at high pressure and temperature [Sun, 2003]. pH levels showed an appreciable increase as well as did ferrous ions concentration with time. Linear polarization resistance technique was employed to study the corrosion rates which were high at the early time periods of the experiments. The corrosion products formed in these conditions and they were effectively protective in lowering the corrosion rates interestingly in these specific multiphase flow

conditions. Both pipeline steel coupons exhibited well spreaded corrosion attacks but with slight variations on the corrosion surfaces.

Ruzic et al. reported the significance of single phase flows on the stability of the corrosion products proposing a mechanism describing the deterioration of protective corrosion products and the consequent corrosion behavior [Ruzic, 2006]. The supersaturation of iron carbonate decreased with the higher velocities making the corrosion products less protective. It was proposed that corrosion product removal in single-phase flows results from hydrodynamic factors acting in subsequent steps. They include the vertical cracking of the corrosion products driven by the intense localized vortices followed by crack propagation in different fashions ending with accelerated widening. Full or partial corrosion product detachment from the steel surface consequently occurs. The partial removal of corrosion products leads to an establishment of galvanic cells comprised of dispersed covered and exposed surface areas making the corrosion attacks be more localized.

2.4. Corrosion products formed in CO_2 corrosion conditions

The performance of the developed pipeline steels in carbon dioxide corrosion environments comparatively depends on the tendency of formation and on the properties of the corrosion products precipitating upon saturation and/or electrochemical reactions. Stability, adherence, compactness as well as the compositional characteristics were of a great research interest when considering long term corrosion reactions or when proposing mechanisms or predicting dissolution rates [Gao, 2008]. Besides the environmental factors, the chemical composition of the corrosion products varying upon the long term

interactions were reported to influence the nature of corrosion attacks and/or corrosion surfaces [John, 1998].

Iron carbonate ($FeCO_3$) is the most predominant corrosion products that form in CO_2-saturated environments. It has protective capabilities depending on its thickness and compactness [Nesic, 2002] and, differently from iron sulfide (FeS), it is not conductive. The formation upon the achieved supersaturation is conventionally described by:

$$Fe^{2+} + CO_3^{2-} \leftrightarrow FeCO_{3\,(s)} \qquad (1.23)$$

The precipitation of iron carbonate occurs when the solubility limit is exceeded. It is the multiplication of concentrations of Fe^{2+} and CO_3^{2-}. The concentration of carbonate is dependent on the local pH levels and the supersaturation is achieved more effectively at higher pH levels [Van Hunnik, 1996]. When the multiplication of ferrous and carbonate concentrations exceeds unity, the precipitation occurs expressed mathematically in relation to the solubility product as:

$$\text{Supersaturation} = \frac{[Fe^{2+}][CO_3^{2-}]}{K_{SP}} \qquad (1.24)$$

Precipitation rate depends therefore on supersaturation limit and on temperature leading to the formation of possibly stable corrosion products decelerating the corrosion rates and acting as natural barriers intervening the transport processes of the corrosion species.

2.5. Carbon dioxide corrosion models

Some models were proposed from 1970's for predicting corrosion rates in CO_2 saturated media considering the partial pressure of carbon dioxide and temperature. There was a model received a wide recognition among experts community with respect to those

two physical factors mentioned. It was proposed by De Waard and Milliams [De Waard, 1975]. Depending on the laboratory corrosion measurements performed on selected pipeline steels, the theoretical basis of that model was provided on the cathodic prevalence of (H_2CO_3) reduction on the corrosion behavior. The corrosion rate expressed as metal loss in millimeters per year; was mathematically represented as:

$$\log CR = 7.96 - \frac{2320}{T + 273} - 5.55 \times 10^{-3}\, T + 0.67 \log P_{CO_2} \qquad (1.25)$$

Temperature and partial pressure of carbon dioxide are expressed in this relation by (^oC) and (bar) respectively in conditions saturated with carbon dioxide, free of salinity, and with pH levels less than 4. The model was repeatedly corrected to provide an appreciable extensive reliability in accounting for other physical and chemical factors influencing the corrosion behavior such as higher pH levels, total pressures, flow velocity, oil wetting, as well as inhibitors as performed in [De Waard, 1995] and [De Waard, 1993]. The proposed corrections to the early proposed models resulted in contradictories making the assumptions valid but for increasingly limited conditions. Therefore, the proposed models generally became more to be semi-empirical rather than being purely mechanistic achieving good reliability at least with selected field conditions. Additionally, the empirical relations were being modified and calibrated by extensive laboratory investigations taking into account the possibly forming corrosion products at higher temperatures [Franco, 2010]. In literature, there is still a considerable recognition for a mechanistic model proposed by Gray et al. for prediction CO_2 corrosion rates with respect to the variations in temperature, P_{CO2}, as well as pH levels. However, there are some drawbacks with the applicability of this model to some cases especially in reference

to the wide range of pH levels from 2 to 11 that this model can handle with no well corrected factors [Gray, 1990].

2.6. Mitigation and control techniques

Mitigation and inhibition methods for carbon dioxide corrosion problems in pipelines were based on fundamental concepts considered for decelerating corrosion reactions. In most cases, mitigation techniques are dealt with the possibly exposed anodic and/or cathodic regions, the corrosive medium, or with the electronic field by which the anodically released electrons are conducted through; the pipeline steel. In oil and gas industry, where the corrosion problems occur in complex environments of multi-interrelated variables, inhibition and corrosion management strategies are based on achieving effective and long-term corrosion suppression. The common mitigation methodologies include chemical inhibition, protective coatings, and cathodic protection. Alternatively, when a better understanding on the significance of corrosive media is attained, proper selection of materials of greater corrosion resistance can provide extended reliability and save fortunes on maintenance and replacements.

2.6.1. Chemical inhibition

Chemical inhibitors injection is one of the most conventional methods utilized for corrosion control in oil and gas industry from 1940's. Inhibitors interfere with the dissolution processes at the corroding metal/environment interfaces decreasing the corrosion rates by as much as 10 times [Heidersbach, 2011]. Inhibitors act on the steel surfaces with different fashions decreasing the anodic or the cathodic reactions depending

on their functional groups and/or the environmental conditions such as temperature. Organic inhibitors such as amine-based and other associate derivatives comprised in long dipolar chain organic surfactants are utilized widely for decelerating the corrosion reactions. In conditions where the environmental factors influencing the corrosion reactions are easily controlled, inorganic inhibitors are also considered [Hedges, 2000]. Corrosion inhibition is achieved, depending on the chemical characteristics, by direct physical adsorption or chemisorption reducing the corrosion rates with efficiencies directly proportional with the fractional active surfaces covered [Nesic, 2007]. Inhibitors injection in the field can be performed continuously during operation with the corrosive media or intermittently depending on the environmental factors or depending on the extent of other natural barriers in reducing the corrosion rates such as the corrosion products. As discussed in chapters V, VI, and VII, crude oil can act as a natural inhibitor decreasing the corrosion rates upon existence with few proportions of 10, 20, and 30 vol%.

2.6.2. Coatings

Coatings of different types provide a very good protective mean against CO_2 corrosion especially in conditions when the flow effects such as erosion or other hydrodynamic forces are induced along with those of pure electrochemical dissolution [Garverick, 1994]. They play a very good role in extending the expected life time of the important mega structures such as pipelines or tankers containing low-pH-level multiphase CO_2-saturated media. The basic effect is impeding the transfer processes of the species involved in the corrosion reactions going to or out of the corroding interfaces. Lots of research efforts were performed, whose results are not reported in this context, in

investigating the corrosion behavior [Naiming, 2010] with respect to the coating types and the associated environmental hazards and/or effects. In some cases, cathodic protection is considered to support the protective coatings in extremely corrosive media such as acidic low-pH level ones.

2.6.3. Cathodic protection

Cathodic protection techniques are generally applied for large structures requiring continuous protections. A controlled impressed potential is applied across the steel-environment interface to spread electrons readily participating in the cathodic reactions not driven necessarily by the anodic dissolution. In other conditions when the corrosive media is extremely acidic, sacrificial anodes are utilized to provide enhanced protectiveness which could be supplemented by inhibitors injection or by coating.

2.7. High Strength Low Alloy (HSLA) steels

High Strength Low Alloy (HSLA) steels are exclusively developed for achieving better structural integrity and strength towards greater operation pressures in oil and gas pipelines. Conventionally, alloying elements are added with controlled proportions by mass to the steel where the enhanced mechanical properties and corrosion resistance are achieved. (HSLA) pipeline steels are produced by rolling and accelerated cooling methods and they contain low carbon contents in a range from 0.05 to 0.25 wt% in consideration with the extent of formability and weldability required.

American Petroleum Institute (API) issued some standards for categorizing high strength pipeline steels which are conventionally called API X-series. These standards are worldwide and they are recognized for materials selection and design practices in oil and

gas industry. Additionally, these pipeline steels are treated with respect to their yield strength, microstructure, as well as the chemical composition which is shown in Table 1.1 for selected pipeline steels.

Table1.1. Chemical composition of selected API- series pipeline steels [Wang, 2009]

Pipeline Steel	Composition (wt%)					
	C	Mn	Si	S	P	Others
API X-52	0.12	1.25	-	0.02	0.025	-
API X-60	0.13	1.5	-	0.05	0.02	-
API X-65	0.15	1.5	0.26	0.0046	0.017	<0.1
API X-70	0.04	1.46	0.24	0.0025	0.0084	<0.1
API X-80	0.07	1.86	0.27	0.001	0.015	<0.1
API X-100	0.09	1.6	0.35	<0.001	<0.002	<0.1

In these classifications, the higher the grade, the higher the yield strength and the lower the toughness are. In the early oil and gas steel structures, API X-52 was quite conventionally considered as a low-grade pipeline steel, selected for its low price and good weldability. However, the greater demand for higher production rates delivered by greater operation pressures lead to develop higher grade steels such as X-65, X-80, and X-100. These newly developed generations of pipeline steels allowed for optimizing the material amounts required for higher pressures leading to achieve economic and environmental benefits. API-X100, which is the subject material in this study, has exceptional strength properties and it is exclusively utilized for some pipeline networks in Canada. Comparatively, with X-65, the required thickness considered for the same pressure in certain operation conditions can be minimized by as much as 10 times with greater reliability and good cost effectiveness. It is shown in Figure 2.3 a graphical representation of the historical development of the pipeline steels with respect to the yield strength attained.

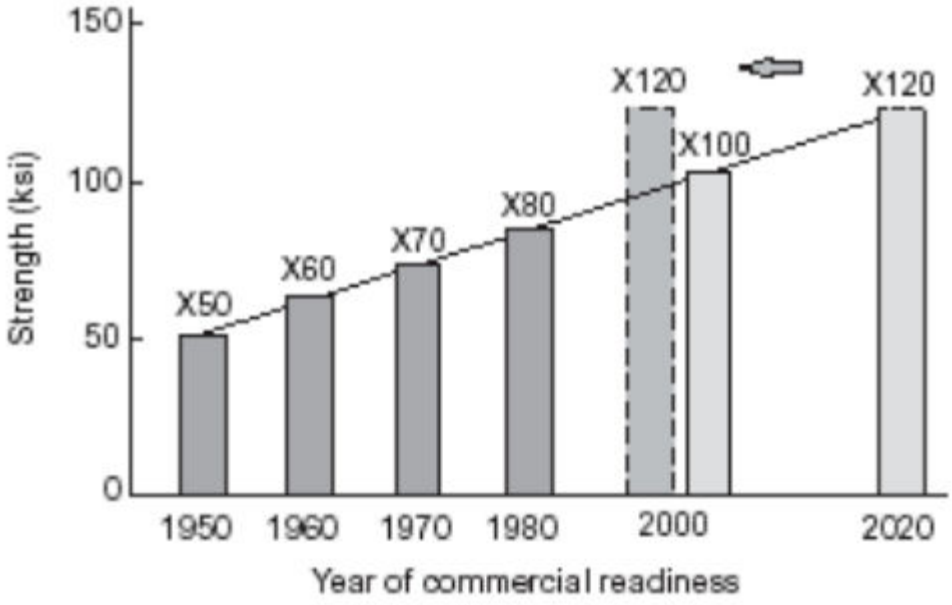

Figure 2.3. Evolution of yield strength of pipeline API steels [Asahi, 2004]

The possible reductions in the steel weight are apparently significant when considering higher grade steels as depicted below from Figure 2.4. The total reduction can be as much as almost 25% when considering X100 instead of X70; which is in fact a high strength steel of a very good reliability, but in terms of total weight, X100 is very beneficial.

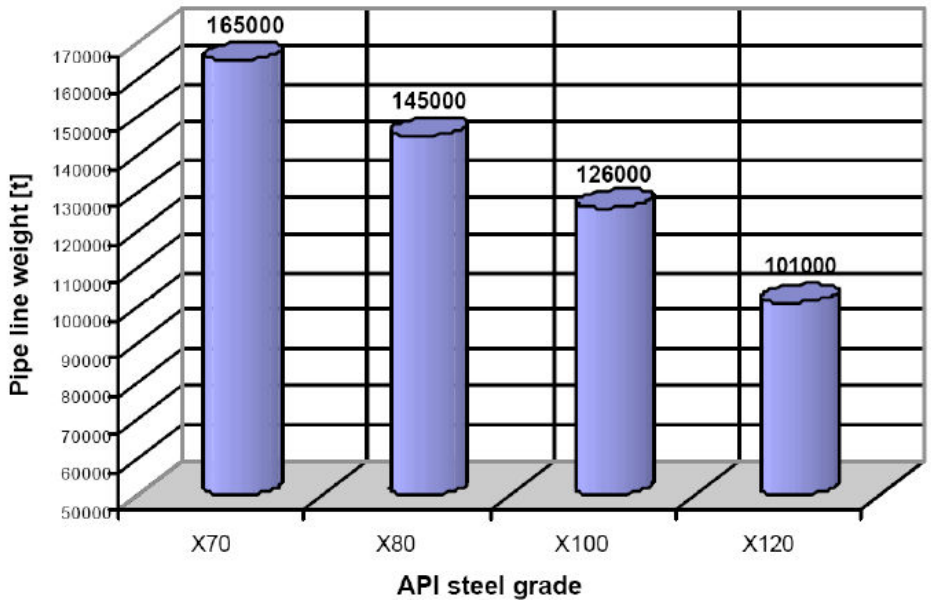

Figure 2.4. Possible material savings bythe use of high strength steels [Graf, 2003]

The small amounts of the alloying elements; chromium, niobium, vanadium, and molybdenum can contribute to, beside the enhanced strength, a better corrosion resistance. It is widely recognized that the addition of chromium in a range from 0.5 to 3 wt% to the carbon steels promotes the corrosion resistance. In that context, the stability of the protective corrosion products was attributed to the formation of chromium oxide films forming at greater proportions as reported in [Nyborg, 1997]. Kermani et al. reported a detailed study on the effect of the compositional content of many pipeline steels on the corrosion behavior (or resistance) and on the subsequent corrosion products and their properties [Kermani, 2001]. V, Ti, and Nb are strong carbide forming elements in normal conditions leading to preserve Cr and Mo uncombined to contribute in forming protective corrosion products during ferrite dissolution. Nb and Si achieve the required strength and compensate for the lowered carbon content. It is shown below in Figure 2.5 a schematic representation showing the relative effect of alloying elements in decreasing the corrosion rates.

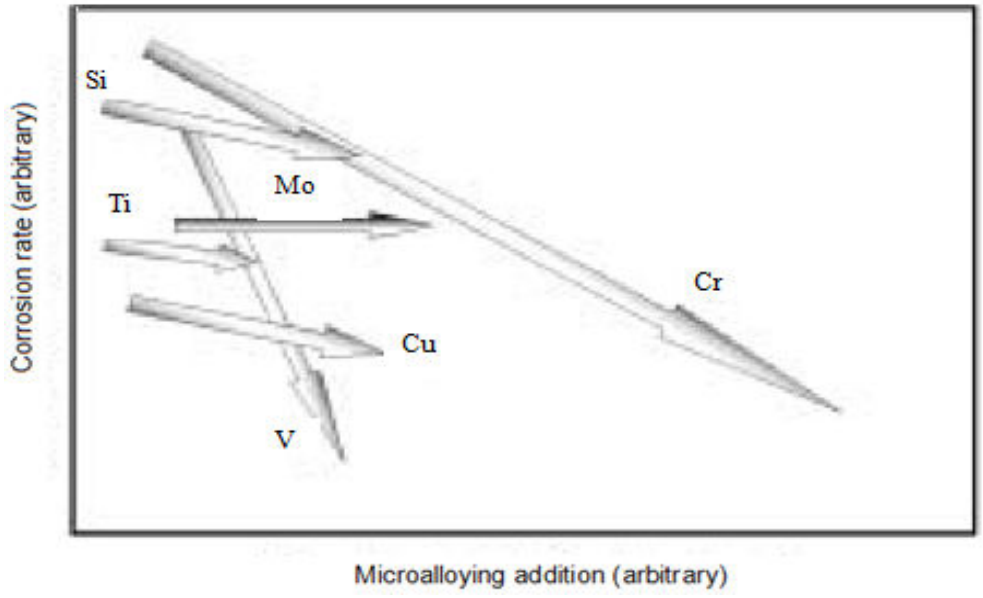

Figure 2.5. Relative effect of increased microalloying elements on the corrosion rates [Kermani, 2003]

2.8. Potentiodynamic polarization

2.8.1. Technique and parameters

Potentiodynamic polarization is a direct electrochemical measurement utilized for investigating the corrosion performance. In that technique, corrosion current density and potential are extrapolated from the polarization profiles scanned across the cathodic and anodic regimes. With respect to the selected polarization ranges and potential scan rates, the characteristic performance of the tested material is revealed in a specific environmental condition as an electrochemical fingerprint. Potentiodynamic polarization can provide a better understanding on the possible multi-step anodic dissolutions, as discussed in Chapters V and VI, from the variations in the potential/current slopes in the prepassivation ranges. Additionally, it indicates the significance of the environmental conditions on the passivation from the potential ranges, anodic peaks, as well as the transpassivation and from the associated accelerated and/or decelerated current densities. As discussed also in Chapter VII, the total cathodic reactions controlling hydrogen evolution can be remarkably discerned as the mass-transfer-limited reduction of (H_2CO_3) is separably identified out from the charge-transfer-controlled reduction of (H_2O). In addition, this technique, as discussed in detail in Chapters V and VI, helped in identifying the inhibition characteristics of a tested crude oil. From the variations of the corrosion potentials along with the decelerated corrosion current densities, it was found that oil can act as an anodic or a cathodic inhibitor with respect to temperature variations, and from the sudden acceleration in the anodic current densities at high overpotentials, important hints on the oil adsorption were revealed accordingly. In this study, the passive current densities were numerically integrated with the elapsed time to calculate the overall charge

transfer released from which a model for passivation incorporating oil in bicarbonate solutions was proposed as explained in Chapter V.

To illustrate a typical potentiodyanmic polarization response, it is shown below in Figure 2.6. a polarization profile considered for investigating the anodic part of a polarized solid material. The polarization conventionally starts from a potential appreciably below the corrosion potential which is assigned with number 1. The polarization is then swept with a constant scan rate (mV/sec) in the direction of positive overpotential passing through the characteristic regions until it is terminated at point 2.

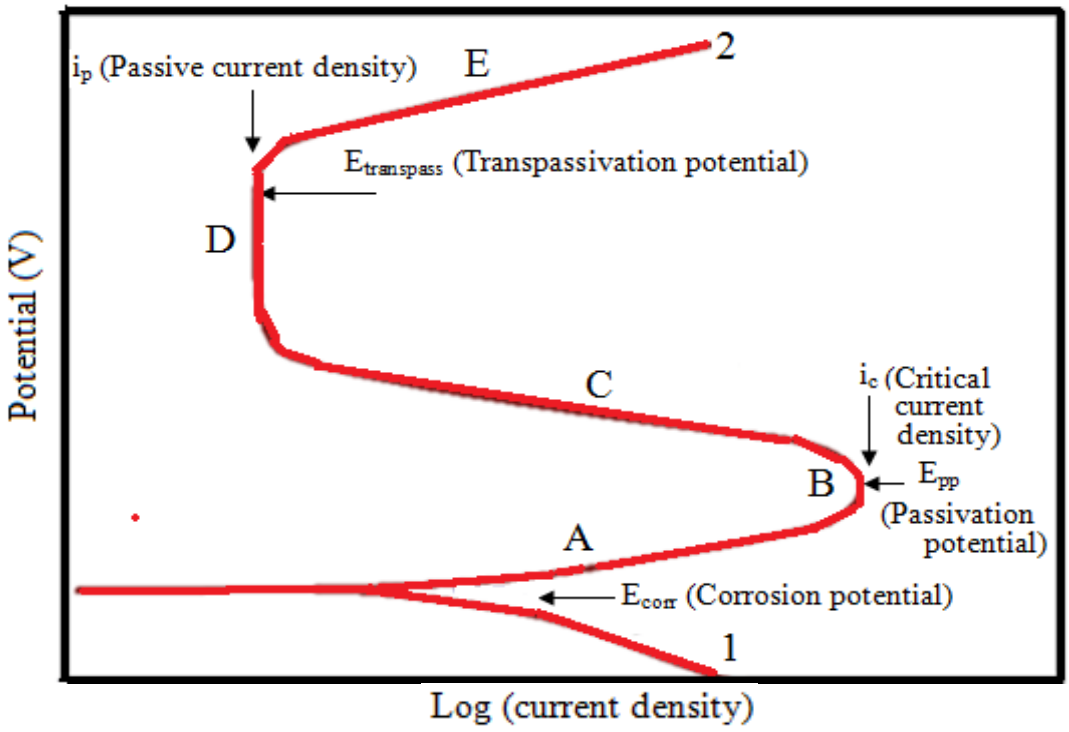

Figure 2.6. Typical potentiodynamic polarization profile

In the anodic region (A), the current density shows a considerable acceleration with the higher overpotential where the polarization within a relatively short range of potential reveals the pure active response. The slopes of potential-current correlations can

reveal hints on the prepassivation behavior or can reflect any electrochemical roles of introduced inhibitors. Consequently, in cases where effective corrosion-decelerating passive films formed, the current densities show an anodic peak corresponding to the onset of that effective formation of stable passivation. In that "critical" condition where the polarization response dramatically changes, assigned with point (B), the potential and the corresponding current density are denoted as passivation potential (E_{pp}) and critical current density (i_c) respectively. The current density then shows a slow gradual decrease as the passive film covers greater active areas or thickens to incorporate mixture of metal oxides or multilayered film acting as effective physical barriers between the surface and the corrosive medium. These processes with respect to the gradual decrease of current density before the existence of a stable passive film are designated electrochemically in region (C). In region (D), the passivation governs the polarization response at which the developed physical barrier becomes stable within an identifiable range of potential and at which the current density shows a relative stability (i_{pass}). When the applied potential is sufficiently high, the current density shows a sudden, active-like, acceleration as depicted from region (E). The potential at which the onset of current acceleration is detected corresponds to transpassivation potential ($E_{transpass}$) at which local deterioration to the passive film occurs accompanied, in some cases, by oxygen evolution.

Cathodic reactions can also be investigated by potentiodynamic polarization with the same scan rates sweeping from low negative overpotentials to the corrosion potential as performed in Chapters V, VI, and VII. Cathodic reduction from the mass-transfer limits, mixed controlled, to the purely kinetic controlled conditions can provide a wide understanding on the capabilities of the reducible species in generating for example

hydrogen. A typical cathodic polarization profile produced with that respect is shown below in Figure 2.7. where the polarization is performed from point 1 and terminated to point 2.

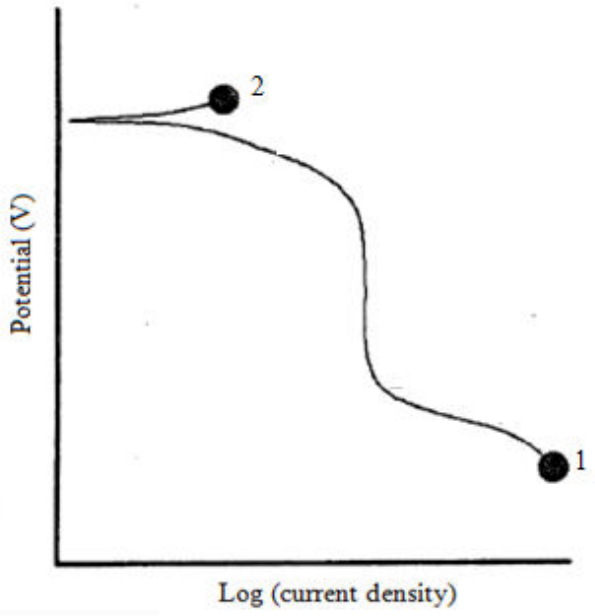

Figure 2.7. Typical cathodic potentiodynamic polarization profile

2.8.2. Potentiodynamics for CO_2 corrosion evaluation

Potentiodynaimc polarization was utilized widely for investigating many aspects of carbon dioxide corrosion behavior of pipeline steels at different environmental conditions [Liu, 2009], and [Zheng, 2008], and [Ren, 2005]. As shown in Figure 2.8, potentiodynamic profiles are presented with respect to the effect of temperature on the polarization behavior at 22, 40, and 80 ^{o}C in CO_2-saturated media. The corrosion rates showed expected increase with the higher temperature and the effect on the cathodic branches was apparent on both (H_2CO_3) and (H_2O) reduction reactions at lower overpotentials. The collective plots indicated the prevalent anodic influence in accelerating the corrosion rates as the corrosion potentials were more negative.

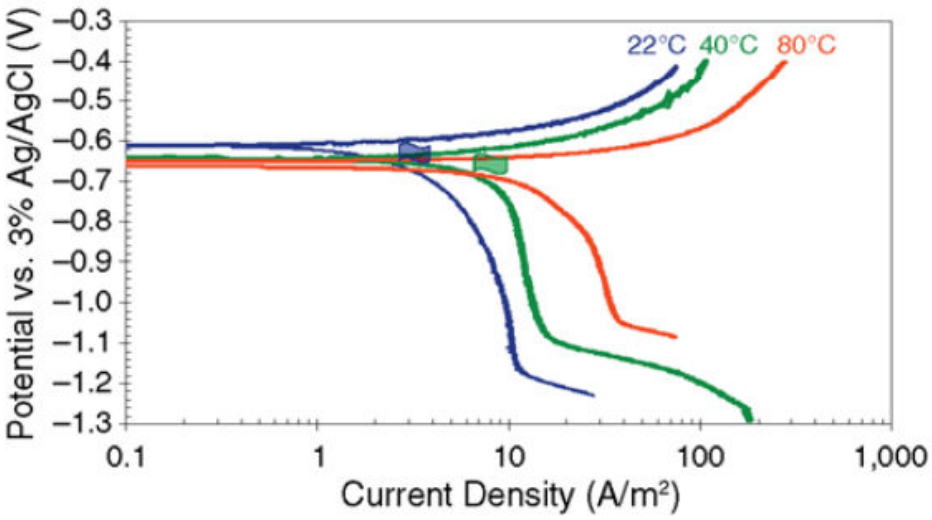

Figure 2.8. Potentiodynamic polarization profiles produced from polarized API X-65 steel static electrodes in continuously CO_2 purged conditions [Nesic, 2007]

The retardations in the anodic regimes were considered in respect to the preliminary physical changes introduced at the corroding interfaces before the effective passivation. These retardations, as shown below in Figure 2.9, indicate the multi-step oxidation reactions leading to form inner hydroxide layers contributing to the subsequent passivation reactions.

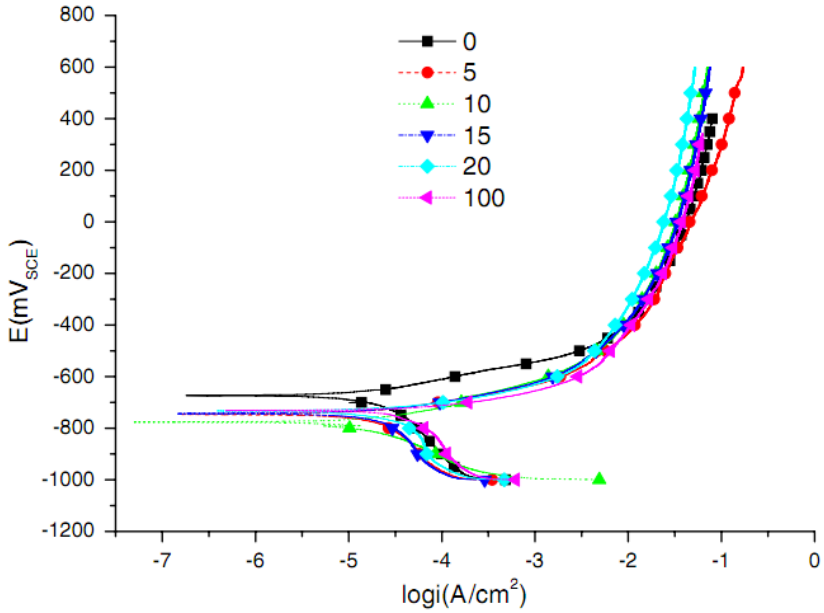

Figure 2.9.Polarization curves of X70 steel in the solution with different CO_2 partial pressures [Zhang, 2009 (B)]

In conditions, when the corrosive media is dominantly governed by bicarbonate, effective passivation with relatively broad ranges is established. Mao et al. considered different amounts of bicarbonate in deoxygenated solutions, but the multiple anodic peaks presented were attributed to new oxide phases formed as depicted below from Figure 2.10.

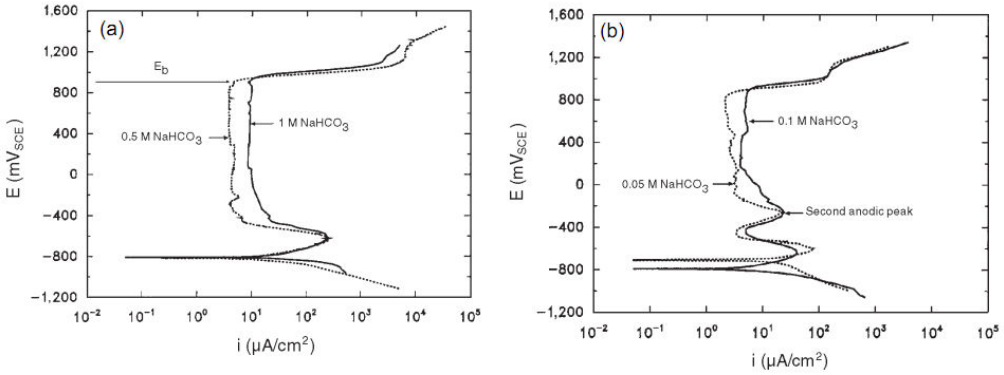

Figure 2.10. Potentiodyanmic polarization profiles produced from (a) 1 M and 0.5 M, (b) 0.1 M and 0.05 M [Mao, 1994]

In a similar work, potentiodyanmic polarization technique provided a better understanding on the effect of the bicarbonate content, temperature, as well as silicate and chloride contents. In addition, the anodic peaks and the associated potential ranges, which are selectively shown in Figure 2.11, were correlated to the basic characteristics of the passive films.

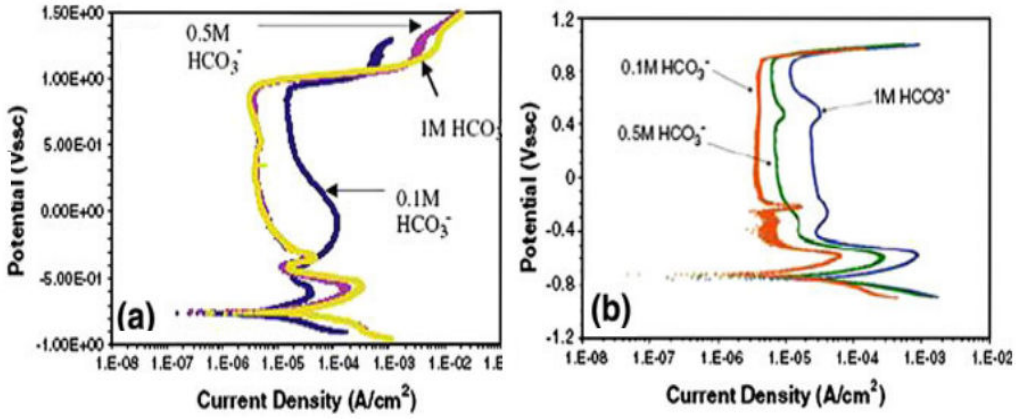

Figure 2.11. Potentiodynamic polarization profiles of API X-70 steel at 25 and 45°C in 0.1, 0.5, and 1 M bicarbonate solutions [Mohorich, 2010]

Interestingly, there are few works utilizing the polarization techniques to measure, electrochemically, the significance of the corrosion products formed with time as shown below in Figure 2.12. The basic morphological and compositional characteristics as well as compactness were also studied in relation to the electrochemical results discerned from the anodic and/or cathodic branches.

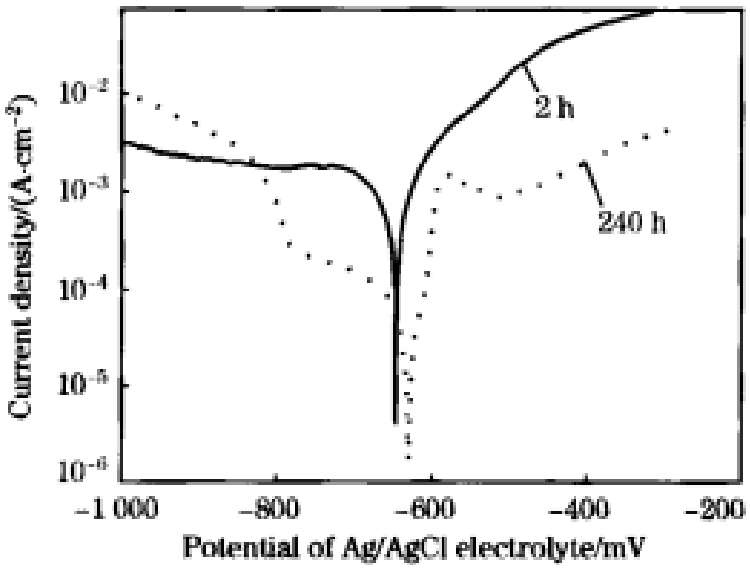

Figure 2.12. Potentiodynamic polarization profiles produced from polarized P110 steel at 90°C and 2.5 MPa during 2h and 240h [Guo-xian, 2009]

2.9. Electrochemical Impedance Spectroscopy (EIS)

2.9.1. Technique

Electrochemical Impedance Spectroscopy (EIS) is a direct electrochemical technique utilized for investigating the possible interactions at the corroding interfaces depending on the surface sensitivity towards alternating currents. From the early investigations on the corrosion phenomena, and although of the difficulties and ambiguities associated, that technique achieved a very good reliability in analyzing

corrosion mechanisms and the associated processes [Kinsella, 1998] and [Keddam, 1981]. In addition, EIS is recently being utilized for investigating the mitigation methods such as coatings and inhibitors providing a reliable electrochemical mean at which equivalent circuits can also be proposed [Jovancicevic, 1999**]**.

EIS provides specific impedance plots produced in relative to the resistance and capacitance exhibited across the double layer, passive films, and the outer regimes at which the transport and diffusion occur. In addition, equivalent electrochemical circuits are proposed with respect to the experimental data to indicate the significance of the corrosion processes.

2.9.2. EIS for CO_2 corrosion evaluation

In many corrosion studies investigating the performance in CO_2-saturated media, EIS was utilized to monitor the electrochemical changes exhibited by the corroding steel over a considerable elapsed time of testing. The changes in the corrosion resistance as well in corrosion mechanisms are monitored to evaluate the significance of the corrosive, H_2CO_3 containing media and that of the developing adherent corrosion products. As shown, for example, in Figure 2.13, the impedance profiles produced on the left; denoted as Nyquist plots are comprised of fairly depressed semicircles getting larger with time. These impedance changes, which are detected from corroding G10350 steel immersed in CO_2-saturated, 3 wt% NaCl containing autoclave conditions, indicated the greater corrosion resistance over time as well as the same persistent mechanisms governing the dissolutions. Interestingly, the alternate impedance diagrams produced at the right; designated as impedance phase bode plots, showed a multi-time constant impedance

response. That referred to the double peaks exhibited getting more discernible with time as the second-high-frequency peaks was shifting to the right over the test time. This indicated the enhanced protectiveness that the corrosion products acquired over time resulting in at least two-time-constant based impedance response in reference to impedance across the double layer and passivation respectively.

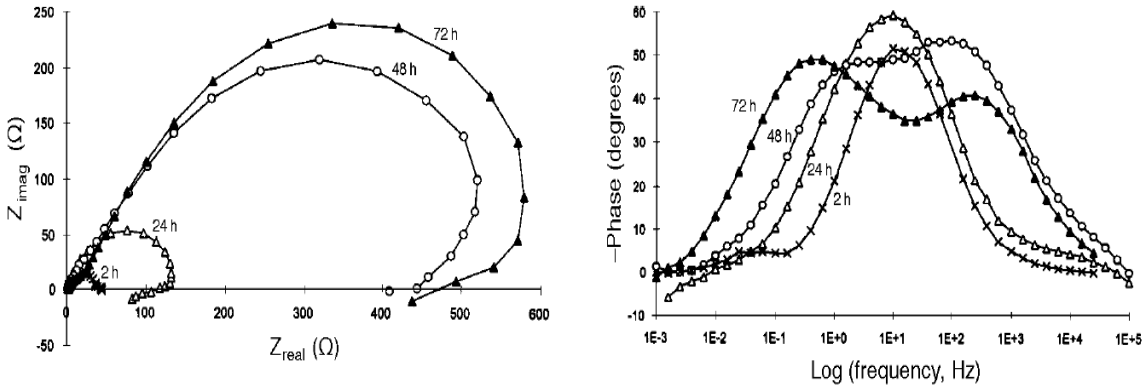

Figure 2.13. Nyquist and phase bode impedance profiles in 3 wt% NaCl containing, CO_2-saturated media at 70 ^oC produced after 2, 24, 48, and 72 hr [Kinsella, 1998]

In other cases of carbon dioxide corrosion environments dominated by bicarbonate species at almost mildly alkaline pH levels, the electrochemical investigations performed by EIS revealed important hints on role of bicarbonate adsorption in driving the corrosion reactions. As discussed in detail in chapters IV and V, the adsorption fields established by the reduced bicarbonate species influenced noticeably the impedance response. As shown in Figure 2.14, impedance at low frequency was characterized by appreciably overlapped semicircles representing adsorption and/or relaxation of the intermediate carbon carrying species. In these conditions, the significance of adsorption is necessarily associated with the size of the capacitive loops exhibited modeled by nested equivalent circuits. Although that in similar conditions at

higher temperatures where the response could be multi-time-time-constant based where the formation of passive films is more facilitated, but the presence of single phase peaks at intermediate peaks makes adsorption elements impeded within those of double layer.

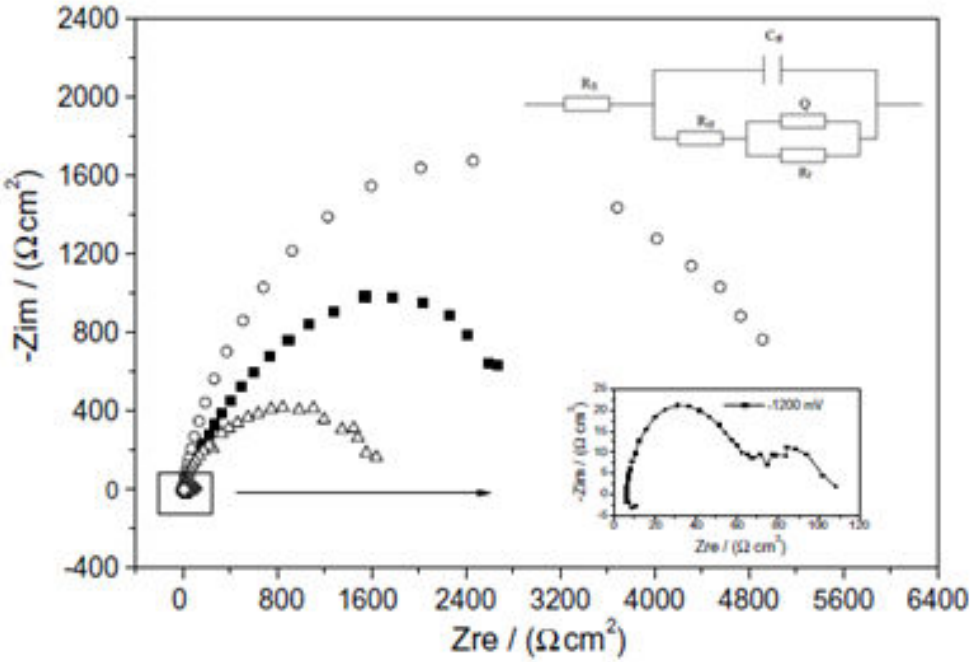

Figure 2.14. Nyquist impedance representations at different concentrations of bicarbonate where the the greatest loop corresponds to the lowest bicarbonate concentration [Li, 1999]

Chapter 3: Test material and experimental details

3.1 Test material and corrosion test coupons preparation

API-X100 is the test material developed for providing the greater strength integrity of pipelines at high pressure. The chemical composition analysis on weight percent basis was performed using Inductive Coupled Plasma (ICP) and LECO carbon analysis. The summarized results for the compositional content are shown below in Table 3.1 and the microstructural characteristics investigated under the optical microscopy, are shown in Figure 3.1.

Table 3.1. The chemical composition and carbon equivalent of the working electrode

Composition (wt. %)										
C	Mn	Mo	Ni	Al	Cu	Ti	Nb	Cr	V	C.E.
0.10	1.67	0.21	0.13	0.02	0.25	0.01	0.043	0.016	0.003	0.47

Prior to the microstructural analysis, the mounted specimens were wet ground up to 1200 grit silicon carbide finish and then polished with 6 and 1 μm diamond suspensions. The steel sample was etched by 2% nital (2 ml nitric acid + 98 ml ethyl alcohol) and then treated with alcohol swapping and finally dried by air stream. The material shows a complex microstructure consisting of acicular ferrite and dispersed bainite colonies with localized variations in color referring possibly to localized variations in the compositional content.

Corrosion test samples prepared for the electrochemical investigation were cut out of a pipeline segment manufactured from API-X100 steel. They were machined to be proper rectangular coupons of nominal dimensions of 15 mm by 10 mm and they were soldered to copper wires by a conductive silver paste. Afterwards, they were mounted in

special hard cold-curing epoxy resins. Prior to each corrosion test, they were sequentially wet ground by silicon carbide emery papers of 120, 320, and 600 grit. Afterwards, they were degreased ultrasonically with ethyl alcohol for 10 minutes and then were rinsed with distilled water and finally dried in a cool air stream.

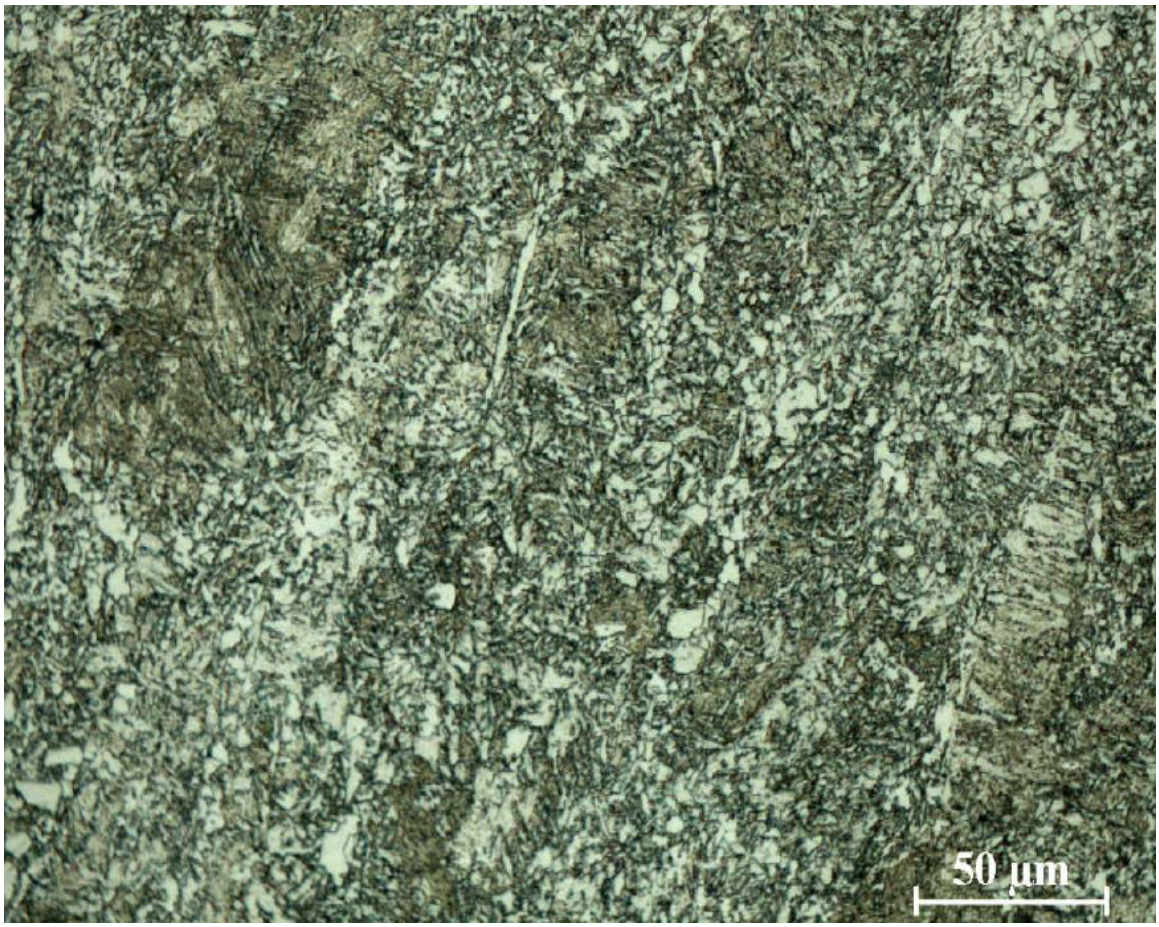

Figure 3.1. Optical micrograph of API-X100 steel microstructure

3.2 Corrosion test setups

The experimental test setups were considered to simulate selected CO_2 corrosion conditions commonly encountered in the field. The glass jacket test cell was convenient for performing the corrosion investigations in naturally aerated and deoxygenated

bicarbonate solutions as well as in oil free and oil containing CO_2-saturated brines. An autoclave was utilized to perform the weight loss measurements in the low oil containing CO_2-saturated stratified flows.

3.2.1. Standard three-electrode jacket cell

The electrochemical measurements were first performed in a standard three-electrode jacket cell of a total volume capacity of 1 L. The working electrode was the studied pipeline material, the counter electrode was a graphite rod, and the reference electrode was a Saturated Calomel Electrode (SCE) of +0.241 V_{SHE}. The electrochemical contact between the reference electrode and the working electrode was achieved by a Luggin capillary tube whose Vycor frit was appreciably close to the steel surface. The cell was connected to a heater manufactured by Cole-Parmer and equipped with a digital controller to provide accurate temperature measurements. The test setup is shown below in Figure 3.2.

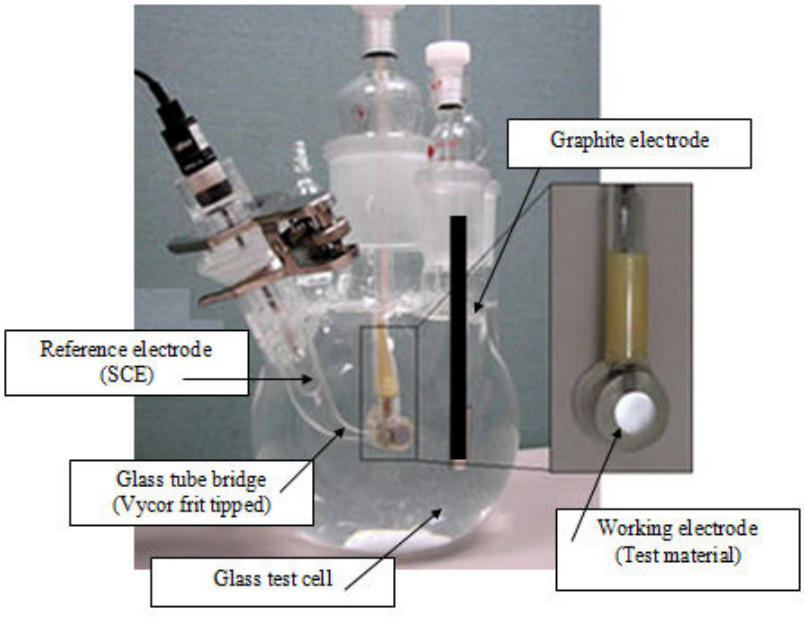

Figure 3.2. Corrosion test setup for electrochemical measurements, Standard glass test cell

The deoxygenated and CO_2-saturated corrosion tests were performed in the same setup but a special gas bubbler was properly inserted and sealed to the test cell. The gas flow was regulated by a mass flow meter to ensure a sufficient positive pressure inside the cell to prevent strictly oxygen contamination whose level was continuously detected by a dissolved-oxygen sensor probe (OMEGA DOB21 accuracy = 12 ppb). In addition, the test solutions were stirred magnetically throughout the test time periods to maintain the effective mixing between the test solutions and the emulsified oil.

The three electrodes were connected to a Princeton Applied Research (PAR) Versastat 4 potentiostat/galvanostat controlled by VersaStudio v1.50.3712 software. The produced free potential variations with time, potentiodynamic polarization responses as well as Electrochemical Impedance Spectroscopy (EIS) results were processed, presented, and then analyzed to reveal the environmental effects on the electrochemical corrosion behaviors.

3.2.2. High pressure 4383 PARR autoclave

The corrosion behavior was further studied in a high pressure/temperature titanium autoclave with a capacity of 1.8 L. The autoclave is manufactured by Parr © and is controlled by a digital interface at which pressure, temperature and rotation speed are controlled and their values are presented. The functional description of the autoclave is shown in Figure 3.3 showing the reactor, gas line connections, sample holder, and the shaft.

The rectangular test samples were fitted by teflon screws to a teflon sample holder installed on the autoclave shaft as shown in Figure 3.4. The samples were numbered and

fitted at the specified places on the shaft were the corresponding numbers are sculptured. Carbon dioxide gas line was connected to the reactor allowing the regulated gas flow to be continuously fed during the test time periods. Operation temperature and pressure of the autoclave were set to be as 100 ^{o}C and 50 psi, respectively.

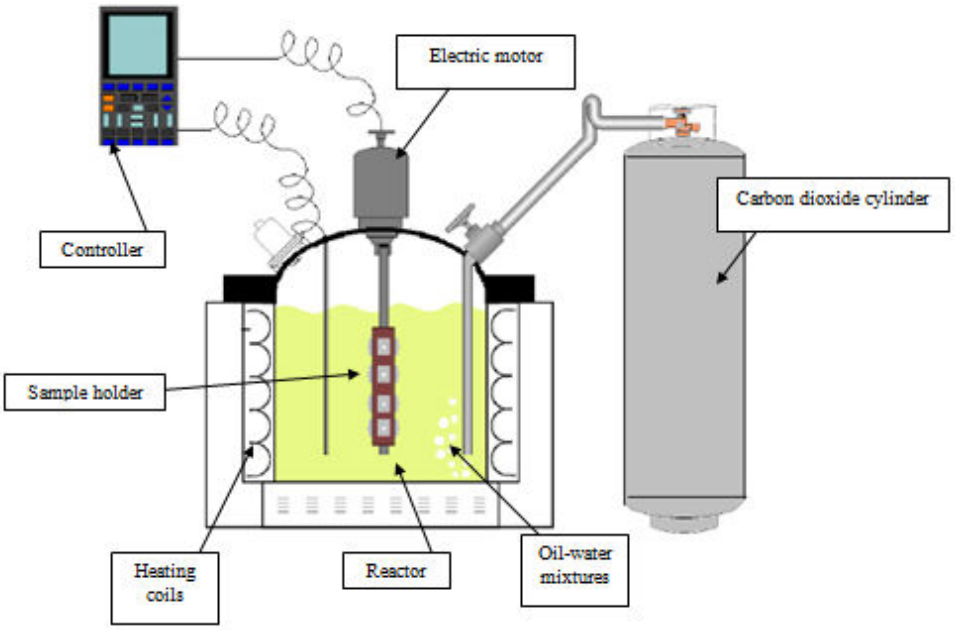

Figure 3.3. Schematic diagram illustrating the functional description of the autoclave utilized for weight loss tests

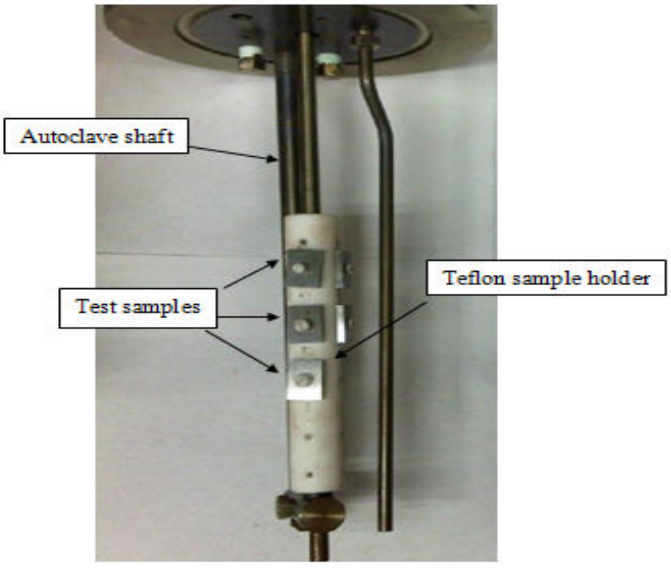

Figure 3.4: Autoclave sample holder

3.3. Experimental procedures

3.3.1. Electrochemical tests

In both aerated and deoxygenated conditions, when the working temperatures were reached, pH levels were measured, when applicable, and then the electrochemical tests were performed. Open circuit potential variations with time were first monitored. The relatively stable OCP values with small fluctuations of about ± 0.1 mV/sec were attained after in time periods generally not less than 4000 seconds. Consequently, Electrochemical Impedance Spectroscopy (EIS) technique was utilized to study the interfacial interactions more thoroughly at the OCP conditions. The frequency range was from 0.01 to 10,000 Hz with a sampling rate of 10 points per decade. Afterwards, the potentiodynamic polarization sweep measurements were performed at a scan rate of 0.50 mV_{SCE}/sec within potential ranges at which the key kinetic characteristics at the anodic and cathodic branches were fairly revealed. Cathodic polarization measurements were performed separately to investigate the charge transfer and mass transport controlled cathodic reactions in the deoxygenated bicarbonate and CO_2-saturated solutions. Prior to the electrochemical tests, the experimental setup and procedures were validated by the practices ASTM Standard G 5-94 [ASTM, 2004].

3.3.2. Weight loss measurements

The test coupons were weighed with a high precision balance before the autoclave immersion tests taking three measurements and then considering the mean value. Based on an experimental schedule, the autoclave was shut down at regularly spaces time periods to take out the corrosion samples and the operation was resumed. Three samples

were taken at each run and then cleaned with hot water and acetone before being weighed to measure the weight loss. The corrosion rates over the test time periods were calculated and the corrosion surfaces were examined by the Scanning Electron Microscopy (SEM).

.

Chapter 4: Results and discussion of the electrochemical investigations in naturally aerated bicarbonate solutions

4.1. Test solutions

The corrosion behaviour is studied in naturally aerated solutions synthesized from analytical grade Fisher procured reagent of sodium bicarbonate ($NaHCO_3$) added with 0.1, 0.5, and 0.8 M concentration in double distilled deionized water. 3 wt% chloride was added to the same bicarbonate conditions investigating the effect of chloride in a separate scheme. Although that such a high concentration of bicarbonate of 0.8 M is seldom reached in typical oil pipeline flows, but to be compliant with the considerations stated in the introduction part of this paper, the study was set to be performed with an extended range of bicarbonate concentrations. The test temperatures were selected to be 20, 40, and 60 ^{o}C and maintained within $\pm$ 1 ^{o}C.

4.2. Open Circuit Potential (OCP) measurements

OCP variations were monitored to account first for the changes that mixed potentials could show before other electrochemical aspects are investigated. OCP profiles were taken within test time periods of about 7100 seconds at which relatively stable OCP's are achieved with minimal fluctuations. OCP in chloride free bicarbonate solutions at the corresponding temperatures are shown in Figure 4.1.

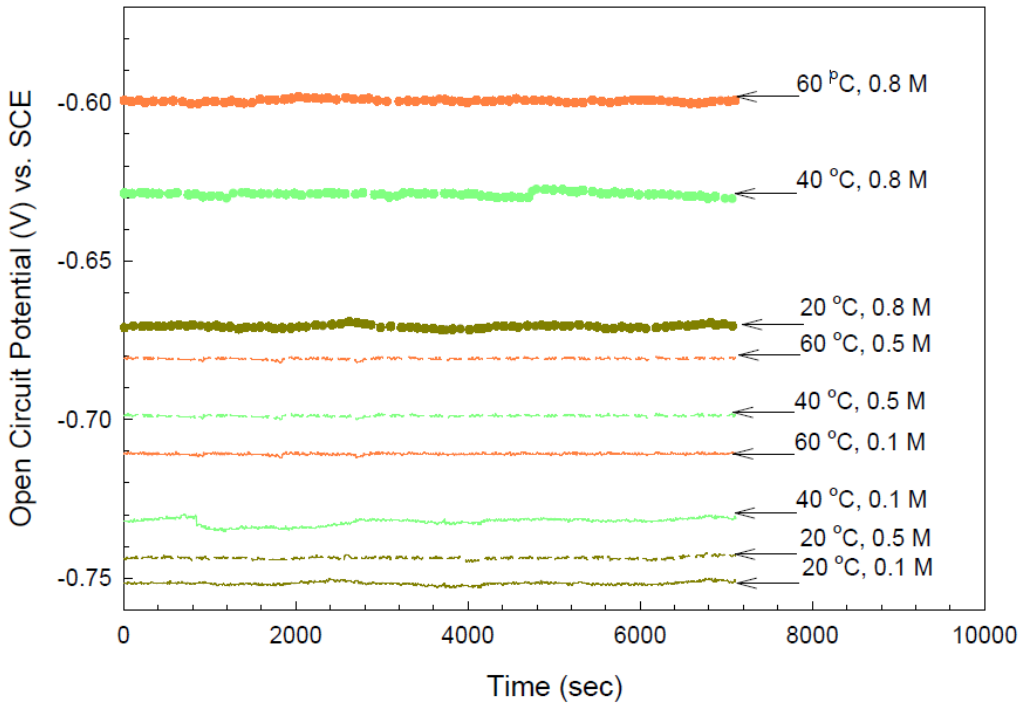

Figure 4.1. Open Circuit Potential (OCP) variations in chloride free bicarbonate test solutions.

Apparently, OCP exhibited an increase with the bicarbonate content at all temperatures. As discussed in the polarization test results section, the accelerated bicarbonate content – dependent cathodic reactions could be greatly responsible for that behaviour where the higher temperatures exerted also the same influence in these mildly alkaline media. In addition, this temperature-dependent behaviour suggests that the cathodic reactions, rather than the anodic ones, are more sensitive to the higher temperatures as previously argued in [Brossia, 2000]. Interestingly, the band of variation between the highest and lowest OCP values at 0.1 and 0.8 M respectively broadened with the higher temperatures.

OCP in all bicarbonate solutions was lower upon the chloride addition as shown in Figure 4.2., as expectedly in accelerating the anodic reactions [Fang, 2006], and confirming with

the polarization test results, the accelerated corrosion rates were accompanied by lower corrosion potentials when chloride was introduced.

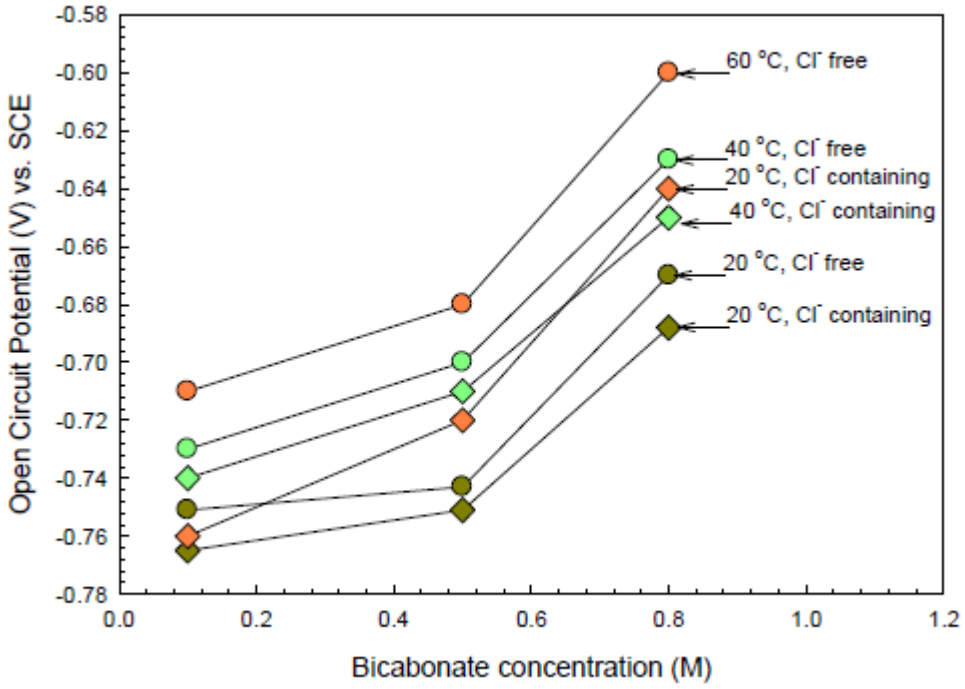

Figure 4.2. Open Circuit Potential (OCP) variations as a function of bicarbonate content at 20, 40, and 60 °C in chloride free and chloride containing test solutions.

The effect of chloride on OCP was more prevalent at higher temperatures and in dilute bicarbonate conditions. The anodic dissolutions are proposed to involve hydroxyl (OH^-) forming iron (II) hydroxide ($Fe(OH)_2$) [Ahmed, 2006] as:

$$Fe + 2OH^- \rightarrow Fe(OH)_2 + 2e^- \qquad (4.1)$$

The cathodic branch is considered to involve the simultaneous reduction of bicarbonate and dissolved oxygen, represented by equation (10). Bicarbonate is reduced substantially in these conditions [Paolinelli, 2008] and [Veawab, 2002] which is represented as:

$$HCO_3^- + e^- \rightarrow CO_3^{2-} + 1/2H_2 \qquad (4.2)$$

$$HCO_3^- + e^- \rightarrow CO_3^{2-} + H_{ads} \qquad (4.3)$$

$$1/2\,O_2 + H_2O + 2e^- \rightarrow 2OH^- \qquad (4.4)$$

The standard half cell potentials are calculated from the standard Gibbs free energy [Dean, 2000] of the involved species and, by utilizing Nernst equation [33], the theoretical anodic and cathodic potential limits are calculated taking into account temperature, pH, and bicarbonate concentration. OCP variations and the associated theoretical potential limits are selectively presented for chloride free and chloride containing solutions at 20 and 60 ^oC respectively in Table 4.1.

Table 4.1. Open Circuit Potentials (OCP) and the calculated half cell equilibrium potentials of the expectedly associated anodic and cathodic reactions for the chloride free and chloride containing conditions at 20 and 60 ^oC respectively.

Salinity	Temperature	HCO_3^- concentration	pH	OCP	Reaction (4.1) equilibrium potential	Reaction (4.3) equilibrium potential	Reaction (4.4) equilibrium potential
	(^oC)	(M)		(V_{SCE})	(V_{SCE})	(V_{SCE})	(V_{SCE})
Chloride free	20	0.1	7.7	-0.751	-0.968	-0.762	0.506
		0.5	7.9	-0.743	-0.974	-0.763	0.519
		0.8	8.4	-0.67	-0.988	-0.768	0.526
Chloride containing	60	0.1	7.8	-0.759	-0.971	-0.756	0.53
		0.5	8.4	-0.721	-0.988	-0.796	0.56
		0.8	8.5	-0.64	-0.991	-0.803	0.57

Apart from the specific potential theoreticals, the accelerated bicarbonate content-dependent cathodic reactions seemed to make OCP more sensitive to the cathodic reduction of dissolved oxygen, existing appreciably with the same amount in these bicarbonate solutions, with the absence and presence of chloride [Vaidya, 2007].

4.3. Potentiodynamic polarization measurements in chloride free bicarbonate solutions

The potentiodynamic polarization profiles at 20 ^oC, are shown in Figure 4.3a for 0.1, 0.5, and 0.8 M bicarbonate conditions. Similar polarization behaviours were

exhibited at 40 and 60 ^{o}C at the characteristic regions. It is apparent that the anodic and cathodic current densities accelerated with the increased bicarbonate contents.

Kinetically, corrosion current density (i_{corr}), and anodic and cathodic Tafel slopes (β_a), (β_c) are iteratively, with the best fit with the experimental data, calculated from Butler-Erdey-Volmer (BEV) equation for the purely charge-transfer controlled polarization [Stansbury, 2000] as:

$$i = i_{corr}\left(\exp\left[\frac{2.3\eta_s}{\beta_a}\right] - \exp\left[\frac{-2.3\eta_s}{\beta_c}\right]\right) \qquad (4.5)$$

The corrosion rate, or (i_{corr}), was proportional with the bicarbonate content and confirming with OCP findings, the corrosion potential (E_{corr}) increased accordingly at all temperatures as illustrated in Table 4.2. These two preliminary trends suggest the strong sensitivity of the corrosion reactions to the cathodic evolution of hydrogen generated from electrochemical bicarbonate consumption.

Interestingly, the higher temperatures seemed to induce a similar electrochemical influence where the corrosion rates progressively increased as did the corrosion potentials accompanied by a noticeable decrease of (β_c) with slightly appreciable changes in (β_a).

Additionally, the influence of bicarbonate content on the accelerated corrosion reactions was less significant as the temperature increased from 20 to 60 ^{o}C where the acceleration factor was almost 4:1 respectively.

Starting with the active dissolution regime, an evidence for a multi-step corrosion mechanism appeared where two anodic slopes resulted, more noticeably with the concentrated bicarbonate solutions, in the pre-passivation range.

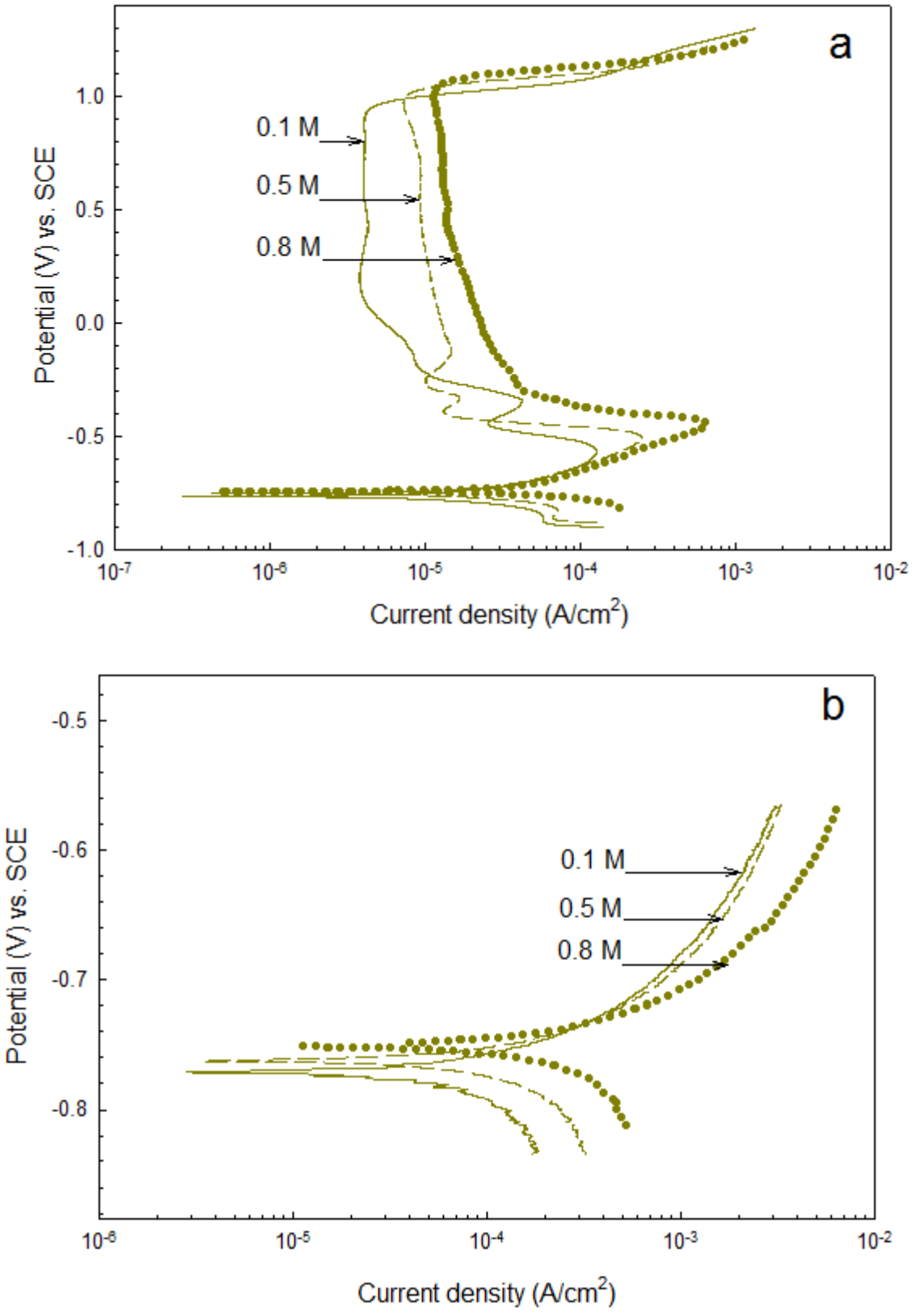

Figure 4.3. Potentiodynamic polarization in 0.1, 0.5, and 0.8 M bicarbonate solutions at 20 ^{o}C in a) chloride free and b) chloride containing conditions.

Dissolution reactions showed a retardation at an anodic transition overpotential of about -750 mV_{SCE} appreciably irrespective from temperature where the consecutive pre-passive slopes increased. This behaviour, in these mildly alkaline media, is very attributable to an introduced physical influence at the active corrosion interface [Talbot, 1998]. Hydroxyl (OH^-) species, getting involved in the dissolution mechanism, could contribute to this active behaviour in our case where a defective iron hydroxide passive film resulted. Despite of the possibly defective nature [Zhang, 2009 (B)] of this hydrous film, it was capable to interfere with a decreased rate of anodic dissolution.

Table 4.2. Potentiodynamic polarization test results in chloride free conditions

Temperature	Bicarbonate concentration	E_{corr}	i_{corr}	β_a	β_c	i_{pass}	E_{pass}	$E_{transpass}$
(°C)	(M)	(mV_{SCE})	($\mu A/cm^2$)	(mV /d)	(mV /d)	($\mu A/cm^2$)	(mV_{SCE})	(mV_{SCE})
20	0.1	-766	9.6	58	56	4.2	-603	894
	0.5	-754	20	53	46	9.3	-538	970
	0.8	-743	45	52	55	13.8	-470	1000
40	0.1	-753	33	51	48	11.5	-667	877
	0.5	-748	47	53	44	41	-652	912
	0.8	-739	63	55	42	43.4	-624	934
60	0.1	-750	56	51	45	14.2	-662	875
	0.5	-743	62	52	43	43.1	-658	920
	0.8	-735	73	49	40	53.7	-655	931

The formation of such a hydroxide-based film [Castro, 1991] within a short range of potential in Pourbiax diagram of Fe-H-C-O [Hirnyi, 2001] is illustrated as:

$$Fe + OH^- \leftrightarrow FeOH^-_{ads} \quad (4.6)$$

$$FeOH^-_{ads} \rightarrow FeOH_{ads} + e^- \quad (4.7)$$

$$FeOH_{ads} \rightarrow FeOH^+_{ads} + e^- \quad (4.8)$$

$$FeOH^+_{ads} + OH^- \rightarrow Fe(OH)_2 \rightarrow Hydrous\left[Fe(OH)_2\right] \quad (4.9)$$

Iron carbonate ($FeCO_3$) can be consequently incorporated with the preliminary formed film with sufficient bicarbonate contents but at a different transition point where

the electrochemical retardation became temporary at potentials, in our case, between 100 to 150 mV above the first retardation.

Iron carbonate formation results in a double-layered film where iron hydroxide becomes a distinct inner layer at this oxidation stage as pointed out by detailed voltammetric investigations [Castro, 1986]. In our case, the relatively continuous acceleration of the current densities could be explained by the bicarbonate-based-partial removal of iron hydroxide film as [Moiseeva, 2005]:

$$Fe(OH)_2 + HCO_3^- \rightarrow CO_3^{2-} + OH^- + Fe^{2+} + H_2O \qquad (4.10)$$

The second transition was not very evident in low bicarbonate conditions and at higher temperatures where the active dissolution was quite prevalent on the polarization performance. At the onset of passivation, distinct anodic peaks appeared with intensities proportional to the bicarbonate content, at overpotentials more positive with the bicarbonate content where the accordingly dependent dissolution delayed the onset of effective passivation.

Depending on (HCO_3^-) content and on the associated pH level, ($FeCO_3$) formation, before that of iron oxides, is facilitated via carbon carrying complexes including $[FeHCO_3^-]_{ads,}$ $[FeHCO_3^+]_{ads,}$ and $[FeOH^-]$ [Moiseeva, 2005].

The adsorption of these intermediates, for example $[FeHCO_3^-]_{ads,}$ is part of the dissolution mechanism as:

$$Fe + HCO_3^- \leftrightarrow FeHCO_3^- \qquad (4.11)$$

$$FeHCO_3^- \rightarrow FeHCO_3 + e^- \qquad (4.12)$$

$$FeHCO_3 + OH^- \rightarrow FeCO_3 + H_2O + e^- \qquad (4.13)$$

The gradual structure of the passive films could comprise miscellaneous oxides such as (Fe_3O_4) and (Fe_2O_3) via reaction complexes along with (OH^-) contribution [Alves, 2002 (A)].

($FeCO_3$) contribute to the formation of iron oxides [Lu, 2006] as:

$$3FeCO_3 + 5OH^- \rightarrow Fe_3O_4 + 3HCO_3^- + H_2O + 2e^- \qquad (4.14)$$

$$3FeCO_3 + 4OH^- \rightarrow Fe_2O_3 + 2HCO_3^- + H_2O + 2e^- \qquad (4.15)$$

From our polarization results, it is evident that more effective passivity is facilitated at lower temperatures where passive current density (i_{pass}) was lower accordingly and where, as shown in Table 4.2; (E_{pass}) was nobler also. In the same proposed context, two distinct anodic peaks appeared exclusively at 20 ^oC for 0.1 and 0.5 M solutions referring possibly to purely chemical oxidation of the already formed products as [Zhang, 2009 (A)]:

$$4FeCO_3 + O_2 + 4H_2O \Rightarrow 2Fe_2O_3 + 4HCO_3^- + 4H^+ \qquad (4.16)$$

$$6FeCO_3 + O_2 + 6H_2O \Rightarrow 2Fe_3O_4 + 6HCO_3^- + 6H^+ \qquad (4.17)$$

$$4Fe(OH)_2 + O_2 \Rightarrow 2Fe_2O_3 + 4H_2O \qquad (4.18)$$

It is observed that, at all temperatures, the transpassivation in these chloride free media occurred at a high overpotential of about 1 V_{SCE} appreciably irrespective from the bicarbonate content. This behaviour is subject for future investigations where the electrochemistry of oxygen at this high overpotential can be further investigated in bicarbonate solutions.

Bicarbonate content-dependent accelerated cathodic reactions in 0.8 M conditions seemed to prevail over the cathodic reduction of water, at least at the charge-transfer

and/or mixed control mass and charge transfer regions, which appeared at lower bicarbonate containing conditions at about -0.89 V_{SCE}.

4.4. Potentiodynamic polarization measurements in chloride free bicarbonate solutions

Potentiodynamic polarization profiles at 20 ^{o}C are shown in Figure 4.3b for 3 wt% containing, 0.1, 0.5, and 0.8 M bicarbonate solutions. Chloride introduced significant kinetic changes in the polarization performance in all bicarbonate solutions where the corrosion rates increased. In comparison to the chloride free solutions, that kinetic behaviour was accompanied by more negative corrosion potentials suggesting in turn the anodic sensitivity towards chloride as discussed previously in [Jelinek, 1980]. Even though, the increased bicarbonate content induced the same cathodic influence in making (E_{corr}) nobler as the corrosion rates increased accordingly as shown in Table 4.3. The anodic reactions proceeded continuously with no clear evidence for temporary-retardation, or for multistep dissolution. The higher conductive chloride containing environments prevented effective formation of stable prepassivation films where the behaviour in that region was quite active [Al-Kharafi, 2002].

Table 4.3. Potentiodynamic polarization test results in chloride containing conditions

Temperature	Bicarbonate concentration	E_{corr}	i_{corr}	β_a	β_c
(°C)	(M)	(mV_{SCE})	($\mu A/cm^2$)	(mV /d)	(mV /d)
20	0.1	-771	25.2	52	50
	0.5	-763	41.3	54	48
	0.8	-750	73.1	52	42
40	0.1	-772	43.5	50	45
	0.5	-758	55.4	51	41
	0.8	-746	80.2	50	39
60	0.1	-768	73	49	44
	0.5	-755	84.9	52	38
	0.8	-752	100.6	46	37

At higher temperatures, 40 and 60 ^{o}C, the anodic behaviour was similar to that at 20 ^{o}C where it was very active and the corrosion rates were higher and the chances for effective passivation or for anodic peaks to appear were inconsiderable. Differently from the cases of chloride free conditions, the sensitivity for (E_{corr}) towards higher temperature was less, especially in the dilute bicarbonate solutions of 0.1 M where both anodic and cathodic reactions could show comparable kinetic responses [El-Naggar, 2006]. The effect of chloride in our bicarbonate solutions seemed to be more associated with the activated autocatalytic generation of cation/oxygen pairs across the unstable pre-passive films [Li, 2007]. Across the interfacial fields where the corrosion processes were occurring, the significant localized pH gradients accelerated the anodic processes and the pitting susceptibility could be consequently higher [REn, 2010].

4.5. Electrochemical Impedance Spectroscopy (EIS) measurements in chloride free bicarbonate solutions

The electrochemical interactions at the free open circuit potentials were further studied by Electrochemical Impedance Spectroscopy (EIS) where a better insight is achieved from the governing interaction mechanisms [Cottis, 1999]. The significance of the environmental factors in aerated chloride free and chloride containing 0.1, 0.5, and 0.8 M bicarbonate solutions at 20, 40, and 60 ^{o}C could be appropriately understood in terms of the charge transfer and the diffusion processes across the adsorption fields and the developing passive films.

Nyquist impedance representation plots for chloride free test solutions are shown in Figure 4.4 for all bicarbonate and temperature conditions established. The relatively

similar profiles seemed to indicate the significance of kinetics as well as parallel diffusion-limited processes across fairly effective passive films.

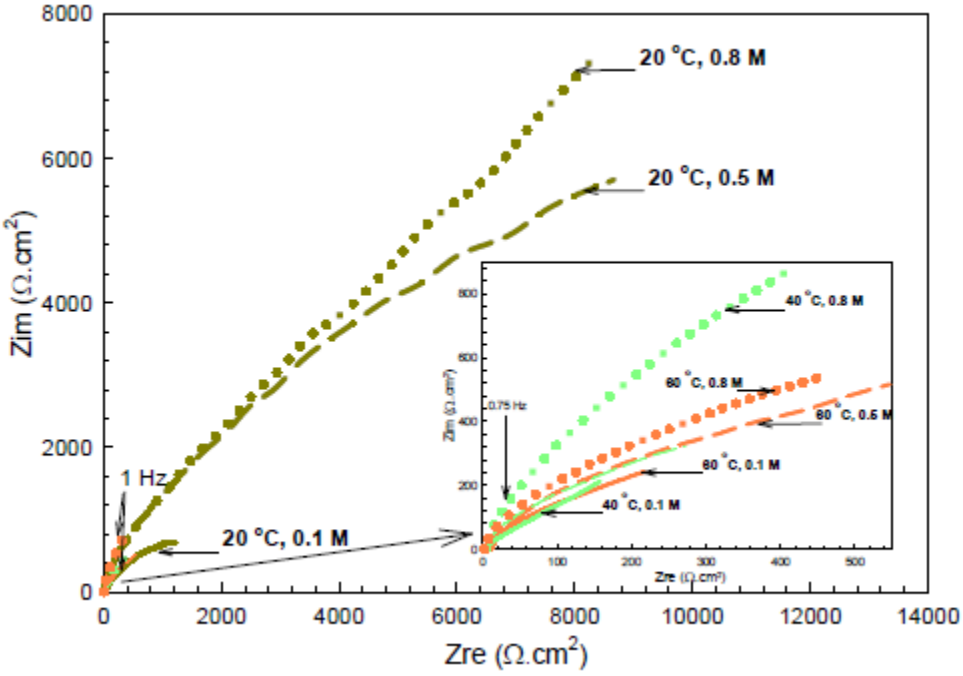

Figure.4.4. Nyquist impedance representation in chloride free bicarbonate test solutions

More specifically, the high-frequency capacitive arc expanded at different extents, in greater association with the bicarbonate content, to produce a second capacitive semicircle. The other part at low and medium-frequency regions flattened to indicate a diffusion-influenced process of the parameter (Y_W). In comparison with the polarization results, Nyquist semicircles achieved an agreement in terms of temperature effect where the charge transfer resistance and the other associated resistances were higher at lower temperatures; i.e. with larger Nyquist semicircles. The medium-frequency capacitive arcs, produced where the charge transformation of electrochemical process is controlled in parallel with other diffusion-limited process are related in most cases to localized active

sites where the corrosion rates were high [Mu, 2010]. Although that in conditions where carbon carrying species dominating the electrochemical processes could induce a separate time constant where the significance of adsorption is specified for [Castro, 1986], adsorption and/or relaxation of reaction intermediates of these species were excluded. The passive film formation, which was facilitated with greater amounts of bicarbonate, induced the prevalent electrochemical influence over any other associated processes which might occur when no effective passivation is established. Therefore, the similar electrochemical interactions seemed to be fundamentally a function of the passive film compactness whose properties are, for example, intrinsically related to temperature.

Impedance is represented in bode plots to elucidate the complimentary understanding on the possible electrode/electrolyte interfaces established as shown in Figure 4.5a at 20 ^{o}C. Impedance moduli |Z| in 0.5 and 0.8 M conditions followed quite similar dependence on frequency at all regions where kinetics and diffusion significances appear. Additionally, in these two bicarbonate conditions, |Z| was noticeably higher than that in 0.1 M. These profiles showed a slight inflection at about 1 Hz where the rate of dependence on frequency changed; i.e. where the overall mechanism could show a transitional dependence on other processes [Ma, 1998]. Bode phase peaks were considerably broad in all bicarbonate conditions and they showed a shift with greater bicarbonate contents as well discernible peaks appeared at high frequencies while the phase values were still high at lower frequencies. The associated processes occurring outside the double layer are related to that impedance behavior as the passive films were developing. At 40 and 60 ^{o}C, relatively similar trends and behaviors were exhibited but the character of multi-time constant based impedance response seemed to be more apparent. Especially, that

occurred in the dilute bicarbonate solutions of 0.1 M where the diffusion component seemed to be more compliant in a second time constant as shown in Figure 4.5b.

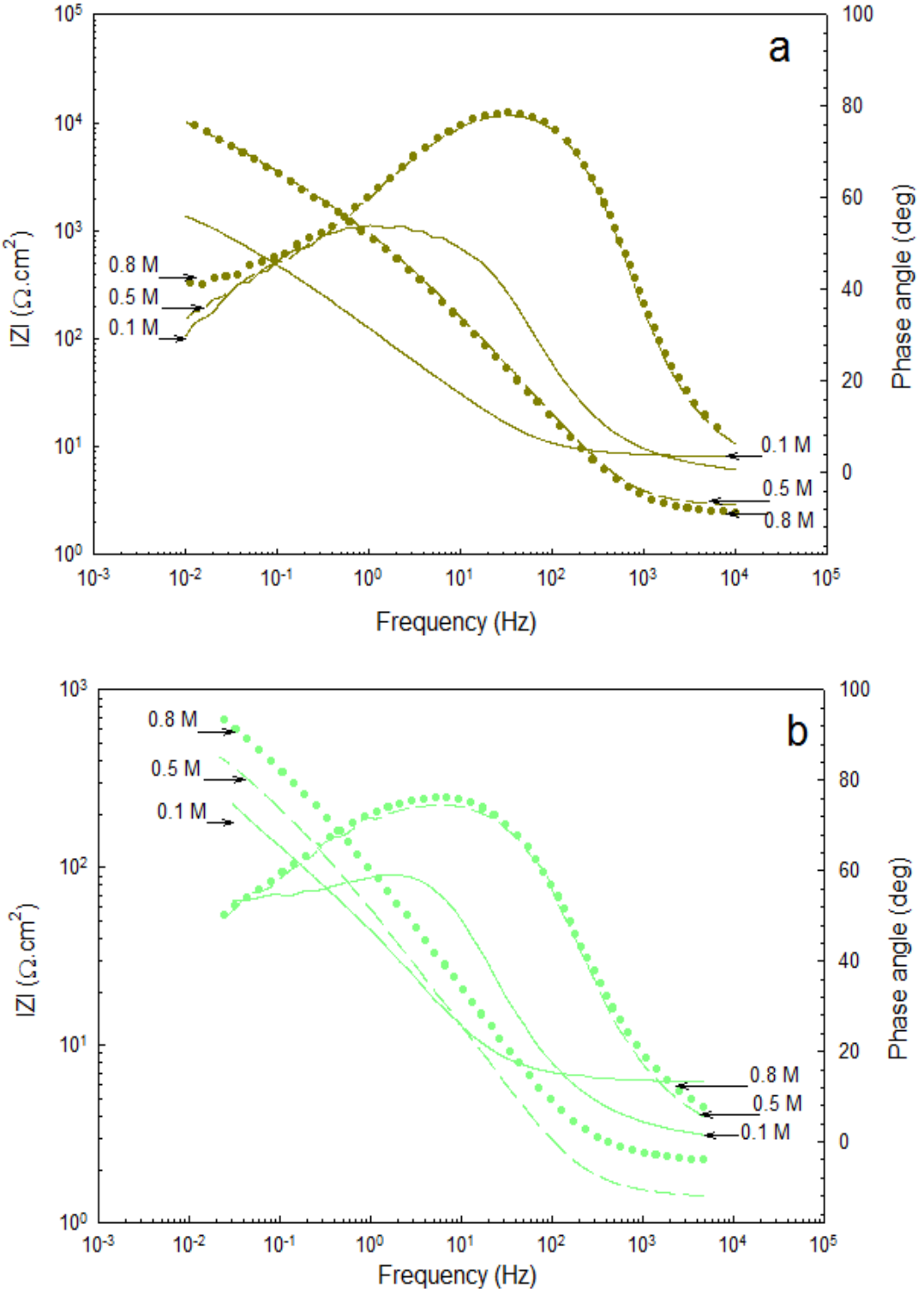

Figure. 4.5. Bode impedance representation plots in 0.1, 0.5, and 0.8 M chloride free bicarbonate solutions at a) 20 °C and b) 40 °C.

The proposed equivalent circuit for the electrochemical impedance response in the chloride free conditions is shown in Figure 4.6 where the contribution of the double layer and the parallel processes are considered in two separate time constants. As explained previously, the applicability for nested equivalent circuits of the configurations of

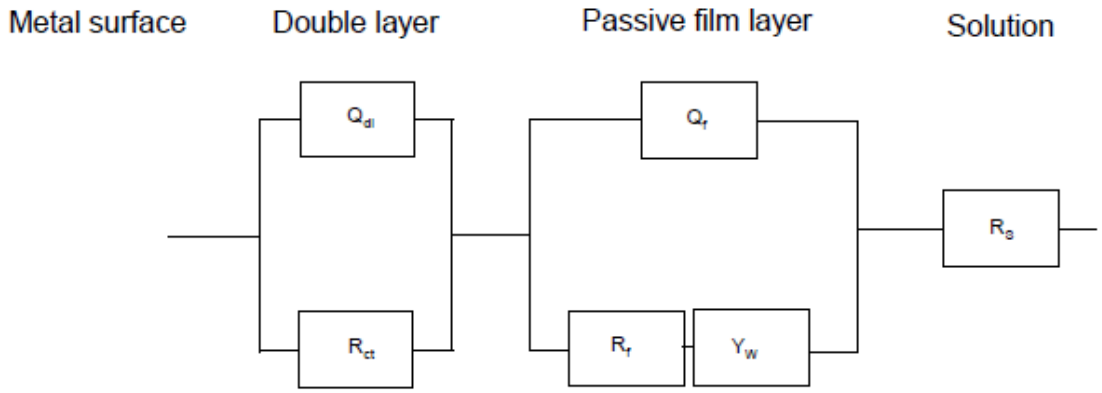

Figure.4.6. Equivalent circuits proposed for the electrochemical impedance response in chloride free bicarbonate test solutions

{R(Q(R(Q(RW))))} or {R(C(R(Q(RW))))} was quite limited although of the consideration of diffusion-limited processes occurring in the active areas, but such configurations were more compliant to adsorption fields rather than to effective passivation [Guo-xian, 2009]. Although of the arguments that are usually raised on those two equivalent circuits utilizable for similar passivation conditions [Chen, 1999] and [Liang, 2009], but the perfect fitting to the experimental data in our case seemed to be very achievable if Nyquist representations showed two depressed partial semicircles or at least a discernible semicircle with a diffusion character in the low frequency.

The electrochemical configuration attempted for the chloride free conditions considered is {R(QR)(Q(RW))}. A Constant Phase Element (CPE) was utilized for the double layer

(Q_{dl}) to account for the surface heterogeneity and it is expressed by equation (4.19) as:

$$Z_{CPE} = \left[Q(j\omega)^n\right]^{-1} \qquad (4.19)$$

(ω) represents frequency, (j) equals to $\sqrt{-1}$, and (n) is (CPE) exponent. The electrical parameters of concern are calculated after the perfect fitting is achieved with the experimental data and their values are shown in Table 4.4.

Table 4.4. Electrochemical Impedance Spectroscopy (EIS) component values in chloride free bicarbonate solutions at 20, 40, and 60 ^{o}C

Components	20 °C			40 °C			60 °C		
	0.1 M	0.5 M	0.8 M	0.1 M	0.5 M	0.8 M	0.1 M	0.5 M	0.8 M
R_s (Ω.cm^2)	8.09	2.955	2.471	6.263	1.421	1.1275	2.805	1.6	3.532
Q_{dl} (F/cm^2)	0.00005192	0.0000432	0.00001678	0.00009369	0.00003856	0.00001482	0.0000701	0.00003172	0.00001616
n_{dl}	0.8339	0.8186	0.7514	0.783	0.878	0.602	0.9365	0.722	0.763
R_{ct} (Ω.cm^2)	580.44	1513.2	1973	22.5	83.1	132.157	21.1	77	96.21
Q_f (F/cm^2)	0.00002674	0.00001384	0.00001212	0.0000284	0.0000161	0.00001127	0.00002379	0.00009986	0.00001047
n_f	0.9841	0.914	0.84	0.995	0.987	0.9383	0.981	0.987	0.9724
R_f (Ω.cm^2)	11.3	160.1	246.3	3.7	32.11	82	2.12	47.7	64.9
Y_{Wf} ($\Omega^{-1}s^{-0.5}$)	0.003404	0.000483	0.0003182	0.004346	0.0009547	0.0005373	0.004606	0.0009633	0.0005331
Chi-square	3.39E-05	2.97E-04	2.14E-05	6.37E-05	7.87E-05	1.36E-05	4.97E-05	4.86E-05	3.11E-05

Charge transfer (R_{ct}) decreased with higher temperatures, confirming with the polarization results where the corrosion rate increased accordingly. In addition, it was proportional with the bicarbonate content in conditions where the effectiveness of passive films seemed to be linearly proportional with the bicarbonate content. Interestingly, and confirming with anticipated capacitive nature, (Q_{dl}) exhibited an opposite trend with the greater bicarbonate content at all temperatures and the capacitive character was less also as revealed from the trend of (n_{dl}). Resistance across the passive films (R_f) decreased to about an order of magnitude at higher temperatures and it followed the trend of the that of (R_{ct}) with the bicarbonate content indicating clearly the better passivation as indicated in [Liu, 1995] with the bicarbonate content at the free open circuit potentials. To support that concept, the decreasing (R_f) trends with lower bicarbonate contents and with higher temperatures were accompanied by a greater diffusion parameter (Y_w) indicating the greater mobility of the active corrosion species through the increasing transfer channels

in the passive films [Li, 2007]. It should be noted that a three time constant-based equivalent circuit was attempted to fir our results where the absorption and/or insertion phenomena [Hamadou, 2005] occurring at an auxiliary deposit layer could induce an effect on the impedance performance. However, no satisfactory agreement was achieved suggesting that such a model is more applicable to higher temperatures, or in conditions where carbonic acid drives the corrosion reactions; i.e. at low pH levels. The perfect applicability of the proposed equivalent circuit is exclusively presented for 20 ^{o}C conditions where the electrochemical interactions at this low temperature show the distinct changes with bicarbonate as shown in Figure 4.7.

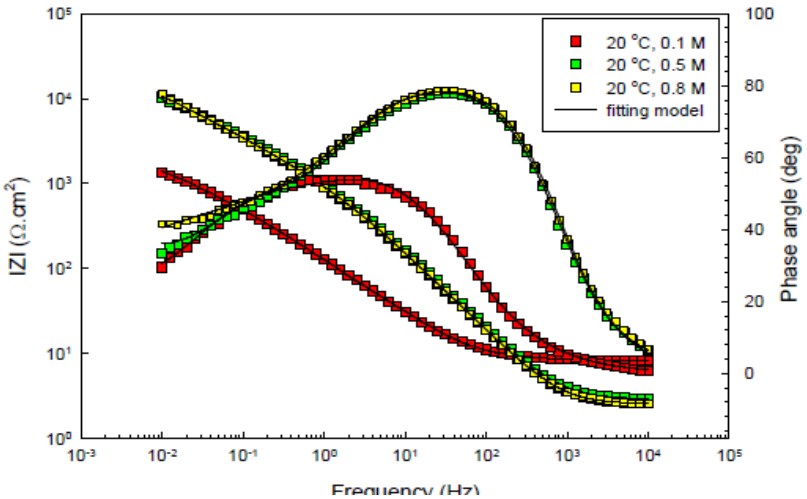

Figure 4.7. Experimental and calculated bode representations of impedance for selected chloride free bicarbonate test solutions.

4.6. Electrochemical Impedance Spectroscopy (EIS) measurements in chloride containing bicarbonate solutions

Nyquist representations in 3wt% chloride containing bicarbonate solutions at 20, 40, and 60 ^{o}C are shown in Figures 4.8a, b, and c respectively. Introduction of chloride changed noticeably associated processes of adsorption and/or passive film formation.

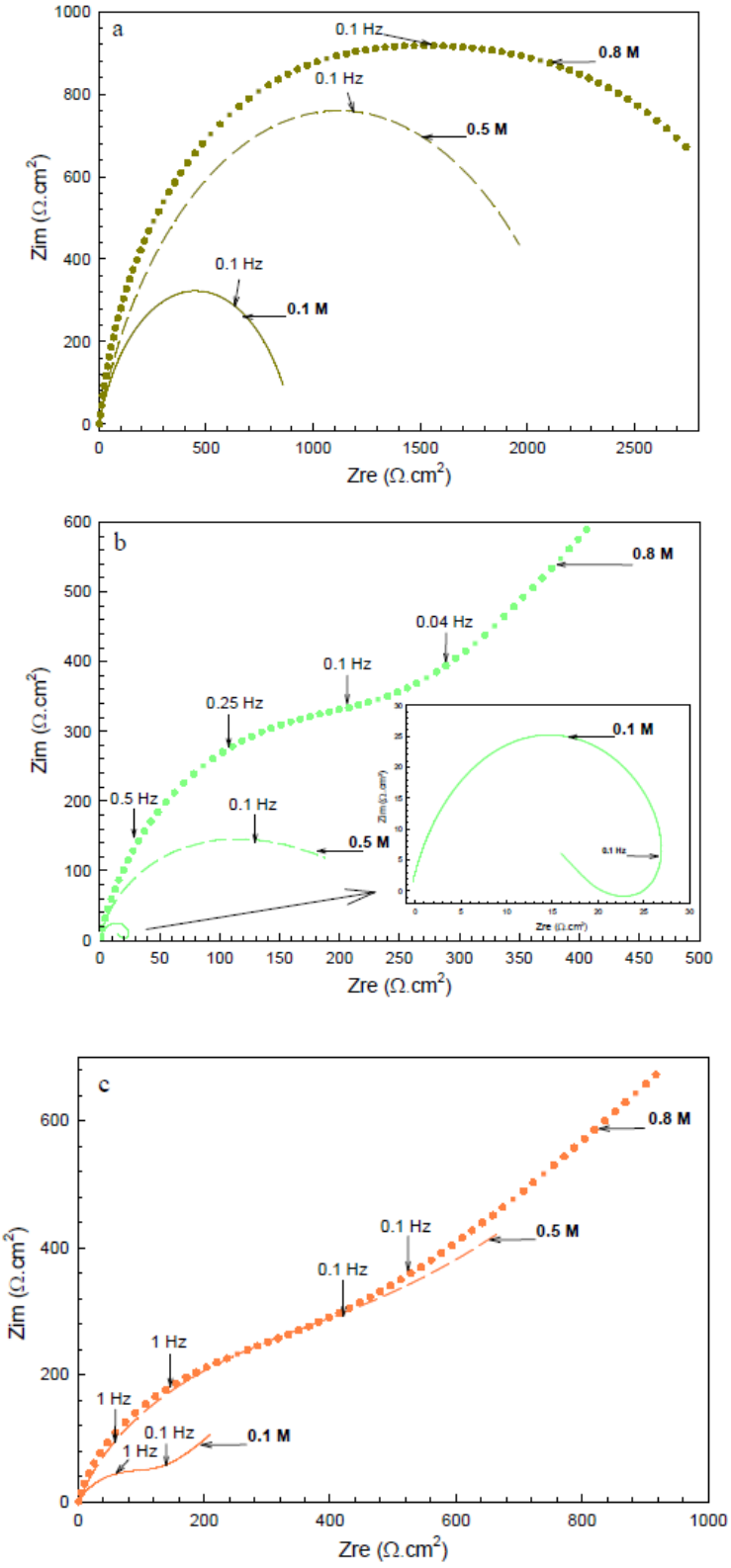

Figure 4.8. Nyquist impedance representation in chloride containing bicarbonate test solutions at a) 20 ^{o}C, b) 40 ^{o}C, and c) 60 ^{o}C.

At 20 ^{o}C, although of the still relatively large impedance semi-circles produced, it seemed that the possibility for effective diffusible passive films to form was quite limited. In all bicarbonate solutions at this low temperature, the chloride-influenced interactions resulted in two fairly overlapped depressed semicircles at medium-to-high and low frequency regions respectively. In a proportional manner, and similarly to the chloride free conditions, the profiles were larger with the bicarbonate content and the significance of the new electrochemical influence was more apparent accordingly. In these conditions, it is reasonable to refer that to the adsorption of bicarbonate species getting involved in the cathodic regime or more possibly to the relaxation of the intermediate species in the dissolution mechanisms in more concentrated bicarbonate conditions [Wu, 2004]. As shown in Figure 4.9a, this is confirmed by the appearance of single phase peaks of intensities proportional to the bicarbonate content at 10 Hz reflecting the adsorption significance but not necessarily in a multi-time constant based equivalent circuit.

The equivalent circuit proposed at 20 ^{o}C is shown in Figure 4.10a, comprising the (CPE) at the double layer and at a special adsorption field of bicarbonate driving the charge transfer reactions on fairly active steel surfaces.

It is of the configuration of {R(Q(R(QR)))} and it achieved a very good fit with the experimental data. At 40 ^{o}C, at which the corrosion behaviour in our bicarbonate conditions could be electrochemically transferable as previously found in other harsher corrosion CO_2 systems [Lin, 2006]. As shown in Figure 4.8b, the presence of chloride made bicarbonate influence the electrochemical interactions differently depending exclusively on its content. In 0.1 M condition, the influence of chloride was significant in facilitating inductive adsorption fields as already found in [Moiseeva, 2005].

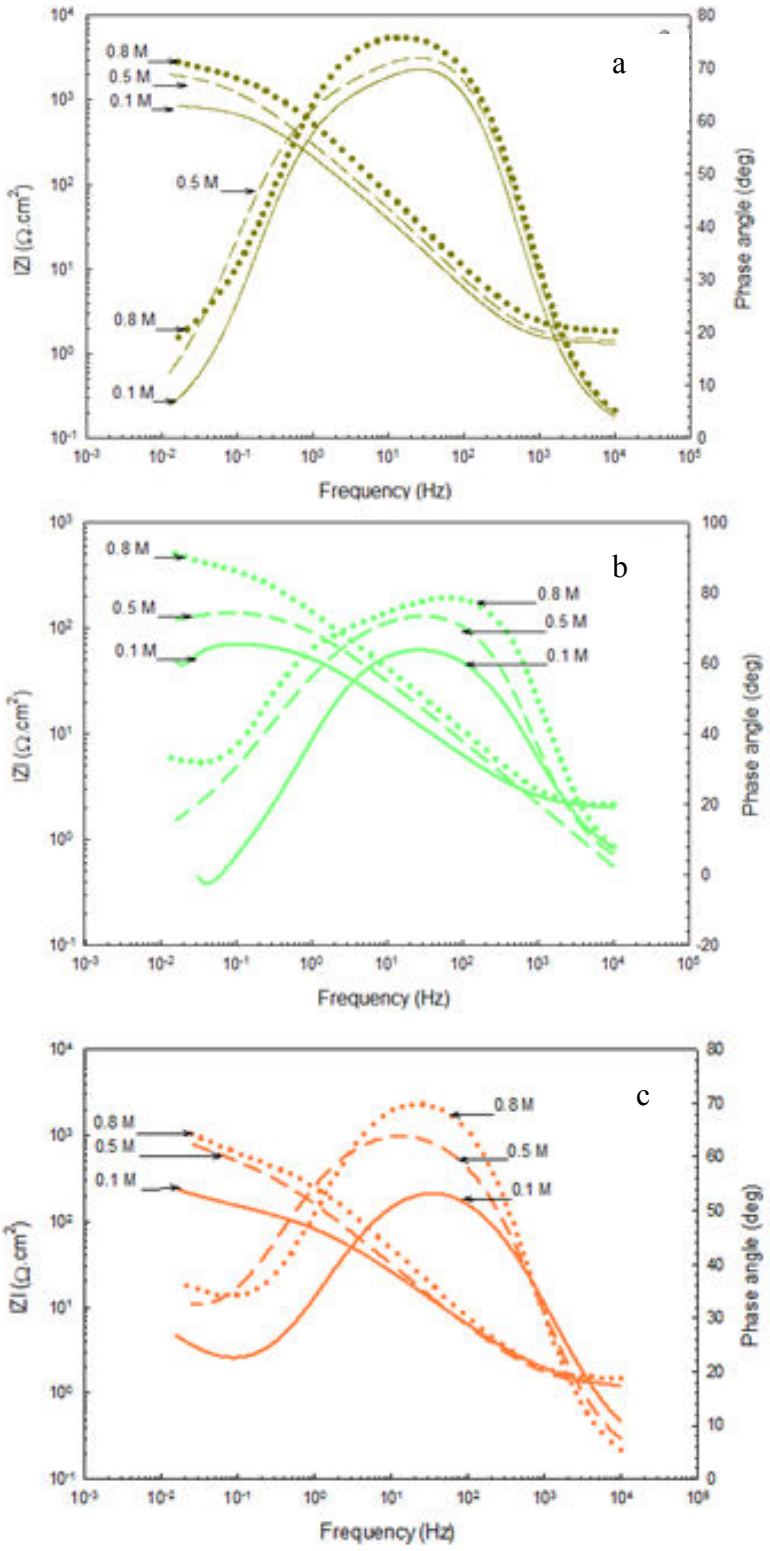

Figure 4.9. Bode impedance representation plots in 0.1, 0.5, and 0.8 M chloride containing bicarbonate solutions at a) 20 ^{o}C, b) 40 ^{o}C, & c) 60 ^{o}C

The proposed equivalent circuit for this special system is shown in Figure 10b and it is of the configuration of {R(Q(R(RL)))}. The new elements (L) and (R_L) represent adsorption resistance and adsorption inductance respectively and the model achieved a pe

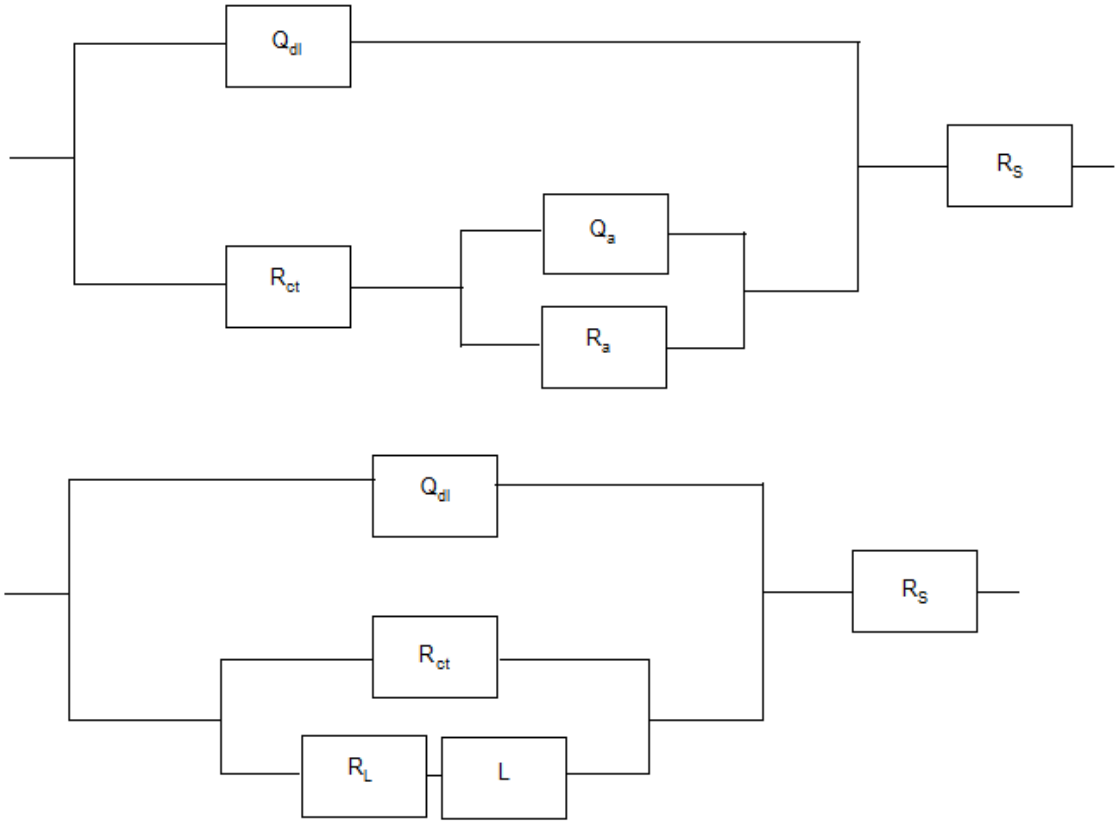

Figure. 4.10. Equivalent circuits proposed for the electrochemical impedance response at a) 20 ^{o}C and at 40 ^{o}C in 0.5 M chloride containing bicarbonate test solutions and b) at 40 ^{o}C in 0.1 M chloride containing bicarbonate test solution.

However, in an increased bicarbonate content of 0.5 M, the behavior changed to be similar to that at 20 ^{o}C and finally the competitive passive film formation process resulted in the two-time constant impedance response in 0.8 M condition. The behavior achieved the expected applicability to the circuit proposed for chloride free conditions in Figure 4.6. As shown in Figure 4.9b, the bode phase peaks were broader with the bicarbonate content, and they showed a shift to appear at a frequency ranging from 60 to

80 Hz. At 60 ^{o}C, the mechanisms seemed to be irrespective from the bicarbonate content and they all showed the significance of diffusion-influenced processes. Following the model proposed in figure 7, the passive films seemed to show, and in a proportional manner with the bicarbonate content at this high temperature, a greater tendency to be more effective or at least to exhibit the diffusion character more apparently. As shown in Tables 4.5, 6, and 7, charge transfer (R_{ct}) resistances were noticeably lower than those in chloride free conditions, and they decreased with higher temperature and oppositely behaved with higher bicarbonate content but reflecting also the decaying effect of chloride with greater bicarbonate content. (Q_{dl}) seemed to be more capacitive in the chloride containing conditions at it showed an opposite trend of that of (R_{ct}) and interestingly, the associated (R_f) and (R_a) along with the CPE's followed the same trends across either the adsorption fields and passive films.

Table 4.5. Electrochemical Impedance Spectroscopy (EIS) component values in chloride containing bicarbonate solutions at 20^{o}C

Components	0.1 M	0.5 M	0.8 M
R_s (Ω.cm^2)	1.809	1.436	1.328
Q_{dl} (F/cm^2)	0.00005946	0.00004514	0.00003292
n_{dl}	0.8819	0.8848	0.8834
R_{ct} (Ω.cm^2)	133.6	220	1781
Q_a (F/cm^2)	0.00005796	0.00004411	0.00001924
n_a	0.6883	0.6221	0.6814
R_a (Ω.cm^2)	771.8	1679	2021
Chi-square	1.78E-05	5.56E-05	4.91E-05

Table 4.6. Electrochemical Impedance Spectroscopy (EIS) component values in chloride containing bicarbonate solutions at 40°C

Components	0.1 M	Components	0.5 M	Components	0.8 M
R_s ($\Omega.cm^2$)	0.9526	R_s ($\Omega.cm^2$)	0.9652	R_s ($\Omega.cm^2$)	0.9179
Q_{dl} (F/cm^2)	0.00006356	Q_{dl} (F/cm^2)	0.00005594	Q_{dl} (F/cm^2)	0.000019
n_{dl}	0.7824	n_{dl}	0.801	n_{dl}	0.9182
R_{ct} ($\Omega.cm^2$)	1.56	R_{ct} ($\Omega.cm^2$)	67.5	R_{ct} ($\Omega.cm^2$)	127.1
R_L ($\Omega.cm^2$)	53.3	Q_a (F/cm^2)	0.00003464	Q_f (F/cm^2)	0.00002189
L (H/cm^2)	120.4	n_a	0.9021	n_f	0.851
Chi-square	3.20E-05	R_a ($\Omega.cm^2$)	1303	R_f ($\Omega.cm^2$)	24.41
		Chi-square	3.83E-05	Y_{Wf} ($\Omega^{-1}s^{-0.5}$)	0.001204
				Chi-square	1.62E-05

Table 4.7. Electrochemical Impedance Spectroscopy (EIS) component values in chloride containing bicarbonate solutions at 60°C

Components	0.1 M	0.5 M	0.8 M
R_s ($\Omega.cm^2$)	0.506	0.896	0.4835
Q_{dl} (F/cm^2)	0.00009225	0.0000849	0.000039
n_{dl}	0.9285	0.8137	0.8671
R_{ct} ($\Omega.cm^2$)	1.009	52.8	91.23
Q_f (F/cm^2)	0.00002064	0.00001312	0.00005935
n_f	0.6839	0.7606	0.8466
R_f ($\Omega.cm^2$)	3.30	36.2	48.3
Y_{Wf} ($\Omega^{-1}s^{-0.5}$)	0.002224	0.004924	0.003057
Chi-square	3.90E-05	0.003454	8.18E-05

The confirmative fitting between the proposed models and some selected experimental data are shown in Figure 4.11.

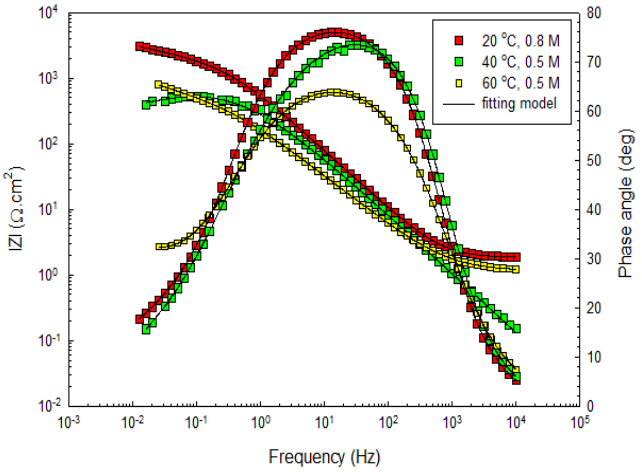

Figure 4.11. Experimental and calculated bode representations of impedance for selected chloride containing bicarbonate test solutions.

Chapter 5: Results and discussion of the electrochemical investigations in deoxygenated low oil containing bicarbonate solutions

5.1. Test solutions

The electrochemical tests were performed in test solutions simulating the carbon dioxide corrosion conditions in transportation pipelines containing high water cuts and decreasing oil amounts. In addition, bicarbonate was considered to be the predominant species resulting from carbon dioxide dissolution in alkaline media [19]. Therefore, the deoxygenated solutions were synthesized to contain 0, 10, 20, and 30 vol% oil mixed with double distilled deionized water electrolytes containing 0.05, 0.1, 0.5, and 1 M bicarbonate and 30 ppm of chloride. The present amount of chloride is one of the typical levels in pipeline oil emulsions after being desalted in oil processing facilities [20]. Analytical grade Fisher procured reagent of sodium bicarbonate ($NaHCO_3$) was utilized for synthesizing the test electrolytes. Dioctyl sulfosuccinate sodium ($C_{20}H_{37}NaO_7S$) salt, an anionic surfactant, was added with 0.2 wt% to maintain the homogeneity of bicarbonate oil emulsions. Selected physical and chemical properties of the emulsified oil are shown in Table 5.1. According to the classification criteria for crude oils in [21], our oil is a medium-weight type containing a complex mixture of hydrocarbons with carbon numbers ranging from C9 to C25. The test temperatures were set to be 30 and 70 ^{o}C.

Selected physical and chemical properties of the considered hydrocarbon in the deoxygenated bicarbonate and CO_2 saturated solutions are shown below in Table 5.1.

Table 5.1. Selected chemical and physical properties of the hydrocarbon considered

Property	Details
Appearance	Pale Yellow
Carbon number	C3-C12
Initial Boiling Point (°C)	25
Boiling Range (°C)	25 - 170
Flash point (°C)	>10
Lower / upper Flammability (V)	1 - 6 %
Auto-ignition temperature (°C)	> 250
Vapor pressure (kPa)	< 38 at 20 °C
Density (g/cm^3)	0.63 at 15 °C

5.2. Open Circuit Potential (OCP) measurements at 30 ^oC

OCP variations with time were monitored in oil free bicarbonate solutions of 0.05, 0.1, 0.5, and 1 M concentration and then they were monitored also in 10, 20, and 30 vol% oil containing conditions. The influence of bicarbonate content on the mixed potentials was apparent as shown in Figure 5.1a and 1b for oil free and 10 vol% oil containing conditions.

OCP profiles were in a band of variation between -0.818 to -0.855 V_{SCE}, and it was evident that OCP decreased with greater bicarbonate content in the oil free conditions. The reason for this behaviour can be related, as discussed in the polarization tests part, to the accelerated anodic reactions. The anodic reaction is proposed to involve bicarbonate and hydroxyl species to form iron carbonate ($FeCO_3$) in mildly alkaline solutions of pH levels around 8 as represented by equation (1) [Moiseeva, 2003] and [Neshati, 2007] as:

$$Fe + HCO_3^- + OH^- \rightarrow FeCO_3 + H_2O + 2e^- \qquad (5.1)$$

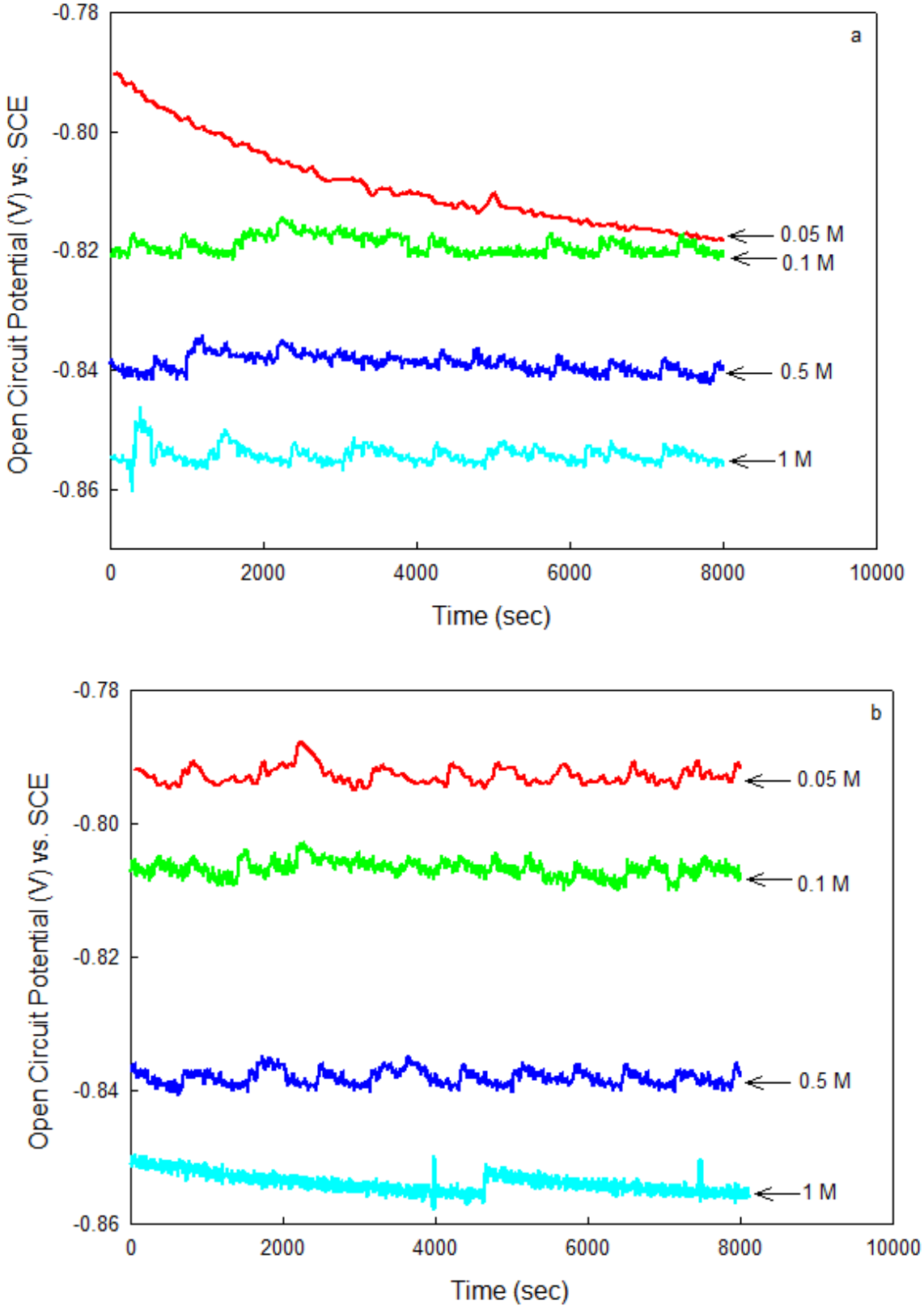

Figure 5.1. Open Circuit Potential (OCP) variations in oil free bicarbonate solutions at 30 ^{o}C in a)oil free and b)10vol% oil containing conditions

Bicarbonate is involved also in the cathodic reactions [Paolinelli, 2008] and [Veawab, 2002]. This is represented by equation (2) or equation (3) as:

$$HCO_3^- + e^- \rightarrow CO_3^{2-} + 1/2H_2 \qquad (5.2)$$

$$HCO_3^- + e^- \rightarrow CO_3^{2-} + H_{ads} \qquad (5.3)$$

The standard half cell potentials are calculated utilizing Gibbs free energies of chemical species listed in [Dean, 2000]. Additionally, the theoretical equilibrium half cell potential limits of anodic and cathodic reactions are calculated taking into account temperature, pH, and bicarbonate concentration using Nernst equation [Ahmed, 2006]. OCP values were well bounded by the theoretical limits as revealed in Table 5.2.

In low bicarbonate containing solutions of 0.05 and 0.1 M solutions, the mixed potentials seemed to be more influenced by the cathodic reduction of bicarbonate. However, with higher bicarbonate amounts of 0.5 and 1 M, OCP decreased as the influence of the accelerated anodic reactions became greater.

This suggests that the accelerated anodic reactions dominate the mixed potentials, especially in conditions where bicarbonate content is high. In addition, this supports the idea that bicarbonate could be involved in the basic dissolution mechanism of steel at different extents depending on its concentration and pH level.

OCP values in oil containing solutions were all nobler than those in oil free ones and the significance of oil was quite pronounced in low bicarbonate containing solutions of 0.05 and 0.1 M. OCP data and calculations at 30 ^{o}C are shown exclusively for the oil containing conditions of 20 vol% in Table 5.2 where similar trends were exhibited in the other oil conditions.

Table 5.2. Open Circuit Potentials (OCP) and the calculated half cell equilibrium potentials at 30 and 70 °C at selected oil conditions

Temperature	Oil	Bicarbonate concentration	OCP	pH	Equilibrium Potential (Reaction(5.1))	Equilibrium Potential (Reaction(5.2))
(°C)	(vol %)	(M)	(V) vs. SCE		(V) vs. SCE	(V) vs. SCE
30	0	0.05	-0.818	8.35	-0.934	-0.734
		0.1	-0.820	8.83	-0.958	-0.762
		0.5	-0.840	8.85	-0.979	-0.763
		1	-0.855	8.94	-0.991	-0.768
	20	0.05	-0.770	8.26	-0.932	-0.728
		0.1	-0.777	8.33	-0.943	-0.732
		0.5	-0.818	8.46	-0.968	-0.74
		1	-0.855	8.69	-0.984	-0.754
70	0	0.05	-0.840	9.62	-0.950	-0.809
		0.1	-0.845	9.77	-0.965	-0.817
		0.5	-0.877	10.1	-1.001	-0.838
		1	-0.883	10.3	-1.016	-0.847

As shown in Figure 5.2, the effect of oil in changing the active state of steel surfaces in 0.5 M bicarbonate solutions started to diminish and in 1 M conditions, the OCP values were stable irrespectively from the oil content. Bicarbonate and oil act synergistically on the steel surfaces, and as the former played an electrochemical role, the latter got adsorbed at different extents depending on bicarbonate concentration. From the physical observations where the conditions of effective miscibility are facilitated, oil was less miscible in highly concentrated bicarbonate solutions. The nobler OCP values are associated to the inhibited anodic reactions where the stable organic films were partially or fully covering steel surfaces. The greater the amount of oil, greater surface areas were more effectively covered as already indicated in [Cook, 1951], and consequently the OCP showed quite noticeable variations in the low bicarbonate containing solutions. In additions, as discussed in the polarization tests part, the current densities showed a noticeable retardation at the anodic branches and the corrosion potentials became nobler.

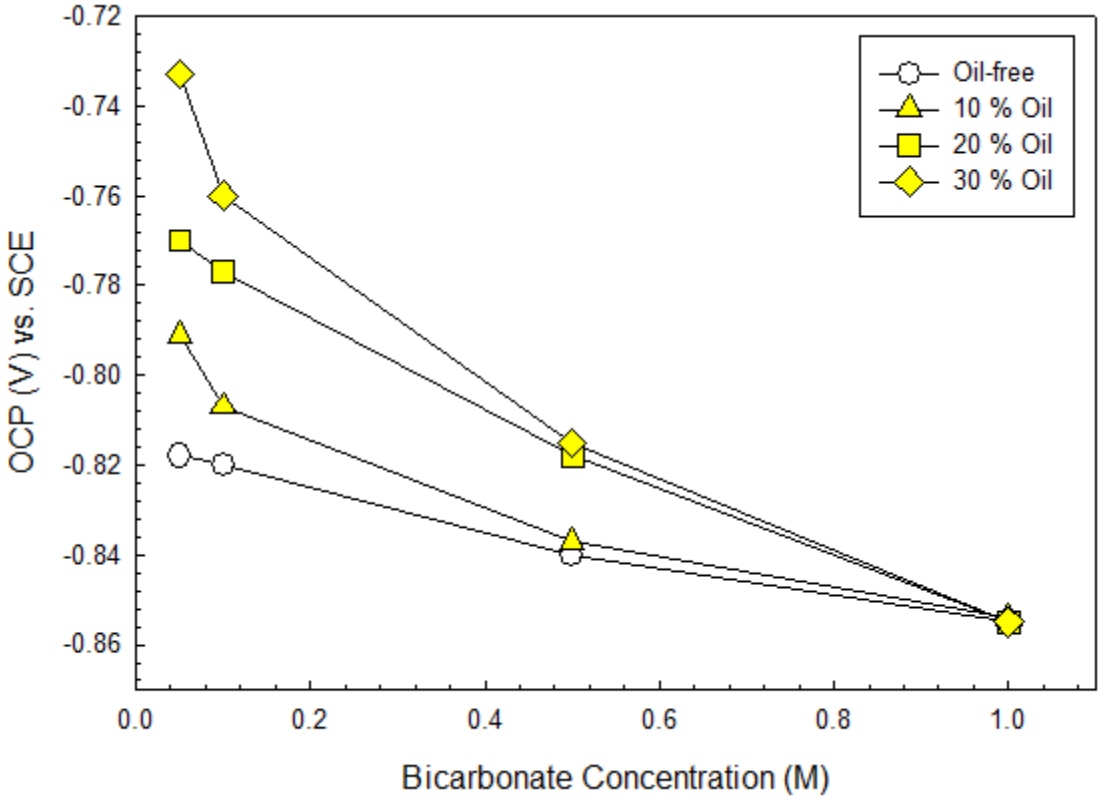

Figure 5.2. Open Circuit Potential (OCP) variations with oil content and with respect to the bicarbonate content at 30 ^{o}C.

5.3. Open Circuit Potential (OCP) measurements at 70 ^{o}C

OCP variations were also monitored at the high temperature 70 ^{o}C in the same bicarbonate and oil conditions established at 30 ^{o}C. OCP profiles in all oil free bicarbonate solutions were more negative than those at 30 ^{o}C, and showing the same trend with the bicarbonate content. The potential variation band between the maximum and minimum OCP was about 40 mV which was comparable to that at 30 ^{o}C. The theoretical anodic and cathodic reaction potentials were calculated taking into account the high temperature, bicarbonate concentration and the calculated pH level. A corrected Nernst equation from Maxwell equation in thermodynamics was considered [Brett, 1993]

as:

$$\frac{\partial \Delta G^{O}}{\partial T} = -\Delta S \qquad (5.4)$$

ΔG^{O} and ΔS are the standard Gibbs free energy and the entropy changes respectively. Assuming a small confined variation of temperature, the entropy change is assumed to be constant; $\Delta S = C$. The equilibrium potential is therefore expressed as:

$$E_T^o = E^o + \frac{\Delta S}{nF}(T - 298) \qquad (5.5)$$

Entropy variations with temperature were taken from [Dean, 2000] for the different species. pH levels were calculated at the high temperature, 70 ^{o}C considering the dissociation constant of water, Kw = 21.2×10^{-14} [Dean, 2000], and the equilibrium constant, Kb = 4.55×10^{-7} [Dean, 2000], for bicarbonate protonation according to the equation:

$$HCO_3^- + H_2O \rightarrow H_2CO_3 + OH^- \qquad (5.6)$$

The effects of the few amounts of chloride added with 30 ppm as well as that of oil were assumed to be negligible in pH calculations. OCP values were well bounded by the theoretical anodic and cathodic limits, but differently from the case of 30 ^{o}C, the mixed potentials in all bicarbonate conditions in oil free conditions were apparently closer to those of the cathodic reactions as shown in Table 5.2.

OCP profiles exhibited similar trends, as found at 30 ^{o}C, with the bicarbonate content in 0, 10, 20 and 30 vol% oil containing solutions. From the physical observations, oil films were showed a relative stability on the steel surfaces, but differently from the conditions at 30 ^{o}C, OCP decreased upon the addition of oil in a proportional fashion with the oil content as shown in Figure 5.3. This suggests that the inhibition mechanism of oil is

temperature dependent. That is; oil inhibits the cathodic reactions at elevated temperatures but its role can be predominately anodic at low temperatures.

Interestingly, significance of oil addition at 70 ^{o}C was apparent in all bicarbonate solutions, while at 30 ^{o}C, only at low bicarbonate containing solutions, OCP showed a change.

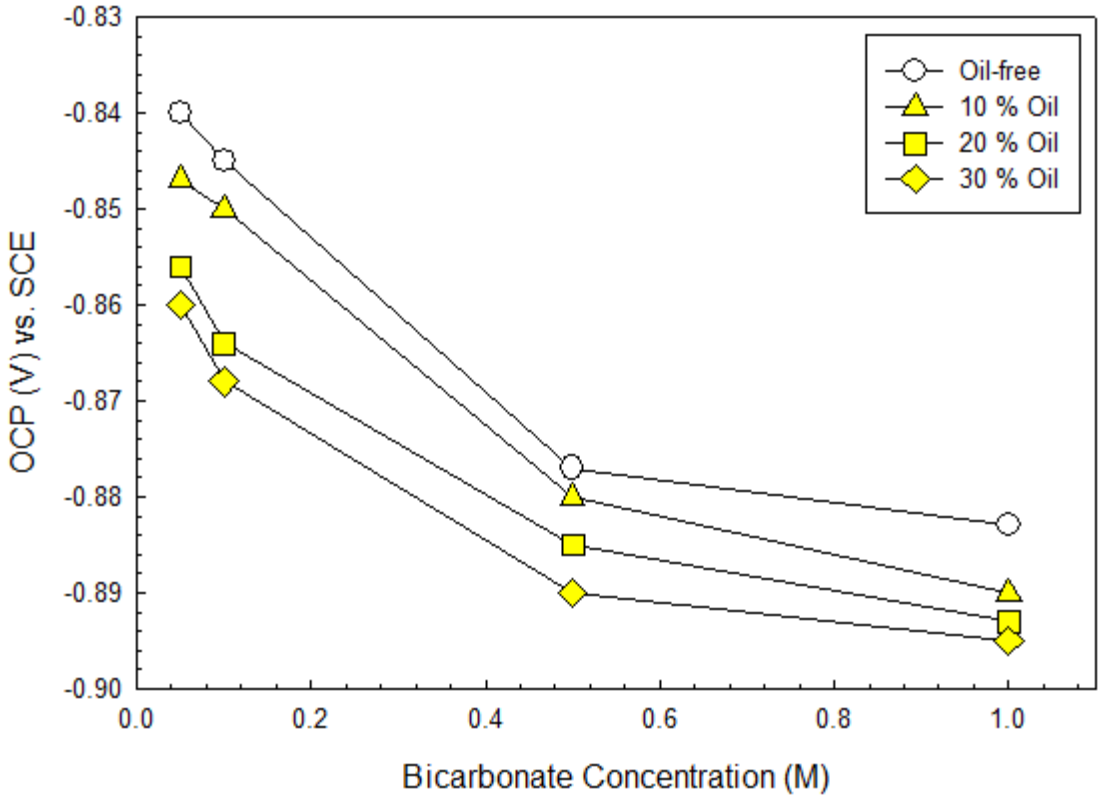

Figure 5.3. Open Circuit Potential (OCP) variations with oil content and with respect to the bicarbonate content at 70 ^{o}C.

5.4. Potentiodynamic polarization measurements at 30 ^{o}C

Potentiodynamic polarization test profiles at 30 ^{o}C in bicarbonate oil free, 10, 20, and 30 vol% solutions are shown in Figure 5.4 a, b, c, and d respectively. The effect of bicarbonate content of 0.05, 0.1, 0.5, and 1 M as well as that of bicarbonate free conditions were studied in the three oil conditions. In oil free conditions, which are

presented in Figure 5.4 a, it is evident that both anodic and cathodic reactions were accelerated in a proportional fashion with the bicarbonate content. The kinetic parameters, corrosion current density (i_{corr}), and anodic and cathodic Tafel slopes (β_a), (β_c) are calculated from Butler-Erdey-Volmer (BEV) equation utilized for the purely kinetic controlled polarization as [Ahmed, 2006]:

$$i = i_{corr}\left(\exp\left[\frac{2.3\eta_s}{\beta_a}\right] - \exp\left[\frac{-2.3\eta_s}{\beta_c}\right]\right) \qquad (5.7)$$

The parameters are iteratively calculated with the best fit with the experimental data. The corrosion rate increased with bicarbonate content and confirming with the OCP test results, the corrosion potential (E_{corr}) decreased accordingly suggesting the prevalent anodic role of bicarbonate in increasing the corrosion rate as already found with the static electrode measurements performed in [Parkins, 1997]. The corrosion rate in bicarbonate free-oil free condition was almost one order of magnitude less than that in the least bicarbonate content of 0.05 M condition. The potentiodynamic profiles in the active anodic dissolution region exhibited two anodic slopes corresponding to different stages of pre-passivation. The two stages from kinetic perspective were well discernable in greater bicarbonate containing conditions of 0.5 and 1 M. The anodic dissolution rates were retarded at a transition point of about -880 mV_{SCE}. This change in the kinetic performance is related to the onset of a passive barrier formation involving hydroxyl (OH^-) species in these mildly alkaline oil free test solutions [Talbot, 1998].

Despite of the defective nature of the hydrous iron hydroxide film studied by EIS means in [Zhang, 2009 (B)], it was evident that it can reduce the anodic dissolution rates.

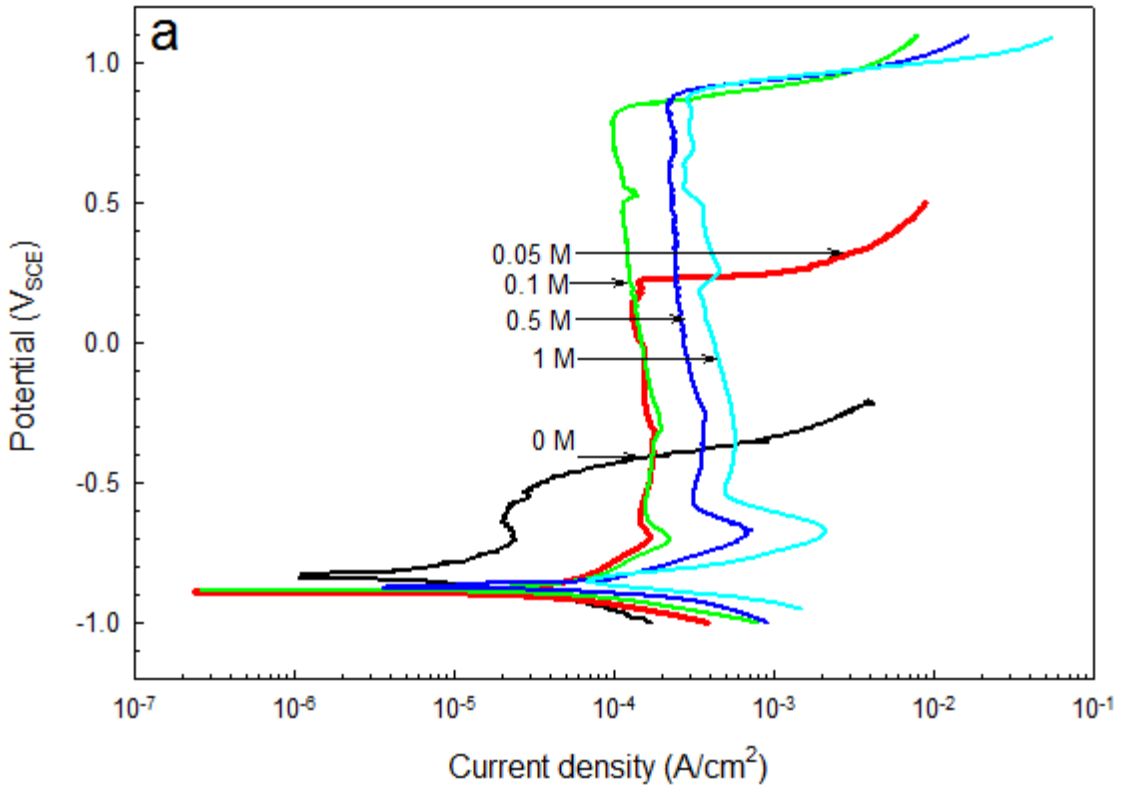
a
1.0
0.5
0.0
-0.5
-1.0
Potential (V_{SCE})
0.05 M
0.1 M
0.5 M
1 M
0 M
10^{-7}
10^{-6}
10^{-5}
10^{-4}
10^{-3}
10^{-2}
10^{-1}
Current density (A/cm^2)

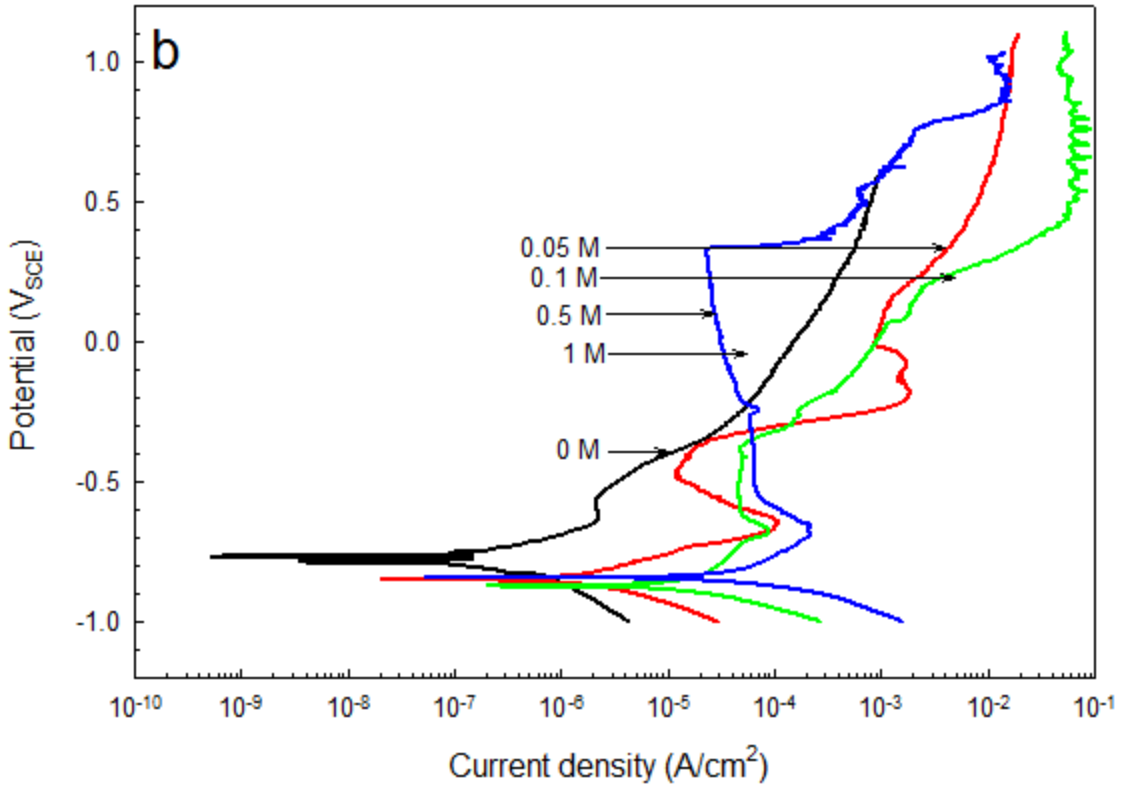
b
1.0
0.5
0.0
-0.5
-1.0
Potential (V_{SCE})
0.05 M
0.1 M
0.5 M
1 M
0 M
10^{-10}
10^{-9}
10^{-8}
10^{-7}
10^{-6}
10^{-5}
10^{-4}
10^{-3}
10^{-2}
10^{-1}
Current density (A/cm^2)

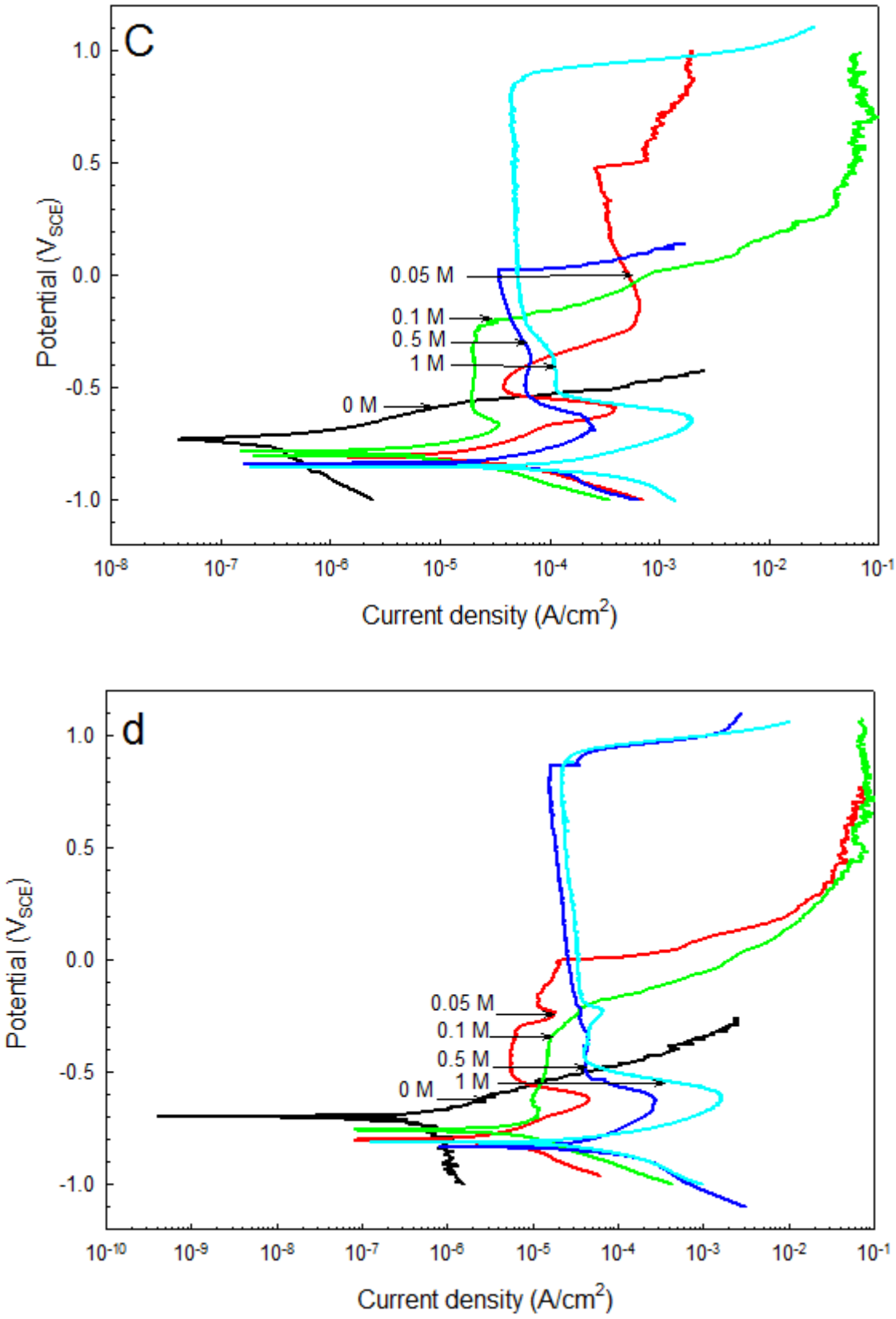

Figure 5.4: Potentiodynamic polarization profiles at 30 ^{o}C in bicarbonate solutions of 0, 0.05, 0.1, 0.5, and 1 M in a) oil free, b) 10, c) 20, and d) 30 vol% oil containing conditions.

A considerable formation of a hydrous passive film [Castro, 1991] in a short range of potential, as illustrated in the Pourbiax diagram of Fe-H-C-O system generated in [Hirnyi, 2001], could be described with the following mechanism:

$$Fe + OH^- \leftrightarrow FeOH^-_{ads} \qquad (5.8)$$

$$FeOH^-_{ads} \rightarrow FeOH_{ads} + e^- \qquad (5.9)$$

$$FeOH_{ads} \rightarrow FeOH^+_{ads} + e^- \qquad (5.10)$$

$$FeOH^+_{ads} + OH^- \rightarrow Fe(OH)_2 \rightarrow \text{Hydrous}\left[Fe(OH)_2\right] \qquad (5.11)$$

The early incorporation of iron carbonate ($FeCO_3$) with the deposit iron hydroxide layer by sufficient bicarbonate contents of 0.5 and 1 M made the anodic current densities to accelerate after a temporary retardation at about -817 mV_{SCE}. The formation of iron carbonate at this new transition point makes iron hydroxide to be a distinct inner layer at this oxidation stage as studied by the voltammetric techniques in [Castro, 1986]. In our case, the current densities showed a continuous acceleration with the higher overpotentials which could be explained by the partial removal of iron hydroxide film described by equation (11) as [Niu, 2007]:

$$Fe(OH)_2 + HCO_3^- \rightarrow CO_3^{2-} + OH^- + Fe^{2+} + H_2O \qquad (5.12)$$

In conditions of low bicarbonate contents of 0.05 and 0.1 M as well as in bicarbonate free condition, the anodic dissolution did not show a second distinct transition point at the same potential of -817 mV_{SCE}.

With the elevated anodic overpotentials, a distinct anodic peak appeared at -700 mV_{SCE} in all bicarbonate containing conditions but with different intensities increasing proportionally with the bicarbonate content. Depending on pH and HCO_3^-/CO_3^{2-}

concentration, the formation of iron carbonate layer as a preliminary adherent compound is facilitated before the formation of iron oxides. Iron carbonate is formed via iron complexes such as $FeHCO_3^+$ which exist in the simultaneous equilibrium as [Himyi, 2001]:

$$Fe + HCO_3^- \rightarrow FeHCO_3^+ + 2e^- \quad (5.13)$$

$$FeHCO_3^+ \leftrightarrow Fe^{2+} + HCO_3^- \quad (5.14)$$

Alternatively, $FeHCO_3^-$ could be involved in $FeCO_3$ formation according to the proposed mechanism:

$$Fe + HCO_3^- \leftrightarrow FeHCO_3^- \quad (5.15)$$

$$FeHCO_3^- \rightarrow FeHCO_3 + e^- \quad (5.16)$$

$$FeHCO_3 + OH^- \rightarrow FeCO_3 + H_2O + e^- \quad (5.17)$$

Complex passive films comprised from a mixture of iron oxides such as (Fe_3O_4) and (Fe_2O_3) are then formed via iron complexes in the presence of (OH^-) species [Alves, 2002 (B)]. It was proposed in [Lu, 2006] that iron carbonate can contribute to the formation of iron oxides according to the equations:

$$3FeCO_3 + 5OH^- \rightarrow Fe_3O_4 + 3HCO_3^- + H_2O + 2e^- \quad (5.18)$$

$$3FeCO_3 + 4OH^- \rightarrow Fe_2O_3 + 2HCO_3^- + H_2O + 2e^- \quad (5.19)$$

When effective passivation states were established, the transpassivation occurred at lower potentials in less bicarbonate containing solutions. Additionally, passivation current density (i_{pass}) in 0.05 and 0.1 M solutions was about two times less than that in 0.5 and 1 M solutions. There was no clear evidence for effective passivation to occur in bicarbonate free-oil free condition.

The addition of oil resulted in changes in both active and passive states at different extents depending on the oil content. Polarization profiles in bicarbonate 10 vol% oil containing solutions are shown in Figure 5.4b. (i_{corr}) in all bicarbonate solutions was less than that in oil free conditions. The effect of oil was very pronounced in low bicarbonate containing solutions of 0.05 and 0.1 M and in bicarbonate free solution where it was almost three times less than that in oil free conditions. Additionally, (E_{corr}) values were nobler than those in oil free conditions indicating the inhibitive influence of oil on the anodic reactions [Mendez, 2001]. The adsorbed oil on the polarized steel surfaces altered the passivation states where the solubility of the species involved in passive film formations is changed in the emulsified aqueous layers adjacent to the steel surfaces [Castillo, 2000]. Comparing the passivation potential (E_{pass}) values in 10 vol% conditions with those in oil free ones, the adsorbed oil layers seemed to delay the formation of effective passive films where (E_{pass}) was higher in these conditions. Additionally, the passivation in 0.05 and 0.1 M solutions was noticeably disturbed and a short passivation range resulted, for example, in 0.1 M condition followed by an extensive dissolution. In 0.5 M solution, the transpassivation potential ($E_{tranpass}$), was about 500 mV lower than that in oil free condition although the onset of passivation was almost identical. The passivation state in 1 M condition did not exhibit a significant change upon the addition of oil. The passive current density (i_{pass}) in all bicarbonate conditions was greatly less than that in oil free conditions, indicating that effective hydrocarbons were involved noticeably in the passivation state. The greater amount of oil of 20 vol% caused further changes. The corrosion current density (i_{corr}) was further reduced accompanied by nobler corrosion potential (E_{corr}). The anodic dissolution was

proportional with the bicarbonate content but the onsets of passivation were variant, differently from the cases of oil free and 10 vol% conditions as shown in Figure 5.4c. The increased amount of oil in these conditions enhanced the passive film structures and ($E_{tranpass}$) values were higher than those in 10 vol% condition. Anodic and cathodic current densities in 30 vol% oil containing conditions followed the same trends found previously. The greater oil contents had a better chance to cover greater areas of the polarized steel surfaces leading to accordingly to further reduced corrosion current densities. In addition, confirming with the OCP test results, (E_{corr}) was nobler where the anodic current densities decreased further. Interestingly, in 30 vol% oil containing conditions, passivation disturbance was quite diminished where the anodic peaks occurred at close passivation potentials (E_{pass}) and the passivation in all bicarbonate containing conditions was enhanced as shown in Figure 5.4d. (i_{pass}) was noticeably reduced indicating that by increasing the oil content, oil could get involved in forming more effective passive films. Tafel anodic slopes (β_a) were in general low in low bicarbonate containing solutions but in conditions where they showed an increase with greater bicarbonate contents in certain conditions, better passivation could be facilitated as discussed in [Glass, 1986]. The summary of kinetic data obtained in all selected bicarbonate and oil conditions at 30 ^{o}C is shown in Table 5.3.

The passivation characteristics are studied further to elucidate the synergistic contributions of both bicarbonate and oil during passive film formation. The consequent electrochemical influence is studied from the charge transfer density perspective where ambiguities associated with the variations in the passivation and transpassivation potentials as well as passive current densities are resolved.

The current density measured from the onset of passivation till the transpassivation is numerically integrated with the time elapsed during the passivation process to calculate the charge density in Columb/cm^2.

Table 5.3. Selected Potentiodynamic polarization results at 30 and 70 ^{o}C

Temperature	Oil	Bicarbonate Concentration	E_{corr}	i_{corr}	β_a	i_{pass}	E_{pass}	$E_{transpass}$	β_c	i_{ll}
(°C)	(vol %)	(M)	(mV)	(μA/cm^2)	(mV/d)	(μA/cm^2)	(mV)	(mV)	(mV/d)	mA/cm2
30	0	0	-833	5	35	22	-730	-580	-	-
		0.05	-870	63	45	82	-710	100	121	22
		0.1	-876	70	58	105	-713	755	80	37
		0.5	-880	82	38	230	-700	810	62	105
		1	-885	120	39	270	-698	830	56	136
	10	0	-780	4	44	2	-640	-580	-	-
		0.05	-850	16	47	15	-667	-417	56	7
		0.1	-872	28	31	49	-687	-400	46	34
		0.5	-844	66	33	53	-700	270	75	88
		1	-854	88	35	65	-688	840	55	120
70	0	0	-794	10	45	16	-703	-500	-	-
		0.05	-812	62	57	17	-704	-353	52	57
		0.1	-848	80	52	123	-703	-54	44	73
		0.5	-883	180	63	280	-702	460	48	157
		1	-890	240	62	980	-704	795	39	208
	10	0	-867	10	68	-	-	-	-	-
		0.05	-873	20	57	59	-753	-503	36	25
		0.1	-883	40	54	490	-793	-93	38	65
		0.5	-898	130	53	616	-802	550	36	128
		1	-900	208	48	892	-800	700	35	177

The significance of oil during passivation, as previously found with the anodic dissolution, is more pronounced with small bicarbonate amounts. In 0.05 M solutions, the addition of oil disturbed the passivation process where oil had the best chance for direct adsorption even during passive film formations.

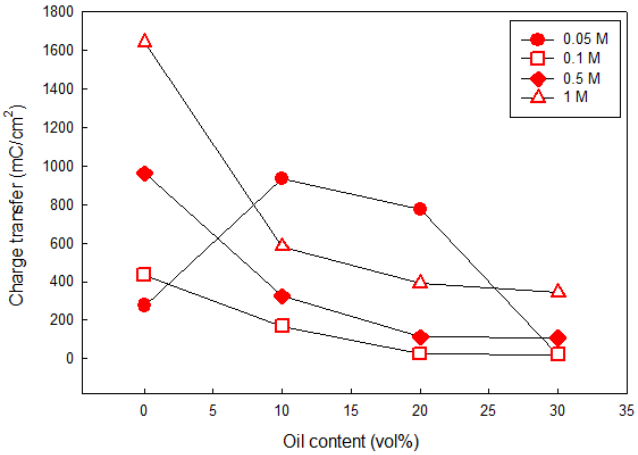

Figure 5.5. Charge transfer during passivation at 30 ^{o}C for 0.05, 0.1, 0.5, and 1 M bicarbonate solutions as a function of oil content.

Therefore, as shown in Figure 5.5, the charge transfer increased noticeably by the addition of 10 vol% oil and then decreased gradually with the increased amounts of oil of 20 and 30 vol%.

This can be explained by the impeded growth of passive films in the partially covered surface areas by oil resulting in greater charge transfer but it decreased with greater amounts of oil where it became incorporated in the passive film structure. In the more discernible short passivation ranges in 20 and 30 vol% conditions, the passive film structures were possibly improved as illustrated in the schematic proposed in Figure 5.6a. Although the passivation in 0.1 and 0.5 M conditions is not as greatly disturbed as in 0.05 M conditions, the reduced adsorption effect of oil with greater bicarbonate contents resulted in reduced charge density release with greater oil contents. In these conditions, the charge density decreased steadily while the greater amounts of oil got adsorbed on the passive films or getting involved in passive film layering as explained in Figure 5.6b. Oil seemed not to alter significantly the passivation states in 1 M conditions where the role of bicarbonate was more prevalent than that of oil.

The cathodic characteristics were evaluated in the same environments established in the anodic polarization test part to evaluate the cathodic capabilities of bicarbonate represented by equations (2) and (3). The cathodic polarization sweeps were performed from -2 V_{SCE} to the corrosion potential. It was clearly evident from the cathodic polarization profiles presented that cathodic reduction rates of bicarbonate were directly proportional to the bicarbonate content. In oil free conditions as shown in Figure 5.7a, cathodic current densities in the mass transfer region were noticeably separated within an overpotential range of about 800 mV.

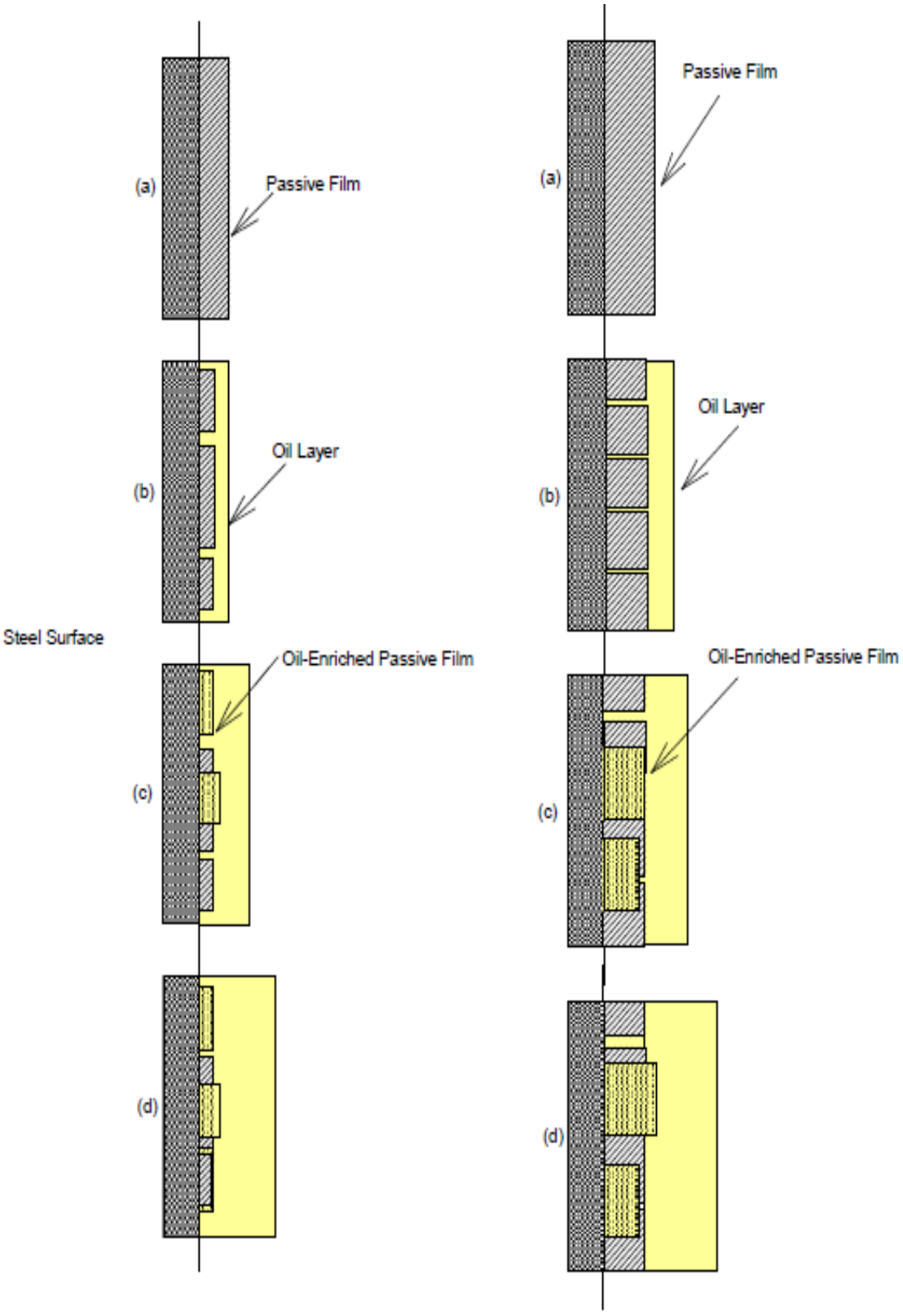

Figure 5.6. Passive films structures formation in oil free(a), 10(b), 20(c), and 30(d) vol% oil containing solutions at 30 ^{o}C in a) 0.05 and b) 0.1, 0.5, 1 M bicarbonate solutions.

The current densities in the mixed mass transfer/charge transfer region were closer and the charge transfer influence became more prevalent at lower overpotentials. In this context, limiting current densities (i_L), which are shown in Table 5.2, in oil free conditions were three orders of magnitude greater than (i_{corr}) in all bicarbonate conditions. The corrosion behaviour, considering the proportional increase of both corrosion and limiting current densities, is under both charge and mass transfer control. Tafel cathodic (β_c) slopes, which are shown in Table 5.3, were in general lower with increased bicarbonate content indicating the sensitivity of charge transfer cathodic reactions towards bicarbonate content.

The adsorption of oil induced changes in the cathodic responses as shown in Figure 5.7b representing 10 vol% oil containing bicarbonate conditions. Cathodic reaction rates exhibited the same trend found in oil free conditions where the cathodic current densities were proportional with the bicarbonate content. Nevertheless, due to the reduced solubility of bicarbonate diffusing through the emulsified interface, the limiting current densities were less than those in oil free conditions. The addition of oil improved the cathodic shoulders in low bicarbonate containing emulsions of 0.05 and 0.1 M where the cathodic reactions became more mass transfer influenced. These behaviours reflected the greater adsorption efficiency of oil with less bicarbonate contents where the surface tensions between oil and water with steel are altered noticeably with respect to the concentrations of carbon carrying species in carbon dioxide saturated environments [Danielson, 2006]. The effect of oil in reducing the mass flux of bicarbonate species during high cathodic overpotnetials in 0.5 and 1 M solutions was less.

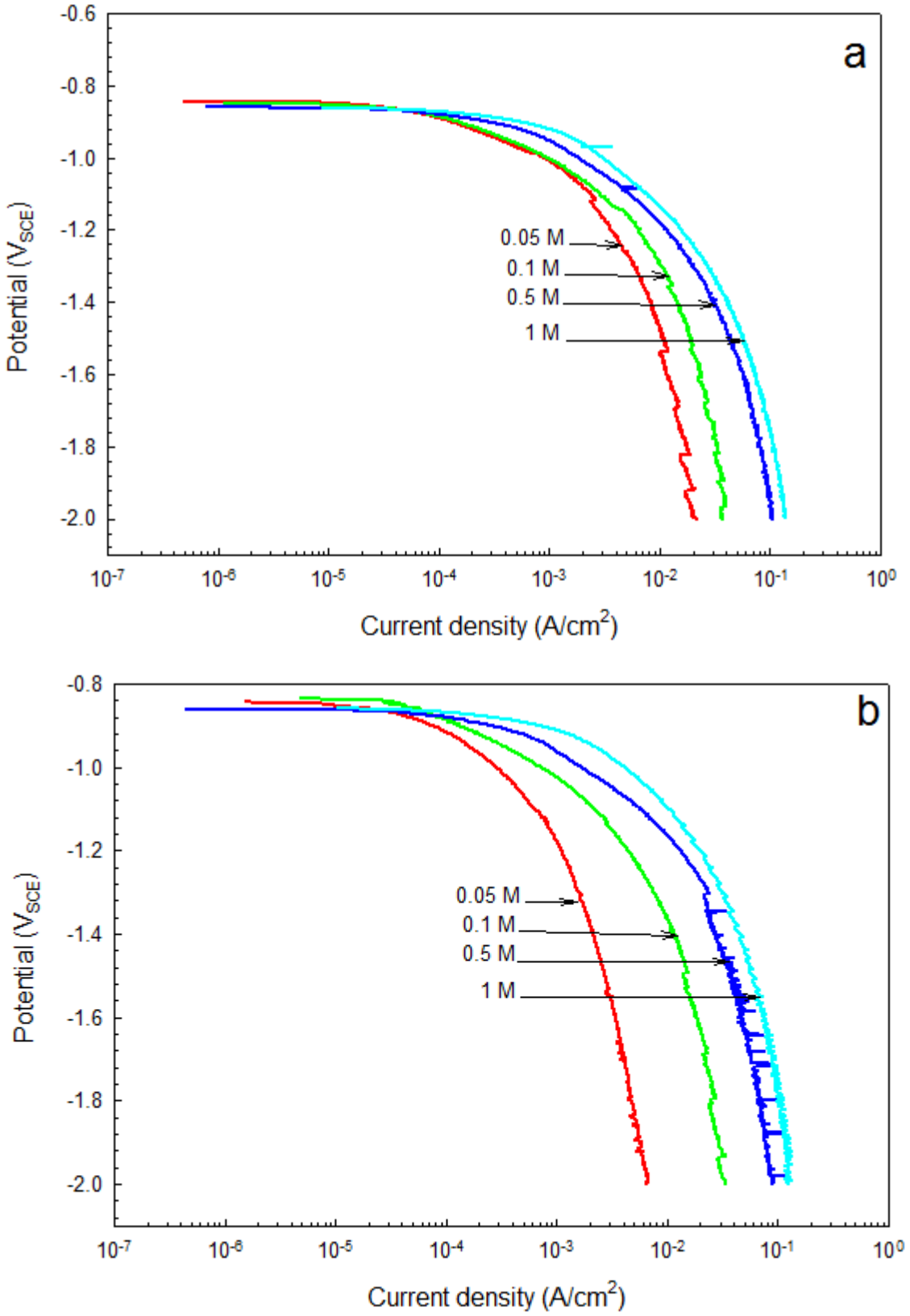

Figure 5.7. Cathodic polarization profiles at 30 ^{o}C in bicarbonate solutions of 0.05, 0.1, 0.5, and 1 M in a) oil free, and b) 10 vol% oil containing conditions.

Due to the greater agglomerative hydrogen evolution in these two conditions, the adsorbed oil layer was disturbed showing considerable fluctuations in the mass transfer region. The cathodic currents were slightly reduced with greater oil contents of 20 and 30 vol% and they showed similar behaviours in the cathodic reduction stages. Tafel cathodic slopes (β_c) in oil containing solutions were generally higher with increased oil contents especially with low bicarbonate containing solutions showing the effectiveness of oil in reducing the charge transfer reactions. Due to the reduced solubility of ferrous ions (Fe^{2+}) in the adsorbed oil layers as already reported in [Tian, 2008], the physical significance of possibly formed passive films in affecting the cathodic charge transfer was not taken into account.

5.5. Potentiodynamic polarization measurements at 70 ^{o}C

The corrosion performance is investigated at a higher temperature, 70 ^{o}C in the same corrosion environments established. The potentiodynamic profiles in bicarbonate oil free, 10, 20, and 30 vol% oil containing solutions are shown in Figure 5.8 a, b, c, and d respectively. The polarization features were similar to those exhibited at 30 ^{o}C, but with considerable changes in the active dissolution and passivation regions. In oil free conditions, as shown in Figure 5.8a, (i_{corr}) was almost two times greater with the higher temperature.

Additionally, the corrosion potentials (E_{corr}) in low bicarbonate containing solutions of 0.05 and 0.1 M was higher than those at 30 ^{o}C, while they were relatively comparable in 0.5 and 1 M solutions. That reflects the sensitivity of corrosion reactions to the cathodic reduction of bicarbonate if it exists with low concentrations in high temperature media.

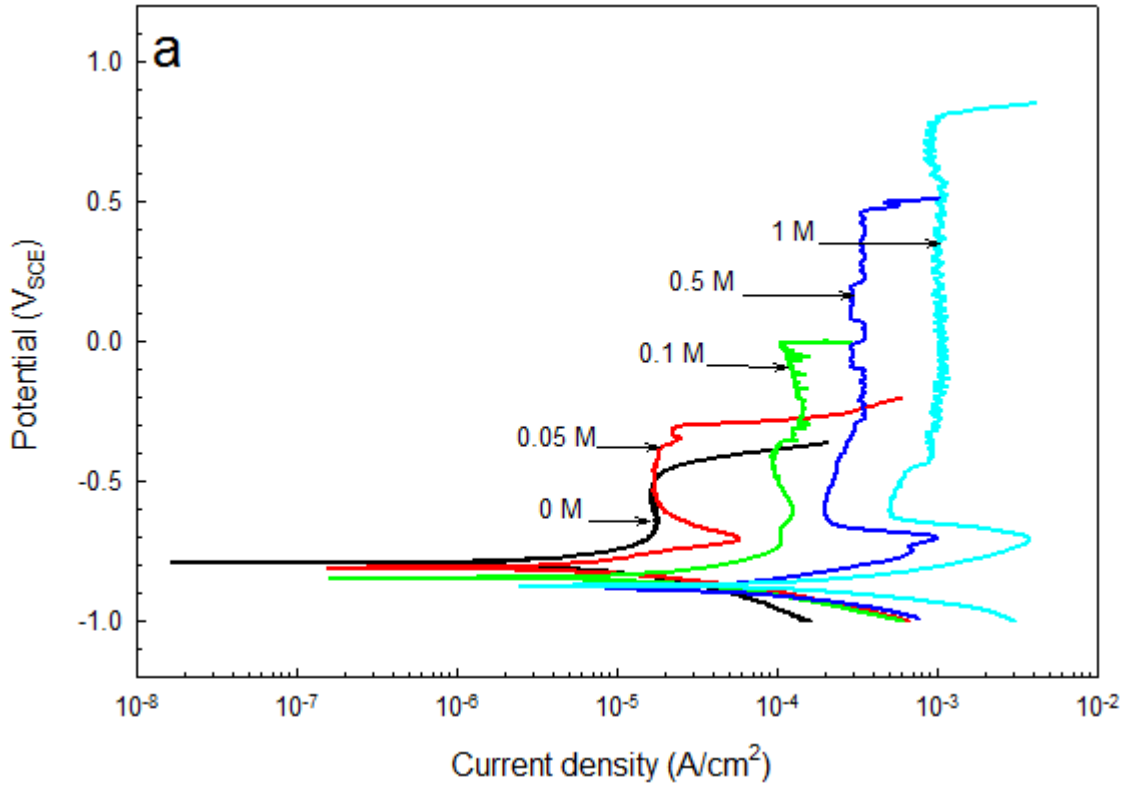
a
1.0
0.5
0.0
-0.5
-1.0
Potential (V_{SCE})
1 M
0.5 M
0.1 M
0.05 M
0 M
10^{-8}
10^{-7}
10^{-6}
10^{-5}
10^{-4}
10^{-3}
10^{-2}
Current density (A/cm^2)

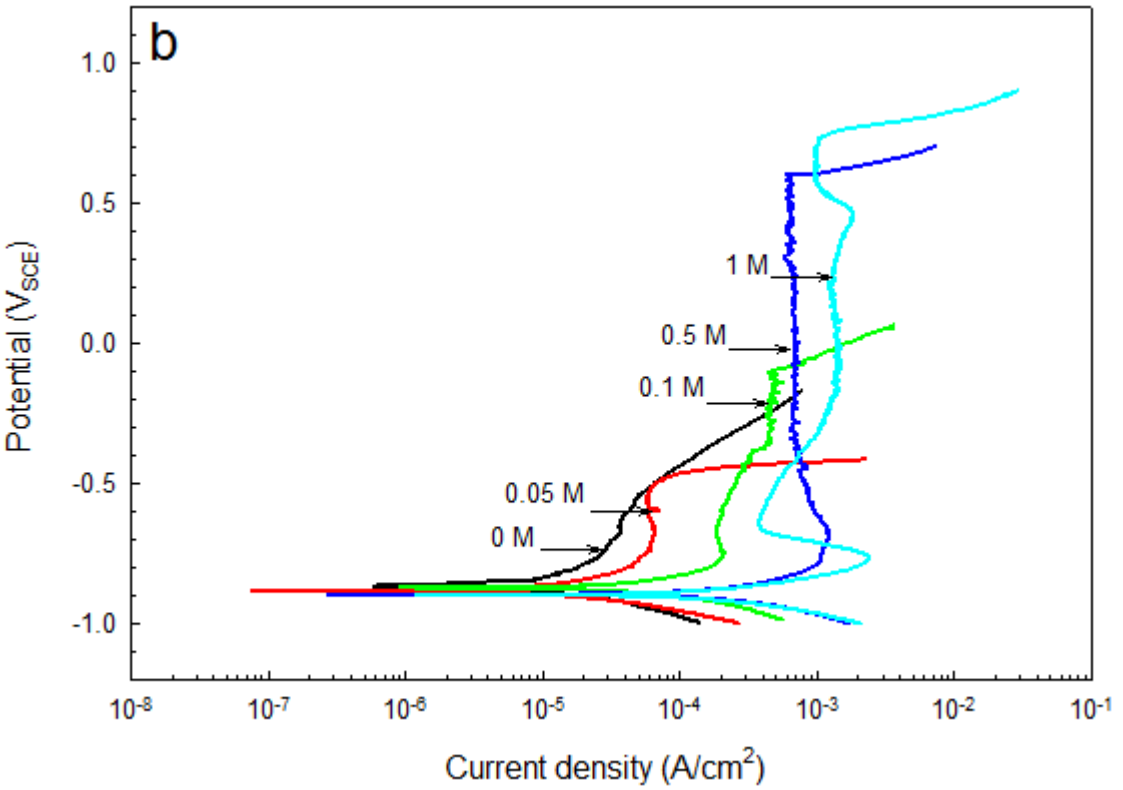
b
1.0
0.5
0.0
-0.5
-1.0
Potential (V_{SCE})
1 M
0.5 M
0.1 M
0.05 M
0 M
10^{-8}
10^{-7}
10^{-6}
10^{-5}
10^{-4}
10^{-3}
10^{-2}
10^{-1}
Current density (A/cm^2)

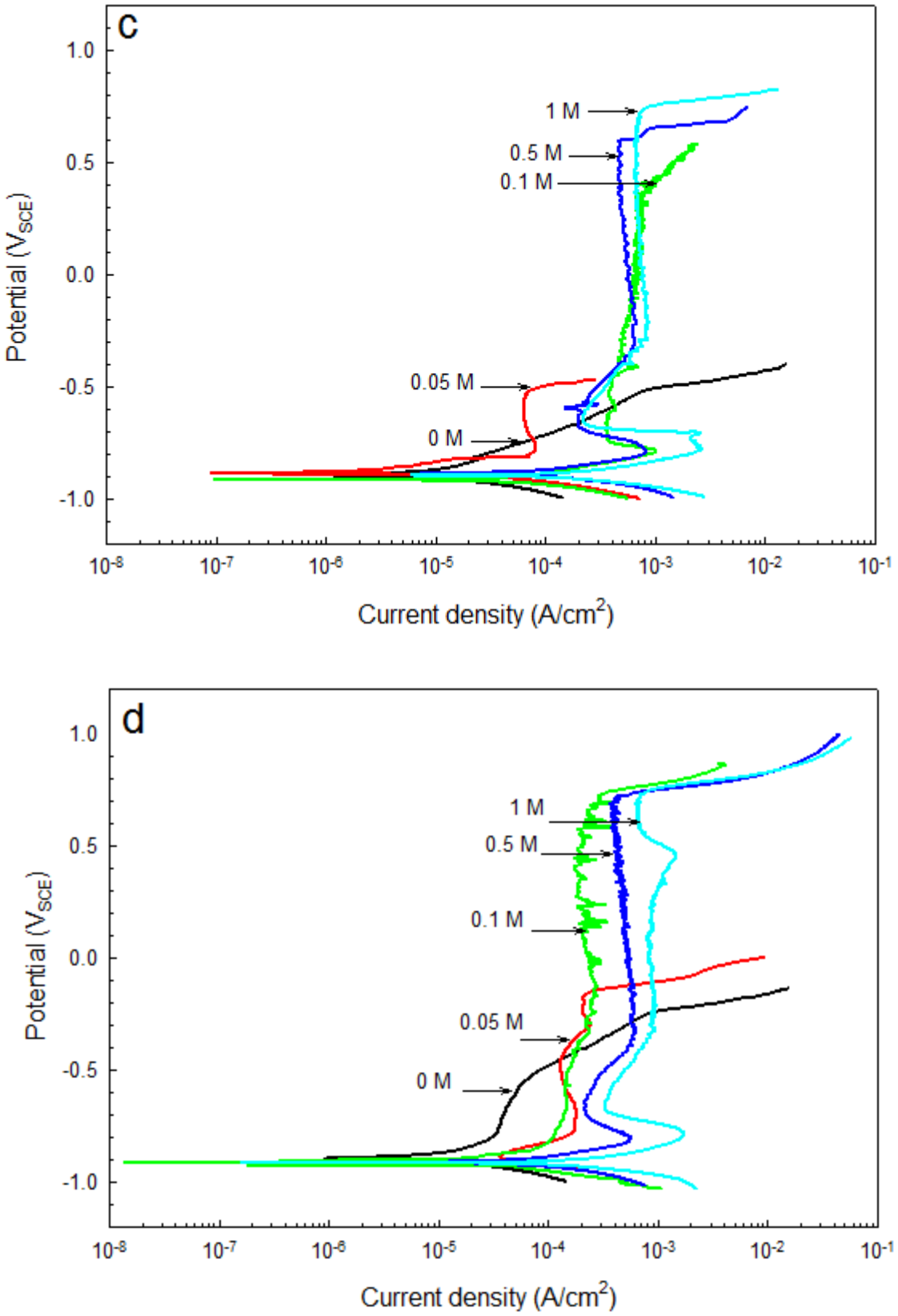

Figure 5.8. Potentiodynamic polarization profiles at 70 ^{o}C in bicarbonate solutions of 0, 0.05, 0.1, 0.5, and 1 M in a) oil free, b) 10, c) 20, and d) 30 vol% oil containing conditions.

Corrosion potentials (E_{corr}) decreased accordingly with greater bicarbonate contents as a result of the dominant influence of the accelerated anodic reactions in increasing the corrosion current density confirming the experimental findings in [Mu, 2010]. The anodic dissolution seemed to proceed proportionally with the bicarbonate content but with similar mechanisms where the multi slopes exhibited at 30 ^{o}C were not apparently discernable in 70 ^{o}C polarization profiles. In the active region, steel dissolution resulted in ferrous ions adsorbed at the interface according to the basic equation:

$$Fe \rightarrow Fe_{ads}^{2+} + 2\,e^{-} \qquad (5.20)$$

The dissolution mechanism could involve hydroxyl and bicarbonate as illustrated in the mechanisms in section 3.2.1. Iron bicarbonate formation is further facilitated with the higher temperature as visualized on the steel surfaces covered with white silver-like products at the end of polarization tests.

Similarly to the conditions at 30 ^{o}C, anodic peaks appeared at almost identical potentials of about -720 V_{SCE} decreasing slightly with the bicarbonate content. Although that the onset of passivation was almost independent from temperature in oil free conditions but the stability of the passive films formed deteriorated with the higher temperature. Transpassivation potential ($E_{transpass}$) markedly varied and it appeared to be proportional to the bicarbonate content. Additionally, (i_{pass}) was significantly high in high bicarbonate containing solutions. As found in other experimental work in [Li, 2007], the donor densities of the passive films comprising Fe_2O_3/FeO increased with temperature where the tendency for of the oxidation reaction Fe^{2+}/Fe^{3+} become greater leading to reduced protectiveness. In bicarbonate free- oil free condition, an indication of stable

passivation appeared in a short range with no distinct peak and with a passive current density very close to that in 0.05 M condition.

The addition of oil decreased the corrosion rates effectively at this high temperature in all bicarbonate solutions. Corrosion potentials (E_{corr}) with the addition of 10 vol% oil were less than those at 30 ^{o}C indicating the accelerated temperature-influenced anodic current densities. Confirming with the OCP test results, the corrosion potentials were all less than those in oil free conditions indicating the inhibitive effect of oil active compounds on the cathodic reactions [Schmitt, 1998]. The onset of passivation in oil containing solutions occurred at a lower potential of about -800 mV_{SCE} and the range of passivation in low bicarbonate containing solutions of 0.05 and 0.1 M was identifiable and was not as greatly disturbed as in 30 ^{o}C as shown in Figure 5.8b. Although the passive current densities were still high, the adsorbed oil could facilitate the formation of adherent passive films at this high temperature. With greater bicarbonate content, 0.5 M, the passivation range extended and the passive current density in 1 M solution was slightly less than that in oil free condition. The corrosion rates in 20 and 30 vol% oil containing condition were further reduced and the corrosion potentials decreased with greater oil contents. The passivation range in 0.05 and 0.1 M solutions increased and the passivation state in 0.5 and 1 M solutions enhanced where the passive current densities decreased in comparison with the lower oil containing condition of 10 vol% as shown in Figure 5.8c and 5.8d. The potentiodynamic data related to the anodic dissolution and the passivation characteristics are shown selectively in Table 5.3.

Charge transfer density at this high temperature was greater and the effect of oil was different in terms of stability and protectiveness of passive films. In 1 M bicarbonate

solutions, the increased amounts of oil decreased the charge density release, as shown in Figure 5.9, as a result of an effective absorption on the passive films or by the direct involvement in their formations in a mechanism similar to that proposed in Figure 5.5b.

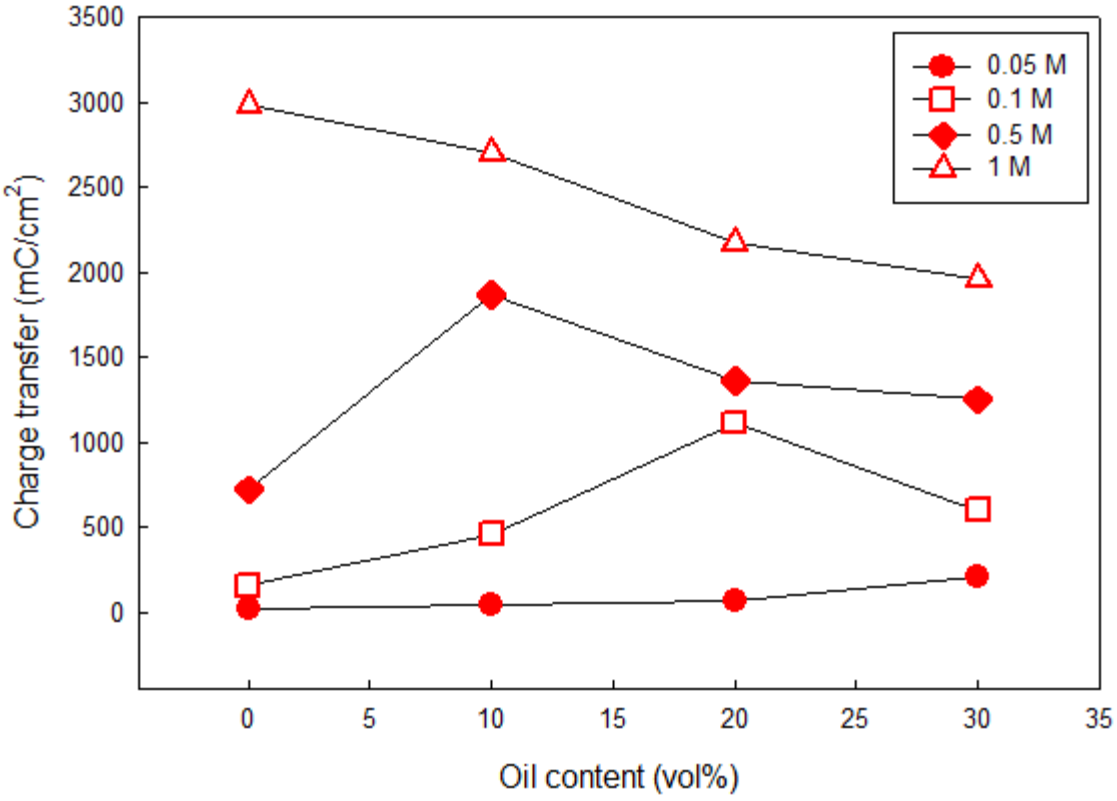

Figure 5.9. Charge transfer during passivation at 70 ^{o}C for 0.05, 0.1, 0.5, and 1 M bicarbonate solutions as a function of oil content.

As previously illustrated, the passivation ranges extended and the passive current densities decreased with greater oil contents in 1 M solutions. In 0.5 and 0.1 M solutions, oil had a better chance for relatively stable adsorption on the steel surfaces where the effective contribution of oil in enhancing the passive film structures, not from the potential range perspective only, but in decreasing the current density was delayed. The charge density started to decrease when the oil amount was 20 vol% in 0.5 M conditions, and when the oil amount was 30 vol% in 0.1 M conditions. Charge density showed a

steady increase with greater oil contents in 0.05 M conditions with no indication for effective passivation of better protectiveness although of the increased passivation range.

Cathodic polarization measurement features in the high temperature conditions were similar to those at 30 ^{o}C, but the rates of reduction of bicarbonate and water were accelerated as shown in Figure 5.10a representing the oil free conditions. The greater diffusion coefficients (D) and the reduced viscosity of the bicarbonate solutions at 70 ^{o}C increased the cathodic current densities as previously found in [Nesic, 1996].

The greater limiting current densities (i_L) in the mass transfer controlled regions suffered from excessive fluctuations for relatively broad overpotential ranges where the measured current densities interfered with the hydrogen gas evolutions. The mass transfer processes of bicarbonate in the deoxygenated oil free conditions can be further characterized in a separate future work utilizing the viscosity and hydrodynamic data at different temperatures. The charge transfer controlled reactions were accelerated when the temperature is increased leading to shorter potential range for mixed mass transefer-controlled and charge-transfer controlled regions. The addition of oil decreased considerably the cathodic current densities at the different stages where effective oil adsorption occurred at this high temperature as shown in Figure 5.10b representing the 10 vol% containing solutions. The limiting current densities decreased but they were still higher than those at 30 ^{o}C. The effect of oil in inhibiting the cathodic reactions decreased when the temperature was higher and the mixed transfer control region was shorter. The intensity of current fluctuations was appreciably limited with the addition of oil.

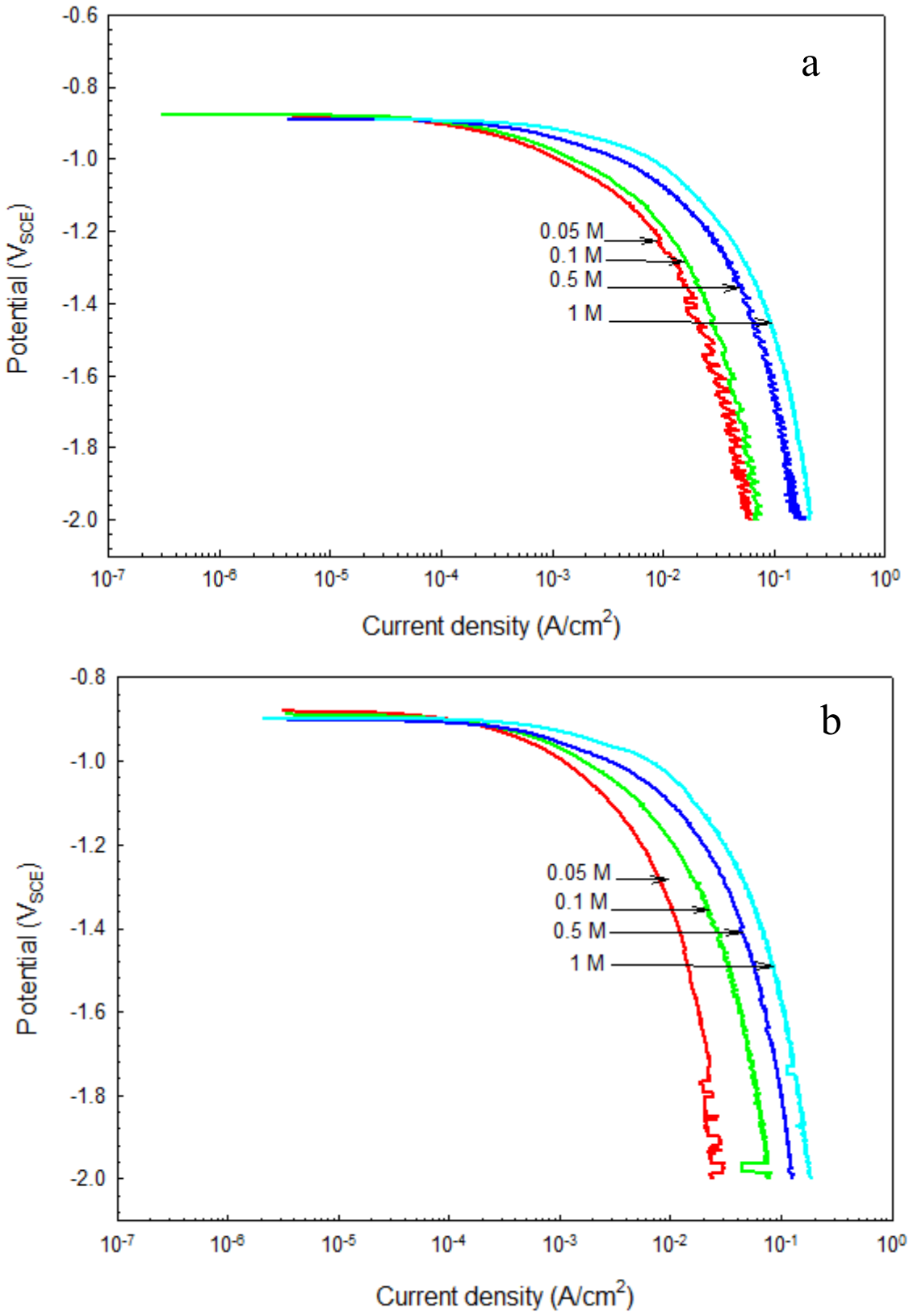

Figure 5.10. Cathodic polarization profiles at 70 ^{o}C in bicarbonate solutions of 0.05, 0.1, 0.5, and 1 M in a) oil free, and b) 10 vol% oil containing conditions.

It seemed that hydrogen evolution occurred in a fashion with no significant disturbance with the adsorbed oil as already indicated in the low temperature high bicarbonate containing solutions. This could be attributed to the limited adsorption of oil on the polarized steel surfaces especially at higher temperatures with greater bicarbonate contents. The increased amounts of oil of 20 and 30 vol% induced similar changes on the cathodic polarizations and they are not shown here. Selected cathodic polarization data are presented in table 5.3.

5.6. Electrochemical Impedance Spectroscopy (EIS) at 30 ^{o}C

The electrochemical interactions at the electrode/electrolyte interfaces were further investigated from the impedance characteristics exhibited at different conditions of bicarbonate and oil. Charge transfer resistance (R_{ct}), double layer capacitance (C_{dl}), mass transfer resistance (Warburg impedance W) and solution resistance (R_s) were identified. These elements contribute to the complex impedance behaviour in equivalent circuits proposed for simulating the mechanisms and electrochemical kinetics [Cottis, 1999]. Nyquist plots for oil free conditions containing 0.05, 0.1, 0.5, and 1 M bicarbonate are shown in Figure 5.11a at which the imaginary part of impedance is displayed as a function of the real part of it at open circuit conditions after 8000-second immersion. Typical Nyquist representations were produced with considerable changes in shapes and sizes as found with the low bicarbonate containing solutions of 0.05 and 0.1 M. As expected, and in agreement with the polarization test results, a relatively large partial capacitive loop was produced in 0.05 M reflecting the greatest polarization resistance.

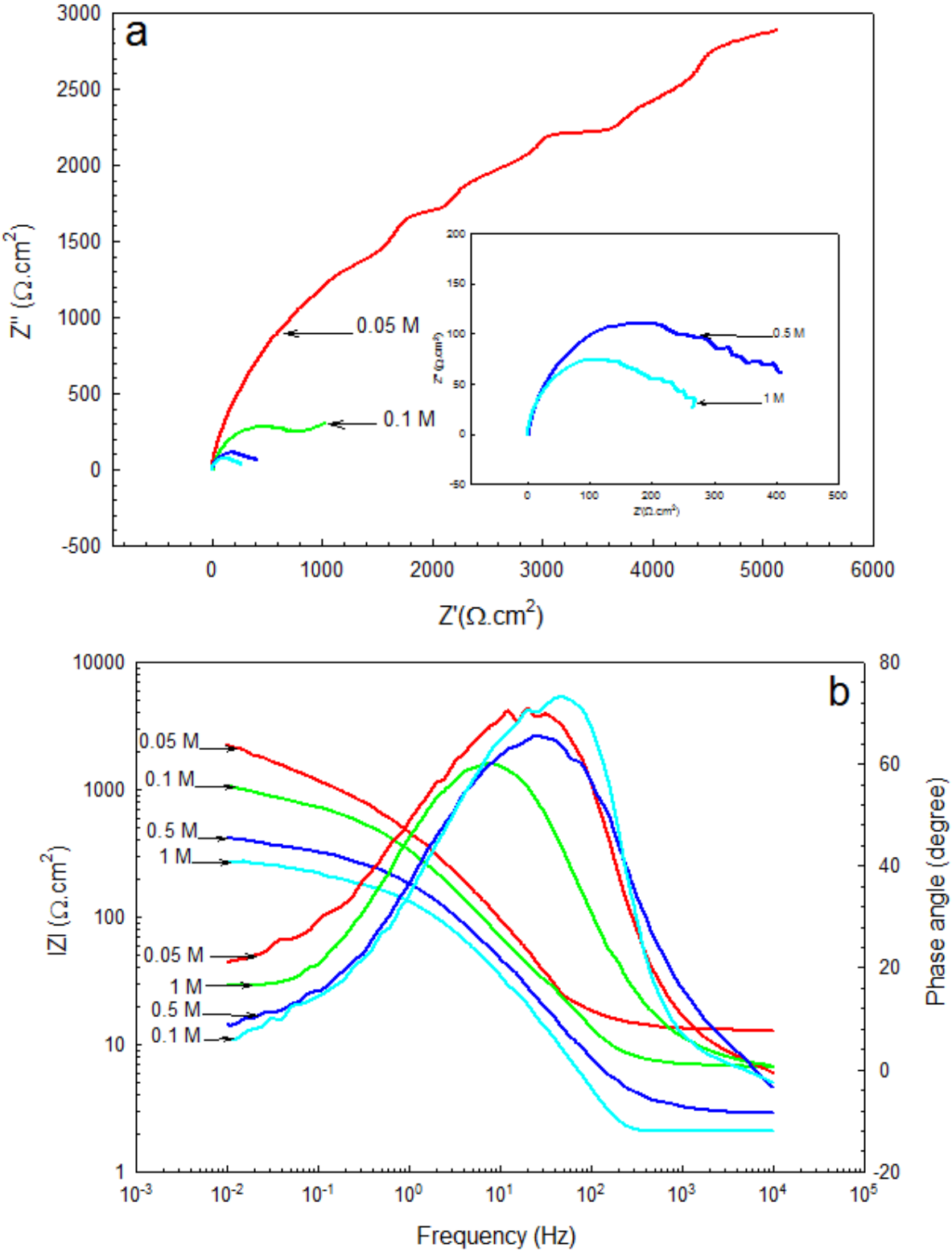

Figure 5.11. Electrochemical Impedance Spectroscopy at 30 °C in oil free bicarbonate solutions of 0.05, 0.1, 0.5, and 1 M represented in a) Nyquist and b) bode diagrams.

Although of the presence of relatively straight line at an identifiable shoulder at about 0.25 Hz, the first impression for the presence of diffusion-influenced process in 0.05 M was excluded for reasons explained in the following context. Nyquist plot shape changed in 0.1 M condition where the first capacitive loop was more identified followed by an extension starting from the same frequency of about 0.25 Hz. The polarization resistance seemed to decrease with the bicarbonate content where the size of the partial semi circles decreased accordingly similarly to the results found in [Louafi, 2010]. In 0.5 and 1 M conditions, the second capacitive loops seemed to get overlapped with the high frequency loop at about 0.25 Hz. The significance of overlapping in these two cases, where plentiful amounts of bicarbonate were available, is strongly associated with adsorption of bicarbonate as they drive the corrosion reactions [Ma, 1998] and [Wu, 2004]. Alternatively, overlapping could be associated with the relaxation of adsorbed carbon carrying intermediates in the corrosion reactions. The relaxation of these adsorbed species which might include $[\,FeHCO_3^-\,]_{ads,}$ $[\,FeHCO_3^+\,]_{ads,}$ and $[\,FeOH^-\,]_{ads}$ induced a change in the electrochemical systems resulting in identifiable peaks in the bode phase impedance representations as shown in Figure 5.11b. Therefore, the adsorption effect can be thought to be more discernible with the increased bicarbonate content where the extent of overlapping between low and high frequency portions increased accordingly. In 0.1 M condition, the second portion does not indicate diffusion-controlled process where the amount of bicarbonate was low and the slope of the linear portion was as small as 0.26. Additionally, (n) values, the Constant Phase Element (CPE) exponent, for 0.05 and 0.1 M conditions, were closer to represent a second capacitive element rather than a Warburg diffusion element. Impedance modules $|Z|$ decreased with greater bicarbonate content

along with the frequency range and their rate of change in the low frequency region were less in the high bicarbonate containing solutions. The proposed equivalent circuit for the oil free conditions at 30 ^{o}C is shown in Figure 5.12 showing the elements representing the condition at the double layer and explaining the adsorption effect. It should be noted that two-time constant based circuit {R(QR)(QR)} was attempted to simulate the experimental data as already proposed in [Alves, 2002], but that did not achieve a very good fit. Additionally Warburg resistance was included in another proposed circuit{R(QR)(Q(RW))} as proposed in [Li, 2008] but no satisfactory agreement was obtained especially at low frequencies.

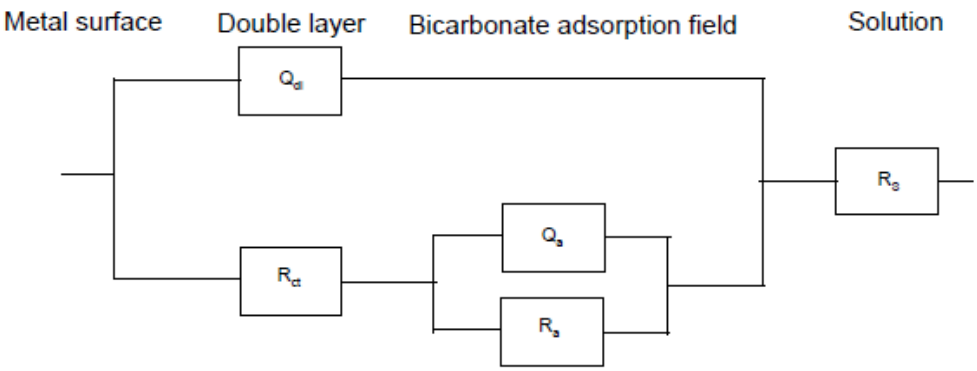

Figure 5.12. Equivalent circuit proposed for the electrochemical impedance response at 30 ^{o}C in oil free bicarbonate solutions of 0.05, 0.1, 0.5, and 1 M.

The proposed equivalent circuit for our case was finally of the configuration {R(Q(R(QR)))}. A Constant Phase Element (CPE) was considered for the double layer (Q_{dl}) to account for the surface heterogeneity at which the capacitive semicircles are depressed [Jüttner, 1990]. (CPE) element is expressed by equation below [Chen, 1999] as: $Z_{CPE} = \left[Q(j\omega)^{n}\right]^{-1}$ (5.21)

(ω) represents frequency, (j) equals to $\sqrt{-1}$, and (n) is (CPE) exponent. The electric elements and their values are shown in Table 5.4 for the oil free conditions at 30 and 70 ^{o}C where the corrosion mechanisms were independent from temperature.

Charge transfer resistance (R_{ct}) as well as that for solution (R_s) decreased with the bicarbonate content confirming with the polarization test results and a capacitive behaviour was exhibited at the adsorption field.

The addition of oil induced noticeable changes in 0.05 and 0.1 corrosion conditions where the influence of oil is significant with low bicarbonate contents. Nyquist plots are shown in Figure 5.13a for 10 vol% oil conditions and they seemed considerably larger than those in oil free conditions where the charge transfer resistance increases as already indicated by EIS means studying corrosion inhibition by crude oil compounds in [Hernandez, 2001].

Table 5.4. Impedance parameters obtained from the corrosion conditions in oil free bicarbonate solutions at 30 and 70 ^{o}C

30 °C					70 °C				
Elements	HCO_3^- Concentration (M)				Elements	HCO_3^- Concentration (M)			
	0.05	0.1	0.5	1		0.05	0.1	0.5	1
R_s (Ω.cm^2)	12.9	3.3	2.9	2.8	R_s (Ω.cm^2)	6.8	2.2	2.1	2.0
Q-Y_{dl} (μS.s^n/cm^2)	0.00156	0.00046	0.00156	0.00158	Q-Y_{dl} (μS.s^n/cm^2)	0.00075	0.00027	0.00276	0.00277
n_{dl}	0.714	0.830	0.789	0.770	n_{dl}	0.685	0.983	0.791	0.760
R_{ct} (Ω.cm^2)	416.90	251.80	10.20	8.40	R_{ct} (Ω.cm^2)	96.84	46.10	0.46	0.42
Q-Y_{ads} (μS.s^n/cm^2)	0.00042	0.00378	0.00042	0.00042	Q-Y_{ads} (μS.s^n/cm^2)	0.00014	0.00141	0.00023	0.00020
n_{ads}	0.694	0.765	0.702	0.810	n_{ads}	0.988	0.502	0.832	0.842
R_{ads} (Ω.cm^2)	2575.9	1061.4	595.2	575.4	R_{ads} (Ω.cm^2)	1305	725.9	345.7	321.3
Chi-square	4.67 E-05	8.1 E-05	5.46 E-05	5.16E-05	Chi-square	4.06E-05	3.02E-05	1.66E-05	2.43E-05

Although Nyquist features in 0.05 M condition seemed to be similar to that of oil free suggesting a similar corrosion mechanism, however, the presence of oil probably established a multi-time constant based impedance behaviour. As evident from the bode

diagram for 0.05 M in Figure 5.13b, the bode phase representation seemed to have two peaks at about 0.5 and 45 Hz respectively but not sufficiently separated.

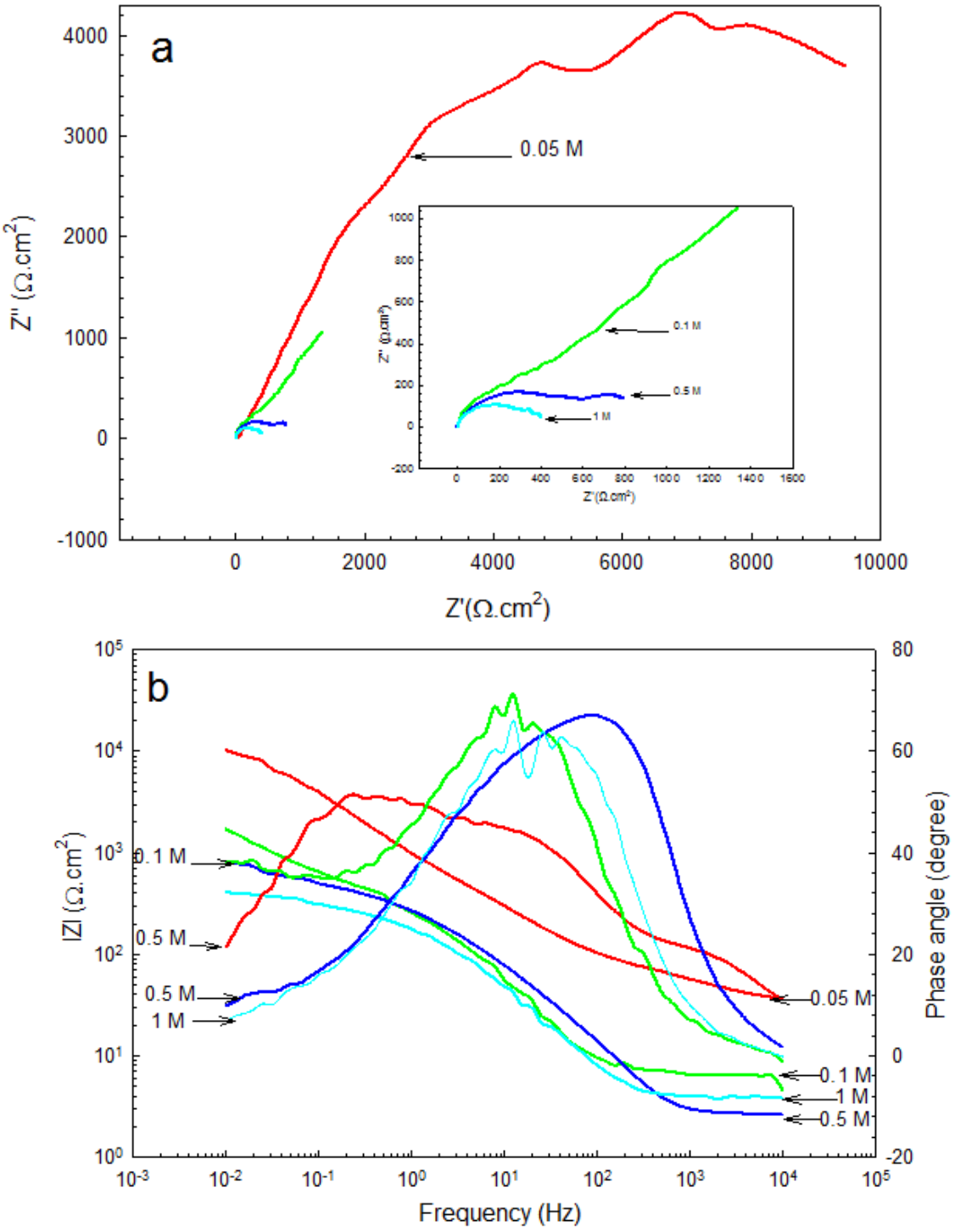

Figure 5.13. Electrochemical Impedance Spectroscopy at 30 ^{o}C in 10 vol% oil containing bicarbonate solutions of 0.05, 0.1, 0.5, and 1 M represented in a) Nyquist and b) bode diagrams.

Therefore, the electrochemical performance could be affected by the presence of a new interface at which bicarbonate adsorption occurred in the oil phase or by the presence of oil enriched film. Two-time constant based equivalent circuits {R(CR)(QR)} and {R(QR)(QR)} were first attempted but no satisfactory agreement was achieved and the same also resulted for Warburg element containing circuits as already suggested for similar corrosion conditions [Sridharan, 2009]. The presence of a high-frequency small peak at about 800 Hz in the bode phase plot led to attempt a third-time constant based equivalent circuit where the adsorption of oil in addition to the presence of the passive film are considered. The equivalent circuit, which is shown in Figure 5.14a of the configuration {R(QR)(QR)(QR)} was attempted and a perfect fit between the simulation and experimental data was then achieved. Similar Nyquist and bode responses were obtained for 20 and 30 vol % oil conditions and the corresponding impedance parameters are shown in Table 5.5.

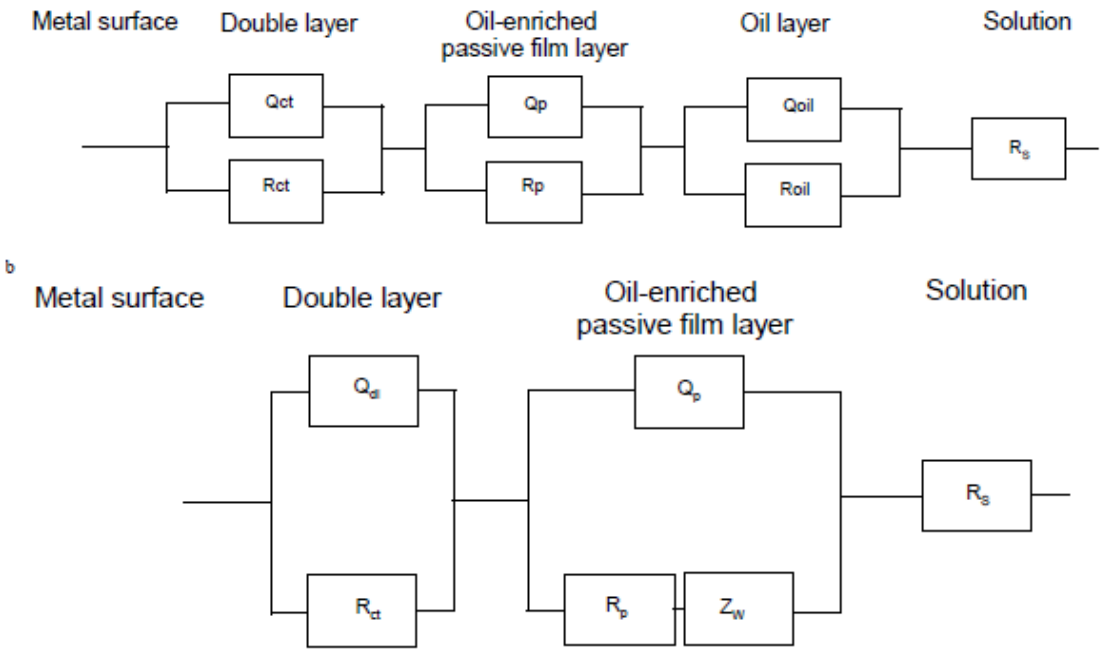

Figure 5.14. Equivalent circuits proposed for the electrochemical impedance response at 30 ^{o}C in 10, 20, and 30 vol% oil containing bicarbonate solutions of a) 0.05 and b) 0.1 M.

Table 5.5. Impedance parameters obtained from the corrosion conditions in 10, 20, and 30 % oil 0.05 M bicarbonate solutions at 30 and 70 ^{o}C

30 °C				70 °C			
Elements	Oil content (vol%)			Elements	Oil content (vol%)		
	10	20	30		10	20	30
R_s ($\Omega.cm^2$)	13.10	13.40	12.00	R_s ($\Omega.cm^2$)	7.61	6.37	7.21
$Q\text{-}Y_{dl}$ ($\mu S.s^n/cm^2$)	0.00703	0.00635	0.00750	$Q\text{-}Y_{dl}$ ($\mu S.s^n/cm^2$)	0.00243	0.00241	0.00310
n_{dl}	0.628	0.634	0.644	n_{dl}	0.839	0.875	0.843
R_{ct} ($\Omega.cm^2$)	690	783	727	R_{ct} ($\Omega.cm^2$)	106.7	112.5	103.7
$Q\text{-}Y_p$ ($\mu S.s^n/cm^2$)	0.00243	0.00185	0.00185	$Q\text{-}Y_p$ ($\mu S.s^n/cm^2$)	0.00703	0.00852	0.00579
n_p	0.839	0.866	0.857	n_p	0.628	0.675	0.741
R_p ($\Omega.cm^2$)	6.731	5.523	6.514	R_p ($\Omega.cm^2$)	690.1	678.3	716.3
$Q\text{-}Y_{oil}$ ($\mu S.s^n/cm^2$)	0.00032	0.00023	0.00041				
n_{oil}	0.976	0.938	0.961				
R_{oil} ($\Omega.cm^2$)	4.541	5.26	4.328				
Chi-square	2.22E-05	7.22E-05	1.38E-05	Chi-square	5.61E-04	4.28E-05	8.11E-05

In these conditions, charge transfer (R_{ct}) was greater than that in oil free condition. The adsorbed oil layers exhibited a capacitive nature where (n_{oil}) values were greater than 0.9. The effect of oil in changing the electrochemical characteristics of 0.05 M conditions was quite similar to that caused by imidazoline inhibitor in carbon dioxide corrosion environments [Lo´pez, 2005].

Interestingly, the corrosion mechanism changed in 0.1 M bicarbonate solutions to exhibit an evidence for diffusion-controlled processes. The capacitive loop was followed by a straight line in the low frequency region at about 1.5 Hz and the bode phase peak was relatively broad with slight fluctuations. The proposed equivalent circuit for 0.1 M conditions involved Warburg impedance (W) in a second-time constant equivalent circuit. The equivalent circuit of the configuration {R(QR)(Q(RW))}, which is shown in Figure 5.14b showed a perfect fit between the simulation and experimental data. In addition, that impedance behaviour was quite similar to 20 and 30 vol% oil containing 0.1 M bicarbonate solutions. In these conditions, oil had a better chance to develop oil-enriched passive films from which diffusion influence became apparent similarly to the conditions

studied in [Hong, 2000]. The electrochemical parameters are shown in Table 5.6 and the corrosion mechanism was irrespective from the high temperature 70 ^{o}C.

Table 5.6. Impedance parameters obtained from the corrosion conditions in 10, 20, and 30 % oil 0.1 M bicarbonate solutions at 30 and 70 ^{o}C

30 °C				70 °C			
Elements	Oil content (vol%)			Elements	Oil content (vol%)		
	10	20	30		10	20	30
Rs (Ω.cm^2)	6.36	6.15	6.74	Rs (Ω.cm^2)	4	3.87	3.93
Q-Ydl (μS.s^n/cm^2)	0.00080	0.00086	0.00080	Q-Ydl (μS.s^n/cm^2)	0.00030	0.00033	0.00038
n_{dl}	0.99	0.97	0.97	n_{dl}	0.97	0.98	0.97
R_{ct} (Ω.cm^2)	356.94	371.38	365.42	R_{ct} (Ω.cm^2)	102.64	113.40	107.86
Q-Y_p (μS.s^n/cm^2)	0.00064	0.00057	0.00061	Q-Y_p (μS.s^n/cm^2)	0.00065	0.00061	0.00065
n_p	0.92	0.91	0.94	n_p	0.8163	0.837	0.875
R_p (Ω.cm^2)	328.8	354.9	337.1	R_p (Ω.cm^2)	61.73	68.3	67.2
W_p (Ω.cm^2/s$^{0.5}$)	0.00273	0.00284	0.00351	W_p (Ω.cm^2/s$^{0.5}$)	0.00722	0.00628	0.00615
Chi-square	1.93E-05	2.37E-05	1.19E-04	Chi-square	2.72E-05	1.41E-05	2.28E-05

Charge transfer (R_{ct}) and solution resistance (R_s) in these conditions were higher than those of oil free and the passive film resistance (R_p) was also high. As previously found with the polarization investigations, the chance for oil of different contents in 0.5 and 1 M bicarbonate solutions for effective direct adsorption or for involvement in the passive film formations was limited. Therefore, from the Nyquist representations as well as from the slight changes in the bode diagrams; it seemed that oil did not induce a significant change in the corrosion mechanisms in the high bicarbonate oil containing solutions. The role of bicarbonate adsorption and/or relaxation of intermediate species were prevalent over that of oil. Therefore, the mechanisms were proposed to be quite similar to those in oil free conditions and the equivalent circuit shown in figure 13 achieved a very good agreement with the experimental data. The equivalent circuit parameters are shown in Table 5.7 for 0.5 and 1 M conditions at 30 and 70 ^{o}C. As expected, charge transfer (R_{ct}) in oil containing solutions showed slight changes in both

0.5 and 1 M solutions but (R_{ads}) showed considerable decreases indicating the disrupted bicarbonate adsorption layers.

Table 5.7. Impedance parameters obtained from the corrosion conditions in 10, 20, and 30 % oil 0.5 and 1 M bicarbonate solutions at 30 and 70 ^{o}C

HCO_3^- concentration (M)	30 C				70 C			
		Oil content (vol%)				Oil content (vol%)		
	Elements	10	20	30	Elements	10	20	30
0.5	R_s ($\Omega.cm^2$)	3.20	3.10	2.70	R_s ($\Omega.cm^2$)	2.12	2.25	2.37
	Q-Y_{dl} ($\mu S.s^n/cm^2$)	0.00276	0.00315	0.00283	Q-Y_{dl} ($\mu S.s^n/cm^2$)	0.002763	0.00227	0.00315
	n_{dl}	0.756	0.785	0.776	n_{dl}	0.7292	0.749	0.784
	R_{ct} ($\Omega.cm^2$)	11.7	10.2	10.6	R_{ct} ($\Omega.cm^2$)	0.4593	0.473	0.51
	Q-Y_{ads} ($\mu S.s^n/cm^2$)	0.00022	0.000316	0.00029	Q-Y_{ads} ($\mu S.s^n/cm^2$)	0.000225	0.00033	0.00019
	n_{ads}	0.94	0.92	0.96	n_{ads}	0.95	0.91	0.94
	R_{ads} ($\Omega.cm^2$)	544.8	546.3	551.6	R_{ads} ($\Omega.cm^2$)	344.8	362	324
	Chi-square	1.43E-05	2.51E-05	1.67E-05	Chi-square	2.46E-05	6.43E-05	5.49E-05
1	R_s ($\Omega.cm^2$)	2.76	2.85	2.74	R_s ($\Omega.cm^2$)	2.124	2.41	2.25
	Q-Y_{dl} ($\mu S.s^n/cm^2$)	0.00276	0.002625	0.00271	Q-Y_{dl} ($\mu S.s^n/cm^2$)	0.002764	0.00255	0.00279
	n_{dl}	0.737	0.756	0.78	n_{dl}	0.7291	0.768	0.714
	R_{ct} ($\Omega.cm^2$)	9.4	9.4	9.2	R_{ct} ($\Omega.cm^2$)	0.4594	0.442	0.523
	Q-Y_{ads} ($\mu S.s^n/cm^2$)	0.00023	0.000276	0.00021	Q-Y_{ads} ($\mu S.s^n/cm^2$)	0.000225	0.00039	0.00034
	n_{ads}	0.97	0.97	0.98	n_{ads}	0.958	0.972	0.936
	R_{ads} ($\Omega.cm^2$)	545	564.2	520.7	R_{ads} ($\Omega.cm^2$)	345	337	358
	Chi-square	1.67E-05	2.14E-05	4.55E-05	Chi-square	1.93E-05	2.73E-05	3.80E-05

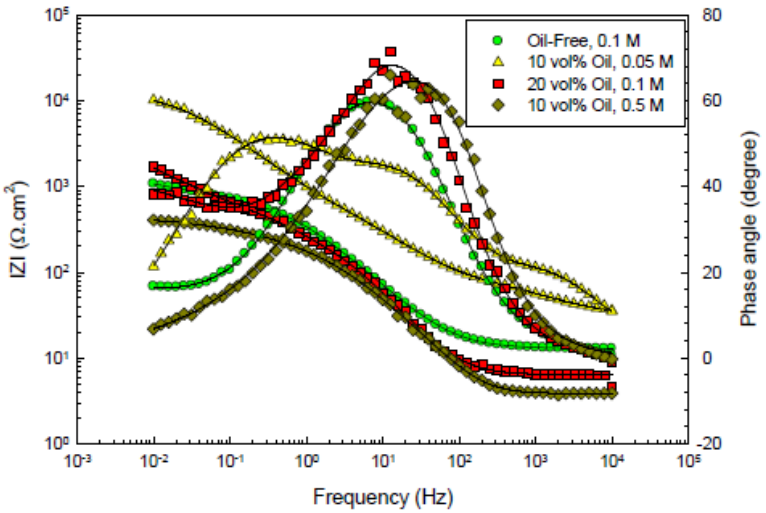

Figure 5.15: Experimental and calculated bode representations for selected conditions

5.7. Electrochemical Impedance Spectroscopy (EIS) at 70 ^{o}C

Nyquist impedance representations at 70 ^{o}C in oil free conditions are shown in Figure 5.16a for 0.05, 0.1, 0.5, and 1 M bicarbonate solutions. The mechanism of electrochemical interactions seemed not to be greatly affected by the higher temperature 70 ^{o}C but rather by bicarbonate contents [Lo´pez, 2003].

In addition, Nyquist plots were considerably smaller than those at 30 ^{o}C, reflecting the decreased polarization resistance as well as that associated with the other interfaces that might exist at this high temperature. Because of the relative Nyquist similarity exhibited for all bicarbonate conditions at both temperatures, adsorption of bicarbonate and/or relaxation of the intermediate species mentioned in section 3.3.1 can be still believed to influence the corrosion mechanisms. The overlapping between the two capacitive loops in 0.5 and 1 M solutions were quite identifiable but occurring at higher frequency, 1 Hz. The changes in Nyquist profiles for 0.1 and 0.05 M conditions occurred at almost the same frequency.

Impedance modules $|Z|$ decreased with the increased bicarbonate content along with the frequency ranges as shown in the bode representations in Figure 5.16b. The same behaviour was exhibited in terms of rate of change of $|Z|$ in the low frequency range with the bicarbonate contents at 30 ^{o}C and the phase bode peaks in 0.05 and 0.1 M conditions appeared at higher frequencies. The previously proposed equivalent circuit in figure 13 for the oil free conditions at 30 ^{o}C showed a very good fit with the experimental data and the calculated electrochemical parameters were produced with small relative errors.

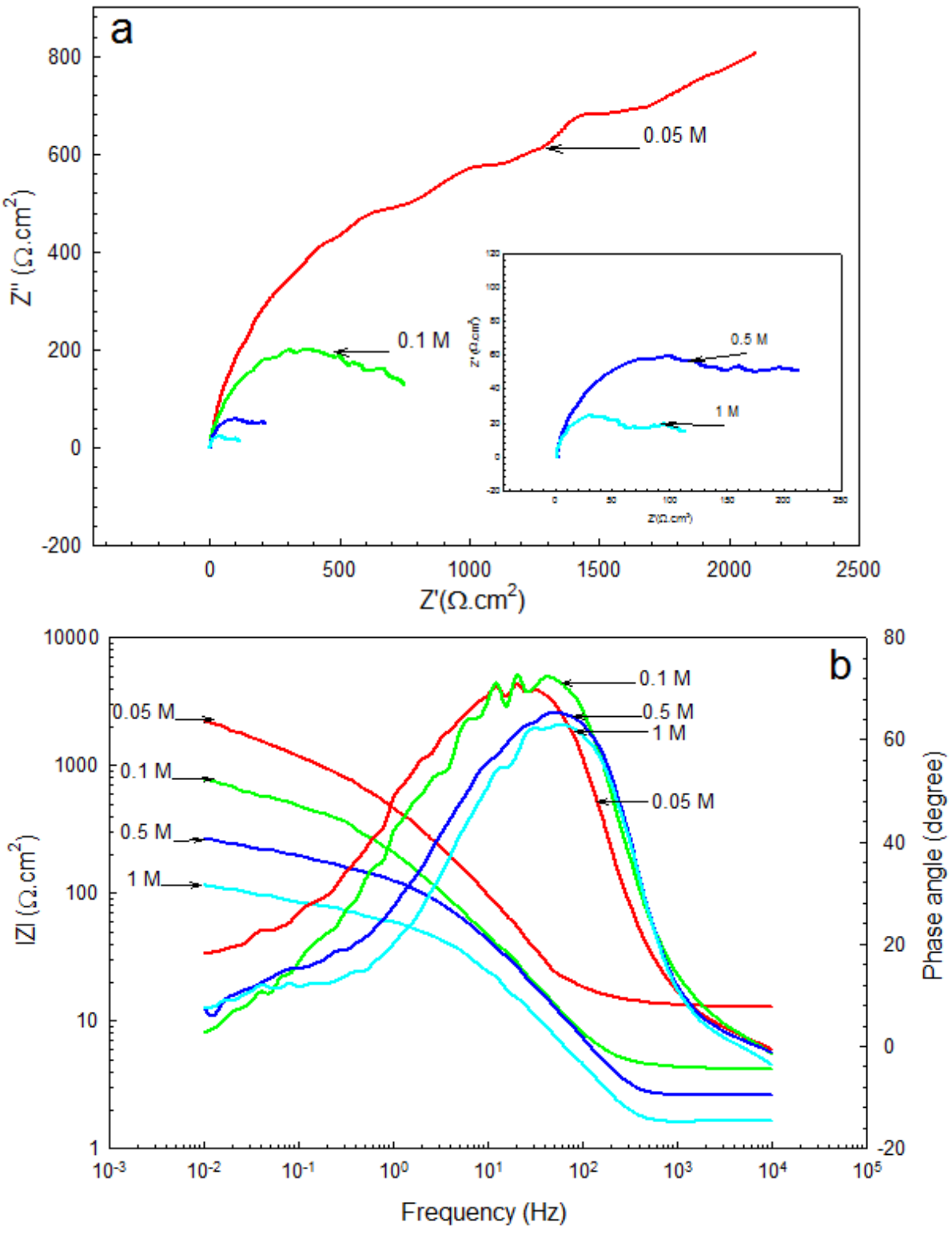

Figure 5.16. Electrochemical Impedance Spectroscopy at 70 °C in oil free bicarbonate solutions of 0.05, 0.1, 0.5, and 1 M represented in a) Nyquist and b) bode diagrams.

Charge transfer (R_{ct}) resistance decreased markedly with the higher temperature and the resistance across the adsorption field decreased also within almost pure capacitances as shown in Table 5.6.

Oil changed the electrochemical interactions in a fashion similar to that at 30 ^{o}C where effect of oil miscibility and adsorption at the higher temperature in different bicarbonate solutions changed. As shown in Figure 5.17a for 10 vol% oil containing conditions, Nyquist plots are smaller compared to those produced at 30 ^{o}C but their shapes showed appreciable similarity. Impedance response in 0.05 M condition seemed to be two-time constant based of the configuration of {R(QR)(QR)} which is shown in Figure 5.18. Differently from the case at 30 ^{o}C, two fairly discernible two peaks in the bode profile appeared as shown in Figure 5.17b with no evidence for another high-frequency third peak.

Although of the possibility for effective oil adsorption in this condition was still high, but the attempted equivalent circuit of the configuration of {R(QR)(QR)(QR)} did achieve a very good fit. As shown in table 8, charge transfer resistance (R_{ct}) decreased about 7 times and the double layer constant phase elements were more capacitive. Interestingly, the passive film resistance was high where the compactness was enhanced or the oil role was to support the passive film structure rather than to get adsorbed on them. Impedance responses in 20 and 30 vol% oil conditions were similar to that shown in 10 vol% oil and their profiles are not shown but the corresponding values with the Chi-square values are listed.

The impedance response in 0.1 M condition, as that at 30 ^{o}C, was also diffusion controlled where the straight line appeared at relatively higher frequency of about 1.5 Hz.

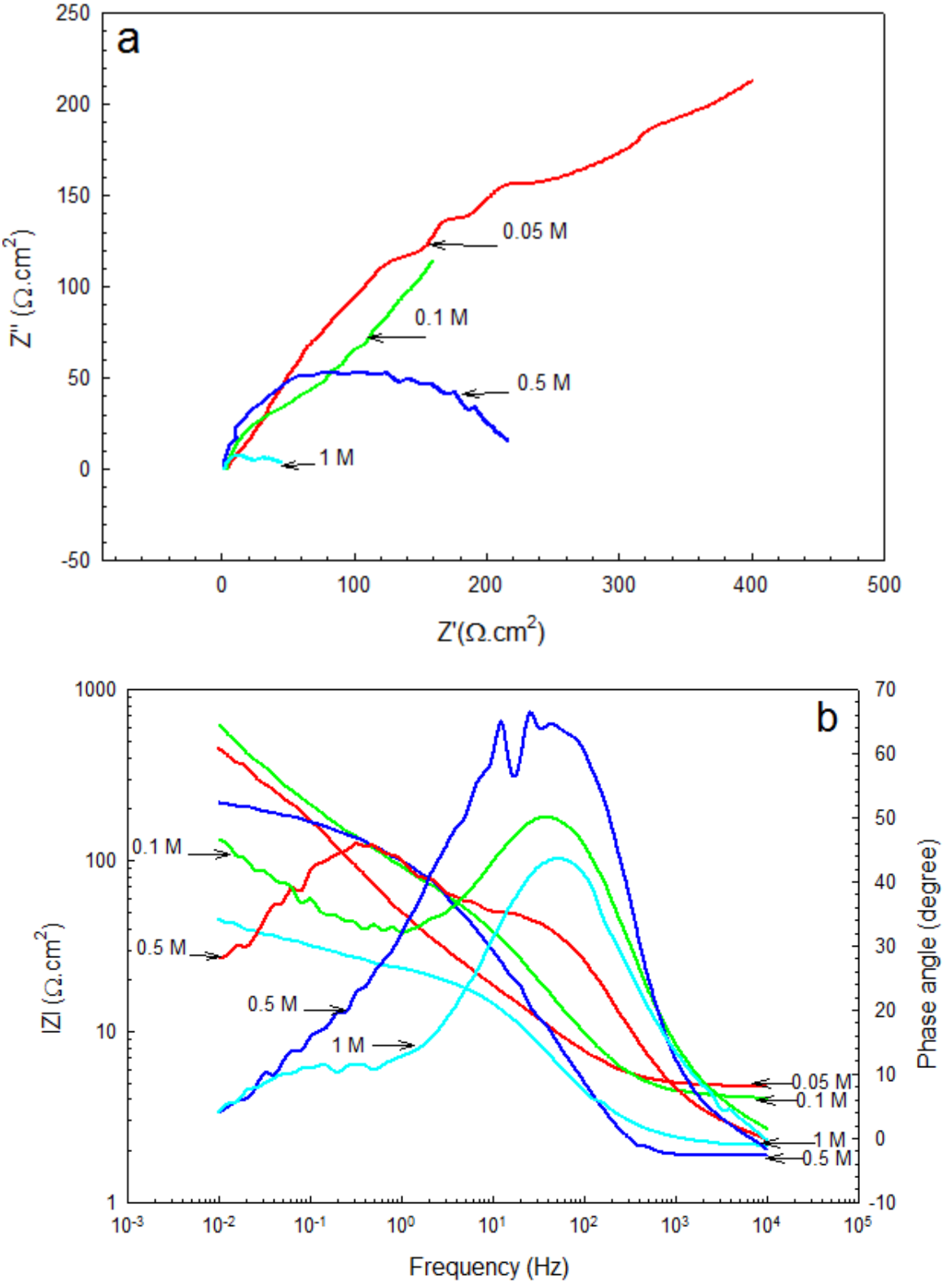

Figure 5.17. Electrochemical Impedance Spectroscopy at 70 °C in oil free bicarbonate solutions of 0.05, 0.1, 0.5, and 1 M represented in a) Nyquist and b) bode diagrams.

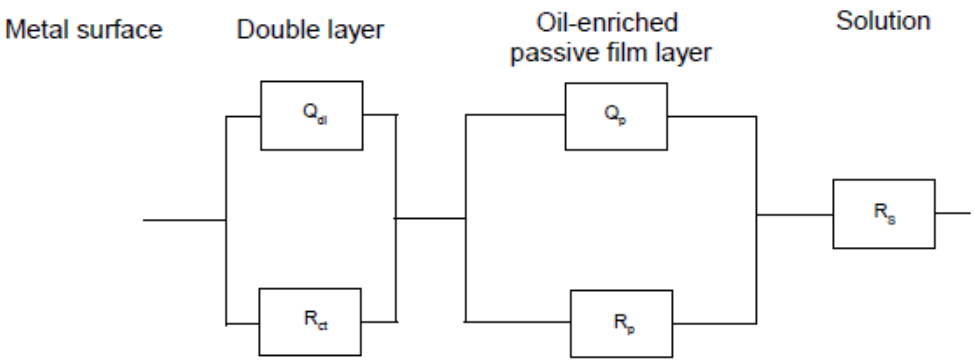

Figure 5.18: Equivalent circuit proposed for the electrochemical impedance response at 70 ^{o}C in 10, 20, and 30 vol% oil containing bicarbonate solutions of 0.05 M.

The equivalent of the configuration {R(QR)(Q(RW))} achieved a satisfactory agreement with the experimental data. It should be noted also that electrochemical characteristics in 0.1 M conditions were almost similar with the different oil contents and their charge transfer resistances were lower than those at 30 ^{o}C as shown in Table 5.6. As already indicated from the polarization test results, the oil-enriched passive films were deteriorated as the tendency for (Fe^{2+}/Fe^{3+}) reactions is greater resulting in lower resistance (R_p) across the passive films as already indicated in simulated bicarbonate solutions [Liang, 2009]. The electrochemical conditions in 0.5 and 1 M solutions, as they were unaffected by the oil contents at 30 ^{o}C, they seemed to show the same response with higher temperatures. In these conditions, the adsorption of bicarbonate or the other associated adsorption processes of intermediate species at this high temperature were more dominant over the adsorption of oil where its miscibility decreases with greater bicarbonate content. The proposed mechanism in the equivalent circuit shown in Figure 5.12 achieved a very good agreement with the experimental data and the calculated

parameters are shown in Table 5.6. As expected, charge transfer resistance showed a considerable decrease, and the resistance across the adsorption field changed slightly. The simulation data are shown with the experimental results for selected bicarbonate and oil conditions at 70 ^{o}C in Figure 5.19 exhibiting the very good fit with the proposed equivalent circuits.

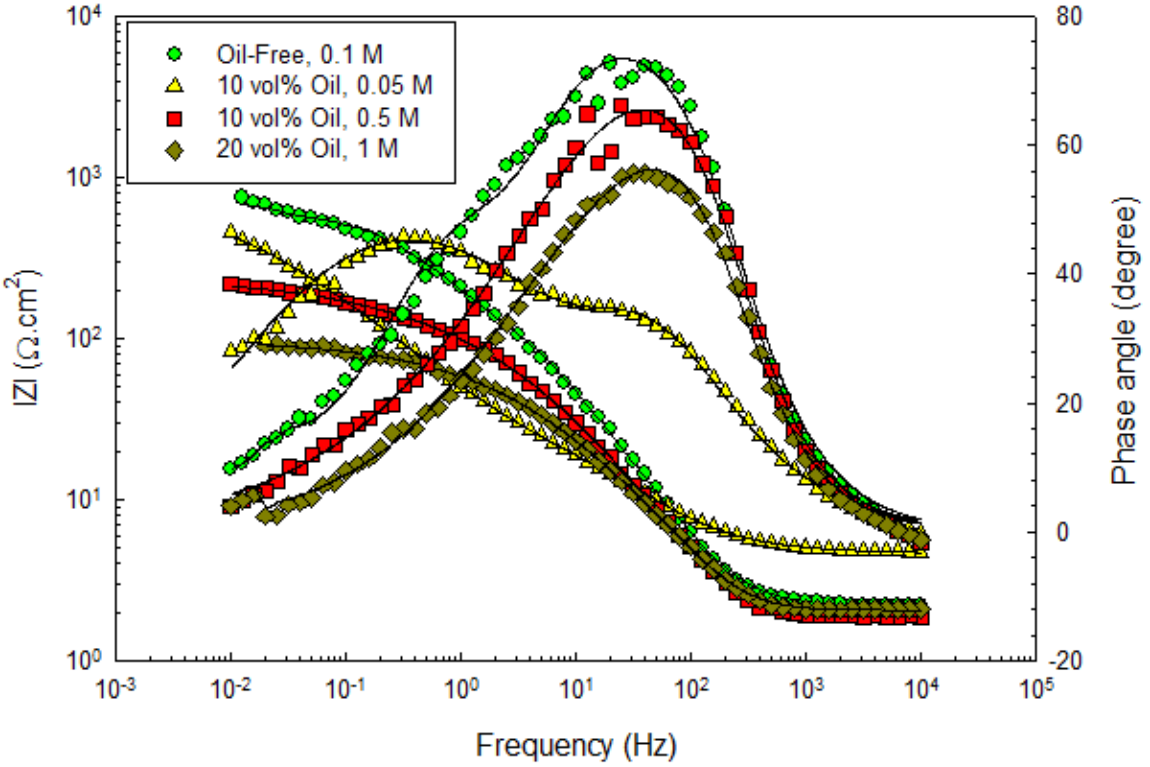

Figure 5.19. Experimental and calculated bode representations of impedance response for selected bicarbonate and oil containing conditions at 70 ^{o}C.

Chapter 6: Results and discussion of the electrochemical investigations in low chloride containing CO_2-saturated media containing low oil amounts

6.1. Test solutions

The electrochemical tests were performed in test solutions simulating the carbon dioxide corrosion conditions in transportation pipelines containing high water cuts with three amounts of a hydrocarbons added with 10, 20, and 30 vol% in unbuffered 1 bar CO_2 saturated emulsions. Selected physical and chemical properties of the emulsified hydrocarbon are shown in Table 6.1.

Table 6.1. Selected chemical and physical properties of the hydrocarbon considered

Property	Details
Appearance	Green
Carbon number	C4-C12
Initial Boiling Point (°C)	25
Boiling Range (°C)	25 - 170
Flash point (°C)	>10
Lower / upper Flammability (V)	1 - 6 %
Auto-ignition temperature (°C)	> 250
Vapor pressure (kPa)	< 38 at 20 °C
Density (g/cm^3)	0.63 at 15 °C
Kinematic viscosity (mm^2/s)	0.5-0.75 at 40 °C

According to the classification criteria of crude oil based on the carbon number as well as on the density stated in [Lyons, 2005], the hydrocarbon considered is a typical medium-weight crude oil. The deoxygenated solutions were synthesized from double distilled deionized water electrolytes, chloride free and 2000-ppm chloride containing. The present amount of chloride is within a range of typical values in pipeline oil flows

after being desalted in oil processing facilities [Manning, 1995]. The test temperatures were selected to be 20, 50, and 80 ^{o}C within ± 1 ^{o}C.

6.2 Open Circuit Potential (OCP) measurements in oil free conditions

OCP variations with time were monitored first at 20, 50, and 80 ^{o}C in chloride free and in 2000 ppm chloride containing oil free solutions. OCP profiles for the six conditions established are shown in Figure 6.1a where OCP decreased with the higher temperature.

Although that the OCP in chloride free conditions was higher than that in chloride containing conditions at each corresponding temperature, the band of variations between the maximum and minimum OCP values in both conditions was similar of about 30 mV. The resulting decrease in OCP with the addition of chloride suggests that the anodic responses became more prevalent during the mixed potential conditions. The anodic reaction (1) representing the direct dissolution of ferrite to ferrous ions (Fe^{2+}) was considered for the theoretical anodic limit as:

$$Fe \rightarrow Fe^{2+} + 2e^{-} \qquad (6.1)$$

Additionally from the mechanisms suggested for the carbon dioxide corrosion reactions, carbonic acid (H_2CO_3) is in equilibrium with the dissolved carbon dioxide gas, and it can get involved in the anodic dissolution in conditions where pH ≤ 5 as represented in equation (2) [Moiseeva, 2003] as:

$$Fe + H_2CO_3 \rightarrow FeCO_3 + 2H^{+} + 2e^{-} \qquad (6.2)$$

The cathodic reactions are driven by both hydrogen cations and carbonic acid which are also in equilibrium expressed from the solubility data [Baraneko, 1990] in aqueous solutions continuously purged with carbon dioxide as represented in equation (3) as:

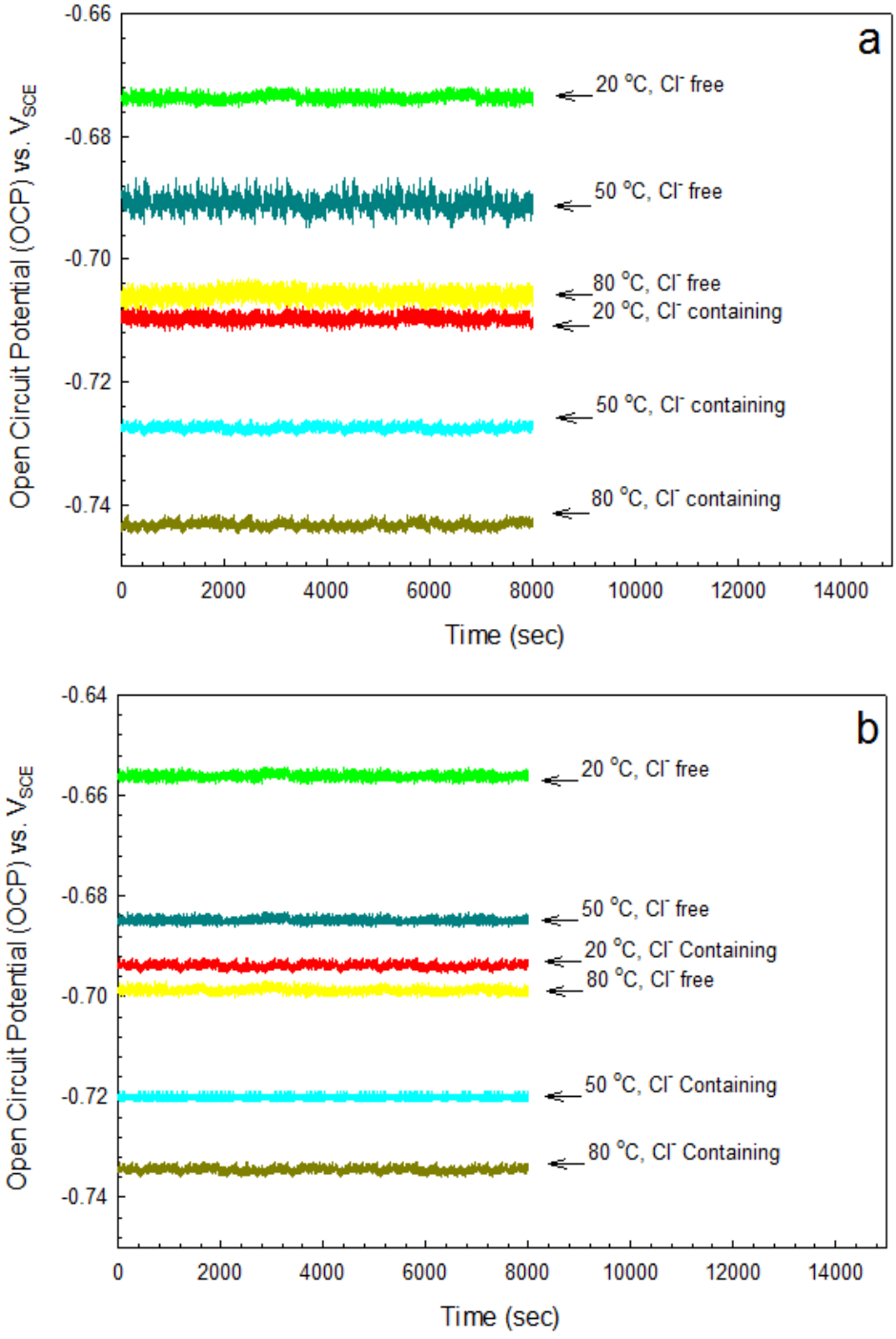

Figure 6.1. Open Circuit Potential (OCP) variations in a) oil free and b) 30 vol% containing oil conditions.

$$CO_2 + H_2O \leftrightarrow CO_2 - H_2O \leftrightarrow H_2CO_3 \leftrightarrow H^+ + HCO_3^- \quad (6.3)$$

It was suggested in a fundamental work [Schmitt, 1983] that carbonic acid acts as a source of hydrogen cations leading to the conventional cathodic reaction (4) as:

$$2H^+ + 2e^- \rightarrow H_2 \quad (6.4)$$

In addition, the direct reduction of carbonic acid as proposed by de Waard and Milliams [De Waard, 1975] participate in the electrochemical hydrogen evolution on the steel surface where carbonic acid acts as a catalyst as proposed in equation (6.5), (6.6), and (6.7) as:

$$H_2CO_3 + e^- \rightarrow H_{ads} + HCO_3^- \quad (6.5)$$

$$HCO_3^- + H^+ \rightarrow H_2CO_3 \quad (6.6)$$

And

$$2H_{ads} \rightarrow H_2 \quad (6.7)$$

Alternatively the cathodic reduction of carbonic acid could also be represented in equation (8) as:

$$H_2CO_3 + e^- \rightarrow HCO_3^- + 1/2\, H_2 \quad (6.8)$$

The standard half cell potentials were calculated based on Gibbs free energies of formation of the individual species of concern as listed in [Dean, 2000]. The theoretical anodic and cathodic limits represent by the half cell reactions, by which the measured OCP profiles are confined within, were calculated as functions of temperature and pH of 1 atm CO_2 saturated solutions utilizing Nernst equation [Ahmed, 2006]. For the high temperatures 50 and 80 ^oC, the corrected Nernst equation was considered from Maxwell relation (9) in thermodynamics [Brett, 1993] as:

$$\frac{\partial \Delta G^{O}}{\partial T} = -\Delta S \qquad (6.9)$$

Where ΔG^{O} is the standard Gibbs free energy and ΔS is the entropy change. Assuming a relatively constant difference in entropy within the temperature range of concern, the equilibrium potential is expressed in equation (10) and the entropy variations with temperature were taken from [Dean, 2005]:

$$E_T^o = E^o + \frac{\Delta S}{nF}(T - 298) \qquad (6.10)$$

pH levels at the high temperatures 50 and 80 ^oC were calculated for oil free and oil containing chloride free solutions based on the temperature-dependant solubility of carbon dioxide purged at 1 bar. The volume fractions of the dissolved carbon dioxide were taken from the improved Beattie volume explicit equation of state for carbon dioxide considering the compressibility and fugacity at different temperatures.

Additionally, the first (k_{a1}) and second dissociation (k_{a2}) constants for the weak carbonic acid as well as that dissociation constant (K_w) of water at 50 and 80 ^oC were obtained from [21] to calculate pH at the corresponding temperatures.

pH levels at 50 and 80 ^oC in 2000 ppm chloride containing solutions were obtained from the model proposed in [Li, 2007]. That model achieved a quite satisfactory agreement with the other experimental work [Crolet, 1983] performed for H_2O-CO_2-NaCl solutions with the maximum deviations of $\Delta pH < 0.2$.

OCP levels were well bounded by the proposed theoretical limits as shown in Table 6.2 where they were along with the equilibrium potentials showing a decrease with the higher temperature.

Table 6.2. Open Circuit Potentials (OCP) and the calculated half cell equilibrium potentials for oil free conditions

Salinity	Temperature	pH	OCP	Equilibrium Potential (Reaction (6.1))	Equilibrium Potential (Reaction (6.2))	Equilibrium Potential (Reaction (6.4))	Equilibrium Potential (Reaction (6.8))
	(°C)		(V) vs. SCE	(V) vs. SCE	(V) vs. SCE	(V) vs. SCE	(V) vs. SCE
Cl^- Free	20	3.5	-0.673	-0.740	-0.744	-0.444	-0.614
	50	4.2	-0.691	-0.746	-0.797	-0.497	-0.667
	80	4.8	-0.705	-0.752	-0.821	-0.521	-0.691
2000 ppm Cl^- containing	20	3.2	-0.71	-0.740	-0.727	-0.427	-0.597
	50	3.9	-0.727	-0.746	-0.797	-0.497	-0.667
	80	4.5	-0.743	-0.752	-0.821	-0.521	-0.691

Additionally, OCP values seemed to be more influenced by the cathodic reactions and the influence of the cathodic reduction of carbonic acid with the higher temperatures seemed to be more pronounced as already indicated from the electrochemical models proposed in [Anderko, 1999]. OCP values in chloride containing solutions were lower than those in chloride free conditions and they were closer to the anodic potentials. As confirmed with the polarization test results, the accelerated anodic reactions upon the addition of chloride could lower the free mixed potentials and where the chances for effective passive film formations were excluded [Agrawal, 2004].

6.3. Open Circuit Potential (OCP) measurements in oil containing conditions

Three proportions of oil of 10, 20, and 30 vol%, were added to the aqueous systems considered with the same salinity and temperature conditions. OCP values exhibited the same trend where they decreased with the higher temperatures and by the chloride additions. The bands of variation between the maximum and minimum OCP values were broader than those in oil free conditions where they were 44 and 40 mV for chloride free and chloride containing conditions respectively as shown in Figure 6.1b for 30 vol% oil containing solutions. Similar OCP trends, within the theoretical limits were exhibited with the higher temperature and by the increased oil content as shown in Figure 6.2.

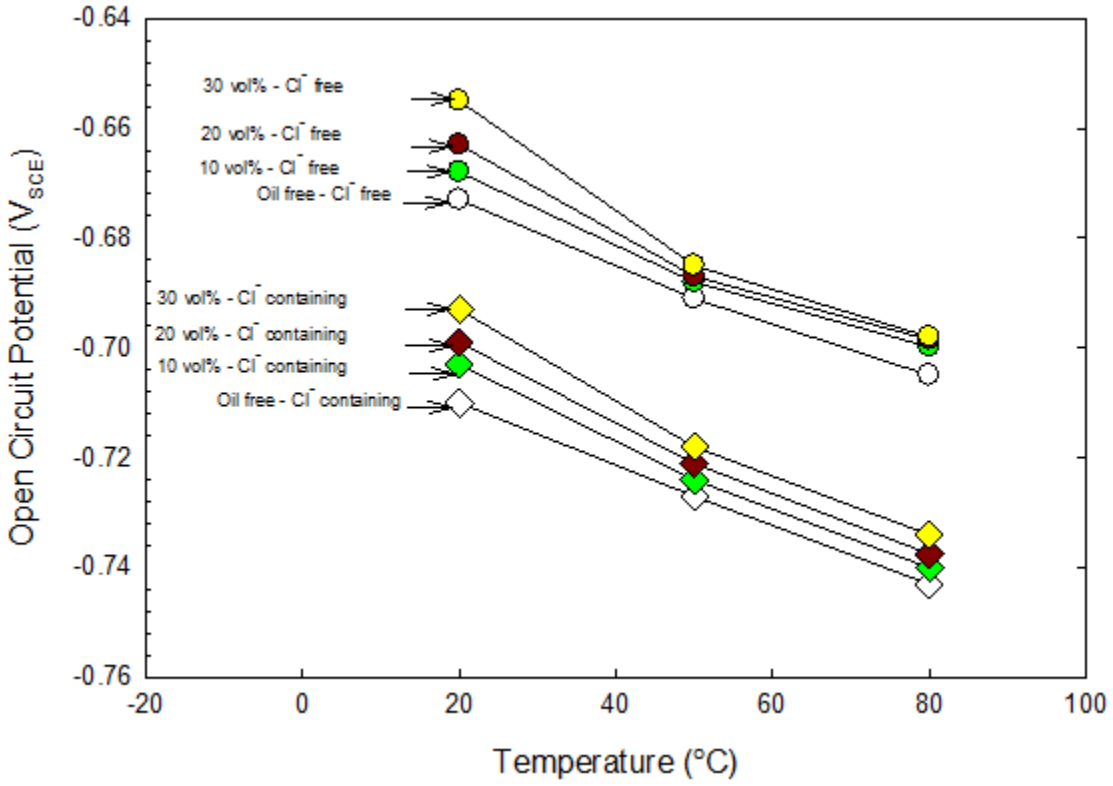

Figure 6.2. Open Circuit Potential (OCP) variations with temperature and oil content in chloride free and chloride containing conditions.

OCP was higher by the addition of oil, and it showed a dependence on oil content in elevating OCP values in both chloride free and chloride containing solutions. Confirming with the polarization test results discussed in section 3.2.2, it was evident that the anodic reactions were inhibited by the stable organic films in a proportional manner with the oil content independently from temperature. The consequent nobler free potentials reflects the unchanged anodic inhibition capability of oil at low pH-CO_2 purged media, and differently from the results found in [Eliyan, 2011], the cathodic reactions could be inhibited upon the temperature variations but in mildly alkaline media. The significance of oil amount in changing OCP in chloride free solutions was less pronounced as the temperature increased, but the effect of oil in chloride containing

solutions was persistent within the full range of temperature, and that is subject for future investigations.

6.4. Potentiodynamic polarization measurements in oil free conditions

The potentiodynamic polarization test profiles in chloride free and chloride containing oil free test solutions at 20, 50, and 80 ^{o}C are presented in Figure 6.3a. Apparently, the reaction rates of the anodic dissolution as well as the cathodic reactions showed an increase with temperature. In addition to the expected acceleration of the corresponding temperature dependent electrochemical reactions, the transport of species involved in the corrosion processes become the dominant step in the dissolution chain [Gray, 1990]. Corrosion current density (i_{corr}) increased with temperature and that was associated with more negative corrosion potentials (E_{corr}) suggesting the prevalence of anodic reactions during polarization as already established in [Kirmani, 2006]. The addition of chloride increased noticeably the electrochemical sensitivity of both anodic and cathodic reactions. The corrosion rates were higher than those in chloride free solutions with more negative potentials as shown in Table 6.3.

Table 6.3. Potentiodynamic polarization results in oil free conditions

Oil condition	Salinity	Temperature (°C)	E_{corr} (mV_{SCE})	i_{corr} ($\mu A/cm^2$)	β_a (mV/d)	β_c (mV/d)	i_L (mA/cm^2)
Oil free	Chloride Free	20	-684	7	60	79	0.841
		50	-689	12	60	78	1.75
		80	-700	63	39	75	3.15
	Chloride Containing - 2 grams	20	-710	58	49	52	25.2
		50	-713	104	64	60	35.3
		80	-718	146	53	54	53.8

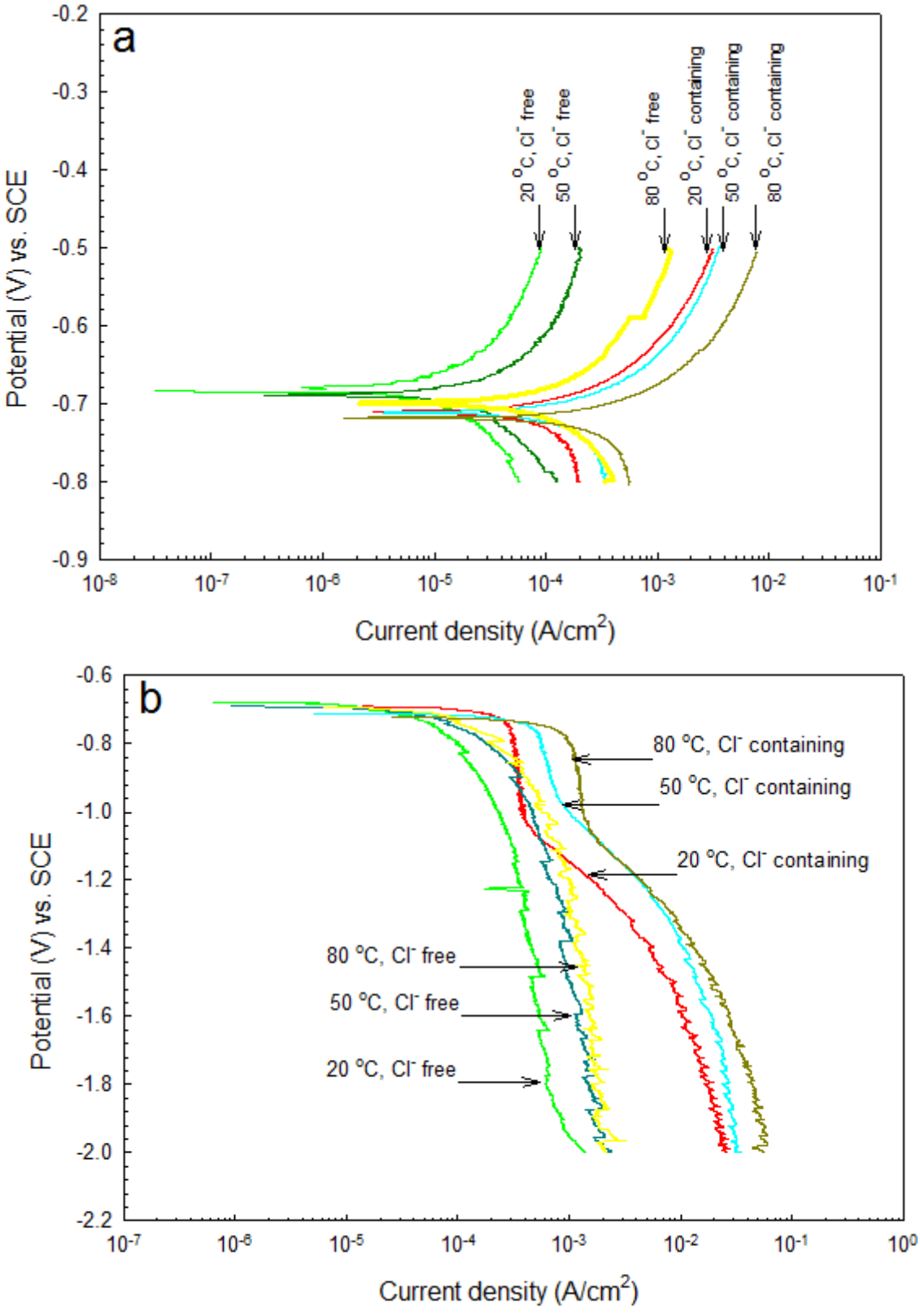

Figure 6.3. Potentiodynamic polarization at 20, 50, and 80 °C in chloride free and chloride containing oil free conditions; a) comprehensive, and b) cathodic profiles

The kinetic parameters, corrosion current density (i_{corr}), and anodic and cathodic Tafel slopes (β_a), (β_c) are calculated from Butler-Erdey-Volmer (BEV) equation utilized for the purely kinetic controlled polarization as [Stansbury, 2000]:

$$i = i_{corr}\left(\exp\left[\frac{2.3\eta_s}{\beta_a}\right] - \exp\left[\frac{-2.3\eta_s}{\beta_c}\right]\right) \qquad (6.11)$$

The parameters are iteratively calculated with the best fit with the experimental data. The decreasing trend of both anodic and cathodic slopes with temperature in chloride free and chloride containing solutions confirmed the accelerated charge transfer reactions.

Although at the high temperature, 80 ^{o}C, the already high corrosion rate doubled upon the addition of chloride, it increased about eight times at low temperature 20 ^{o}C. From the visual observation at the end of the relatively short-ranged polarization for both chloride free and chloride containing conditions, a white/silver passive films were intact on the steel surfaces similarly to those appeared in [Mao, 1994] incorporating iron carbonate ($FeCO_3$). Chloride effect on the accelerated corrosion rates can be greatly attributed to the stability of that iron carbonate film and/or to the greater conductivity of the aqueous media where the effective passive film formation was not favored [Sun, 2003]. As proposed from the Mott-Schottky plots generated for the passive films formed at different temperatures, the autocatalytic formation of cation/oxygen vacancy pairs in the presence of chloride lead to greater donor density in a proportional manner with the higher temperature. That behaviour across the passive films can be proposed to cause a considerable instability of the passive films and/or greater pitting susceptibility within a field where considerable local pH gradients are established [Li, 2007].

The anodic reactions in the active polarization region are represented by the direct dissolution of ferrite colonies as described in equation (1) where the dissolution occurred continuously with no evidence for multistep slopes as reported in many studies [Yin, 2009] and [Zhang, 2005]. Conventionally, ($FeCO_3$) in CO_2-saturated water precipitates on the steel surface where (Fe^{2+}) combines with (HCO_3^-) in the low pH media as described in equation (6.12):

$$Fe^{2+} + HCO_3^- \rightarrow FeCO_3 + H^+ \qquad (6.12)$$

Bicarbonate species, not carbonate ones exist more predominantly in pH ranges greater than 3.8 [Nazari, 2010] and according to CO_2 dissolution mechanism described in equation (3), bicarbonate exist in sufficient local concentrations to precipitate as described in equation (11), or even in an electrochemical manner as described in equation (6.13) [Zhang, 2011] as:

$$Fe^{2+} + HCO_3^- \rightarrow FeCO_3 + H + e^- \qquad (6.13)$$

($FeCO_3$) precipitation, which is also temperature sensitive, can be the major constituent in a stable passive film growing electrochemically with an equilibrium potential of about -650 mV_{SCE} as found in [Zhang, 2009 (A)] at pH 3.8.

The characteristics of the cathodic polarization were also investigated in separate scheme considering polarization sweeps from -2 V_{SCE} to the corrosion potential as shown in Figure 6.3b. The total cathodic reaction rates were quite dependent on temperature in both chloride free and chloride containing conditions. In the mass transfer limited region in the chloride free conditions, the limiting current density (i_L) shown in Table 6.3 was within a range of variation of about an order of magnitude between the maximum and minimum temperatures. In these conditions, the direct reduction of (H_2CO_3) became

more dominant with the higher temperature over that of (H^+) [Nesic, 1996], and the decreased viscosity and the consequent greater diffusion of the reducible species accelerated the hydrogen evolution. At the high temperatures 50 and 80 ^oC at low overpotentials, the cathodic reactions might involve a temperature-insensitive chemical step, probably hydration of carbon dioxide, leading to quite comparable current densities. The current densities at different temperatures were closer in the mixed charge transfer-mass transfer controlled regions, and the onset for the cathodic reactions to be more mass transfer controlled was apparent at the higher temperatures where the cathodic shoulders modified. In chloride containing conditions, the cathodic reactions seemed to follow a different mechanism where the changed kinetics at the interface accompanied by low pH gradients made the reduction of (H^+) as well as that of (H_2CO_3) greatly accelerated. The limiting current density reaching cathodic reactions were intercepted by the cathodic reduction of water as:

$$2H_2O + 2e^- \rightarrow 2OH^- + H_2 \qquad (6.14)$$

Irrespectively from temperature, the onset of charge transfer controlled reduction of water was apparent at about -1 V_{SCE} and where the accelerated reactions became dominated by the reduction of water as already indicated in [Zhang, 2007] and [Louafi, 2010].

6.5. Potentiodynamic polarization measurements in oil containing conditions

The polarization profiles in 10 vol% oil containing solutions at the same conditions established for oil free conditions are shown in Figure 6.4a. The polarization behaviour showed a considerable change upon the addition of oil from many perspectives.

The anodic polarization in the active region seemed to undergo two well discernible steps indicating an electrochemical dependence of oil adsorption on the applied potential especially at the low temperature of 20 ^{o}C.

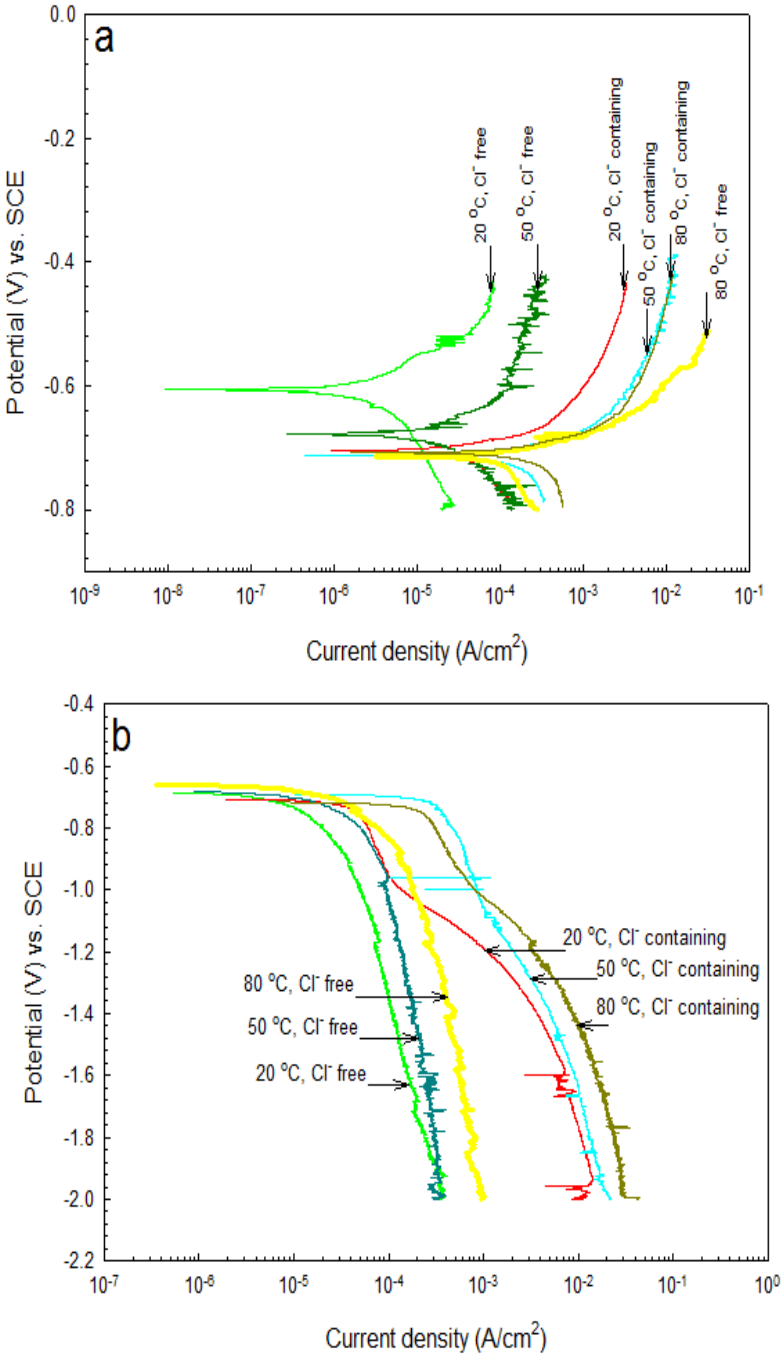

Figure 6.4. Potentiodynamic polarization at 20, 50, and 80 ^{o}C in chloride free and chloride containing 10 % oil containing conditions; a) comprehensive, and b) cathodic profiles.

This behavior encountered was very similar to other polarization studies performed in [Zhang, 2001] and [Ortega-Sotelo, 2010], where the inhibitor stability was related to the applied potential before the desorption occurs at a characteristic potential (E_{des}). As expected, the anodic branch seemed to be more sensitive to oil addition, and in that perspective, the possibility for a multistep anodic dissolution to occur was excluded where the active region in the oil free conditions did not show abrupt changes. In conditions where oil miscibility was high; i.e. at low temperatures, the polarization responses showed a considerable noise where the electrochemical interactions at the emulsified oil layer at the steel surfaces were sensitive to oil adsorption.

Corrosion rates were less upon the addition of oil in a proportional manner with the oil content as shown in Table 6.4 independently from the absence or presence of chloride.

Table 6.4. Potentiodynamic polarization results in oil containing conditions

Oil content	Salinity	Temperature	E_{corr}	i_{corr}	β_a	E_{des}	Efficiency	β_c	i_L
		(°C)	(mV)	($\mu A/cm^2$)	(mV/d)	mV	%	(mV/d)	(mA/cm^2)
10	Chloride Free	20	-606	0.6	63	-570	91.4	82	0.25
		50	-678	2.4	64	-648	80.0	76	0.32
		80	-704	52	73	-688	17.5	69	0.98
	Chloride Containing - 2 grams	20	-705	24	61	-686	58.6	67	12
		50	-708	71	74	-678	31.7	38	21.7
		80	-713	132	51	-702	9.6	62	32.3
20	Chloride Free	20	-603	0.55	65	-566	92.1	79	0.22
		50	-675	1.932	62	-645	83.9	78	0.37
		80	-700	23	76	-682	63.5	71	0.92
	Chloride Containing - 2 grams	20	-703	24	59	-682	58.6	69	13
		50	-709	59	78	-680	43.3	41	23.1
		80	-715	117	50	-702	19.9	52	31
30	Chloride Free	20	-603	0.45	67	-563	93.6	77	0.18
		50	-671	1.3	61	-642	89.2	78	0.32
		80	-700	18	75	-688	71.4	73	0.87
	Chloride Containing - 2 grams	20	-700	19	62	-683	67.2	71	11
		50	-705	47	74	-680	54.8	55	21.2
		80	-710	87	58	-700	40.4	63	28

The decrease of corrosion rates in both conditions were expressed with inhibition efficiency where the performance of oil added with different amounts is compared with the situation in oil free conditions as:

$$\eta = \frac{i - i_{oil}}{i} \qquad (6.15)$$

(η) is the inhibition efficiency expressed in (%), (i) and (i_{oil}) represent the corrosion current density in oil free and oil containing conditions respectively. The inhibition efficiency range was wide in the chloride free conditions and it was as high as 90 % at 20 ^{o}C and as low as 10 % at 80 ^{o}C where the corrosion inhibition was strongly related to temperature-dependent oil miscibility. Although the inhibition efficiency in chloride containing solutions showed the same trend with temperature, it was noticeably lower and the range of variation was narrower. Oil adsorption had an appreciable effect on the cathodic reactions as depicted from the trend of (β_c) in comparison with that of oil free conditions. The effect of oil was, however, more predominant on the anodic reactions where (E_{corr}) was nobler upon the addition of oil and where the active anodic region showed the electrochemical differences. Oil desorption in chloride free solutions occurred at higher (E_{des}) in a range between 30 to 40 mV above (E_{corr}) at 20 ^{o}C but it occurred earlier in a range between 10 to 22 mV above (E_{corr}) at higher temperature. In chloride containing solutions where smaller surface areas were covered by oil as indicated in [Gutzeit, 2000], oil desorption occurred at quite lower (E_{des}) in a range not exceeding 13 mV irrespectively from temperature.

The cathodic polarization reactions were noticeably inhibited in a proportional manner with the oil amount. Oil seemed not to induce a significant electrochemical change on the cathodic reactions where the mechanisms in chloride free and chloride containing solutions were similar to those in oil free conditions as shown in Figure 6.4b. As shown in Table 6.4, the suppressed (i_L) values were more sensitive to the introduction of oil at low temperatures. Oil adsorption/desorption seemed not be electrochemically

influenced in the cathodic branch of our case, but rather, the geometric blocking could be attributable to the noticeable inhibited current densities especially at the mixed charge transfer- mass transfer controlled regions.

6.6. Adsorption isotherms and associated thermodynamics

Oil adsorption and the associated active interactions are further investigated from thermodynamic perspectives. Langmuir isotherms, after other attempts to fit the surface coverage (θ) to different adsorption isotherms, were utilized to evaluate oil adsorption in relation to temperature variations in chloride free and chloride containing solutions. In our case, oil adsorption, occurring in chemisorption fashion as going to be discussed in following context, was greatly possible governed by an aromatic compound sharing its $\pi-$electron density; it is called 1, 2, 3, 4-tetrahydronaphthalene ($C_{10}H_{12}$) and its chemical structure is shown in Figure 6.5.

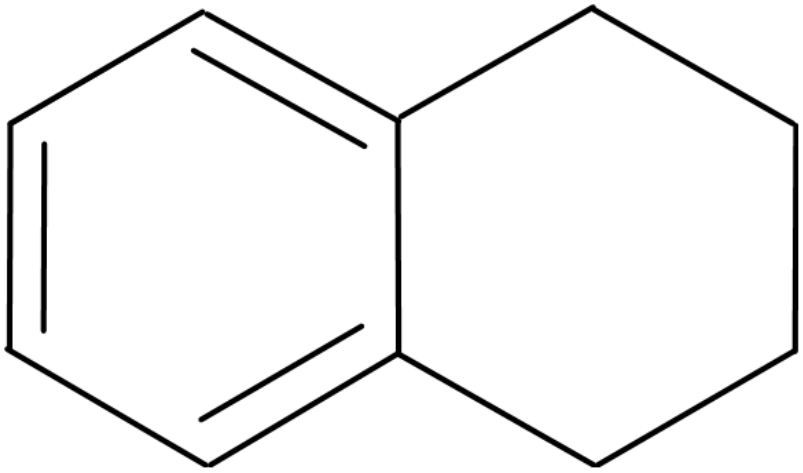

Figure 6.5. Chemical structure of 1, 2, 3, 4-tetrahydronaphthalene ($C_{10}H_{12}$).

As reported in [Ayello, 2011] where the devotion was for the crude oil chemistry effect on the corrosion inhibition, ($C_{10}H_{12}$) adsorption decreases the corrosion rate and it alters

the interfacial tensions of the emulsified phases at the steel surface. Therefore, and according to Langmuir assumptions, it was assumed that there were limited interactions between the adsorbed aromatics with the steel surfaces and a homogenous monolayer of surface saturation was established [Bard, 2001].

Langmuir isotherm for oil adsorption is mathematically represented as [Bard, 2001]:

$$\frac{\theta}{1-\theta} = B\,C \qquad (6.16)$$

(θ) is the fractional coverage of the surface, (B) is the energetic coefficient of proportionality, and (C) is bulk concentration of emulsified oil active species in (mol/L). The concentration of the active adsorbable specie ($C_{10}H_{12}$) is calculated from its molecular weight of 132.2 g/mol from which the average molecular weight of our complex hydrocarbon is calculated for of about 231 g/mol according to the estimates listed in the United States Environmental Protection Agency (EPA) database [EPA, 2010].

The linear relation between $(\theta/(1-\theta))$ and concentration was very evident for both chloride free and chloride containing solutions, as shown in Figure 6.6a and b, with linear regression coefficients (R^2) close to unity.

Oil adsorption dependence on temperature was apparent where the ratio concerned, as it increased with the oil content, decreased with higher temperatures. In chloride containing solutions, the same trend was produced with respect to oil and temperature, but it seemed that the enhanced kinetics at the emulsified interface minimized the areas for stable oil coverage. (B) is related to the free energy of adsorption (ΔG_{ads}), which are both shown in Table 6.5 and they are mathematically related as [Bard, 2001]:

$$B = \exp\left(\frac{-\Delta G_{ads}}{RT}\right) \qquad (6.17)$$

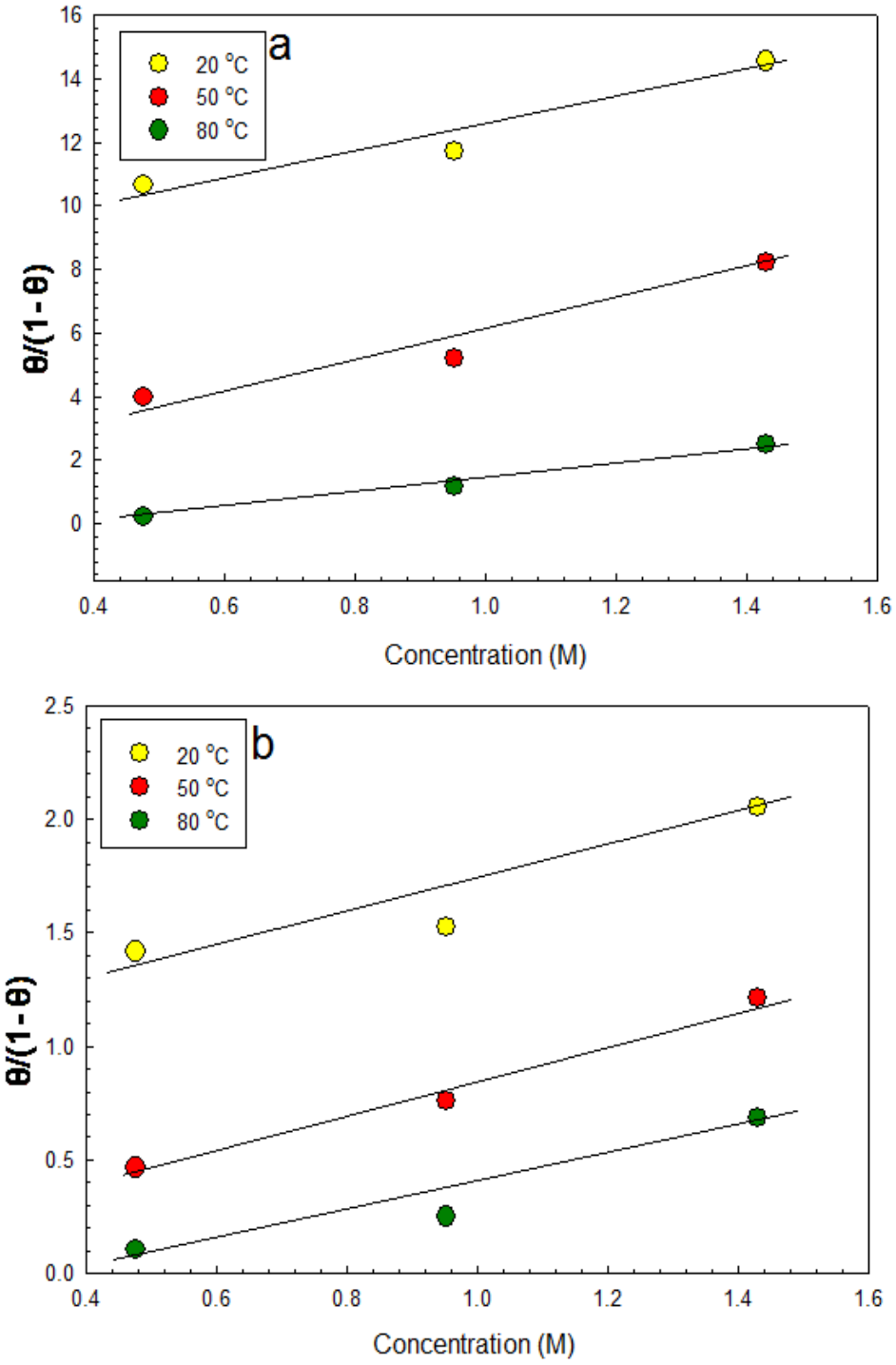

Figure 6.6. Langmuir adsorption plots at 20, 50, and 80 °C in a) Chloride free and b) chloride containing solutions

(T) is the absolute temperature in (K), and (R) is the universal gas constant equals to 8.314 J/K.mol.

Table 6.5. Adsorption Parameters at 20, 50, and 80 ^{o}C

Temperature (°C)	Salinity	B	R^2	Free Energy of adsorption (kJ/mol)	ΔH (kJ/mol)	ΔS (kJ/mol.K)
20	Chloride Free	7.83	0.936	-5.013	4.39	42.69
	Chloride Containing - 2 grams	1.383	0.875	-0.790	5.20	53.49
50	Chloride Free	7.19	0.943	-4.805	10.23	108.64
	Chloride Containing - 2 grams	1.176	0.979	-0.395	13.72	101.22
80	Chloride Free	4.26	0.975	-3.530	35.82	169.41
	Chloride Containing - 2 grams	1.064	0.982	-0.151	26.52	188.82

As expected, (B) decreased accordingly with the higher temperature and it was greater in chloride free solutions than that in chloride containing ones suggesting that the gradual replacement of adsorbed water molecules by oil was impeded by chloride. Additionally, (ΔG_{ads}) was more negative at lower temperatures and its range of variation with respect to temperature in chloride free and chloride containing solutions was relatively short. These trends indicate that the spontaneous adsorption studied is governed by the formation of donor-acceptor bond between the unpaired electrons and the active sites [Brett, 1993].

Langmuir adsorption isotherm can be expressed in an alternative expression involving enthalpy (ΔH) and entropy (ΔS) variations [Brett, 1993] as:

$$\frac{\theta}{1-\theta} = C \exp\left(-\frac{\Delta H - \Delta S}{RT}\right) \qquad (6.18)$$

This relation was plotted to produce linear plots, which are not shown here, of

(Ln(θ /(1- θ)) as a function of temperature reciprocal (1/T) with (R^2) close to unity. Adsorption enthalpy, calculated from ($\Delta H = - R \times slope$), showed an expected increase with the greater oil content and it was greater in chloride free conditions. The positive values indicated that the oil adsorption was an endothermic process and it is then confirmed that the stability of oil layers is chemisorption-based at which the charge transfer can form a coordinate bonding [Dahmani, 2010]. Oil adsorption is, as already found with other organic inhibitors in [Saleh, 2006] and [Solmaza, 2008], associated with an increase in randomness associated with the gradual desorption of multiple water molecules counteracting the expected orderness of oil adsorption. Therefore, the calculated entropy of adsorption showed a positive change and it increased with temperature.

6.7. Electrochemical Impedance Spectroscopy (EIS) measurements in oil free conditions

Nyquist plot impedance representations for chloride free and chloride containing conditions at 20, 50, and 80 ^{o}C are shown in Figure 6.7a and b. The impedance performance is characterized basically at the intermediate to the high frequency ranges by partial depressed semicircles reflecting the pure charge transfer controlled processes at active surfaces.

The semicircle sizes decreased with the higher temperature in both chloride free and chloride containing conditions with no indications to significant changes in the electrochemical interactions. The possibility for mass transfer influenced processes to occur were excluded in our cases differently from the observations studied in [Castro, 1986], instead, at low frequencies, inductive behaviors were indicated.

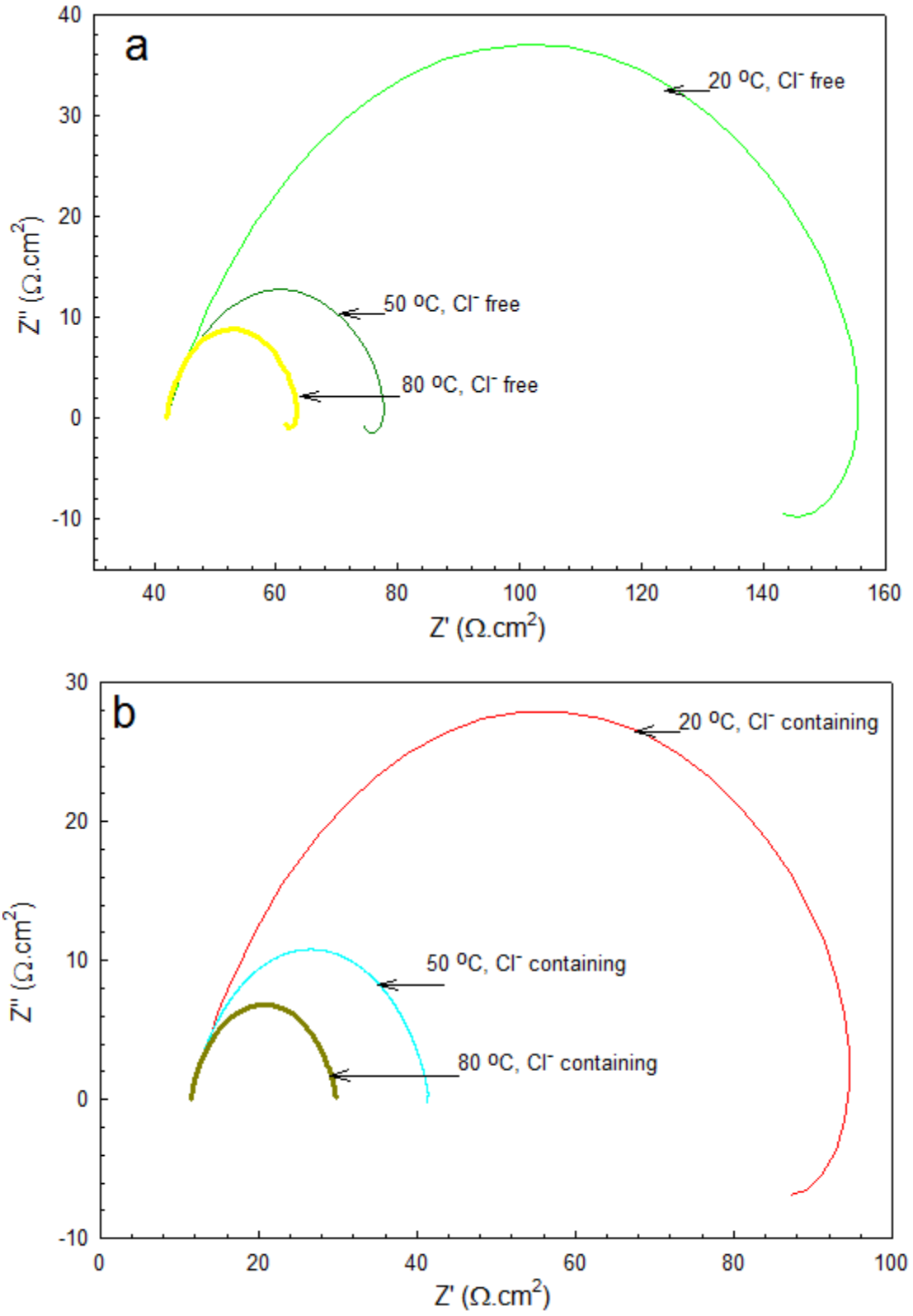

Figure 6.7. Nyquist impedance representation plots at 20, 50, and 80 °C in oil free a) chloride free and b) chloride containing solutions.

At these frequency ranges, important hints were revealed on the multistep nature of the corrosion mechanism in CO_2 saturated solutions where the role of active carbon carrying species became apparent when this electrochemical technique is utilized. In these conditions, the induction can be attributed to the adsorption of the active species acting on the steel surfaces and/or to the relaxation of reaction intermediates such as $[FeHCO_3^-]_{ads,}$ $[FeHCO_3^+]_{ads,}$ and $[FeOH^-]$ [Castro, 1986].

EIS investigations performed on the inductive behaviour [Farelas, 2010], [Moiseeva, 2005] referred $[FeOH^-]_{ads}$ to be in the consecutive steps in the dissolution mechanism as:

$$Fe + H_2O \leftrightarrow FeOH_{ads} + H^+ + e^- \qquad (6.19)$$

$$FeOH_{ads} \rightarrow FeOH^+_{sol} + e^- \qquad (6.20)$$

$$FeOH^+_{sol} + H^+ \leftrightarrow Fe^{2+}_{sol} + H_2O \qquad (6.21)$$

But in other conditions when the temperature-influenced pH level rises, the electrochemical contribution of (HCO_3^-) becomes considerable [Torres-Islas, 2008] where the adsorption of $[FeHCO_3^+]_{ads,}$ becomes important in the dissolution mechanism [Hirnyi, 2001] as:

$$Fe + HCO_3^- \rightarrow FeHCO_3^+ + 2e^- \qquad (6.22)$$

$$FeHCO_3^+ \leftrightarrow Fe^{2+} + HCO_3^- \qquad (6.23)$$

The adsorption and/or relaxation processes resulted in single phase peaks in the bode representations of varying intensities with temperature as shown in Figure 6.8a and 8b.

Impedance modules $|Z|$ decreased accordingly with the higher temperatures throughout the frequency range and the rate of change of $|Z|$ with the low frequency was slower with

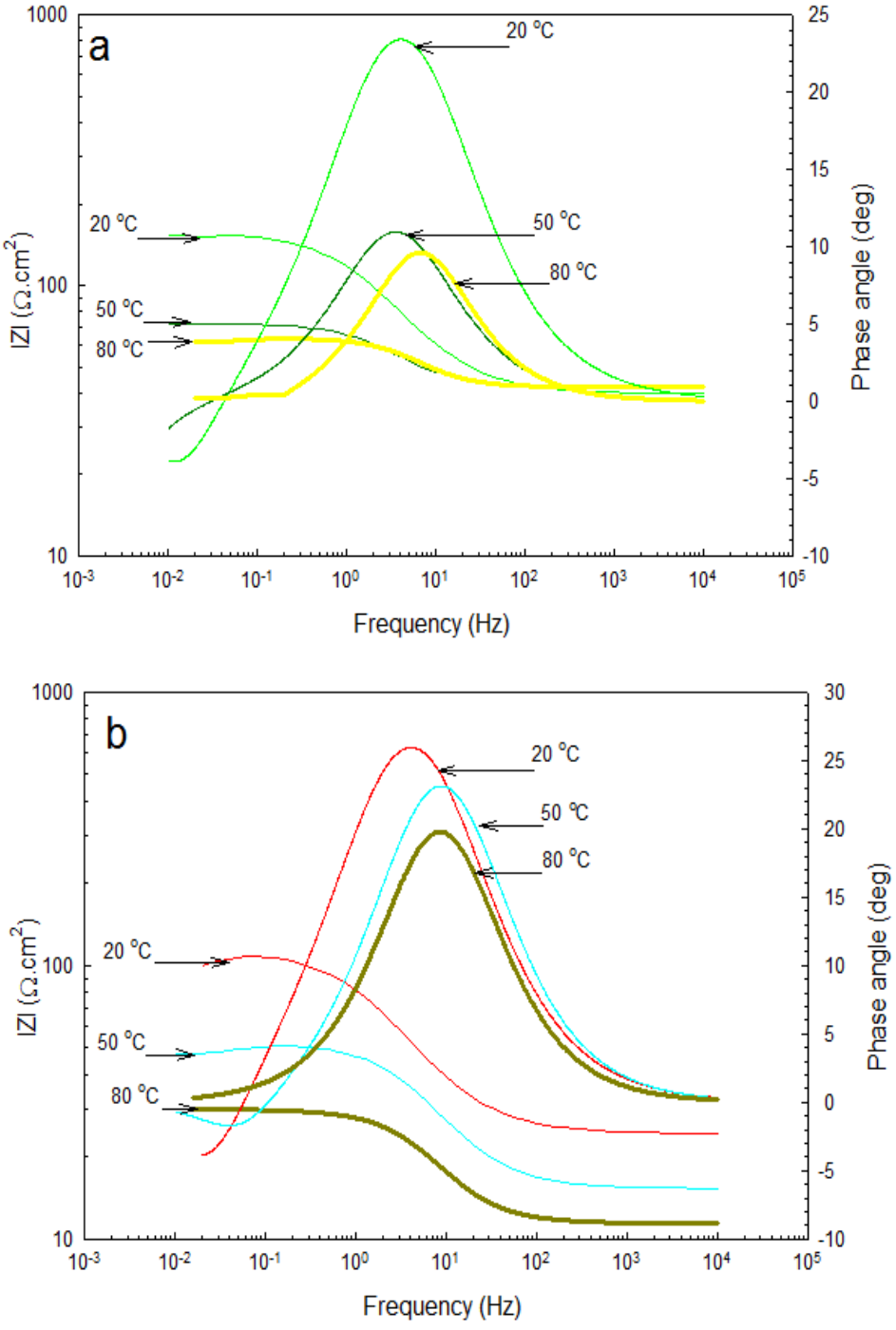

Figure 6.8. Bode impedance representation plots at 20, 50, and 80 °C in oil free a) chloride free and b) chloride containing solutions.

the higher temperatures. The significance of the associated induction-influenced processes at the low frequencies, resulting in small valleys in the bode phase representations, was more apparent at low temperatures. The introduction of chloride seemed not to influence the interfacial interactions but the accelerated kinetics resulted in smaller Nyquist semicircles; i.e. smaller charge transfer resistance and also in making the adsorption fields more inductive. The experimental impedance data were fitted with an equivalent electrochemical circuit of the configuration {R(Q(R(RL)))} and it is shown in Figure 6.9.

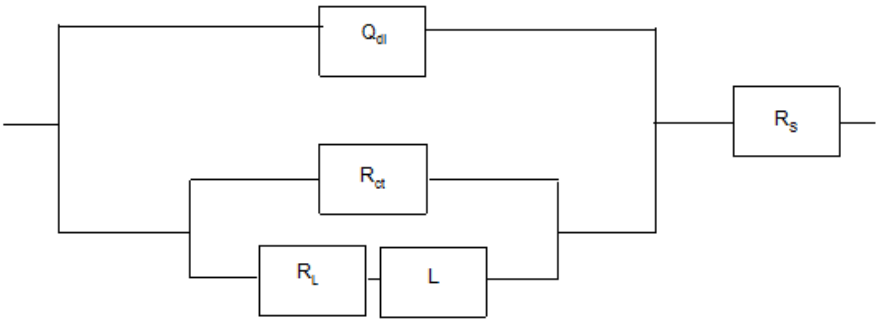

Figure 6.9. Equivalent circuit proposed for the electrochemical impedance response in chloride free and chloride containing oil free solutions

At the double layer, (R_{CT}) represents the charge transfer resistance and (Q_{dl}) is the Constant Phase Element (CPE) to compensate for the capacitance across the heterogeneous surface resulting in depressed capacitive semicircles [Cottis, 1999] and it is mathematically expressed as:

$$Z_{CPE} = \left[Q(j\omega)^{n}\right]^{-1} \qquad (6.24)$$

(ω) represents frequency, (j) equals to $\sqrt{-1}$, and (n) is (CPE) exponent. The solution resistance is represented as (R_S), and (R_L) and (L) represent the adsorption resistance and adsorption inductance respectively. It should be noted that other equivalent circuits were

attempted of two-time constant based type, as previously proposed in [Wang, 2011] and [Ortega-Toledo, 2010], to account for the adsorption and/or for effective electrochemical influence of possibly developed passive films, but no satisfactory fitting was achieved. The electrical components with their values are shown in Table 6.6 for chloride free and chloride containing oil free conditions.

Table 6.6. Impedance parameters in oil free conditions at 20, 50, and 80 ^{o}C

Components	Chloride free			Chloride containing		
	20 °C	50 °C	80 °C	20 °C	50 °C	80 °C
R_S ($\Omega.cm^2$)	42.09	42.18	42.02	11.34	11.39	11.4
Q_{dl} (F/cm^2)	0.0000170	0.0000232	0.0000221	0.0000240	0.0000373	0.0000349
n_{dl}	0.7061	0.7655	0.8046	0.712	0.7878	0.8083
R_{CT} ($\Omega.cm^2$)	93.674	32.15	19.29	68.92	25.02	18.37
R_L ($\Omega.cm^2$)	25.9	5	2.559	20.74	4.347	0.1059
L (H/cm^2)	273.6	25.77	6.313	124.4	16.6	0.09711
CHI-SQUARE	2.34E-05	7.50E-05	3.71E-05	3.55E-05	3.65E-04	7.16E-05

The introduction of chloride decreased the charge transfer resistance as well the associated resistance at the adsorption field and both showed an expected decrease with higher temperatures. The interfacial characteristics at the double layer were appreciably more capacitive in the chloride containing solutions and at higher temperatures. The confirmative fitting between the proposed electrochemical model and the experimental data are selectively shown in Figure 6.10.

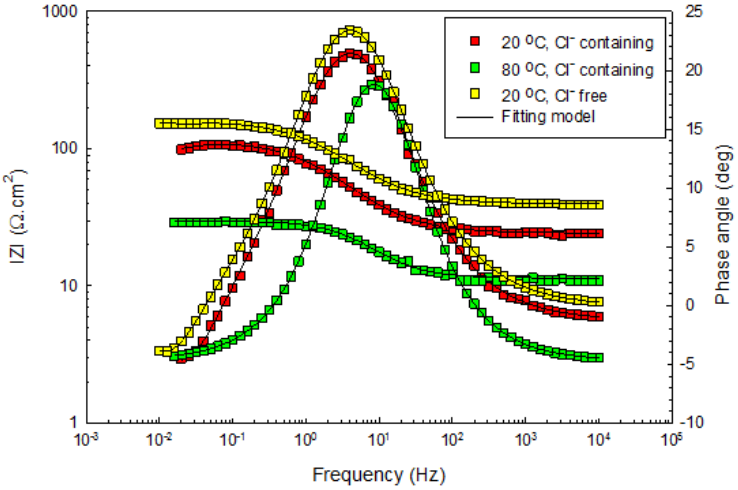

Figure 6.10. Experimental and calculated bode representations of impedance for selected temperature and chloride oil free conditions.

6.8. Electrochemical Impedance Spectroscopy (EIS) measurements in oil containing conditions

Nyquist plot representations for oil containing conditions reflected similar interaction mechanisms but indicated a greater influence from adsorption, rather than diffusion-limited processes, as shown in Figure 6.11a, and 11b for 10 % oil containing chloride free and chloride containing solutions respectively. The induction at low frequency ranges, which was more apparent than that in oil-free conditions, can now be attributed more to the stable oil adsorption. Nyquist semicircles were larger than those in oil free conditions, and confirming with the polarization test results, indicated the greater charge transfer resistance. In chloride containing conditions, Nyquist semicircles were smaller in chloride containing conditions where the active state was stronger, and similarly to the chloride free conditions, the dependence on temperature was very apparent where the dissolution mechanisms accelerated. In regard to the bode representations, single-peak and low-frequency-single valley, as shown in Figure 6.12a and 12b, appeared reflecting the greater role of oil adsorption in a fashion where a significant presence for a second time constant was excluded.

Therefore, the previously proposed electrochemical model for oil free conditions achieved a very good agreement with the experimental data assigning the same electrical components to the processes discussed in this context. In Table 6.7, the parameters and their values in all oil containing chloride free and chloride containing conditions showing the expected increase of (R_{CT}) with the greater oil amounts.

The charge transfer and the associated resistance across oil films decreased with the higher temperature in both salinity conditions. Impedance was more capacitive in the

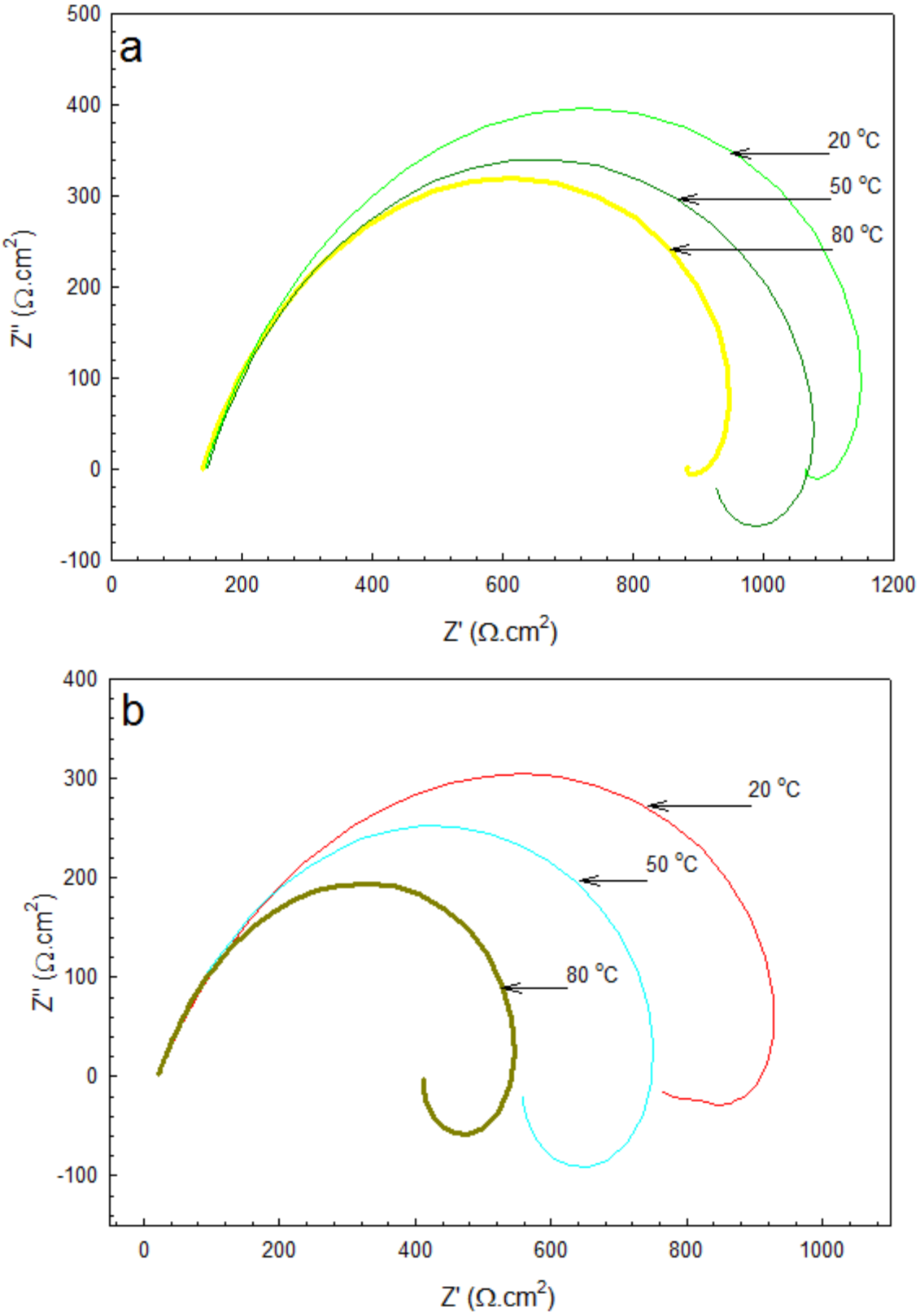

Figure 6.11. Nyquist impedance representation plots at 20, 50, and 80 °C in 10 vol% oil containing a) chloride free and b) chloride containing solutions.

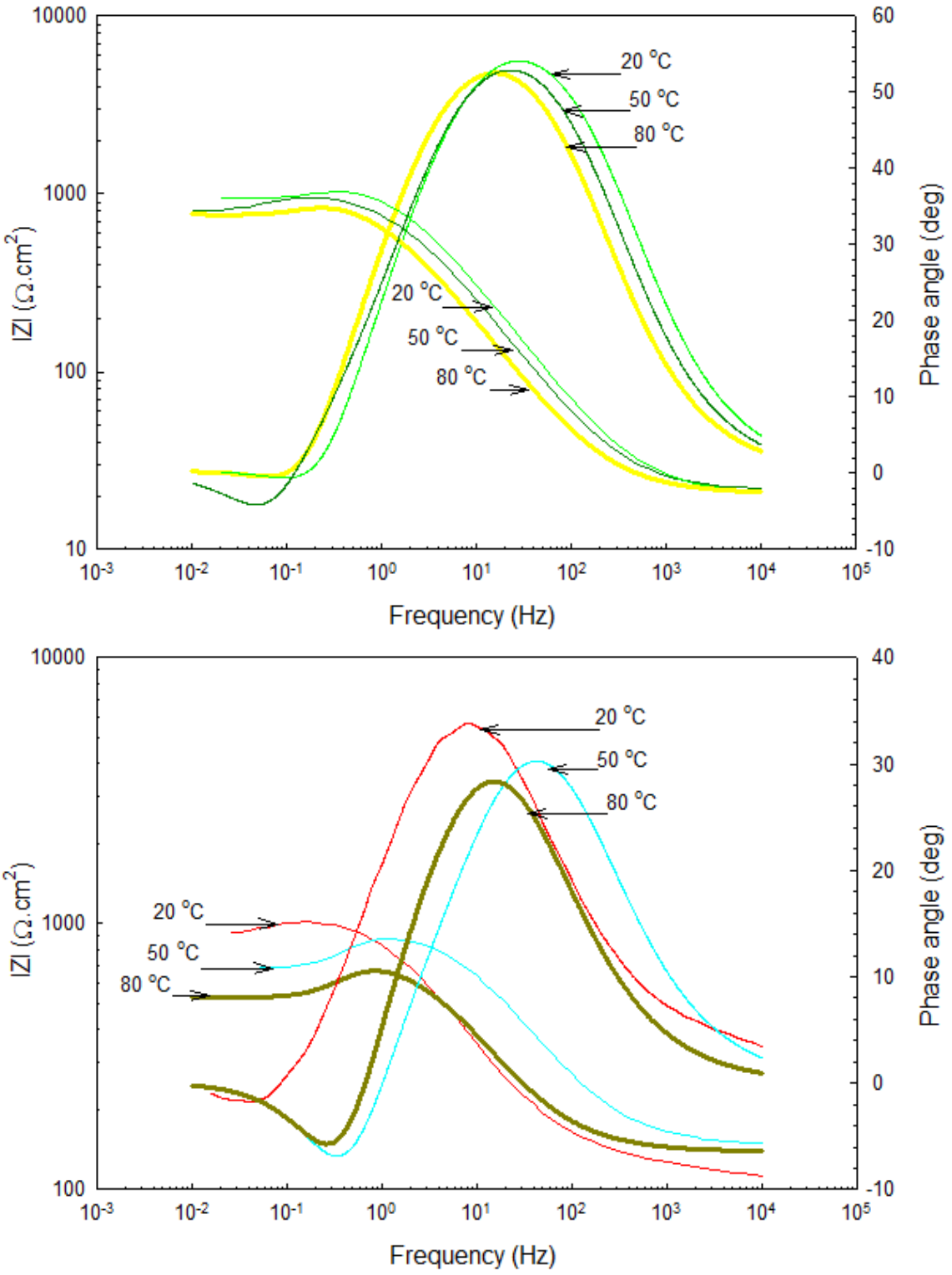

Figure 6.12. Bode impedance representation plots at 20, 50, and 80 ^{o}C in 10 vol% oil containing a) chloride free and b) chloride containing solutions.

chloride containing conditions and correspondingly at higher temperatures in conditions where the oil miscibility was less at higher temperatures and where consequently greater uncovered active areas were exposed [Jiang, 2005]. The confirmative bode plots for oil containing conditions are shown in Figure 6.13 for selected environments.

Table 6.7. Impedance parameters obtained from 10, 20, and 30 % oil containing conditions at 20, 50, and 80 ^{o}C

Components	Oil conditions	Chloride free			Chloride containing		
		20 °C	50 °C	80 °C	20 °C	50 °C	80 °C
R_S (Ω.cm^2)	10% Oil containing	147.8	145.8	138.5	20	21.3	20.5
Q_{dl} (F/cm^2)		0.00001374	0.00001686	0.00004373	0.00005133	0.0000628	0.0000649
n_{dl}		0.7427	0.7453	0.7513	0.7504	0.798	0.779
R_{CT} (Ω.cm^2)		929.5	782.1	752	802	536.4	392.9
R_L (Ω.cm^2)		295.2	253	240.2	291.6	277.8	243.9
L (H/ cm^2)		170.5	501.6	202.9	417.5	86.05	77.3
CHI-SQUARE		2.22E-05	3.42E-05	1.60E-05	5.88E-05	8.05E-05	1.92E-05
R_S (Ω.cm^2)	20% Oil containing	146.8	149.8	144.5	23	21.8	22.5
Q_{dl} (F/cm^2)		0.0000117	0.0000159	0.0000337	0.0000433	0.0000452	0.00004832
n_{dl}		0.7123	0.7111	0.7437	0.727	0.775	0.794
R_{CT} (Ω.cm^2)		1000.3	862.7	801.3	925.3	646.7	463.3
R_L (Ω.cm^2)		297.6	285.7	243.6	263.5	281.6	223.8
L (H/ cm^2)		271.3	346	212.7	418.1	88.03	75.3
CHI-SQUARE		1.46E-05	7.85E-05	1.21E-05	3.45E-05	2.18E-05	5.45E-04
R_S (Ω.cm^2)	30% Oil containing	141.5	151.6	145.2	22	23.7	24.5
Q_{dl} (F/cm^2)		0.0000112	0.0000136	0.0000235	0.0000451	0.0000452	0.0000458
n_{dl}		0.73231	0.7511	0.784	0.7411	0.782	0.787
R_{CT} (Ω.cm^2)		1088.2	891.3	831.6	936.9	687.6	495.1
R_L (Ω.cm^2)		287.3	277.6	223.1	273.7	279.3	213.2
L (H/ cm^2)		556.8	497.3	273.7	438.7	107.13	83.7
CHI-SQUARE		5.47E-05	9.99E-05	8.79E-05	1.17E-05	6.65E-05	8.79E-04

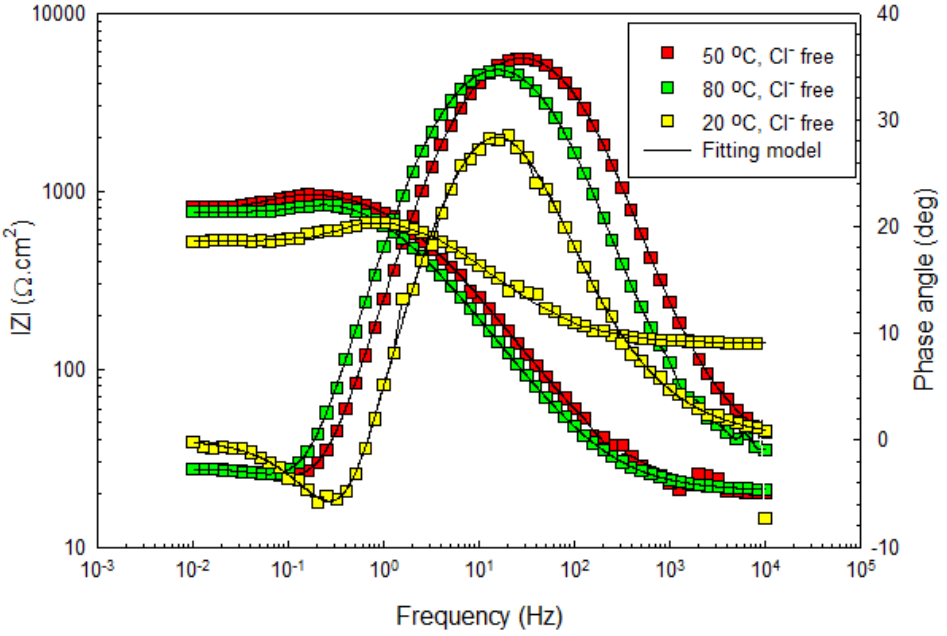

Figure 6.13. Experimental and calculated bode representations of impedance for selected temperature and chloride 10 % oil containing conditions.

Chapter 7: Results and discussion of the electrochemical investigations in high chloride containing CO_2-saturated media containing 10 vol% oil amounts

7.1. Test solutions

Corrosion tests were basically performed in unbuffered 1-bar-CO_2-saturated brines of sodium chloride concentrations of 5, 10, 40, and 80 g, prepared to be oil free solutions and 10 vol% oil containing emulsions. Except only with the potentiodynamic polarization measurements, chloride was introduced incrementally with an amount of 5 g in the range from chloride free to 80 g chloride containing to oil free solutions at 20 ^{o}C. In addition, the effect of carbon carrying species resulting from CO_2 dissolution was isolated in a separate potentiodynamic test performed in continuously N_2-purged brines at the same temperature and basic salinity conditions.

To achieve the effective homogeneity between the aqueous brines and the introduced oil, dioctyl sulfosuccinate sodium ($C_{20}H_{37}NaO_7S$) salt, an anionic surfactant, was added with 0.2 wt% to the oil containing test solutions. Table 6.1 shows selected properties of the emulsified hydrocarbon considered in our study. According to the classification criteria of crude oil based on the carbon number as well as on the density stated in [Lyons, 2005], the test hydrocarbon represents a typical medium-weight crude oil. Double distilled deionized water was utilized for all our test solutions and the salinity range was extended to include chloride up to 80 g considering extreme saline stratum water cuts accompanying the decreasing oil content from aging field wells [Mullin, 2008].

Two relatively extreme temperatures were selected for our electrochemical studies; 20 and 90 ^{o}C maintained within ± 1 ^{o}C.

7.2. Open Circuit Potential (OCP) measurements

Free open circuit potential variations were first measured at 20 and 90 ^{o}C in oil free and oil containing; chloride free, 10, 40 and 80 g chloride containing continuously CO_2 purged solutions. OCP decreased in a proportional manner with the chloride content in oil free and oil containing solutions and it seemed also that the nobler OCP's resulted at the low temperature; 20 ^{o}C accordingly. It is shown in Figure 7.1 selected OCP profiles at 20 ^{o}C specifically for oil free conditions and at 90 ^{o}C specifically for oil containing conditions reflecting the significant influence of oil, in addition to that of temperature's, in lowering OCP.

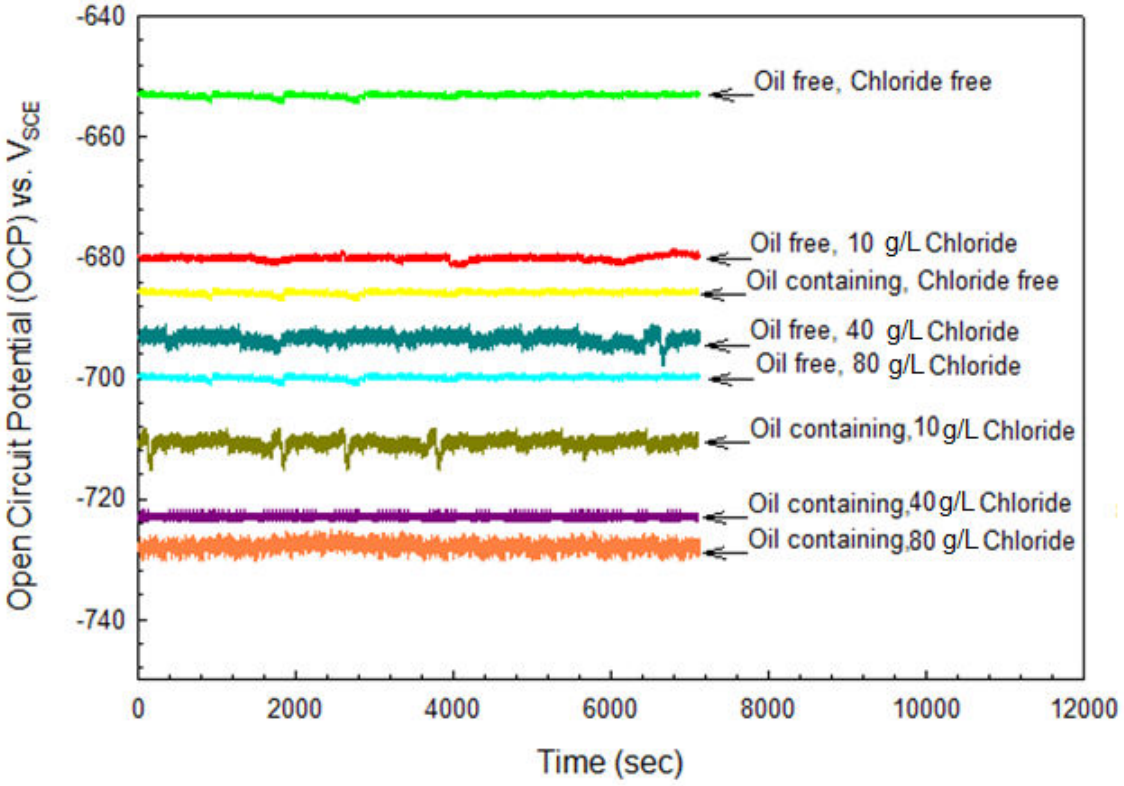

Figure 7.1. Selected Open Circuit Potential (OCP) profiles in oil free at 20 ^{o}C and in 10 vol% oil containing at 90 ^{o}C conditions.

Interestingly, the bands of variation of potentials with respect to the increased amount of chloride at the two "extreme" conditions were similar of as much as approximately 45 mV. During mixed potential conditions in these low-pH-level media between 4 and 5, the anodic dissolution as well as the cathodic reduction of carbon carrying species and hydrogen protons affected the active state depending on temperature, and salinity. Therefore, to consider the theoretical limits, the proposed electrochemical reactions governing the free conditions need to be studied. Basically, the direct oxidation of steel is expressed as:

$$Fe \rightarrow Fe^{2+} + 2e^{-} \quad (7.1)$$

In addition, especially at pH levels less than or equal to 5, in 1-bar-CO_2-saturated media, the plentiful amounts of carbonic acid (H_2CO_3) existing with considerable speciation equilibrium can have a greater role in the dissolution mechanism [Moiseeva, 2003] as:

$$Fe + H_2CO_3 \rightarrow FeCO_3 + 2H^{+} + 2e^{-} \quad (7.2)$$

Cathodic hydrogen generating reductions, which were reported in many studies as the governing reactions in carbon dioxide corrosion environments [Schmitt, 1983] and [De Waard, 1975], are driven by (H_2CO_3) and the associated (H^+) protons as:

$$2H^{+} + 2e^{-} \rightarrow H_2 \quad (7.3)$$

$$H_2CO_3 + e^{-} \rightarrow HCO_3^{-} + 1/2\,H_2 \quad (7.4)$$

Standard half cell potentials were calculated from Gibbs free energies of formation of the species, which are involved in the electrochemical reactions, listed in [Dean, 2000]. The theoretical limits by which the monitored OCP values were confined

within were in turn calculated, depending on temperature and pH, by utilizing Nernst half cell potential equation [Ahmed, 2006].

pH levels at 20 and 90 ^{o}C in the basic saline conditions of concern were obtained from the model proposed in [Li, 2007] for selected speciation equilibriums for H_2O-CO_2-NaCl systems. The model was in a good agreement with a separate experimental work [Crolet, 1983] performed for the same conditions at different molalities of (NaCl) with the maximum deviations of $\Delta pH < 0.2$. The effect of the appreciable amounts of oil of 10 vol% was neglected from the pH calculations. OCP values and the associated environmental factors in the oil free conditions with the calculated half cell potentials are all shown in Table 7.1.

Table 7.1. Open Circuit Potentials (OCP) and the calculated half cell equilibrium potentials for oil free conditions at 20 and 90 ^{o}C

Temperature	Salinity	pH	OCP	Equilibrium Potential (Reaction (7.1))	Equilibrium Potential (Reaction (7.2))	Equilibrium Potential (Reaction (7.3))	Equilibrium Potential (Reaction (7.4))
(°C)	(g)		(V_{SCE})	(V_{SCE})	(V_{SCE})	(V_{SCE})	(V_{SCE})
20	0	3.8	-653	-740	-762	-462	-632
	10	3.8	-680	-740	-762	-462	-632
	40	3.7	-693	-740	-756	-456	-626
	80	3.6	-701	-740	-750	-450	-620
90	0	5.2	-681	-754	-915	-615	-685
	10	5	-708	-754	-901	-601	-671
	40	4.8	-719	-754	-887	-587	-657
	80	4.6	-722	-754	-872	-572	-642

It is revealed the well containment of the measured OCP values within the theoretical limits taking into account the significance of the by-amount chloride on the modified kinetics at both anodic and cathodic regimes. It is interesting to observe that the cathodic sensitivity of OCP towards chloride content as well as towards temperature was accompanied by nobler potentials with the increased chloride content, as pH levels

become accordingly lower, at both temperatures, 20 and 90 ^{o}C, where the pH levels were also accordingly higher at the latter temperature.

All OCP data with respect to the salinity content and temperature in oil free and oil containing condition are presented in Figure 7.2. As discussed previously in this context, OCP decreased proportionally with the salinity content at 20 ^{o}C suggesting the considerable sensitivity of anodic reactions towards the small amount of chloride of 10 g when OCP noticeably decreased 30 mV.

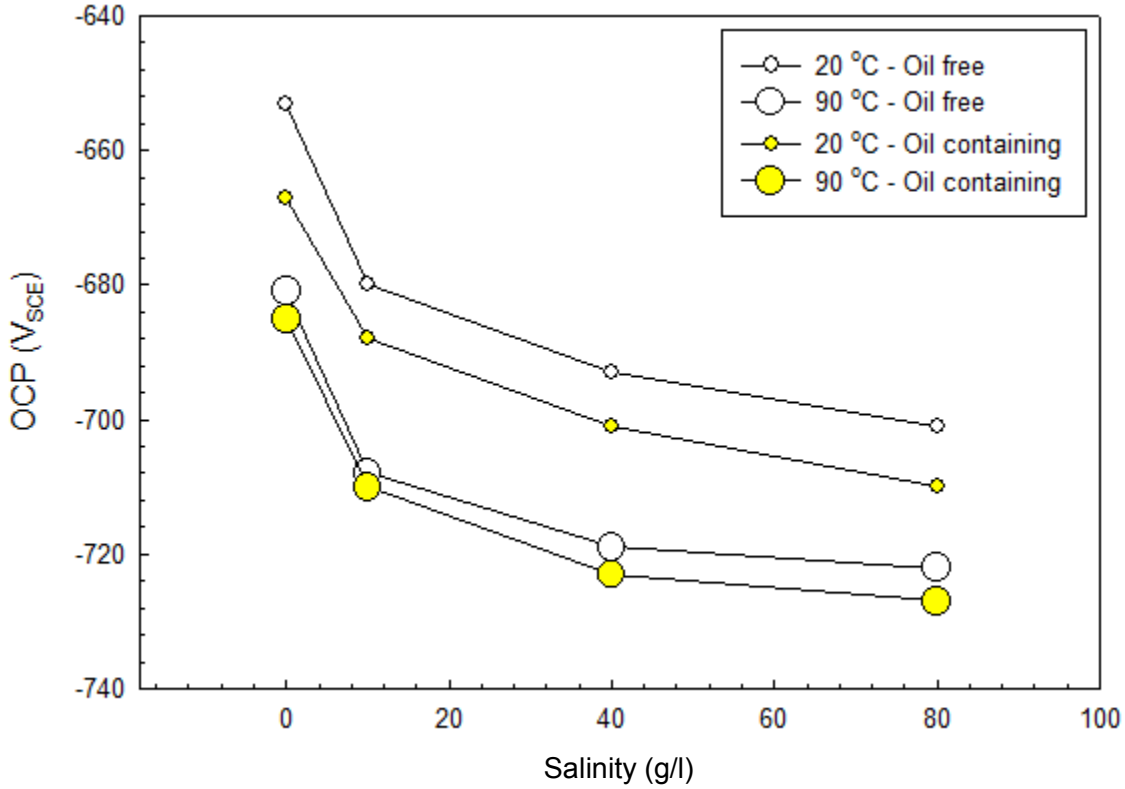

Figure 7.2. Open Circuit Potential (OCP) variations with respect to the salinity content at 20 and 90 ^{o}C in oil free and oil containing conditions.

However, the decaying response at the same temperature, as the chloride amount is doubled from 40 to 80 g, suggests that possibly physical factors at the interface affected the active behavior. At the end of the OCP measurements, considerable changes on the surface appeared suggesting that the mixed potential variations in the concentrated

CO_2-purged brines could be typically related to purely topographic surface factors where the anodic and cathodic regions could change in size or in location [Bard, 2001]. At 90 ^oC, the accelerated kinetics and the associated transport processes activated the surfaces becoming prevalently anodic as shown with the cases of chloride free and 10 g chloride containing solutions. This behaviour confirmed the polarization test results where upon accelerated dissolution reactions, the corrosion potentials decreased noticeably by as much as 20 to 30 mV comparatively with lower temperature conditions. The trend with respect to the whole chloride content range was preserved irrespectively from the high temperature and the justifications on the variations of OCP in 40 and 80 g chloride containing conditions at 20 ^oC could still be valid for this case as discussed from kinetic points of view in the polarization tests part.

Oil seemed to induce purely cathodic inhibitive effect, as the corrosion rates necessarily decelerate and the stable organic films reduced OCP. The significance of oil addition was most effective in conditions where it was most miscible in chloride free and low chloride containing conditions. Interestingly, it seemed also that oil caused OCP to decrease steadily throughout the salinity range at the low temperature 20 ^oC. At 90 ^oC, oil inhibition was still cathodic but its influence was limited as was its temperature-dependent miscibility. The steady range of the reduced OCP was also noticeable even with the concentrated brine of 80 g chloride. Oil in that case could play the same role but more significantly with the more facilitated passivation in such condition as discussed in the polarization test part considering also the physical changes on the steel surface that could be investigated by Scanning Electron Microscopy (SEM) in a separate future work.

7.3. Potentiodynamic polarization measurements in oil free conditions

Potentiodynamic polarization profiles at 20 ^{o}C produced from 5 to 80 g chloride containing oil free solutions are all shown in Figure 7.3. The basic trend reflects the expected anodic sensitivity towards chloride addition with the few amounts and then the continuously decreasing corrosion potential (Ecorr), was accompanied by lower corrosion rates with greater chloride amounts.

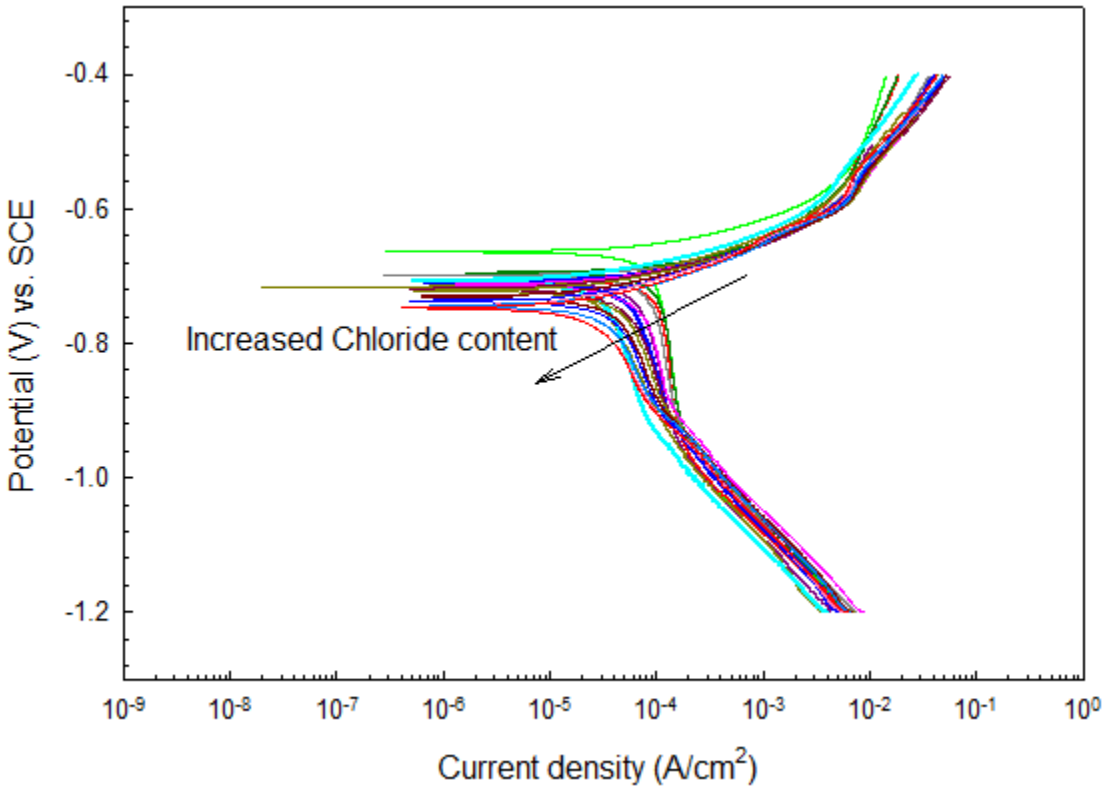

Figure 7.3. Potentiodynamic polarization profiles at 20 ^{o}C produced from oil free CO_2-saturated media containing chloride added incrementally with an amount of 5 g from 5 to 80 g.

In the low cathodic overpotentials right below the corrosion potential down to -1 V_{SCE}, the mass-transfer limited cathodic reduction seemed to control hydrogen evolution reactions in these low-pH media of about 4. However, at lower overpotentials, the total

cathodic reduction reactions seemed to be specifically controlled by charge transfer reactions at which a different specie getting reduced at lower potentials, but showing a considerable higher rate with the chloride content. At the anodic branch, similar trends were also exhibited where the anodic dissolution proceeded with appreciable dependence on the chloride content but before an evidence for retardation appearing at about -0.5 V_{SCE}.

Corrosion current density (i_{corr}), and the associated kinetic parameters (β_a), and (β_c) were calculated from Butler-Erdey-Volmer (BEV) equation as [Stansbury, 2000]:

$$i = i_{corr}\left(\exp\left[\frac{2.3\eta_s}{\beta_a}\right] - \exp\left[\frac{-2.3\eta_s}{\beta_c}\right]\right) \qquad (7.5)$$

The parameters of concern were iteratively calculated with the best fit within the charge transfer controlled reactions, and both (β_a) and (β_c) were within quite similar ranges of variation between about 40 to 80 mV/decade following the similar trends of the anodic and cathodic branches with respect to the chloride content.

As shown in Figure 7.4, for 20 ^{o}C, (i_{corr}) increased with the greater chloride content from the chloride free up to 30 g chloride containing conditions where (E_{corr}) decreased accordingly along the chloride content range.

This interesting behavior reflects the by-amount chloride changing roles with respect to the anodic and cathodic reactions during polarization where the corrosion rate reached a “peak” value. The maximum corrosion current density in this case is associated with the greatest sensitivity that the corroding steel surface could show towards accelerated anodic reactions before the retardation of cathodic reactions start to govern the polarization behavior with the increased chloride contents.

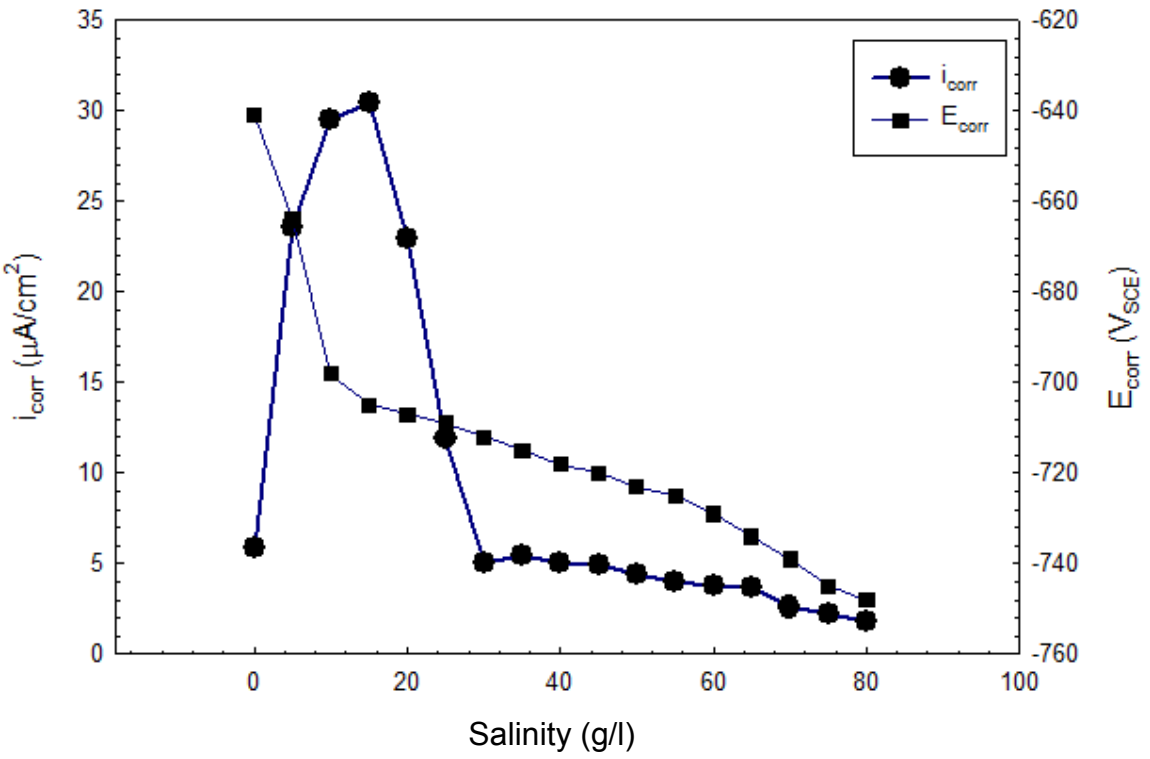

Figure 7.4. Corrosion current density (i_{corr}) and corrosion potential (E_{corr}) variations with respect to the salinity content at 20 ^{o}C in oil free CO_2-saturated conditions.

The behaviors of the anodic and cathodic reduction are further studied with selected salinity profiles but considering also the chloride free conditions and higher-pH-N_2-purged media as shown in Figure 7.5.

Due to the multi-contributing chemically existing species of (H^+), (H_2CO_3), and (H_2O) in the cathodic reactions, the evaluation was performed first in continuously purged nitrogen media at which the contribution of (H_2O) is more specifically determined. As apparently exhibited, the progressively accelerated anodic reactions with the chloride content made the corrosion rates greater along with lower corrosion potentials. Comparatively, the corrosion rates, shown in Figure 7.6, in these conditions were lower than those at CO_2-purged conditions with the respective chloride amounts before and

after the inflection exhibited in Figure 7.4, taking into account the much denser, and more effective carbon-based passivity formed at high chloride containing CO_2-purged conditions.

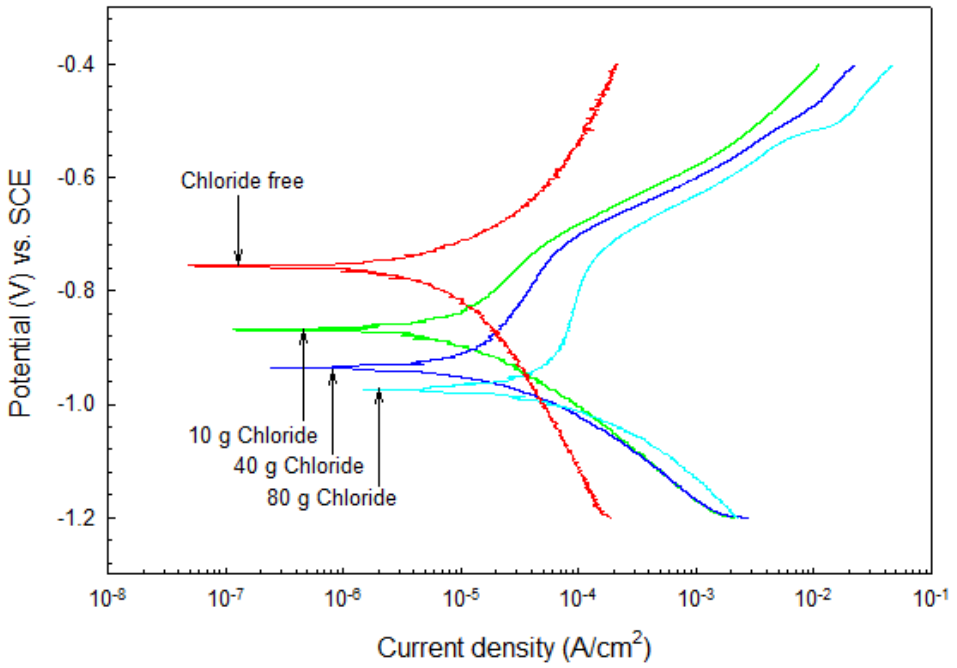

Figure 7.5. Potentiodynamic polarization profiles at 20 ^{o}C produced from oil free N_2-saturated chloride free, 10, 40, and 80 g chloride containing

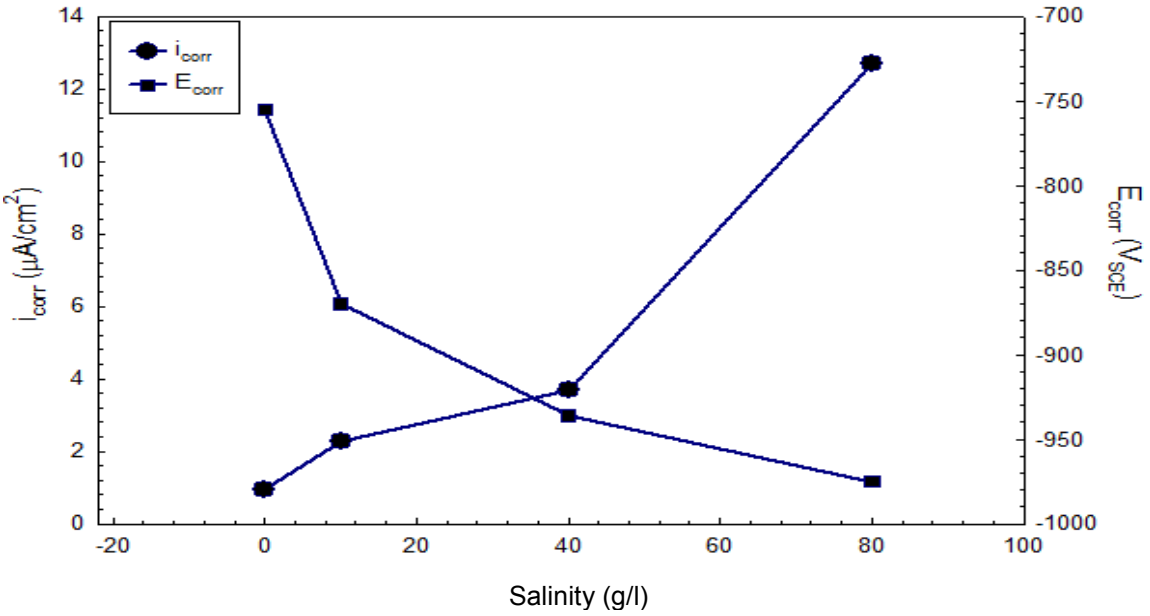

Figure 7.6. Corrosion current density (i_{corr}) and corrosion potential (E_{corr}) variations with respect to the salinity content at 20 ^{o}C in oil free N_2-saturated conditions.

In addition, the corrosion potentials were quite lower than those in CO_2-purged conditions reflecting the important, at least from Nernst-based equilibriums, sensitivity of water reduction expressed in equation (7.6) towards the lower pH levels in CO_2-purged media as already reported in [Sun, 2003] as:

$$2H_2O + 2e^- \rightarrow 2OH^- + H_2 \qquad (7.6)$$

From Figure 7.5, although that the sensitivity towards greater chloride content diminished and the cathodic shoulders of water reduction extended accordingly, exhibiting the enhanced kinetics, or at least in making the reduction to be more charge-mass mixed transfer controlled. At the anodic side, it seemed that due to the absence of readily contributable carbon carrying species in the anodic dissolution mechanisms, the anodic reactions were slower than those in CO_2-purged conditions.

In addition, the dependence on chloride content was clearer in being proportional on its content and where strong retardations in the anodic dissolution appeared. This phenomenon occurred before the second acceleration of the anodic reactions occurring at similar potentials at around -0.735 $V_{SCE.}$ Interestingly, the potential range of effective retardation was broader, indicating the earlier passivity, but at higher current densities ranging from 150 to 230 mV in 10 and 80 g chloride containing conditions respectively. During these potential ranges of concern, the retardations can reveal the multistep role of intermediate species such as ($FeOH^+$) [De Waard, 1975] or alternatively the direct involvement of ($FeOH^-$) [Zhang, 2009 (B)] and water [Davies, 1980] as:

$$Fe + OH^- \leftrightarrow FeOH^-_{ads} \qquad (7.7)$$

$$FeOH^-_{ads} \rightarrow FeOH_{ads} + e^- \qquad (7.8)$$

$$FeOH_{ads} \rightarrow FeOH^+_{ads} + e^- \qquad (7.9)$$

$$FeOH^{+}_{ads} + OH^{-} \rightarrow Fe(OH)_2 \rightarrow Hydrous\left[Fe(OH)_2\right] \qquad (7.10)$$

$$Fe + H_2O \rightarrow Fe(OH)_2 + 2H^{+} + 2e^{-} \qquad (7.11)$$

The distinct difference in the polarization performance in the two conditions, N_2-purged and CO_2-purged are more elucidated considering the chloride free and 10 g chloride addition in Figure 7.7. At the anodic branches, corrosion rates were accelerated at lower overpotentials upon the addition of chloride, but the accelerated irretardatible reactions in CO_2 conditions proceeded simultaneously with the total mass-transfer limited reduction of (H^{+}) (and/or (H_3O^{+})) and (H_2CO_3) as [Schmitt, 1983]:

$$H_2CO_{3\,(ads)} + e^{-} \rightarrow H_{(ads)} + HCO^{-}_{3\,(ads)} \qquad (7.12)$$

$$H_3O^{+}{}_{(sol)} + e^{-} \rightarrow H_{(ads)} + H_2O \qquad (7.13)$$

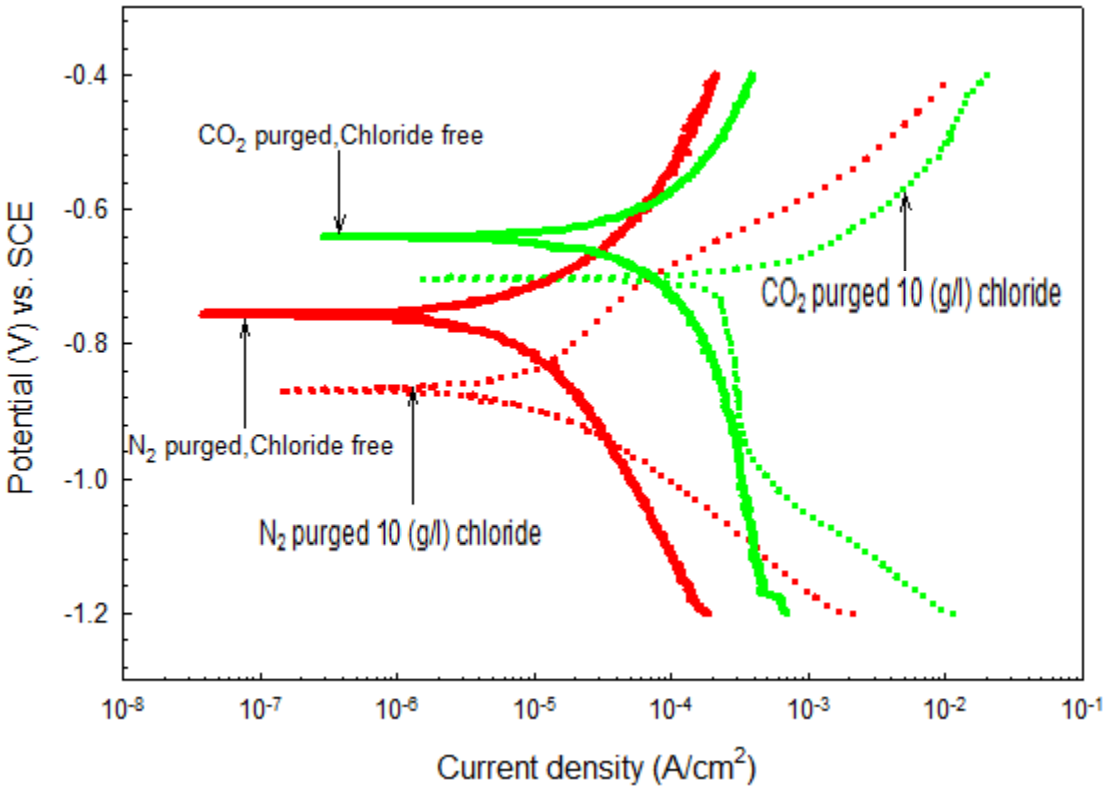

Figure 7.7.Potentiodynamic polarization profiles at 20 °C produced from oil free N_2 and CO_2-saturated chloride free and 10g chloride containing media.

However, the retarded anodic dissolution intersected the accelerated charge-transfer reduction of water in N_2-purged media. In addition, it is also evident the accelerated charge transfer reduction of water, comparing both chloride containing solutions influenced by lower pH levels, by almost an order of magnitude.

Selectively, at 20 and 90 ^oC, polarization profiles are shown for chloride free and chloride containing CO_2-purged solutions in Figure 7.8a, and b. The changes in corrosion rate and in the associated corrosion potential are discussed previously in this context in regard to 20 ^oC where the low-chloride accelerated corrosion rates were finally inhibited with greater amounts of chloride as already reported in a similar work performed at 5 ^oC [Fang, 2006]. In our case, it is interesting to observe a "bow" on Evans map corresponding to that phenomenon where the mechanisms of cathodic reactions, or at least the significance of electrochemical roles of the reducible species changed.

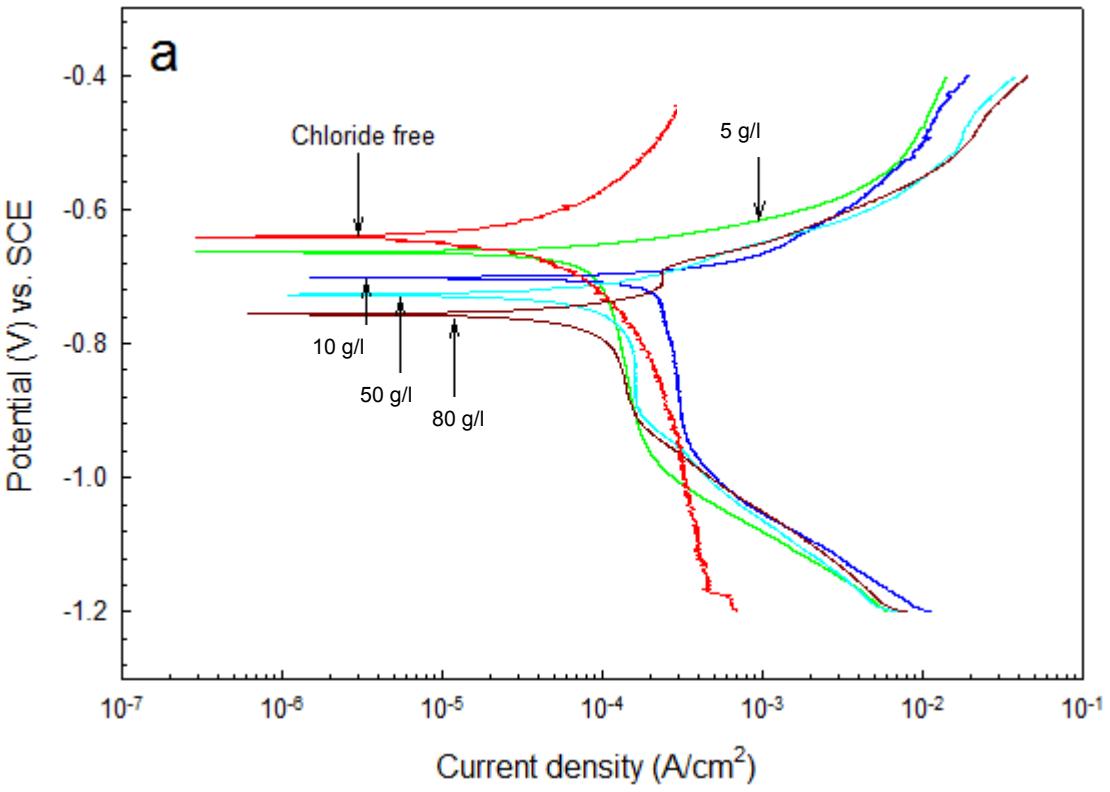

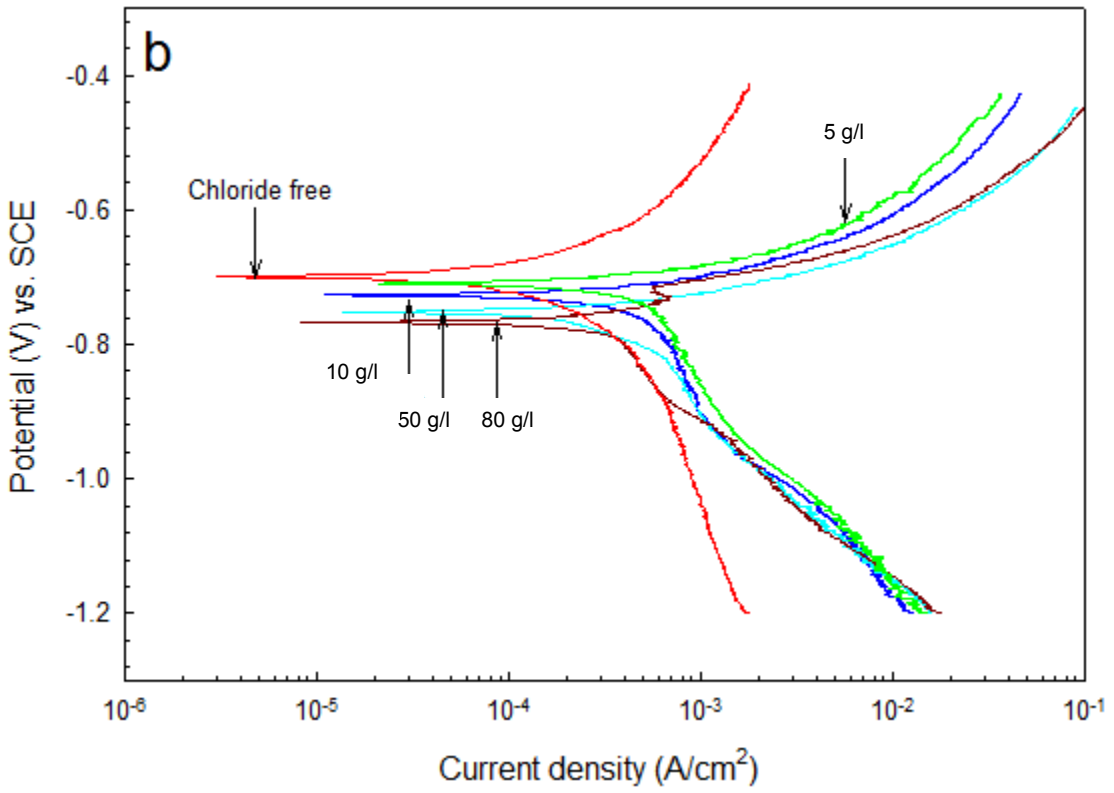

Figure 7.8. Potentiodynamic polarization profiles produced from oil free CO_2-saturated chloride free, 5, 10, 40, and 80 g chloride containing media at a) 20 ^{o}C and b) 90 ^{o}C

With the increased amounts of chloride, the tendency for more effective covering corrosion products seemed to be the controlling parameter in the rates of cathodic reactions. In other words, the decreased corrosion rates along with the decreased corrosion potentials are related to the inhibited cathodic evolution of hydrogen which were possibly occurring, but at lower rates, on the corrosion products rather than on the active surfaces at these ranges of potential. At the higher temperature, 90 ^{o}C, the corrosion current density followed, with the selected data points, the same trend of that of 20 ^{o}C and it was substantially as greater as two orders of magnitude at lower corrosion potentials as shown in Figure 7.9. Although of the similar, but accelerated, trends of the cathodic reduction reactions at this high temperature, however, water reduction seemed to

contribute more greatly in the controlling cathodic reduction reactions as the range of mass-limited reduction of (H^+) and (H_2CO_3) became increasingly shorter with the greater chloride content.

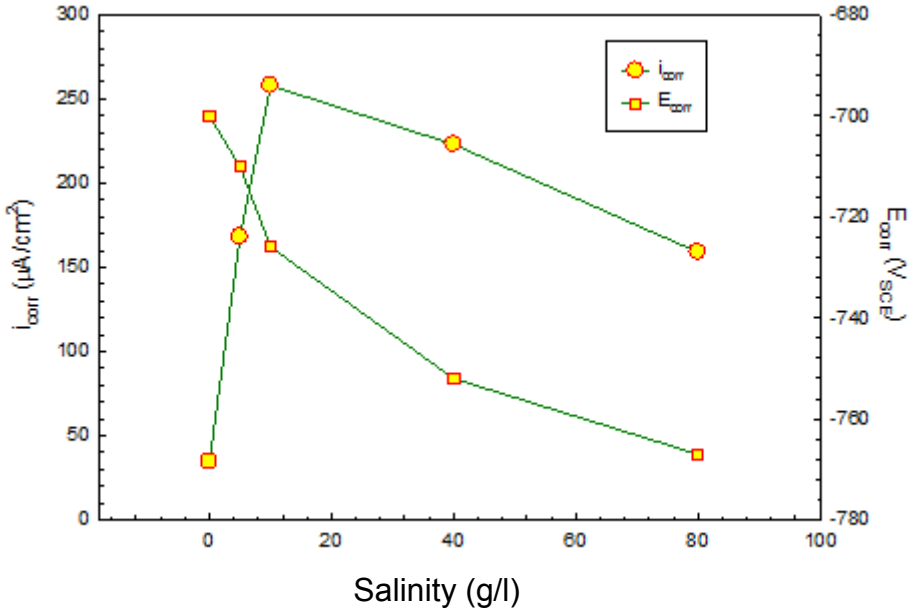

Figure 7.9. Corrosion current density (i_{corr}) and corrosion potential (E_{corr}) variations with respect to the salinity content at 90 ^oC in oil free CO_2-saturated conditions.

At 20 and 90 ^oC, the anodic dissolution in 80 g chloride containing conditions, specifically, exhibited a clear retardation in a form of short, but relatively vertical overpotential, before the continuous dissolution, reflecting the great influence of chloride in facilitating the formation of more effective pre-passive barriers. This behaviour could be very compliant to Linter and Burstein's views [Linter, 1999] on the accelerated active dissolution when $Fe(OH)_2$ became more readily switchable to $FeCO_3$ in the presence of the dissolved CO_2 as:

$$Fe(OH)_2 + CO_2 \rightarrow FeCO_3 + H_2O \qquad (7.14)$$

7.4. Potentiodynamic polarization measurements in oil containing conditions

The corrosion rates were considerably lower upon the addition of oil getting adsorbed on the polarized corrosion surfaces at different extents depending basically on its greater lower-temperature miscibility. As shown in Figure 7.10a, potentiodynamic profiles exhibited similar trends with respect to the increased chloride content but the decreased corrosion rates where also accompanied by lower corrosion potentials suggesting the cathodic inhibitive capability of the hydrocarbon.

At this low temperature, the greatest inhibition at both anodic and cathodic branches was achieved in the absence of chloride where oil had a better chance for effective and direct adsorption but causing considerable current noises. These noises in the current density were more significant at the low negative overpotentials, where as discussed in [Eliyan, 2011 (B)], were possibly related to the agglomerative hydrogen evolution through, the more effective or more covering, organic oil layers. The interfacial role of oil adsorption across the low-leveled-pH gradients in the chloride containing conditions seemed to influence greatly the mass-limit reduction of hydrogen protons and the reducible carbon carrying species at potentials above -1 V_{SCE}.

In these regions right below the corrosion potential, the cathodic shoulders substantially expanded indicating the effective influence of adsorbed oil on the reduction mechanism, where charge transfer for water reduction seemed to have a better role with greater chloride contents. In chloride free and 5 g chloride containing conditions, the anodic retardations occurred earlier and at decelerated current densities reflecting the effect of

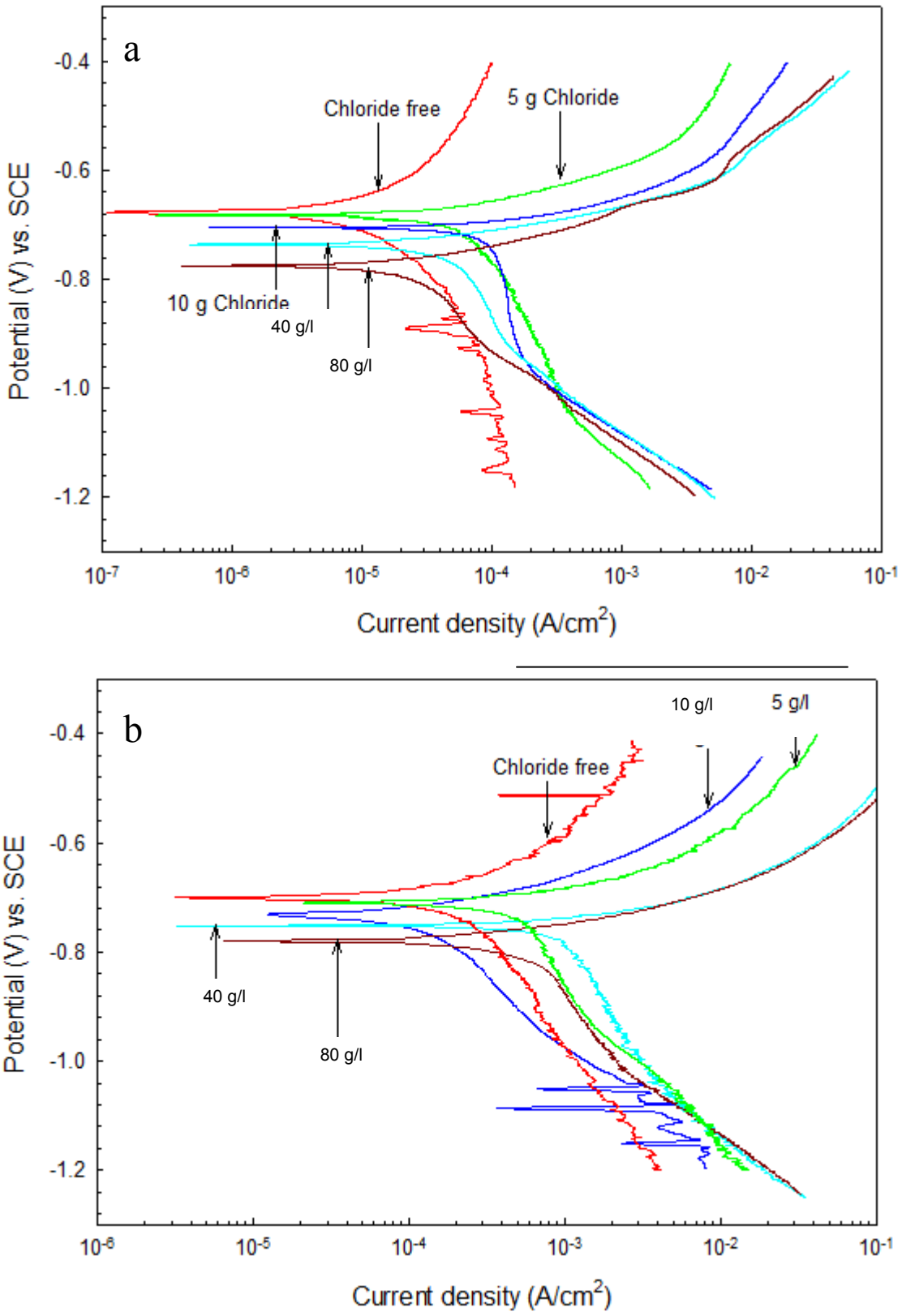

Figure 7.10 Potentiodynamic polarization profiles produced from oil containing CO_2-saturated chloride free, 5, 10, 40, and 80 g chloride containing media at a) 20 ^{o}C and b) 90 ^{o}C

oil although of the lack of good indications of electrochemical oil adsorption as previously reported in [Zhang, 2001] for imidazoline-based inhibitor.

The absence of short-ranged multi slopes in the active region, comparatively with oil free conditions, was accompanied by final passive film retardations occurring at extended, but decelerated current densities in higher chloride containing conditions. Oil seemed to influence the passivity formation process by stable adsorption on the active surface, impeding the passivity, or occurring on the fast already occurring passive films. This argument could be related to the substantial amounts of oil found adsorbed on the white/silver passive films on our corrosion specimens at the end of the relatively less-sloped passive polarizations terminated at about -0.4 V_{SCE}.

Kinetically, the effect of oil on the lower corrosion rates was analyzed from the variations in corrosion inhibition (η) and differences in corrosion potential between oil free and oil containing conditions (ΔE_{corr}) with respect to the salinity content as shown in Figure 7.11a. The efficiency was as high as 50 to 70 % in chloride free and 5 g chloride containing conditions before it decreased with the greater chloride amounts of 10 and 40 g.

The passive films were readily to be more effective and the oil miscibility, an important parameter for good adsorption, was increasingly limited in these more concentrated brines as visualized from the laboratory observations. Oil inhibition was very cathodic where corrosion potentials in all salinity conditions at this low temperature were less than those in oil free conditions. The greatest difference in corrosion potentials was in the chloride free condition of about 35 mV and then decreasing with the greater chloride content before it increases again in 40 and 80 g chloride containing solutions.

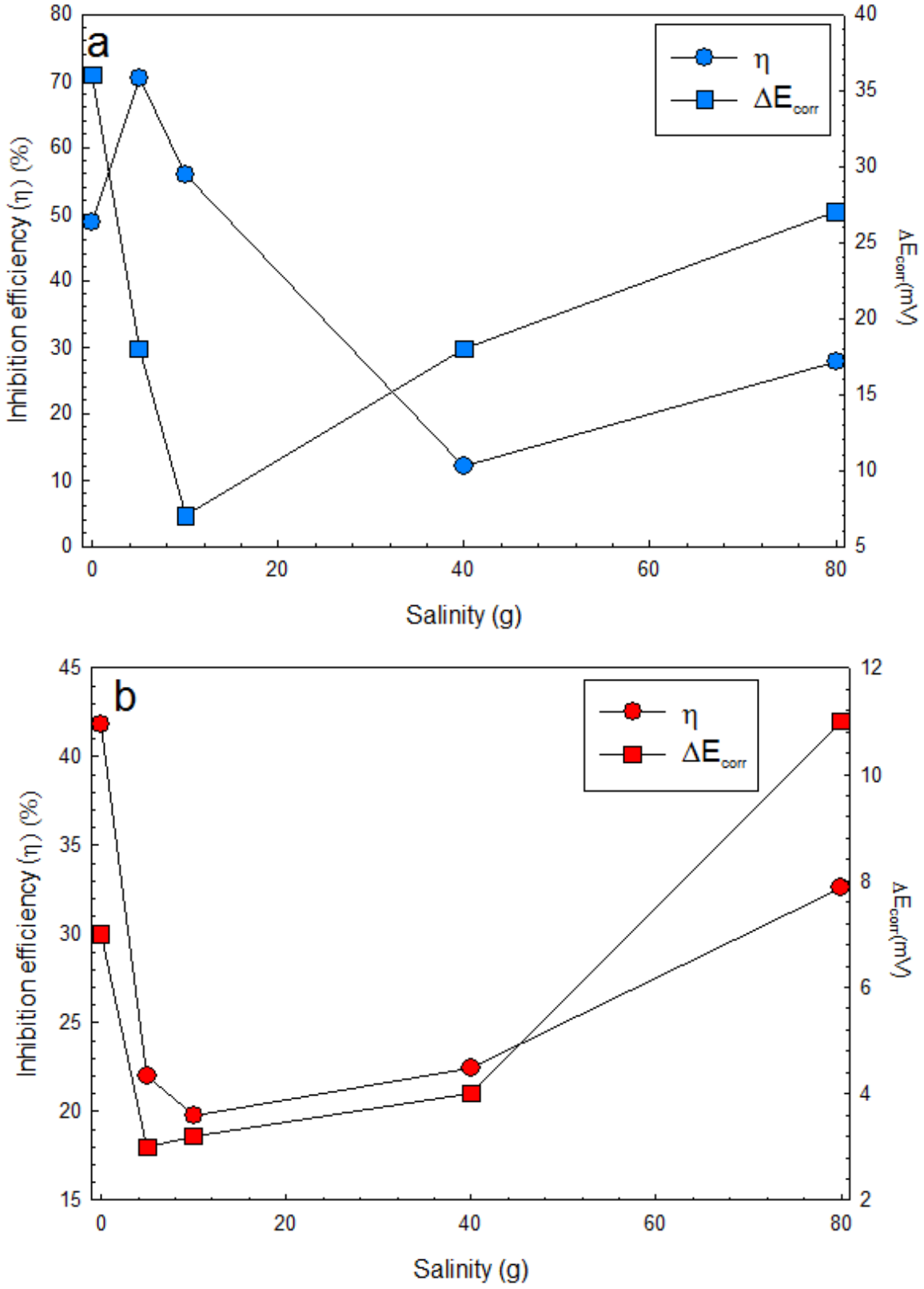

Figure 7.11. Corrosion inhibition efficiency and corrosion potential difference obtained between oil free and oil containing conditions at a) 20 ^{o}C and b) 90 ^{o}C.

This increasing trend along with that similar of (η) with greater chloride additions of 40 g could be greatly related to the effective incorporation, not necessarily to the active adsorption, in the more effective passive film formations leading to better passivity layering. This argument could be also related to a different role acted by oil when strong passivation is formed where oil could also establish good inhibition on the passive films alternatively.

At the higher temperature, 90 ^{o}C, the corrosion rates were considerably higher and the influence on the mass transfer-limited cathodic reactions was greater. The cathodic reactions seemed to be of more mixed charge-mass transfer controlled and the role of water reduction was expectedly higher with considerable current density noises as shown in Figure 7.10b. The corrosion potentials were the least negative among the other temperature and oil conditions with respect to the salinity content. The inhibitive capabilities of oil were still cathodic irrespectively from the high temperature at all salinity conditions. In addition, (ΔE_{corr}) followed appreciably the same trend of that at 20 ^{o}C, as shown in Figure 7.11b, and the proposed justifications in that context would be valid although of the less (ΔE_{corr}) at 90 ^{o}C. Also, oil with less higher-temperature efficiency seemed to preserve the same capabilities during passivation and in a proportional manner with the greater salinity content where the accelerated hydrogen evolution accelerated the anodic dissolutions accordingly allowing oil to be a part, with a considerable proportion, of the passive film structures as discussed also in detail in [34].

7.5. Electrochemical Impedance Spectroscopy (EIS) measurements in oil free conditions

Nyquist impedance representations for oil free conditions at 20 ^{o}C are shown in Figure 7.12a revealing a similarity between the appreciably depressed semicircles produced. In addition, at low frequency ranges, slight extensions developing to be considerable "overlapped" parts as the test brines were more concentrated.

The implied similarity suggests the relative independence of the overall dissolution mechanisms from the chloride content although of the noticeable changes in the rates of the processes involved. In this context, the tendency for greater charge transfer seemed to be proportionally favourable with the chloride content as the interactions at the free conditions are related to the localized, chloride sensitive, pH gradients [Ren, 2010]. Therefore, Nyquist size was the greatest in the absence of the by-amount introduced chloride with solution resistance (R_s) as greater as an order of magnitude than those in chloride containing solutions. It seemed that there is good applicability of a single-time constant based impedance response, where a single identifiable peak appeared within almost the same-order of magnitude of a frequency range of between 25 to 100 Hz in chloride containing conditions. However, the low-frequency extensions in chloride free and low chloride containing solutions as well as the appreciably merged semicircles in the concentrated one of 80 g suggests an impedance responses effectively modeled by an equivalent nested circuit. In that circuit, the associated adsorptions of intermediate species during corrosion are given specific resistive and phase elements but not necessarily a diffusion, non applicable to our data, Warburg element as already suggested for similar responses in [Zhang, 2011] and [Yin, 2010].

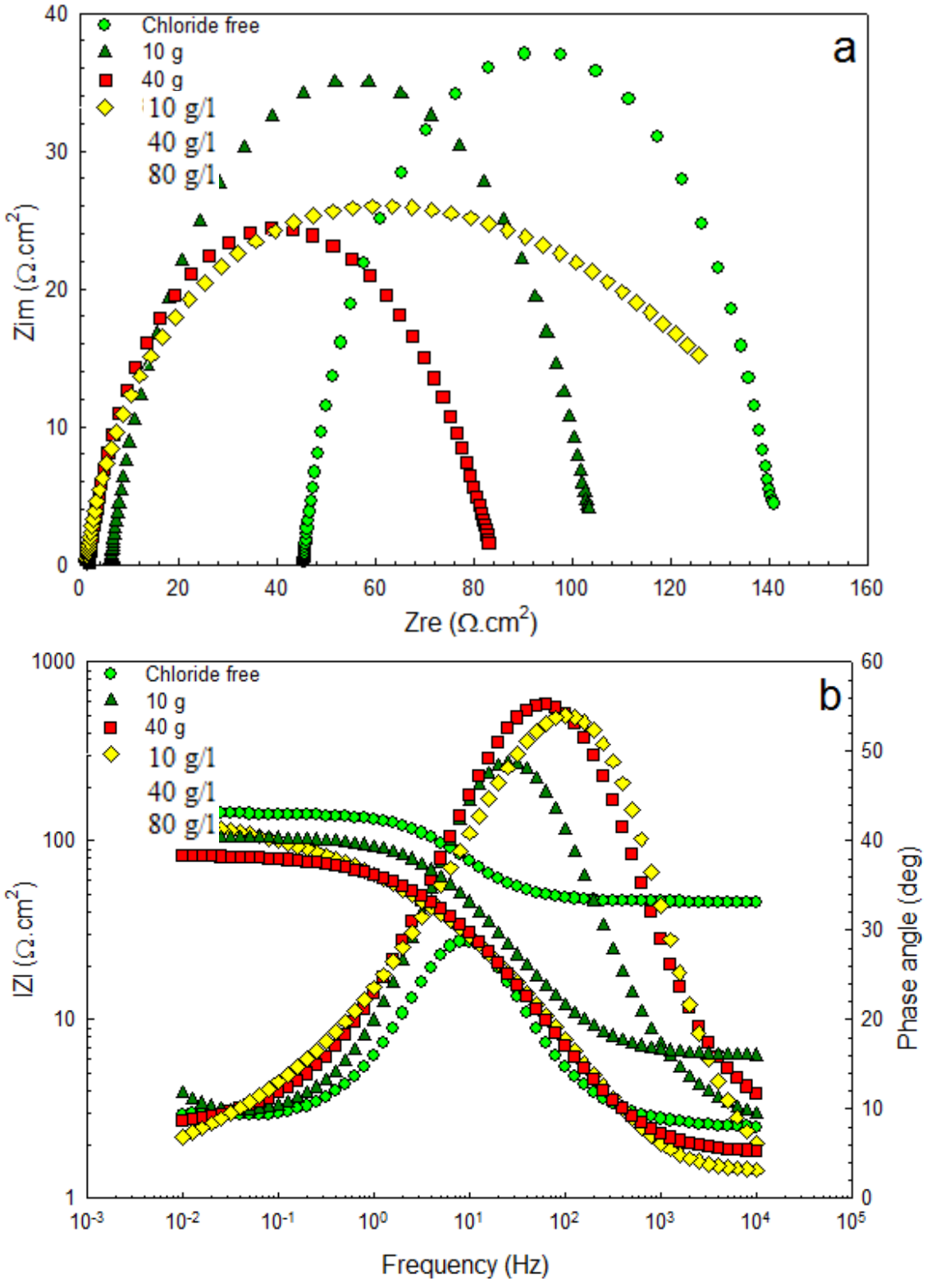

Figure 7.12. Electrochemical Impedance Spectroscopy (EIS) results at 20 ^{o}C produced from the oil free conditions that are chloride free, 10, 40, and 80 g chloride containing media represented by a) Nyquist and b) bode plots.

It was reported that adsorption of the corrosive species [Guo-xian, 2009], especially if they were cathodically reducible ones, and/or the relaxation of the intermediate species [Wu, 2004] can influence the low-frequency impedance producing an overlapped loop with the high frequency one. The increased mounts of chloride seemed to make adsorption effect more apparent as shown from Nyquist plots as well as from the bode ones where the modulus |Z| decreased proportionally as shown in Figure 7.12b. Impedance inflections and transitions seemed to occur, especially in chloride containing conditions, across the same medium to high frequency regions with similar characteristics.

The proposed equivalent circuit for our low temperature cases is shown in Figure 7.13 reflecting the roles of the processes discussed with charge transfer resistance (R_{dl}), and Constant Phase Element (CPE); (Q_{dl}) at the double layer. The adsorption field resistance (R_a) as well as the associated phase element (Q_a) are also shown in the proposed circuit of the configuration {R(Q(R(QR)))}.

(CPE) at the double is proposed for surface heterogeneities considered with a modified element and it is mathematically represented as [Baptiste, 2006]:

$$Z_{CPE} = \left[Q(j\omega)^n\right]^{-1} \qquad (7.15)$$

(ω) represents frequency, (j) equals to $\sqrt{-1}$, and (n) is (CPE) exponent.

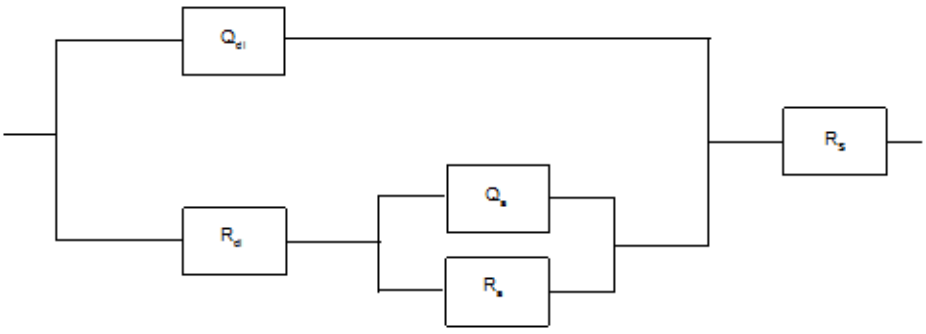

Figure 7.13 Equivalent circuit proposed for the electrochemical impedance response in oil free conditions at 20 ^{o}C.

The calculated electrochemical parameters at 20 ^{o}C are all shown in Table 7.2 for chloride free and chloride containing solutions. (R_s) as well as the associated (R_{dl}) followed an expectedly decreasing trend with the greater chloride content where the latter decreased to almost two orders of magnitude in the most concentrated brine in comparison to the chloride free one. The preserved capacitive nature throughout the salinity range seemed to be less significant with the greater chloride content. Interestingly, the resistance across adsorption followed an opposite trend accordingly, confirming the arguments provided at the beginning of this proposed context.

Table7.2. Electrochemical Impedance Spectroscopy (EIS) electric components calculated from the proposed equivalent circuit in oil free conditions at 20 ^{o}C

Electric components	Chloride content (g)			
	0	10	40	80
R_s (Ω.cm^2)	45.4	6.1	1.8	1.3
Q_{dl} (μF/cm^2)	6.27	6.31	6.40	7.71
n_{dl}	0.837	0.792	0.817	0.744
R_{dl} (Ω.cm^2)	96.1	68.2	47.4	0.11
Q_a (μF/cm^2)	6.83	10.72	11.45	3.72
n_a	0.891	0.763	0.727	0.8759
R_a (Ω.cm^2)	8.31	2.87	34.96	157.1
Chi-square	8.84E-05	8.93E-05	1.84E-05	7.69E-05

At the higher temperature 90 ^{o}C, the interfacial interactions showed noticeable changes where the role of adsorption seemed to be modified and/or limited by physical factors intrinsically dependent on temperature [Li, 2007] as deduced from Nyquist profiles in Figure 7.14a.

In addition, the interactions seemed to be more responsive to the increased amounts of chloride where the diffusion limited processes were more depicted as shown with the cases of 40 and 80 g chloride containing solutions. At the same free potential conditions, the role of active species, especially the cathodically reducible ones, seemed to be more

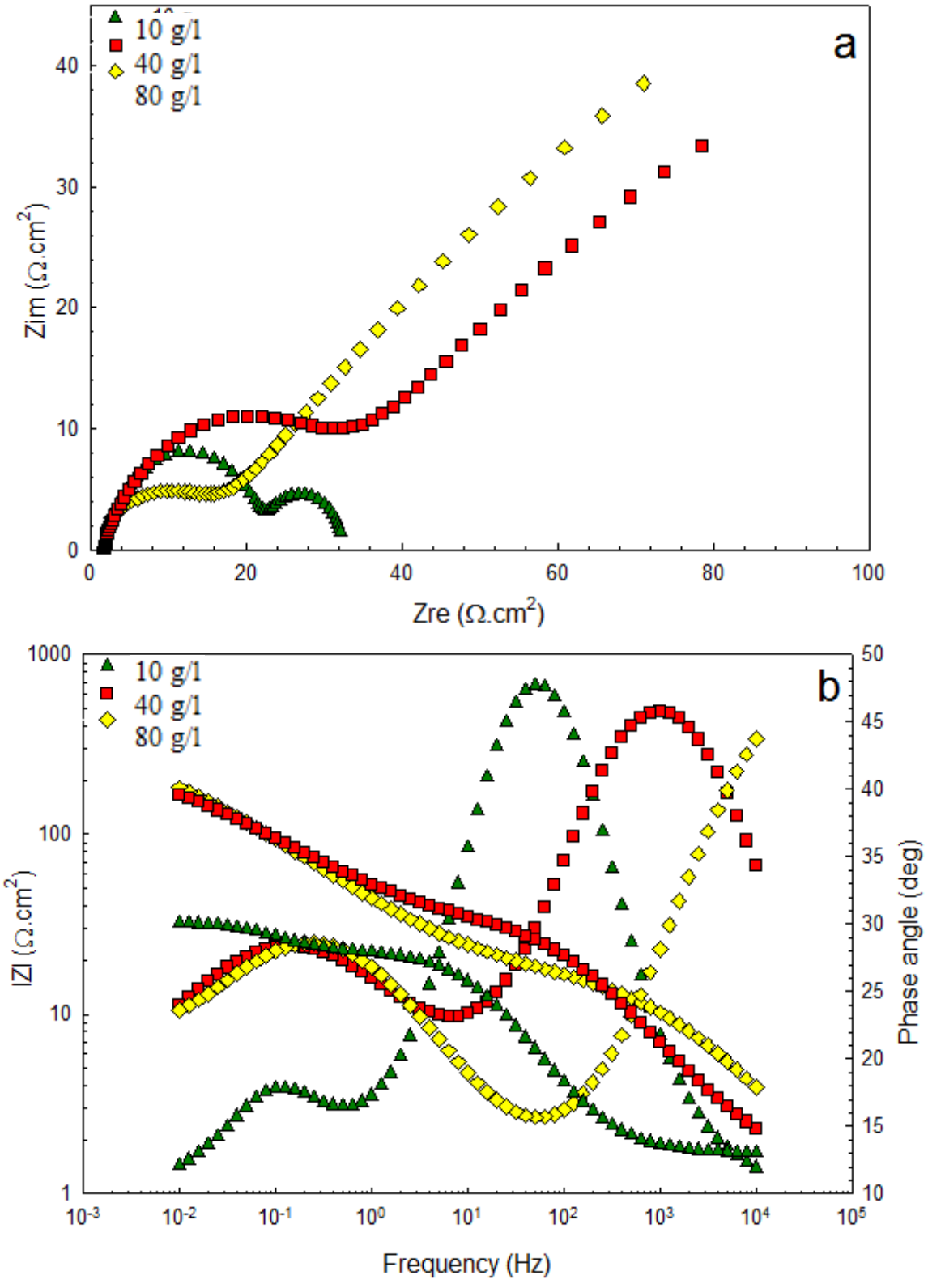

Figure 7.14. Electrochemical Impedance Spectroscopy (EIS) results at 90 ^{o}C produced from the oil free conditions that are 10, 40, and 80 g chloride containing media represented by a) Nyquist and b) bode plots.

compliant in a separate time constant, where in confirmation with the polarization test results, the limited passivity associated, kinetics were attributed to the retarded cathodic reactions. The significance of multi-time constant based impedance response was apparent in all chloride containing solutions as well-discernible phase peaks resulted at the low and high frequencies. That significance, specifically associated with the processes occurring outside the double layer resulted in phase peaks with intensities proportional with the chloride content at the high frequency. In 10 g chloride containing solution, |Z| showed the gradual decreasing transition from low-to-medium to high frequency ranges and the early low frequency phase peak was considerably small as shown in Figure 7.14b.

This behaviors reflects, diffusion-free, but second time constant based impedance to be considered for this low-chloride containing condition at this high temperature. The equivalent circuits proposed at 90 ^{o}C for 10 as well as 40 and 80 g containing conditions are shown in Figure 7.15a and 15b respectively.

The associated electric parameters calculated from the perfect fitting achieved with the experimental data are shown in Table 7.3. Solution resistances were considerably lower with the higher temperatures and they showed the expected decreasing trend with the chloride content. The double layers in all conditions seemed to be less capacitive accordingly and because, of the concurrent effect on the charge transfer acted by the increased chloride content, in addition to that of already high temperature, (R_{ct}) increased an order of magnitude at 40 g and it was comparable to that of 10 g upon the introduction of 80 g chloride.

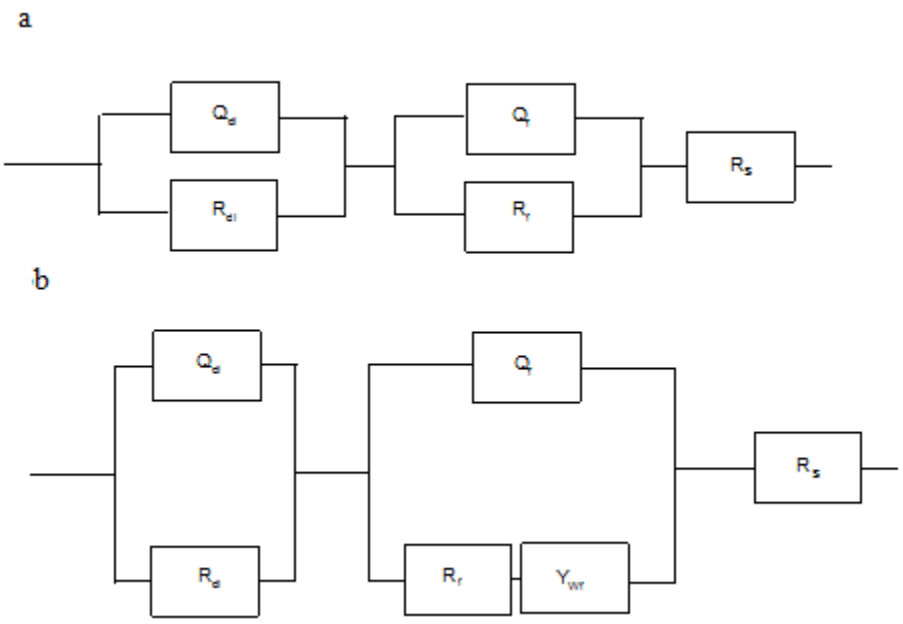

Figure 7.15 Equivalent circuits proposed for the electrochemical impedance response in oil free conditions at 90 ^{o}C for a) 10 g and b) 40 and 80 g chloride containing conditions.

Table 7.3.Electrochemical Impedance Spectroscopy (EIS) electric components calculated from the proposed equivalent circuit in oil free conditions at 90 ^{o}C

Electric components	Chloride content (g)	Electric components	Chloride content (g)	
	10		40	80
R_s ($\Omega.cm^2$)	1.677	R_s ($\Omega.cm^2$)	1.287	0.03116
Q_{dl} ($\mu F/cm^2$)	1.21	Q_{dl} ($\mu F/cm^2$)	1.4	2.9
n_{dl}	0.8284	n_{dl}	0.685	0.6079
R_{dl} ($\Omega.cm^2$)	20.94	R_{dl} ($\Omega.cm^2$)	220.1	15.57
Q_f ($\mu F/cm^2$)	1.834	Q_f ($\mu F/cm^2$)	3.15	1.198
n_f	0.96	n_f	0.7216	0.7881
R_f ($\Omega.cm^2$)	9.983	R_f ($\Omega.cm^2$)	27.79	270.6
Chi-square	3.48E-05	Y_{Wp} ($\Omega^{-1}s^{-0.5}$)	0.3797	0.06531
		Chi-square	2.21E-05	6.18E-05

Confirming with the proposed physical changes at the interfaces and with the polarization results, the resistance across the passive film (R_f) increased with the greater chloride content. In addition, the diffusive mobility, represented by the diffusion parameter (Y_{Wp}), decreased accordingly reflecting a special behaviour differently from the anticipated film deterioration with the greater chloride content. That is attributed to

the enhanced effectiveness that the corrosion products may have upon the accelerated kinetics in by-amount enhanced conductivity of the corrosive chloride containing electrolytes [Sun, 2003].

EIS performance was studied also at specific cathodic ovepotentials where the total mass-transfer controlled total reduction of (H^+) and (H_2CO_3) occurs at -0.8 V_{SCE} and where the charge-transfer controlled reduction of (H_2O) occurs at -1.2 V_{SCE} respectively. Nyquist plot representations at -0.8 V_{SCE} at 20 and 90 ^oC are shown in Figure 7.16a. The diffusion mass-transfer limited processes are apparently reflected from the impedance responses at both temperatures. Nyquist plots at 90 ^oC were considerably smaller; indicating the decreased significance of the associated resistive elements in the two-time based equivalent circuits. In addition, the enhanced kinetics at this high temperature by which it might mixdely interfered with the mass-transfer limited processes could make the diffusion Nyquist tails in the low frequency regions not as sharp as those at 20 ^oC.
Bode representations, which are not shown here, confirmed the two-time constant based response from the peak intensities and from the associated inflections. However, and differently from the cases discussed previously at OCP conditions at 90 ^oC in the concentrated brines, the diffusion limited processes seemed to occur across special diffusion fields by which the concentration gradients of the reduced species controlled the overall process through not effectively considerable passive films. At the lower cathodic overpotential of -1.2 V_{SCE}, the cathodic processes were totally controlled by the charge-transfer reduction of (H_2O), and the resulting Nyquist plots are shown in Figure 7.16b with the assigned potentials.

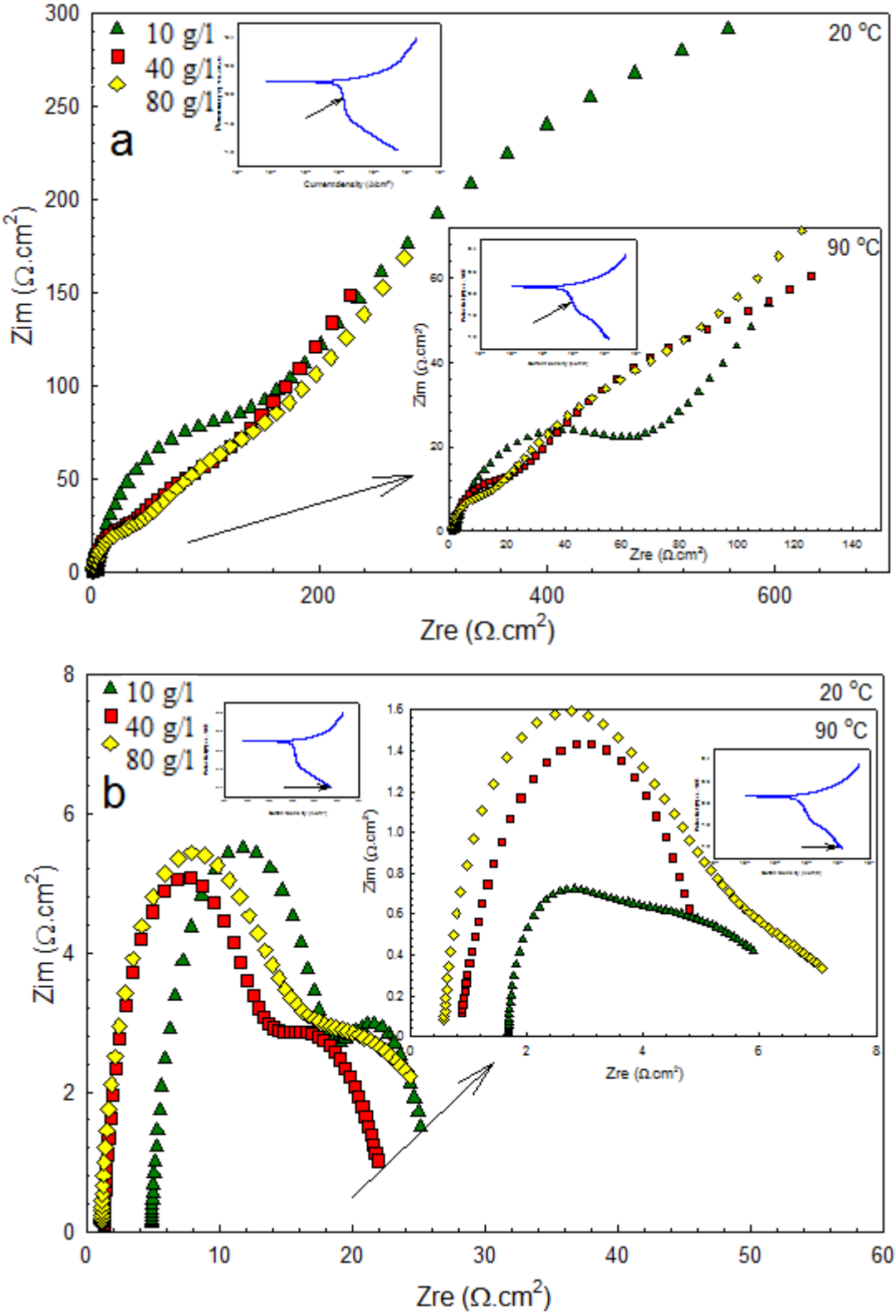

Figure 7.16 Electrochemical Impedance Spectroscopy (EIS) results at 20 and 90 ^{o}C produced from the oil free conditions that are 10, 40, and 80 g chloride containing media at a) -0.8 V_{SCE} and b) -1.2 V_{SCE}

At both temperatures, fairly overlapped semicircle loops appeared decreasing appreciably in size with the chloride content and temperature accordingly. From the bode diagrams, which are not shown here, all the processes seemed not to exhibit a multi-time constant impedance response, but rather, adsorption processes considered in nested equivalent circuits, seemed to govern the reduction process. The confirmative agreements between the experimental and model data at OCP are selectively shown in Figure 7.17 for the oil free conditions.

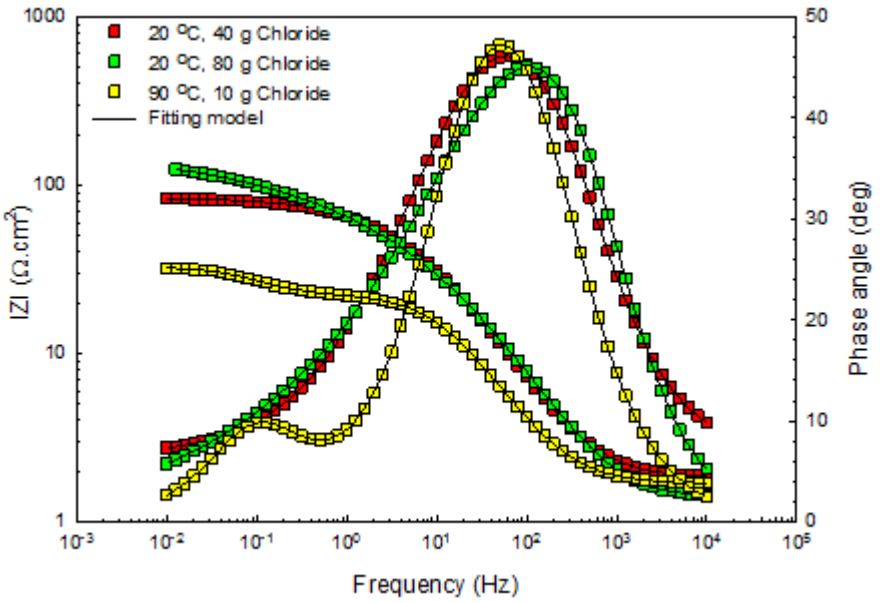

Figure 7.17. Experimental and calculated bode representations of impedance for selected temperature and chloride oil free conditions.

7.6. Electrochemical Impedance Spectroscopy (EIS) measurements in oil containing conditions

Nyquist and bode plot impedance representations are shown respectively in Figure 7.18a and b at 20 ^{o}C. The interfacial mechanisms showed significant changes upon the addition of oil where the extent of corrosion processes became associated to the

by-chloride-amount dependent inhibitive oil adsorption. Impedance responses, irrespectively from

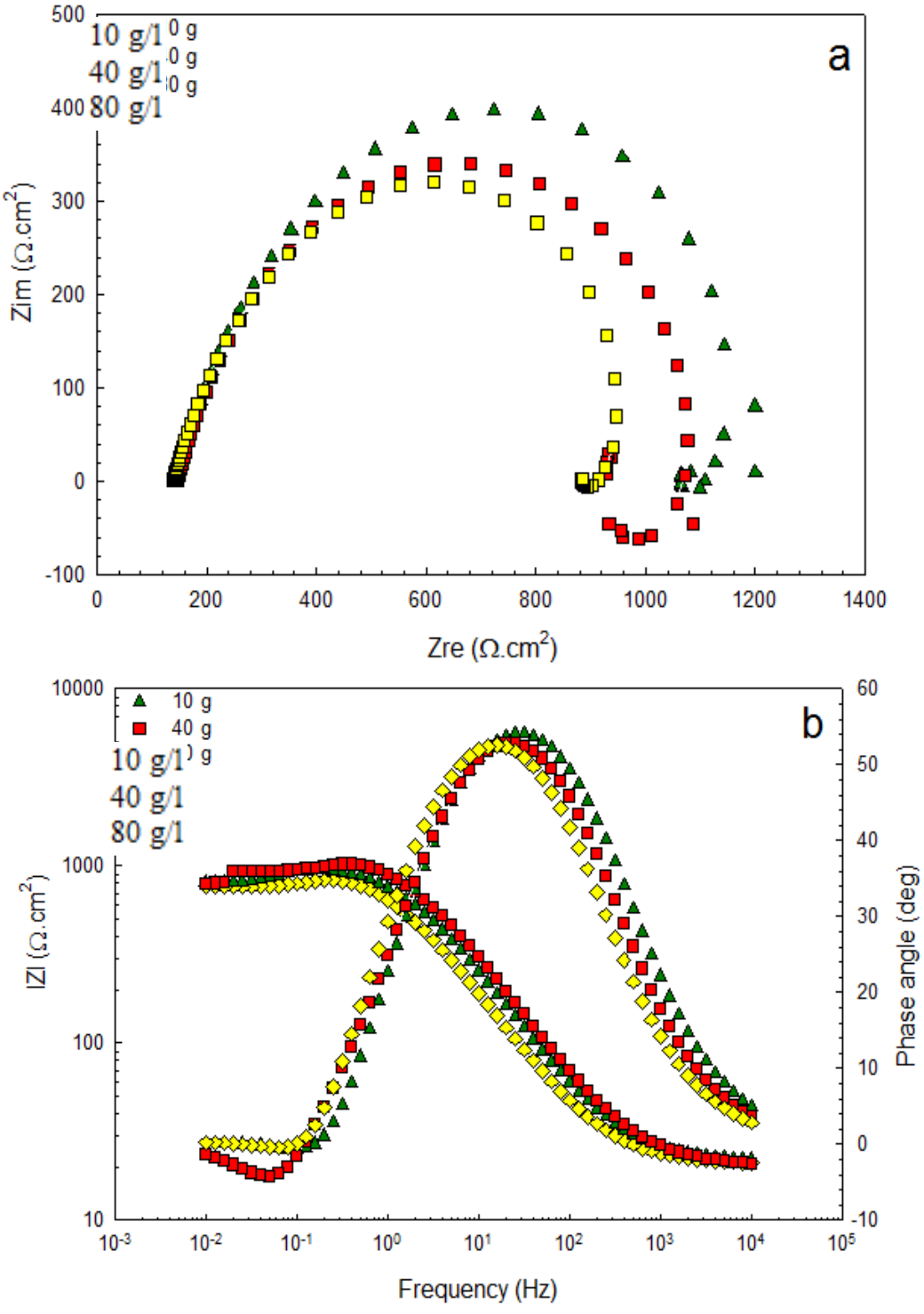

Figure 7.18. Electrochemical Impedance Spectroscopy (EIS) results at 20 °C produced from the oil containing conditions that are 10, 40, and 80 g chloride containing media represented by a) Nyquist and b) bode plots.

the chloride amounts, exhibited inductive behaviors where the partial depressed semicircles showed inward curvatures at the low frequency limits. As expected, the semicircles were considerably smaller with the greater chloride content and they were all greater than those produced in oil free conditions. In addition, comparatively to the oil-free conditions, there was no distinct changes in impedance response with respect to the chloride content where oil was effectively inhibitive with the greater chloride content although of the limited miscibility accordingly. The inductive behaviour was associated with single phase peaks appearing at between 10 to 30 Hz following a lower-frequency valley representing a typical impedance response when ammonium and immidazoline-based inhibitors are added to CO_2-saturated media [Khodyrev, 2011], [Ortega-Sotelo, 2010], and [Garnica-Rodriguez, 2009]. At the higher temperature, 90 ^{o}C, Impedance seemed to be more sensitive to the chloride content and all Nyquist semicircles were considerably smaller than those produced at 20 ^{o}C as shown in Figure 7.19a.

Interestingly, the governing mechanisms studied in oil containing conditions seemed to be independent from the chloride content and temperature reflecting the relative effectiveness of oil inhibition at all conditions. A better effectiveness seemed to be proportionally achieved with lower temperature and/or lower chloride content where the stable inhibiting layers are necessarily associated with the enhanced miscibility accordingly. The bode representations at 90 ^{o}C where similar to those produced at 20 ^{o}C, showing the phase peaks at slightly greater frequencies and the rate and fashion of $|Z|$ transitions from low to medium frequencies were similar and they showed a dependence on the chloride content as shown in Figure 7.19b.

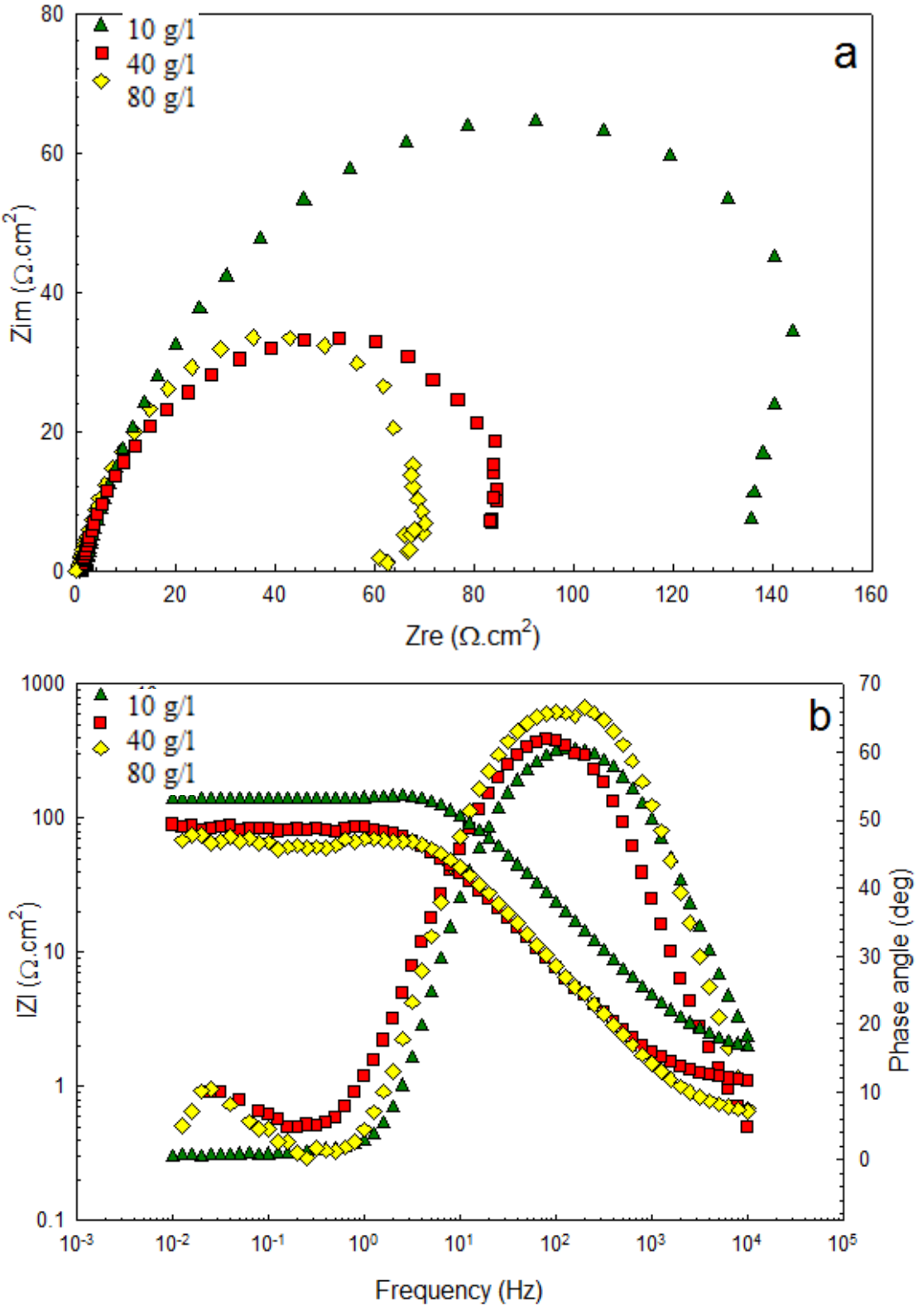

Figure 7.19 Electrochemical Impedance Spectroscopy (EIS) results at 90 ^{o}C produced from the oil containing conditions that are 10, 40, and 80 g chloride containing media represented by a) Nyquist and b) bode plots.

The similar mechanisms in oil containing conditions at both temperatures achieved a very good fitting with the proposed equivalent circuit shown in Figure 7.20 containing (R_L) and (L) representing oil adsorption resistance and inductance respectively.

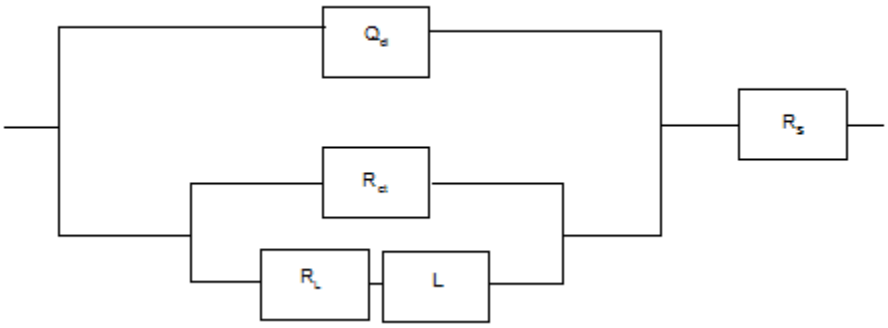

Figure 7.20 Equivalent circuit proposed for the electrochemical impedance response in oil containing conditions at 20 and 90 ^{o}C.

The electric parameters of concern are all shown in Table 7.4 for 20 and 90 ^{o}C. The charge transfer at 20 ^{o}C preserved its great same order of magnitude resistance showing a decreasing trend with the chloride content as well as that of adsorption (R_L).

Table7.4. Electrochemical Impedance Spectroscopy (EIS) electric components calculated from the proposed equivalent circuit in oil containing conditions at 20 and 90 ^{o}C

Electric Components	20 °C			90 °C		
	Chloride content (g)			Chloride content (g)		
	10	40	80	10	40	80
R_s ($\Omega.cm^2$)	145.8	142.7	138.5	1.648	1.062	0.6064
Q_{dl} ($\mu F/cm^2$)	1.38	1.70	2.37	2.83	7.21	5.78
n_{dl}	0.7423	0.8434	0.9314	0.778	0.8063	0.8331
R_{dl} ($\Omega.cm^2$)	943.9	792.9	751.9	139	86.63	67
R_L ($\Omega.cm^2$)	289.3	248.6	240	48.14	21	7.5
L (H/cm^2)	167.5	447.5	202.9	2.904	0.8837	1.469
Chi-square	2.95E-04	2.59E-05	1.95E-04	1.50E-05	4.25E-04	6.23E-05

However, at 90 ^{o}C, distinct variations with chloride were exhibited accordingly; the resistance at the double layer was almost 10 times less than that at 20 ^{o}C in all chloride containing conditions reflecting the electrochemical sensitivity of oil adsorption

towards temperature. Interestingly, (Q_{dl}) exhibited an appreciable opposite trend to that of resistance with respect to both temperature and chloride and the capacitive nature was also more apparent. The confirmative fitting between the experimental data and with those produced from the proposed models are selectively shown in Figure 7.21.

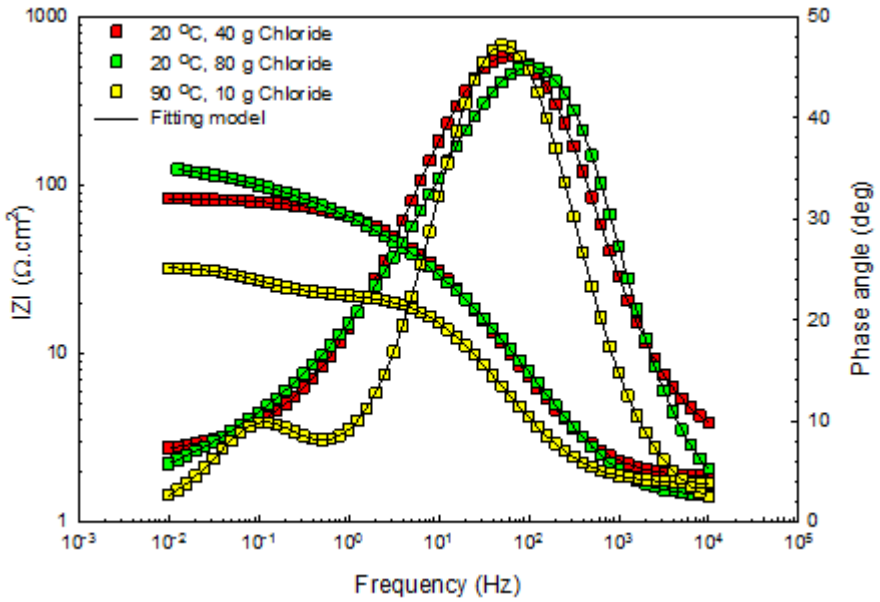

Figure 7.21. Experimental and calculated bode representations of impedance for selected temperature and chloride oil containing conditions.

Chapter 8: Results and discussion of the potentiodynamic polarization investigations in multivariable controlled CO_2 corrosion in a medium containing chloride and acetic acid

8.1. Test solution

Corrosion tests were basically performed in unbuffered 1-bar-CO_2-saturated, 1-L-brines of sodium chloride concentrations of 10, 20, 30, 40, 50, and 60 g, containing also 10, 20, 30, 40, 50, and 60 mL of acetic acid. Two relatively extreme temperatures were selected for our electrochemical studies; 20 and 90 ^{o}C maintained within $\pm$ 1 ^{o}C.

8.2. Potentiodynamic polarization results

The corrosion behavior was first investigated in chloride free conditions to investigate the cathodic effect on the accelerated corrosion reactions. The influences of the basic species driving the polarization behavior were appreciably separated in CO_2-saturated and N_2-saturated media in four polarization profiles shown in Figure 8.1. It is apparent that the least corrosion rate and potential were exhibited in conditions where the reduction of (H_2O) as well as that of (H^+) exclusively dominated the total cathodic reactions. However, upon CO_2-saturation; the cathodic reactions were about an order of magnitude greater, reflecting the expanded reduction process by carbonic acid which results from carbon dioxide dissociation in a low-aroud-4-pH medium. The corrosion rate was consequently greater accompanied by an expected nobler corrosion potential (E_{corr}) by as much as

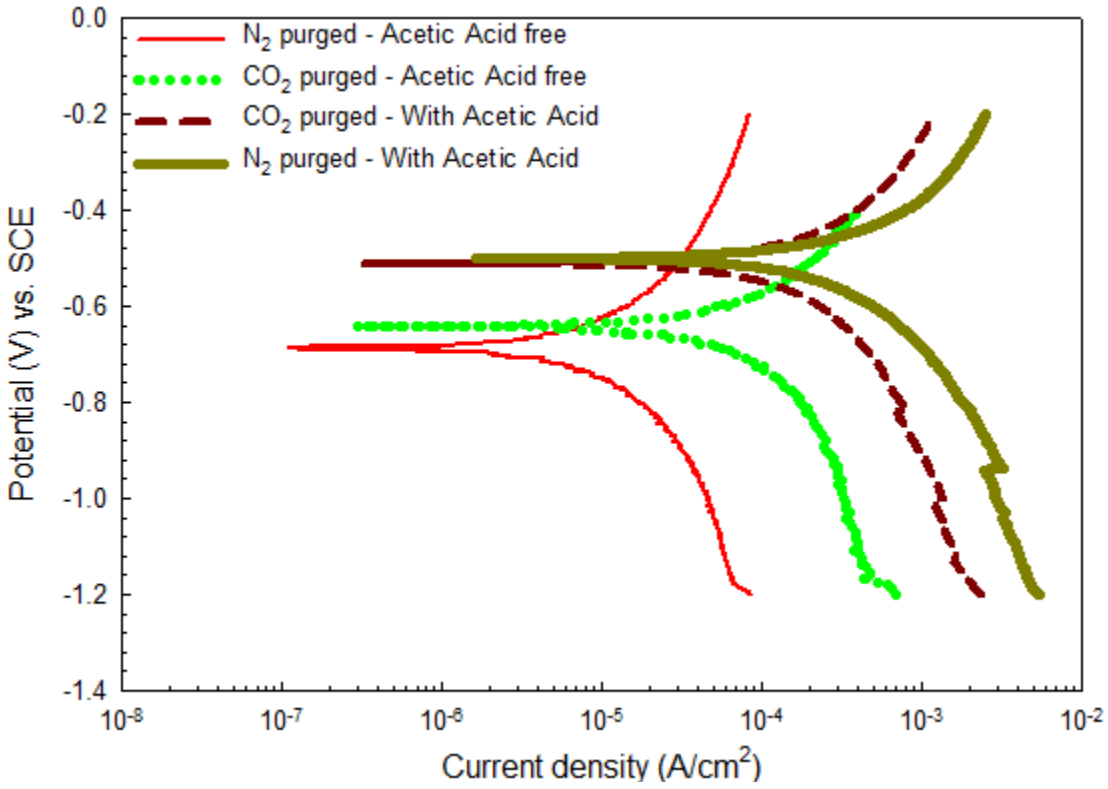

Figure 8.1. Potentiodynamic polarization in chloride free, CO_2-saturated, and N_2-saturated media, free of and containing 10 mL acetic acid.

almost 45 mV. Interestingly, the anodic branch showed a noticeable acceleration in comparison to that of N_2-saturated medium, supporting the proposed views on the direct involvement of (H_2CO_3) and (HCO_3^-) in the anodic dissolution mechanisms; i.e. in the active region [Kermani, 2003].

Introduction of 10 mL of (CH_3COOH) almost multiplied the cathodic regime covering that already established in acetic-acid-free-CO_2-saturated medium. The corrosion rate consequently accelerated as a result of the CH_3COOH-influenced vigorous evolution of hydrogen. Interestingly, the maximum corrosion reaction was attained in acetic acid containing N_2-saturated medium, making the two extremes; maximum and minimum corrosion rates and potentials in acetic acid containing and acetic acid free N_2-

satureated media respectively. There was a similar respect of corrosion which was exhibited in acetic acid containing CO_2-saturated medium. However, the considerable deceleration in both anodic and cathodic branches in that condition indicated the ability of carbon carrying species in facilitating the formation of stable passivity even in the presence of acetic acid. Moreover, that might suggest the occurrence of cathodic reactions, but deceleratingly, on those interfacial barriers, or by impeded diffusion of the reducible species.

As shown in Figure 8.2, the same 4 cases were considered but with the introduction of 10 g chloride. In the case of acetic acid free N_2-saturated medium, the anodic reactions were greatly accelerated leading to a greater corrosion rate and to a more negative (E_{corr}) accompanied by an enhanced kinetics of cathodic reduction of water.

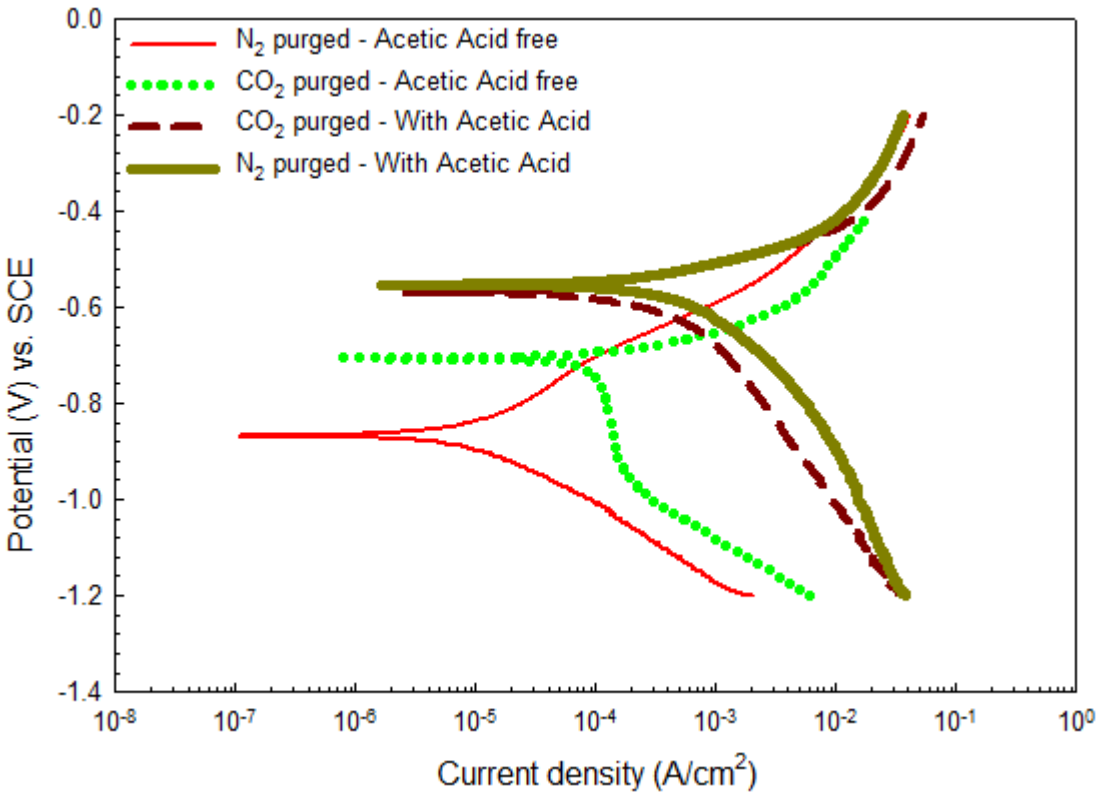

Figure 8.2. Potentiodynamic polarization in 10 g chloride containing, CO_2-saturated, and N_2-saturated media, free of and containing 10 mL acetic acid.

In addition, the polarization exhibited a multi-sloped anodic dissolution corresponding to early formed, hydroxide-based films before a possible further dissolution or transformation to stable oxide films when the current densities varied. However, in CO_2-saturated medium, two distinct cathodic regimes were revealed. In addition, the corrosion behavior was anodically sensitive by the introduction of chloride where the accelerated anodic dissolution also intersected the combined mass-limited cathodic reduction of (H_2CO_3), and (H^+). The active reductions of water in the acetic acid free conditions were within almost the same orders of magnitude. Introduction of acetic acid produced appreciably comparable corrosion behaviors in the active anodic and cathodic regimes in CO_2 and N_2-saturated media. The corrosion rates were also expectedly higher, and were too in comparison to the chloride free conditions. The greatest cathodic reactions, with a modified mixed charge-mass transfer shoulder, were exhibited in N_2-saturated medium with justifications, possibly valid for these cases, proposed for chloride free conditions.

The investigations on the polarization behavior were carried further to study the effect of chloride and acetic acid, separably with specific ranges, at 20 and 90 ^oC. As shown in Figure 8.3a; comparatively with the chloride-free condition at 20 ^oC, the corrosion behavior was apparently anodically sensitive with the small dose of chloride of 10 g. The corrosion rate was as higher as 7 times and the corrosion potential was about 90 mV lower. The cathodic regime exhibited the mass-transfer limited cathodic reduction of (H_2CO_3), and (H^+) upon chloride-influenced kinetics of hydrogen evolution in the more conductive condition. In addition, the total cathodic reduction regime was finally

dominated by purely charge-transfer reduction of water at similar potentials around – 1 V_{SCE}, as already indicated in [Fang, 2010], and irrespectively from the chloride content.

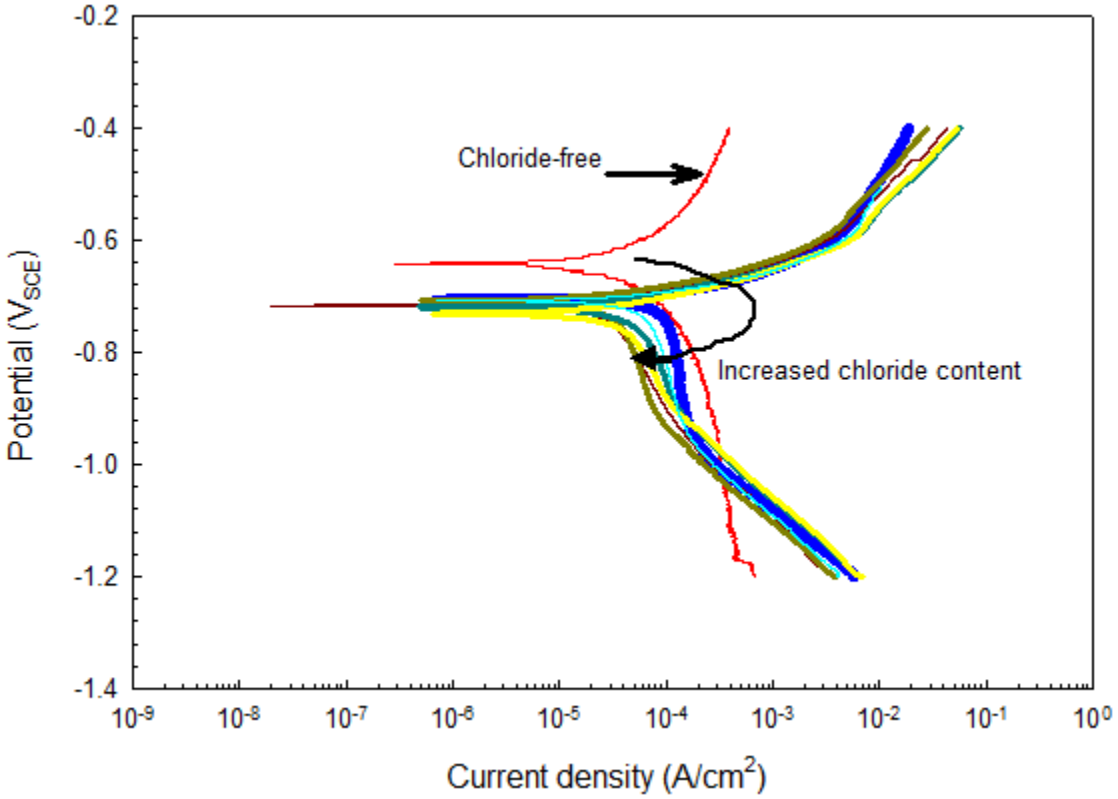

Figure 8.3. Potentiodynamic polarization in CO_2-saturated containing 10, 20, 30, 40, 50, and 60 g chloride at 20 ^oC

Corrosion current densities exhibited a "bow" where the anodic sensitivity was finally restricted by decelerated cathodic reactions where the corrosion rate showed a peak value before it decreased with the greater chloride content. Corrosion potentials showed a steady decrease along with the chloride content range of from 10 to 60 g but influenced initially by anodic acceleration and finally by cathodic deceleration. It seemed that the corrosion behavior in chloride containing CO_2-saturated media is necessarily associated with physical transformations at the corroding interface. The enhanced dissolution with the greater chloride content possibly led to more facilitated, with greater

supersaturation, corrosion products form firmly, intacting to the active areas at which hydrogen evolution is occurring. At 90 ^{o}C, fair similarities to 20 ^{o}C condition were exhibited as a result of the increased chloride content on both anodic and cathodic regimes as shown in Figure 8.4.

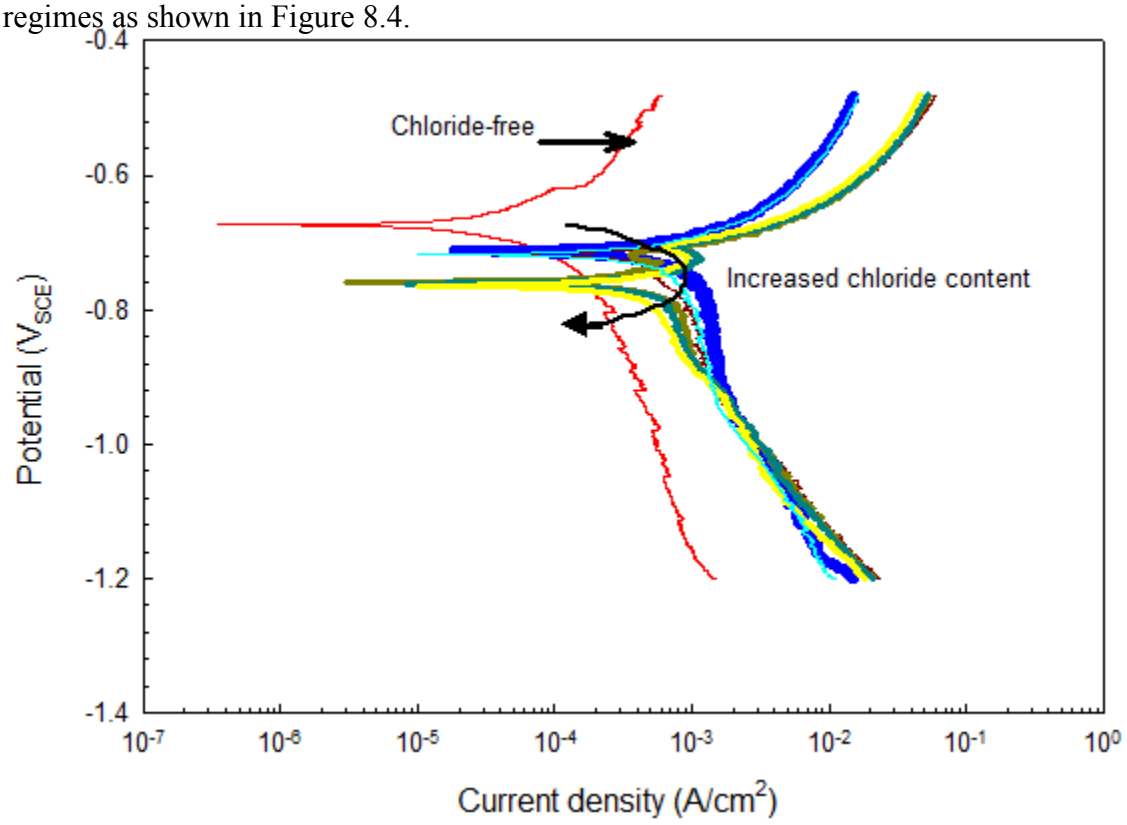

Figure 8.4. Potentiodynamic polarization in CO_2-saturated containing 10, 20, 30, 40, 50, and 60 g chloride at 90 ^{o}C

The reactions were apparently accelerated at the higher temperature, and the cathodic reductions showed an extended kinetics making the total reduction of (H^+) and/or (H_2CO_3), existing with different speciation, more to be mixed charge-mass transfer controlled. The anodic dissolution in the concentrated brines containing 50 and 60 g chloride exhibited appreciable retardations corresponding to facilitatedly formed products resulting from and possibly contributing to the accelerated anodic response.

The effect of increased acetic acid contents from 10 to 60 mL, as shown in Figure 8.5 for 20 ^{o}C, was investigated to evaluate the basic polarization features possibly produced in chloride free conditions.

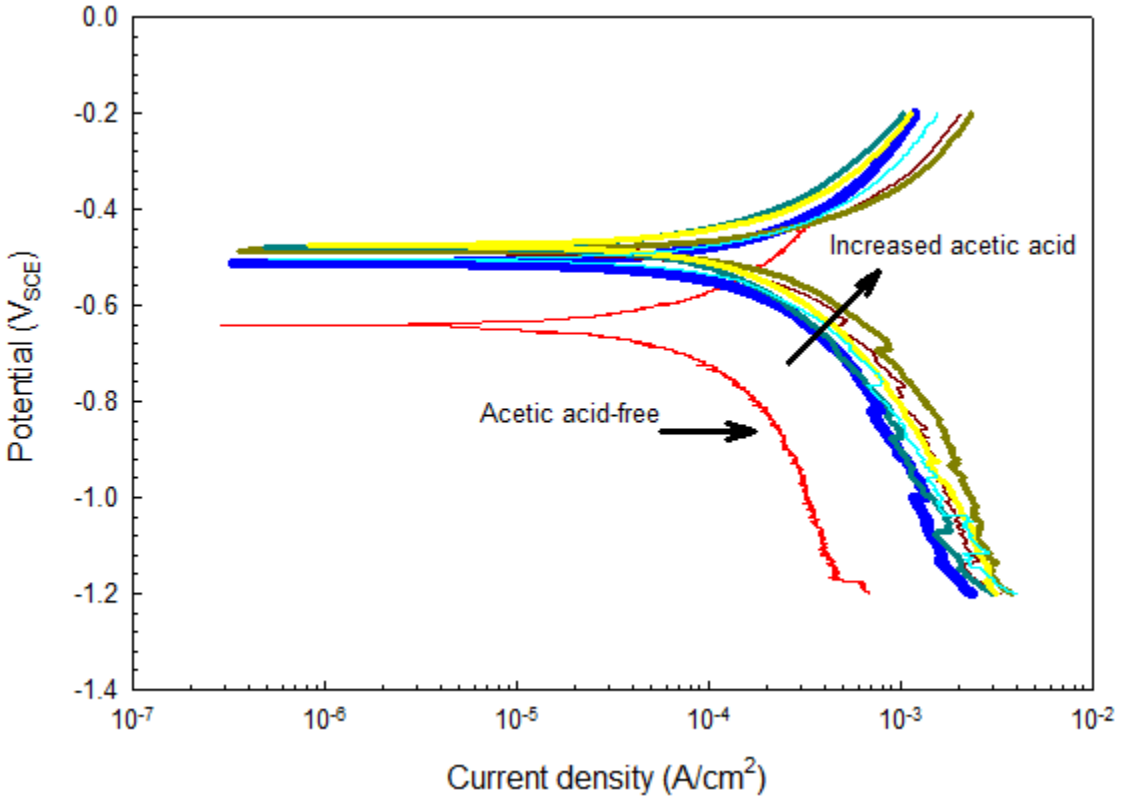

Figure 8.5. Potentiodynamic polarization in CO_2-saturated containing 10, 20, 30, 40, 50, and 60 mL acetic acid at 20 ^{o}C

Acetic acid reduction prevailed greatly the already established cathodic regime of the chloride-free CO_2-saturated media making the cathodic reactions multiplied by as high as almost 5 times.

The cathodic regime in these conditions showed the considerable dependence on the acetic acid content making the corrosion rates consequently higher as well as are the corrosion potentials. The increased corrosion rates were quite sensitive to the few amounts of acetic acid before they showed appreciably slight variations with the greater

amounts and at also corrosion potentials as higher as almost 110 mV than that of acetic acid-free condition. The basic features and trends with the greater acetic acid content at 90 ^{o}C were similar to those at the lower temperature, but the corrosion rates were expectedly higher, and the cathodic shoulders were more separated.

Corrosion current densities and corrosion potentials are collectively presented in Figures 8.6 and 8.7 for acetic acid and chloride containing conditions at 20 and 90 ^{o}C. The corrosion rates were significantly higher at 90 ^{o}C by as much as 17 to 20 times in chloride containing solutions and by almost 8 times in acetic acid containing solutions. For the reasons illustrated previously in this context, corrosion rates were increasingly sensitive towards the few amounts of chloride before they showed peaks and consequently decreasing trends due to the decelerated cathodics.

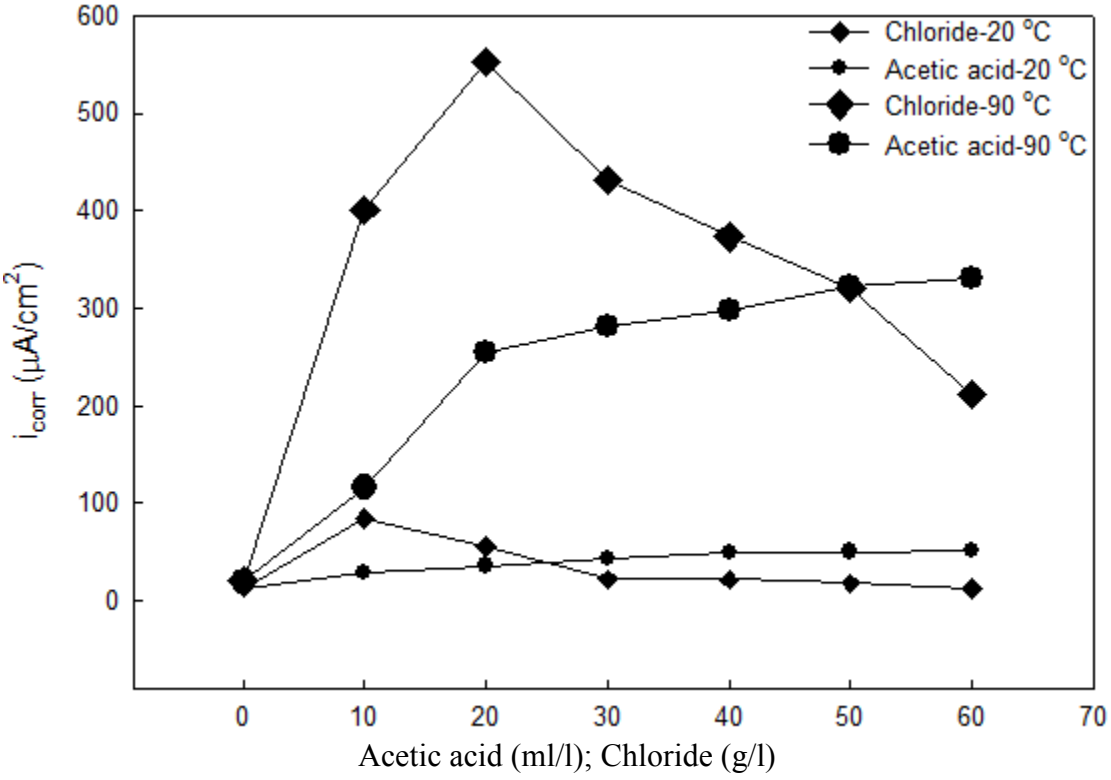

Figure 8.6. Corrosion current density variations with respect to the chloride and acetic acid amounts at 20 and 90 ^{o}C

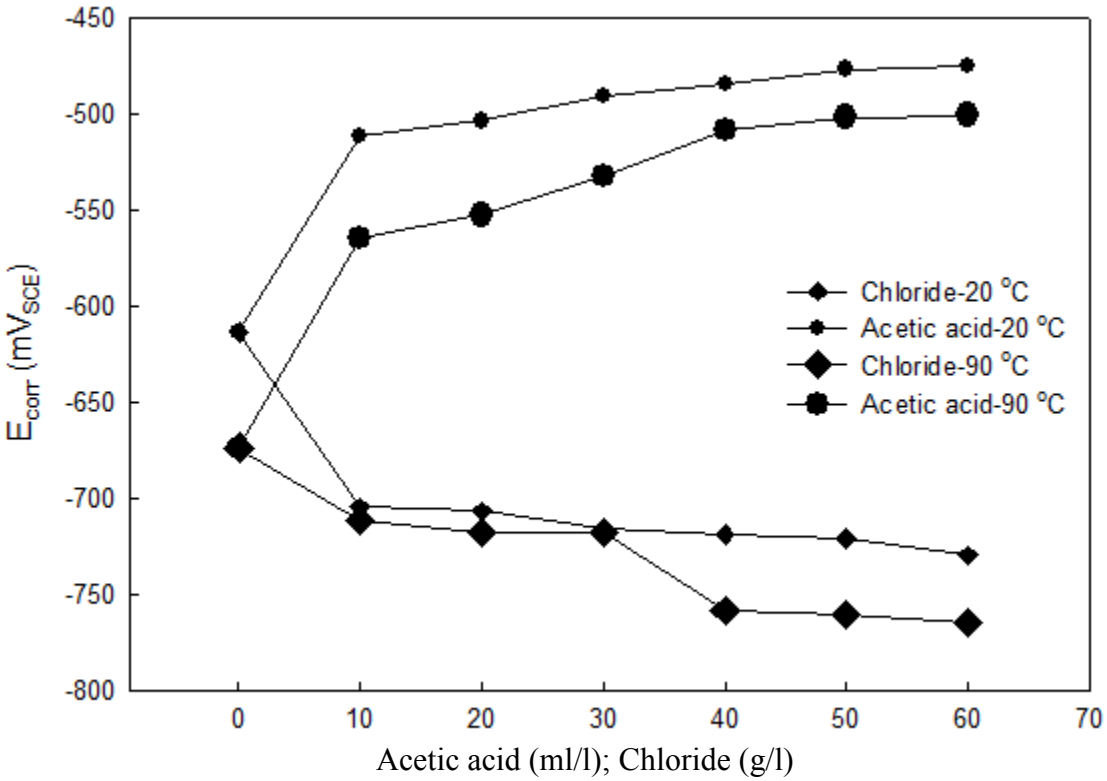

Figure 8.7. Corrosion potential variations with respect to the chloride and acetic acid amounts at 20 and 90 ^{o}C

However the corrosion rates were continuously proportional to the increased acetic acid content but with different significance in comparison to chloride depending on temperature. In other words, chloride seemed to be more significant in increasing the corrosion rates than even the great acetic acid amounts at 90 ^{o}C but that respect was different at 20 ^{o}C. The corrosion potentials, as illustrated previously, increased with acetic acid content and decreased with that of chloride in a steady fashion. Interestingly, the higher-temperature-accelerated anodic reactions made the corrosion potentials in both conditions lower.

The multivariable-influenced corrosion behavior was investigated based on the effect of acetic acid on the variability of the corrosion rates with the increased chloride

content. As shown in Figure 8.8, reduction of acetic acid, introduced with the few amount of 10 mL, prevailed the total cathodic reduction regimes exhibited along the full range of

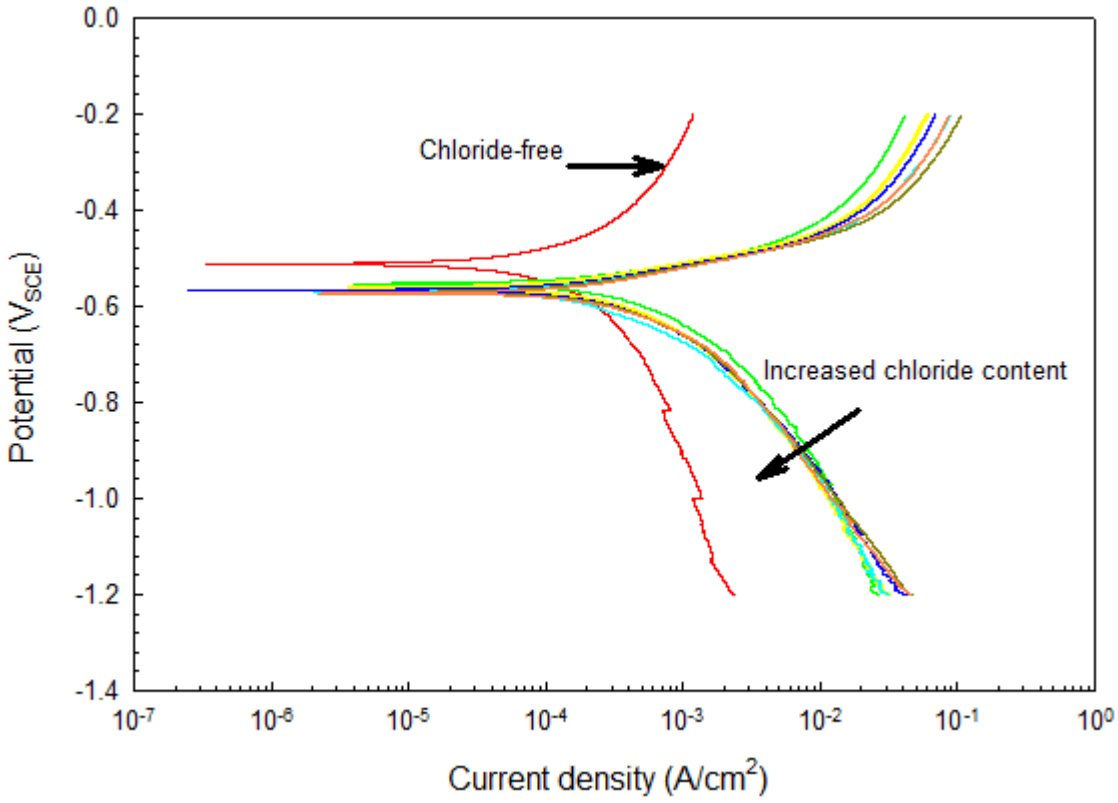

Figure 8.8. Potentiodynamic polarization in CO_2-saturated medium containing 10, 20, 30, 40, 50, and 60 g in the presence of 10 mL acetic acid at 20 ^{o}C

The initial anodic sensitivity towards increased chloride content was preserved but the corrosion potentials were considerably higher than those in acetic acid-free conditions. It seemed also that acetic acid, although of the greater corrosion rates in comparison to those of acetic acid-free conditions, made corrosion rates appreciably independent from the great chloride contents. That could be due to the ability of acetic acid in interrupting the interfacial physical significance by which the variations of E_{corr}-i_{corr} were attributed for when effective passivation had a strong tendency to form. That

respect in terms of the effect greater acetic acid amounts on corrosion in these brines was similar at both temperatures which are not shown here.

3-D comprehensive representations of the corrosion current density with respect to the chloride and acetic acid contents are shown for 20 and 90 ^{o}C respectively in Figure 8.9 and 8.10. The corrosion rates were proportional to the acetic acid content in all chloride containing solutions as the elementary profile of acetic-acid free condition is fairly exaggerated along with the acetic acid contents. Interestingly, the initial sensitivity towards the smallest chloride content producing a peak value was preserved and it was getting greater expectedly with the greater acetic acid content.

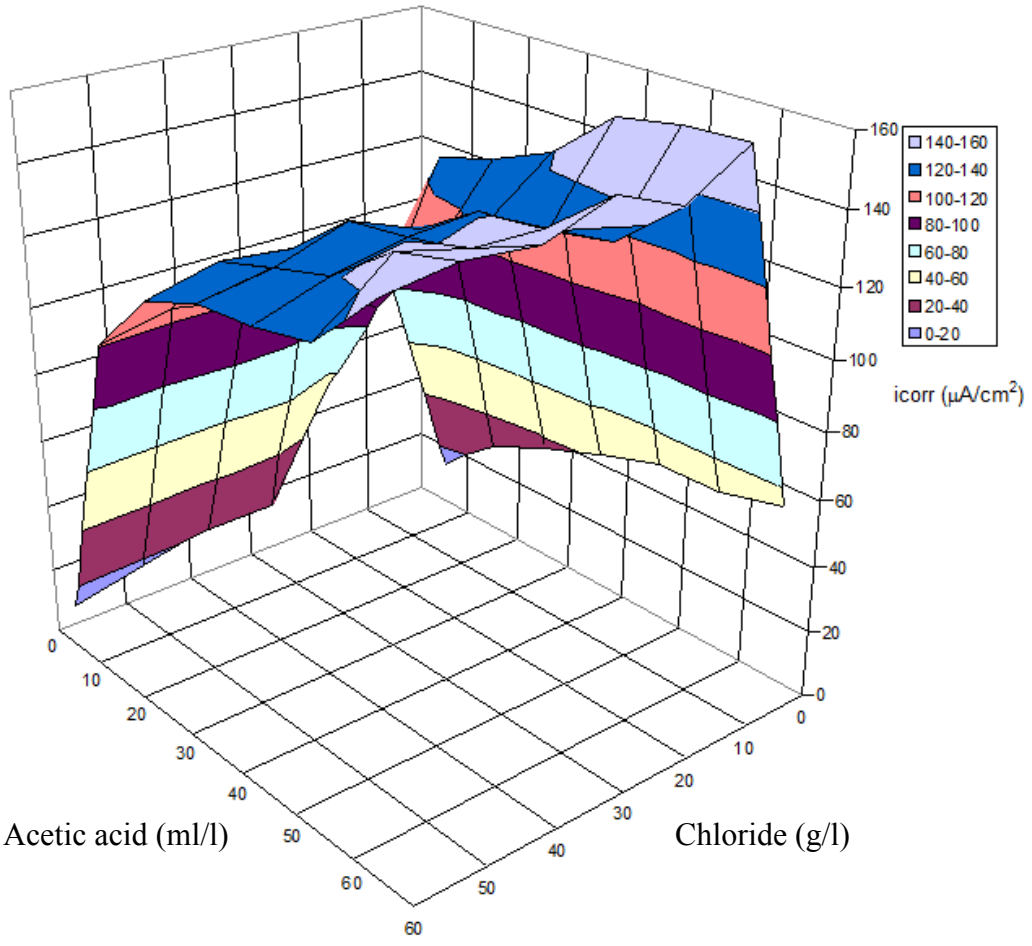

Figure 8.9. 3-D representation of corrosion current density variations with respect to chloride and acetic acid contents at 20 ^{o}C

Acetic acid, introduced with the different amounts, appreciably made the corrosion rates relatively independent from the greater chloride content. The corrosion rates seemed to be necessarily increased-acetic-acid controlled where at the most concentrated acetic acid containing solutions, they showed elevated, but fairly flat 3-D strip of corrosion rates. It is interesting that although of the similar trends that the corrosion rates exhibited with respect to acetic acid at the two chloride extremes; chloride-free and the most concentrated brine, the corrosion rates were almost 4 times greater upon the existence of chloride. The corrosion rates at the higher temperature 90 ^{o}C were significantly greater and although of the appreciable similarity with respect to the simultaneous effects of chloride and acetic acid, however, these effects seemed to be more determined.

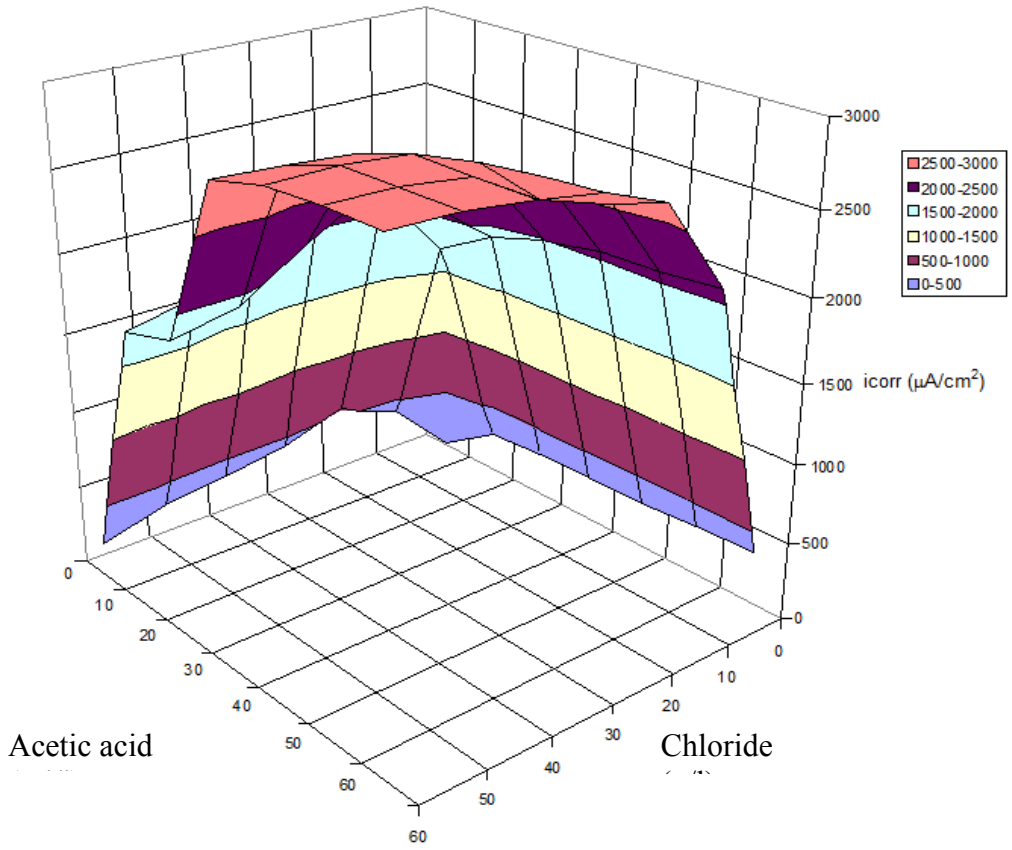

Figure 8.10. 3-D representation of corrosion current density variations with respect to chloride and acetic acid contents at 90 ^{o}C

Except with the acetic acid- free, 10 and 20 mL containing conditions, the corrosion rates were proportional to the chloride content without exhibiting a significant peak. It seemed that there is a temperature dependent acetic acid allowance for increased chloride contents to induce their full anodic effect where the corrosion rates consequently increased without the retardation exhibited at 20 ^{o}C. In addition, the corrosion rates were the greatest as both chloride and acetic acid amounts were increased in a fashion which was not very discerned at 20 ^{o}C.

Chapter 9: Results and discussion of CO_2 saturated autoclave environments

9.1. Test environments

The test solutions in the autoclave were made to simulate the stratified flows at relatively low rotational speed of 50 rpm containing different ratios of oil and water. In our study, three proportions of oil were selected to study the variations in the corrosion rates accordingly of 10, 50 and 90 %. Carbon dioxide was continuously purged into the reactor at a total pressure of 50 psi and the temperature was set to be as high as 100 ^{o}C for 24 days. Selected physical and chemical properties of the considered oil in this study are shown in Table 6.2.

9.2. Weight loss test results

It is shown in Figure 9.1 corrosion rate variations with respect to the oil content across the time elapsed. The corrosion rates at early test time periods were the highest and they started to decay exponentially and in a proportional manner with the oil content. The effect of the greatest oil amount of 90 % at this high temperature was very apparent in suppressing the corrosion rates to about 5 times in comparison to that in 50 % oil containing emulsions. In addition, in that condition; the corrosion rates were almost stable throughout the test time period where oil adsorption interfered the dissolution processes and the associated transfer of the reducible carbon carrying species. However, from a long test time perspective, the effect of oil amount seemed to be similar as the

corrosion products were forming and acquiring enhanced morphological and compositional characteristics similarly to other findings in [Yu, 2007].

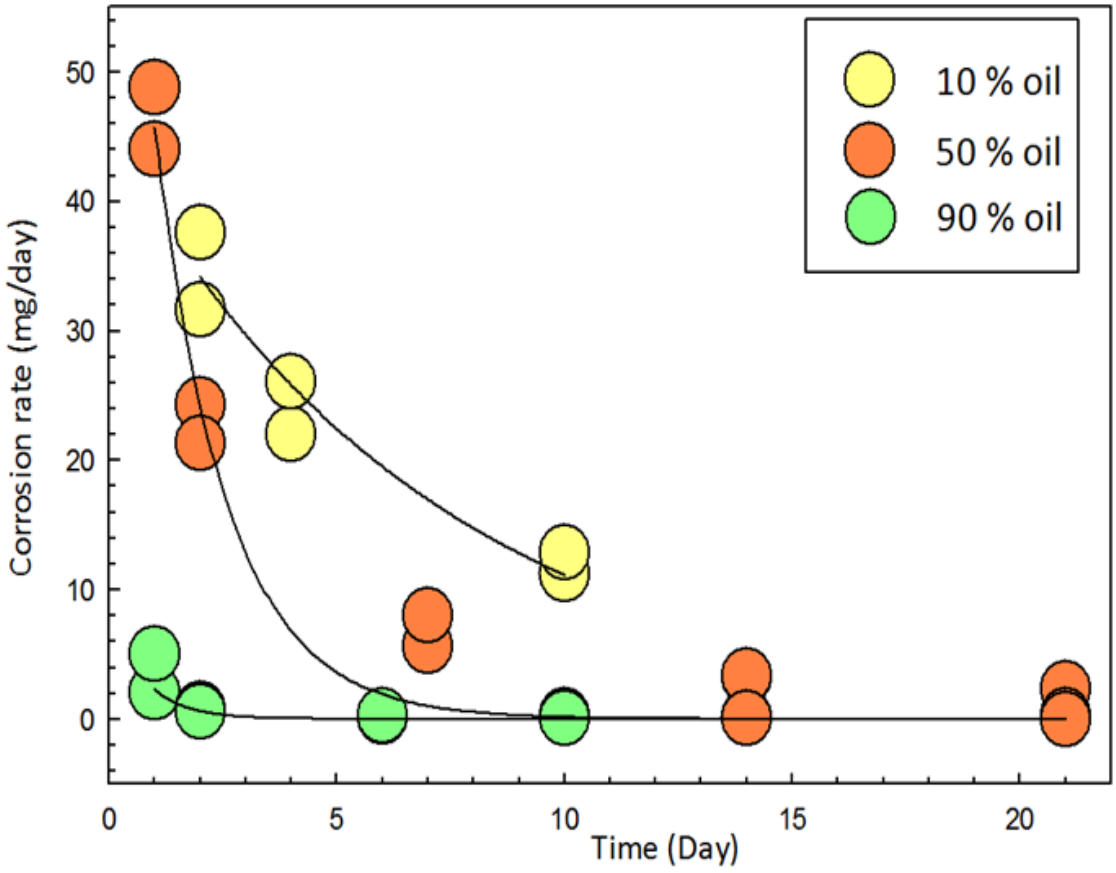

Figure 9.1. Corrosion rates from weight loss measurements taken over the time period of 24 days with respect to the oil content

As the corrosion proceeded, and upon the conditional supersaturation achieved, the corrosion products changed from being dispersed particle-like to be well spread on the steel surface as shown in Figure 9.2, except with few defects decreasing the corrosion rates. The effect on the corrosion rate was fundamentally related to the impeded transfer of the species involved in the corrosion mechanisms protecting the steel from further dissolution and taking over the oil adsorption.

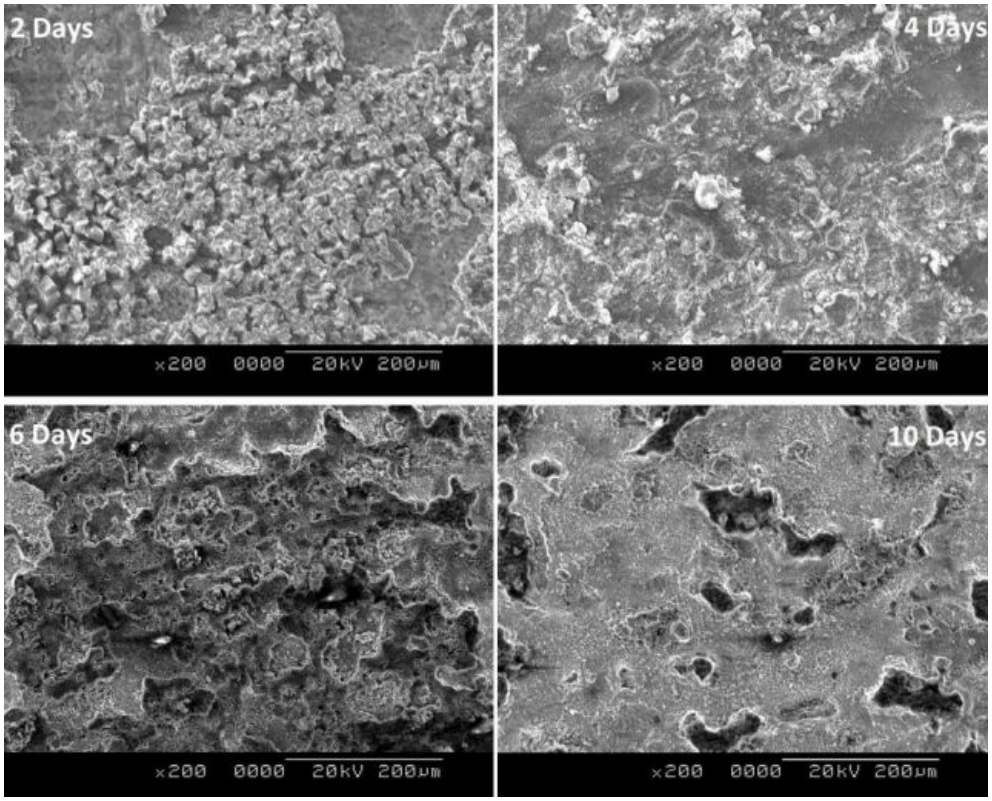

Figure 9.2. Corrosion surface morphology variations over the time period for specimens immersed in autoclave-based environments at 100 ^{o}C in 50 psi CO_2 saturated environments

The corrosion products incorporating iron carbonate are transformable to considerably stable protective oxides these CO2-saturated media. It is shown below in Figure 9.3 a Pourbiax illustrating the possible corrosion products intercontaining (Fe_2O_3) and (Fe_3O_4) as well as ($FeCO_3$)

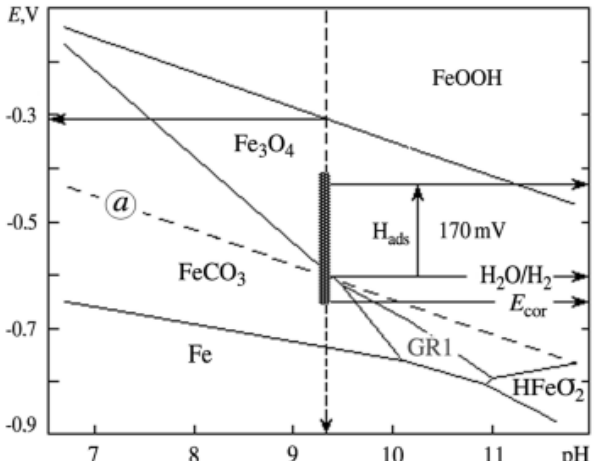

Figure 9.3 Pourbaix diagram for the $Fe - HCO_3^- - CO_3^{2-} - H_2O$ at 325 K [Hirnyi, 2001]

Chapter 10: Conclusion, summary and suggested future tracks

The basic electrochemical investigations were performed in simulated CO_2 corrosion environments that a new generation pipeline steel; API-X100 can be exposed to in conditions where the cathodic protection is not applied. The corrosion rates showed a considerable increase with the bicarbonate content as well as did the anodic and cathodic branches in both aerated and deoxygenated conditions. In addition, effective passivation was established in the bicarbonate solutions where the current density in that regime decreased gradually at different extents depending on temperatures and bicarbonate content. The anodic peaks and the consequent passivation were exclusively established in the chloride free conditions showing a variation in the onset of passivation (E_{pass}). In CO_2-saturated media, corrosion rates increased with temperature and upon the addition of chloride but they decreased upon oil addition. Generally, the interfacial mechanisms were very sensitive to the environmental conditions but in the presence of oil, the behavior was inductive and showed an independence from temperature and other chemical factors. The summarized findings of the performed investigations are stated below.

10.1. Summary of the results from the naturally aerated bicarbonate solutions

In that experimental work, some electrochemical perspectives of the corrosion behavior were investigated in aerated chloride free and 3 wt% chloride containing 0.1, 0.5, and 0.8 M bicarbonate conditions at 20, 40, and 60 ^{o}C. The basic findings of this brief study can be summarized as the following:

1. The free open circuit potentials were nobler with the increased bicarbonate content suggesting the cahtodic influence on the mixed potentials at all temperature conditions where the same influence of higher temperature was also exerted. In chloride containing conditions, OCP was lower respectively and it followed fairly the same trend exhibited in chloride free conditions with respect to bicarbonate and temperature.
2. The corrosion rate increased with the higher bicarbonate content and with higher temperature in both chloride free and chloride containing conditions where also (E_{corr}) was nobler accordingly.
3. An evidence for a multistep dissolution mechanism in chloride free conditions was exhibited where preliminary prepassivation films influenced the anodic dissolution in conditions where the passivation was more effective with lower bicarbonate contents. However, in chloride containing conditions, the anodic dissolution proceeded extensively with no indication for a multistep dissolution or for anodic peaks.
4. EIS interactions were very similar in chloride free conditions irrespectively from bicarbonate content and temperature where the role of diffusible passive films was apparent in a two-time constant based equivalent circuit.
5. The presence of chloride changed markedly the role of bicarbonate in a temperature-dependent fashion. At 20 and 60 ^{o}C, the mechanisms were similar with respect to the bicarbonate content showing adsorption at the former and passive film formation at the latter temperature.

10.2. Summary of the results from deoxygenated low oil containing bicarbonate solutions

The electrochemical aspects of the corrosion behaviour in deoxygenated bicarbonate solutions containing low oil amounts were studied at 30 and 70 ^{o}C. The influence of anodic and cathodic reactions at both free and polarization potentials were evaluated from different considerations including active kinetics, passivation, impedance, and cathodic reduction characteristics. The basic findings of this study are shown below:

1. Bicarbonate species were involved in both anodic and cathodic reactions and OCP decreased with the increased bicarbonate contents at 30 ^{o}C where the anodic reactions dominate the mixed potential conditions.
2. Oil inhibited the anodic reactions in a proportional manner with the amounts it was added with, and the significance of oil in elevating OCP was quite apparent in low bicarbonate containing solutions.
3. OCP values at 70 ^{o}C were more negative than those at 30 ^{o}C in all bicarbonate and oil conditions and they were more negative with the increased bicarbonate contents.
4. The inhibition role of oil seemed to be temperature dependent where the cathodic reactions were noticeably inhibited with the addition of oil in a proportional fashion at 70 ^{o}C. Additionally, the effect of oil in the free potential conditions was apparent even in the concentrated bicarbonate solutions.
5. Corrosion current density was proportional to bicarbonate content and a multistep active dissolution occurred at 30 ^{o}C. In addition, effective passivation was

established for all oil free bicarbonate solutions and the passive current density was proportional to the bicarbonate content.

6. Corrosion current density decreased by the addition of oil and corrosion potential was nobler in a proportional fashion with the oil content in all bicarbonate solutions reflecting the effect of oil in inhibiting the anodic current densities and confirming with the OCP test results at 30 ^{o}C. Oil disturbed the passivation conditions especially in low bicarbonate containing solutions of 0.05 and 0.1 M although of the decreased passive current densities.
7. From the charge transfer results at 30 ^{o}C, it increased in the passivation region primarily with the addition of 10 vol% oil in 0.05 M conditions but it then decreased with the increased oil content where the passivation became oil-enriched. However, in the other bicarbonate conditions, charge transfer decreased with the oil content. Additionally, charge transfer variations are explained in proposed schematics.
8. Charge transfer in the cathodic reactions exhibited a considerable sensitivity to the bicarbonate content at 30 ^{o}C. The limiting current density showed a great dependence on the bicarbonate content in oil free and in all oil containing conditions. Diffusion mass transport of bicarbonate was reduced in a proportional fashion with the oil content where the limiting current density decreased and the cathodic reductions became more mass transport influenced.
9. Corrosion current density increased noticeably in all bicarbonate and oil conditions at 70 ^{o}C and the corrosion potential decreased with the bicarbonate content. Additionally it was lower with the higher temperature confirming with

OCP test results. The active dissolution occurred with no indication for successive electrochemical steps and the passivation conditions were better and showed a dependence on the oil content.

10. Charge transfer release during passivation was higher at the higher temperature 70 ^{o}C, and the maximum charge transfer in the different bicarbonate conditions was dependent on the oil content.
11. The limiting current density increased with the higher temperature and showed a similar trend of variation with oil and bicarbonate at 30 ^{o}C. The range of mixed charge/mass transfer control was shorter in these conditions.
12. EIS responses revealed the role of bicarbonate adsorption and/or relaxation of intermediate species in oil free conditions at 30 ^{o}C. Nyquist plot sizes decreased with the bicarbonate content and the charge transfer resistance as well as that across adsorption field decreased with the bicarbonate content.
13. The addition of oil changed the electrochemical interactions in 0.05 and 0.1 M conditions where the impedance response in the former was third-time constant based and the latter comprised Warburg impedance in a two-time constant based equivalent circuit.
14. Oil with different amounts did not induce significant changes in the impedance responses in 0.5 and 1 M bicarbonate containing conditions where oil was less miscible but the charge transfer decreased.
15. Corrosion mechanisms at the free potential conditions were almost irrespective from the high temperature 70 ^{o}C. The proposed equivalent circuits showed a

satisfactory agreement with the experimental data for both oil free and oil containing conditions.

10.3. Summary of the results from low chloride containing CO_2-saturated media containing low oil amounts

Some electrochemical investigations were utilized to study a special carbon dioxide corrosion case of susceptibility necessarily related to low oil amounts in the transported emulsions. Additionally, some thermodynamic aspects related to the oil adsorption in relation to temperature and chloride were also revealed. The basic findings of this study can be summarized as follows:

1. OCP decreased with the higher temperature and it was higher in chloride free solutions than those in chloride containing ones showing the same trend with temperature and confirming the anodic influence in the oil free conditions.
2. OCP was higher in oil containing conditions and in a proportional manner with the oil content and the sensitivity of OCP towards that was apparent within the full temperature range in chloride containing conditions.
3. The corrosion rate was proportional to the higher temperature and the corrosion potential was lower correspondingly in chloride free and chloride containing oil free conditions. The cathodic reactions were also accelerated with the higher temperature and in the presence of chloride which also induced significant changes in the cathodic mechanisms.

4. The corrosion inhibition efficiency by the addition of oil was quite high at low temperatures and in chloride free conditions and oil adsorption showed a dependence on the applied potential in the anodic branch.
5. 1, 2, 3, 4-tetrahydronaphthalene was very attributable for establishing the stable surface oil films where the endothermic adsorption associated with the greater disorderness revealed the chemisorption nature of oil adsorption.
6. The electrochemical interactions supported the basic OCP and polarization findings where the charge transfer resistance decreased with the higher temperature. Adsorption and/or relaxation of reaction intermediates played the inductive role in both chloride free and chloride containing oil free solutions.
7. The presence of oil did not change the corrosion mechanism, however it increased the charge transfer resistance and the other associated resistance across the oil adsorption fields. The interfacial characteristics were more capacitive at higher temperatures, in chloride containing conditions, and when the oil amount is lower.

10.4. Summary of the results from high chloride containing CO_2-saturated media containing 10 vol% oil amounts

Some fundamental electrochemical aspects of the corrosion performance and corrosion inhibition in CO_2-saturated media of a wide range of salinity at 20 and 90 ^oC of API-X100 pipeline steel. The basic findings of this study can be summarized as follows:

1. OCP decreased proportionally with the greater salinity content irrespectively from temperature in oil free conditions reflecting the anodic sensitivity to small amounts of chloride. OCP exhibited also similar decreasing trend with higher

temperatures. The roles of possibly accelerated or retarded anodic and cathodic reactions changing accordingly with chloride and temperature were studied in separate polarization tests.

2. Oil seemed to act as a cathodic inhibitor leading to lower OCP's at both temperatures and showing a considerable effectiveness along the salinity range considered. OCP appeared to be the lowest in oil containing conditions at 90 ^{o}C and the noblest at 20 ^{o}C in oil free conditions.
3. The corrosion rates increased with the chloride content up to 30 g reaching a peak value before it decreased with the greater chloride content at 20 ^{o}C. The anodic reactions accelerated but finally the retarded cathodic reactions controlled the polarization behavior showing a "bow" in the Evan's map. At 90 ^{o}C, similar trends with respect to corrosion rates and corrosion potentials were exhibited, but the corrosion rates were significantly accelerated and the role of water reduction kinetics was more prevalent.
4. Oil inhibited the corrosion reactions more effectively at lower temperatures and in lower chloride containing solutions and it affected noticeably the mass-limit reduction of (H_2CO_3) and (H^+) extending the cathodic shoulders. In addition, oil seemed to play a different role during passivation, possibly incorporated in the passive films, especially in the concentrated brines and at high temperature 90 ^{o}C.
5. In oil free conditions, Impedance responses were similar at 20 ^{o}C representing the significance of adsorption and or relaxation of intermediate species. At 90 ^{o}C, impedance was two-time constant based and it incorporated Warburg element representing appreciable significance of diffusion-limited processes.

6. In oil containing solutions, the interfacial mechanisms seemed to be independent from temperature showing inductive behaviors. They were more sensitive to the greater chloride content where the charge transfer decreased accordingly and where the capacitive nature was more apparent.

10.5. Summary of the results from the potentiodynamic polarization investigations in multivariable controlled CO_2 corrosion in a medium containing chloride and acetic acid

This brief study was devoted to investigate the capabilities, on amount basis, of chloride and acetic acid on the corrosion behavior. The corrosion rates were accelerated cathodically with the increased amounts of acetic acid. The corrosion rates exhibited a variation with respect to the chloride content exhibiting a maximum value with the respect to the maximum anodic sensitivity. Acetic acid prevailed the corrosion behavior and, in temperature-dependent fashion, chloride role was different in the acetic acid containing conditions.

10.6. Summary of the results from CO_2 saturated autoclave environments

The weight loss was significantly less with the increased oil content and the morphological morphology of the corrosion products governed the dissolution behavior with time.

10.7. Suggested future tracks

This work can be considered as a general base from which more specific cases of CO_2 corrosion can be further studied. From selected materials and construction perspectives, the welded pipeline sections still represent a great challenge for corrosion experts to mitigate the greater susceptibility for corrosion to occur. Apart from the significance of the environmental conditions, CO_2 corrosion seems, from the current research findings, much more influenced by microstructural and compositional characteristics. The future efforts can be tracked in long-term scopes as:

1. This special corrosion phenomenon can be further studied with respect to distinct material characteristics. The effects of microstructure and compositional content can be diagnosed in simulated CO_2-saturated conditions where different pipeline steels are considered.
2. In the next scope, the localized variations induced from the coupled microstructural regimes, across for example the welding zone, can be correlated to the corrosion performance.
3. The corrosion product properties varying with respect to both environmental and material characteristics can be studied but by utilizing cyclic voltammetry. This technique can provide a preliminary route map of the corrosion product properties but on electrochemical basis.
4. The morphological and compositional characteristics of the corrosion products can be studied in the same environmental conditions considered in this study but from hydrodynamic perspectives. The protectiveness of the formed corrosion products in these conditions can be effectively reliable in special flow conditions.

References

Agrawal A. , Durr C., and Koch G., 2004. Sulfide films and corrosion rates of AISI 1018 carbon steel in saline solutions in the presence of H_2S and CO_2 at temperatures up to 175 ^oF, CORROSION/2004. Paper no. 383, NACE.

Ahmad Z., 2006, Principles of corrosion engineering and corrosion control, first ed., Butterworth-Heinemann.

Al-Kharafi F., Ateya B., and Abdallah R., 2002, Electrochemical behaviour of low carbon steel in concentrated carbonate chloride brines, Journal of Applied Electrochemistry, 32. 1363-1370.

Altoe P., Pimenta G., Moulin C., Diaz S., and Mattos O., 1996, Evaluation of oilfield corrosion inhibitors in CO_2 containing media: a kinetic study, Electrochemica Acta, 41. 1165-1172.

Alves V. and Brett C., 2002 (A), Characterization of passive films formed on mild steels in bicarbonate solution by EIS, Electrochimica Acta, 47. 2081- 2091.

Alves V. and Brett C., 2002 (B), Influence of alloying on the passive behaviour of steels in bicarbonate medium, Corrosion Science, 44. 1949-1965.

Alves V., and Brett C., 2002 (C), The influence of alloying on the passive behaviour of steels in bicarbonate medium studied by electrochemistry and XPS, Key Engineering Materials, 232. 436-439.

Anderko A. and Young R., 1999. Simulation of CO_2 / H_2S corrosion using thermodynamic and electrochemical models, CORROSION/1999. Paper no. 31, NACE.

Asahi, H., 2004, Development of Ultra-high-strength Linepipe X120. Nippon Steel.

ASTM Standard G 1-03, 2004, Standard practice for preparing, cleaning, and evaluating corrosion test specimens, Annual Book of Standards, ASTM, Pennsylvania.

ASTM Standard G 5-94, 2004, Standard reference test method for making potentiostatic and potentiodynamic anodic polarization measurements, Annual Book of Standards, ASTM, Pennsylvania.

Ayello F., Sr W., Richter S., and Nesic S., 2011, Crude oil chemistry effects on inhibition of corrosion and phase wetting, CORROSION/2011. Paper no.11060, NACE.

Bai Z., Chen C., Lu M., Li J., 2006, Analysis of EIS characteristics of CO_2 corrosion of well tube steels with corrosion scales, Applied Surface Science. 252 (2006) 7578–7584.

Baptiste J., Orazem M., Pébère N. and Tribollet B., 2006, CPE analysis by local electrochemical impedance, Electrochim Acta. 51. 1473–1479.

Bard A., and Faulkner L., 2001.Electrochemical methods, fundamentals and applications, second ed., John Wiley & sons.

Baraneko V., Kirov V., and Musienko A., 1990, Solubility of oxygen and carbon dioxide in water, translated from Atomnaya Energiya, 68. 342-346.

Brett C., and Brett A, 1993, Electrochemistry; principles, methods, and applications, Oxford University Press.

Brossia C., and Cragnolino G., 2000, Effect of environmental variables on localized corrosion of carbon steel, Corrosion, 56. 505-514.

Bulger J., Lu B. and Luo J., 2006, Microstructural effect on near-neutral pH stress corrosion cracking resistance of pipeline steels, Journal of Materials Science, 41, 5001-5005.

Burke P., 1984, Synopsis: Recent Progress in the Understanding of CO2 Corrosion, CORROSION/1984. Paper no. 2, NACE.

Butler, G. and Ison H., 1966, Corrosion and its prevention in water, Reinhold Publishing Corp.

Cáceres L., Vargas T., and Herrera L., 2009, Influence of pitting and iron oxide formation during corrosion of carbon steel in unbuffered NaCl solutions, Corrosion Science, 51. 971-978.

Castillo M., Rincon H., Duplat S., Vera J., Baron E., 2000, Protective properties of crude oils in CO_2 and H_2S corrosion, CORROSION/2000. Paper no. 5, NACE.

Castro E., and Vilche J., 1991, Electrooxidation/electroreduction processes at composite iron hydroxide layers in carbonate-bicarbonate buffers, Journal of Applied Electrochemistry, 21. 543-551.

Castro E., Valentini C., Moina C., Vilche J., and Arvia A., 1986, The influence of ionic composition on the electrodissolution and passivation of iron electrodes in potassium carbonate-bicarbonate solutions in the 8.4-10.5 pH range at 25°C, Corrosion Science, 26. 791-793.

Chen Y. and Jepson W., 1999, EIS measurement for corrosion monitoring under multiphase flow conditions, Electrochimica Acta. 44, 4453-4464.

Cook E., and Hackerman N., 1951, Adsorption of polar organic compounds on steel, The Journal of physical and colloid chemistry. 55. 549-557.

Cottis R., and Turgoose S., 1999, Electrochemical impedance and noise, NACE International, USA.

Crolet J. ,Thevenot N., Dugstad A., 1999, Role of free acetic acid on the CO_2 corrosion of steels, CORROSION/99, Paper no. 24. NACE.

Crolet J., Thevenot N., Nesic S., 1996, Role of conductive corrosion products on the protectiveness of corrosion layers, CORROSION/96, paper no. 4. NACE.

Crolet J., 1994, Which CO_2 corrosion, hence which in predicting CO_2 corrosion in the oil and gas industry, European federation of corrosion. Paper no. 13. Institute of Materials.

Crolet J., and Bonis M., 1983, pH measurements in aqueous CO_2 solutions under high-pressure and temperature, Corrosion, 39. 39-46.

Dahmani M., Et-Touhami A., Al-Deyab S., Hammouti B., Bouyanzer A., 2010, Corrosion Inhibition of C38 Steel in 1 M HCl: A comparative study of black pepper extract and its isolated piperine, International journal of electrochemical science, 5. 1060-1069.

Danielson T., and Joosten M., 2006, Use of dimensional analysis for evaluation of corrosion inhibitor effectiveness in wet gas pipelines, CORROSION/2006. Paper no. 6569, NACE.

Davis D. and Burstein G., 1980, The Effect of bicarbonate on the corrosion and passivation of iron, Corrosion, 36. 416-422.

De Waard C., Lotz U., and Dugstad A., 1995, Influence of liquid flow velocity on CO_2 corrosion: a semi-empirical model, CORROSION/95, Paper No.128. NACE

De Waard C., Lotz U., 1993, Prediction of CO2 Corrosion of Carbon Steel, CORROSION/1993. Paper No. 69, NACE.

De Waard C., and Millims D., 1975, Carbon Acid Corrosion of Steel, Corrosion, 31. 177-181.

Dean J., 2000, Lange's Handbook of Chemistry, fifteenth ed., McGraw-Hill, New York.

Dodds W., Stutzmal N., and Sollami B., 1956, Carbon dioxide solubility in water, Industrial and engineering chemistry, 1. 92-95.

Dugstad A., Hemmer H. and Seiersten M., 2000, Effect of steel microstructure upon corrosion rate and protective iron carbonate film formation, CORROSION/2000, Paper No. 24, NACE.

Dugstad A., Lunde L. Videm K., 1994, Parametric study of CO_2 corrosion of carbon steel, CORROSION/94, Paper No. 14, NACE.

Dugstad A., 1992, The importance of $FeCO_3$ supersaturation on the CO_2 corrosion of carbon steel, CORROSION/1992, Paper No. 14, NACE.

Efird K. and Jasinski R., 1989, Effect of the crude oil on corrosion of steel in crude oil/brine production, Corrosion, 45. 165-171.

Eliyan F., and Alfantazi A., 2011 (A), How the corrosion is when the oil is less; electrochemical investigations on CO2 corrosion performance of API-X100 steel in low oil containing pipeline flows, Corrosion Science. Under review.

El-Naggar M., 2006, Effects of Cl^-, NO_3^- and SO_4^{2-} anions on the anodic behaviour of carbon steel in deaerated 0.5 M $NaHCO_3$ solutions, Applied surface science, 252. 6179-6194.

EPA, 2010, Site assessment tools for petroleum hydrocarbon fuels guide, EPA, USA.

Ergun M., and Turan A., 1991, Pitting potential and protection potential of carbon steel for chloride ion and the effectiveness of different inhibiting anions, Corrosion Science, 32. 1137-1142.

Fang H., Nesic S., and Brown B., 2006, General CO_2 corrosion in high salinity brines, CORROSION/2006. Paper no. 372, NACE.

Farelas F., Ramirez A., 2010, Carbon Dioxide Corrosion Inhibition of Carbon Steels Through Bis-imidazoline and Imidazoline Compounds Studied by EIS, International journal of electrochemical science, 5. 797-814.

Foss M., Gulbrandsen E., and Sjöblom J., 2010, Oil wetting and carbon dioxide corrosion inhibition of carbon steel with ferric corrosion products deposits, Corrosion, 66. 1- 11.

Franco R., Pacheco J., Wei S., Pugh D., Geurts K., and Robb G., 2010, Applications of corrosion models to oil and gas production, CORROSION/2010. Paper no. 370, NACE.

Gao K., Yu F., Pang X., Zhang G., Qiao L., Chu W., and Lu M., 2008, Mechanical properties of CO_2 corrosion product scales and their relationship to corrosion rates, Corrosion Science, 50. 2796-2803.

Garnica-Rodriguez A., and Genesca J., 2009. Electrochemical evaluation of aminotriazole corrosion inhibitor under flow conditions, Joirnal of Applied Electrochemistry, 39. 1809-1819.

Garverick L., 1994, Corrosion in the Petrochemical Industry, 2nd edition, ASM.

George K., and Nesic S., 2007, Investigation of carbon dioxide corrosion of mild steel in the presence of acetic acid – Part 1: Basic Mechanisms, Corrosion, 63.178-186.

Glass G., 1986, The effect of a change in surface conditions produced by anodic and cathodic reactions on the passivation of mild steel, Corrosion Science, 26. 441-445.

Graf, M. and Hillenbrand H., 2003, High-strength large-diameter pipe for long distance high pressure gas pipelines, Europipe.

Gray L., Anderson B., Danysh M., and Tremaine P., 1990, Effect of pH and temperature on the mechanism of carbon steel corrosion by aqueous carbon dioxide, CORROSION/1990. Paper no. 2281, NACE.

Guo-xian Z., Xiang-hong L., Jian-min X., and Yong H., 2009, Formation characteristic of CO_2 corrosion product layer of P110 steel investigated by SEM and electrochemical techniques, Journal of iron and steel, 16. 89-94.

Gutzeit J., 2000, Effect of organic chloride contamination of crude oil on refinery corrosion, CORROSION/2000. Paper no. 697, NACE.

Hamadou L., Kadri A., and Benbrahim N., 2005, Characterization of passive films formed on low carbon steel in borate buffer solution (pH 9.2) by electrochemical impedance spectroscopy, Applied Surface Science, 252. 1510-1519.

Hedges B., Paisley D., and Woollam R., 2000, The corrosion inhibition availability model, CORROSION/2000. Paper 34, NACE.

Heidersbach B., 2011, Metallurgy and corrosion control in oil and gas production, Wiley, USA.

Hernandez S., Duplat S., Vera J., and Baron E., 2002, A statistical approach for analyzing the inhibiting effect of different types of crude oil in CO_2 corrosion of carbon steel, CORROSION/2002. Paper no. 293, NACE.

Hernandez S. and Bruzual J., 2001, Isolation of potential corrosion inhibiting compounds in crude oils, CORROSION/2001. Paper no. 1044. NACE.

Heuer J. and Stubbins J. , 1999, An XPS characterization of $FeCO_3$ films from CO_2 corrosion. Corrosion Science, 41. 1231 – 1243.

Heuer J and Stubbins J., 1998, Microstructure analysis of coupons exposed to carbon dioxide corrosion in multiphase flow, CORROSION/1998, Paper no. 70566. NACE

Hirnyi S., 2001, Anodic hydrogenation of iron in a carbonate-bicarbonate solution, Materials Science, 37. 491-498.

Hong T., Shi H, Wang H., Gopal M. and, Jepson W., 2000, EIS study of corrosion product film in pipelines, CORROSION/2000, Paper no. 44. NACE.

Hunnik V., Pots E., and Hendriksen B., 1996, The formation of protective $FeCO_3$ corrosion product layers in CO_2 corrosion, CORROSION/96, paper no. 6. NACE.

Ikeda A., Ueda M., and Mukai S., 1984, CO_2 behaviour of carbon and Cr steels, Advances in CO_2 Corrosion, CORROSION/1984, Paper no. 5. NACE.

Jelinek J., and Neufeld P., 1980, Temperature effect on pitting corrosion of mild steel in de-aerated sodium bicarbonate-chloride solutions, Corrosion Science, 20. 489-496.

Jepson W., Bhongale S., and Gopal M., 1996, Predictive model for sweet corrosion in horizontal multiphase slug flow, CORROSION/1996, Paper no.19, NACE.

Jiang X., Zheng Y., and Ke W., 2005, Effect of flow velocity and entrained sand on inhibition performance of two inhibitors for CO2 corrosion of N80 steel in 3% NaCl solution, Corrosion Science, 47. 2636-2658.

John R, 1998, SweetCor: an information system for the analysis of corrosion of steels by water and carbon dioxide**.** CORROSION/1998, Paper no. 20, NACE.

Jovancicevic V., Ramachandran S., and, Prince P., 1999, Inhibition of Carbon Dioxide Corrosion of Mild Steel by Imidazolines and Their Precursors. Corrosion, 55. 449-455.

Jüttner K., 1990, Electrochemical impedance spectroscopy (EIS) of corrosion processes on inhomogeneous surfaces, Electrochimica Acta, 35. 1501-1508.

Keddam M., Mattos O., and Takenouti H., 1981, Reaction model for iron dissolution studied by electrode impedance, J. Electrochem. Soc.,128. 257-266.

Kermani M. and Morshed A., 2003, Carbon dioxide corrosion in oil and gas production-A Compendium, Corrosion, 59. 659-683.

Kermani M., Gonzales J., Linne C., Dougan M., Cochrane R., 2001, Development of low carbon Cr-Mo steels with exceptional corrosion resistance for oilfield applications, CORROSION/2001. Paper no. 65, NACE.

Kermani M. and Smith L., 1997, CO_2 corrosion control in the oil and gas production; design considerations, first ed., The institute of materials, London.

Kermani M., Smith L., 1994, Predicting CO_2 Corrosion in the oil and gas industry, European Federation of Corrosion, Paper no. 13, Institute of Materials.

Khodyrev Y., Batyeva E., Badeeva E., Platova E., Tiwari L., and Sinyashin O., 2011, The inhibition action of ammonium salts of O,O-dialkyldithiophosphoric acid on carbon dioxide corrosion of mild steel, Corrosion Science, 53. 976–983.

Kinsella, B., Tan, Y., Bailey S., 1998, Electrochemical impedance spectroscopy and surface characterization techniques to study carbon dioxide corrosion scales, Corrosion, 54. 835-842.

Kirmani, B., Martin, J., and Esaklul, K., 2006, Materials design strategy: Effect of H_2S/CO_2 corrosion on materials selection, CORROSION/2006. Paper no. 6121, NACE.

Li C., 2009, Effect of corrosion inhibitor on water wetting and carbon dioxide corrosion in oil-water two-phase flow, PhD. Thesis, Ohio University.

Li J. and Zuo J., 2008, Influences of temperature and pH value on the corrosion behaviors of X80 pipeline steel in carbonate/bicarbonate buffer solution, Chinese Journal of Chemistry. 26. 1799-1805.

Li D., Feng Y., Bai Z., Zhu J., and Zheng M., 2007, Influence of temperature, chloride ions and chromium element on the electronic property of passive film formed on carbon steel in bicarbonate/carbonate buffer solution, Electrochimica Acta, 52. 7877-7884.

Li J. and Meier D., 1998, An AFM study of the properties of passive films on iron surfaces, Journal of Electro analytical Chemistry, 454. 53-58.

Liang Z., Xiao-gang L., Cui-wei D., 2009, Effect of Environmental Factors on Electrochemical Behavior of X70 Pipeline Steel in Simulated Soil Solution, Journal of iron and steel research, 16. 52-57.

Lin G., Zheng M., Bai Z., and Zhao X., 2006, Effect of temperature and pressure on the morphology of carbon dioxide corrosion scales, Corrosion, 62. 501-507.

Linter B., and Burstein G., 1999, Reaction of Pipeline Steels in Carbon Dioxide Solutions, Corrosion Science, 41. 117-139.

Liu F., Du M., Zhang J. and Qiu M., 2009, Electrochemical behavior of Q235 steel in saltwater saturated with carbon dioxide based on new imidazoline derivative inhibitor, Corrosion Science, 51. 102-109.

Liu X. and Mao X., 1995, Electrochemical polarization and stress corrosion cracking behaviours of a pipeline steel in dilute bicarbonate solution with chloride ion, Scripta Metallurgica et Materialia, 33. 145-150.

Lopez D., Simison S., de Sanchez S., 2005, Inhibitors performance in CO_2 corrosion EIS studies on the interaction between their molecular structure and steel microstructure, Corrosion Science, 47. 735–755.

Lopez D., Perez T., Simison S., 2003, The influence of microstructure and chemical composition of carbon and low alloy steels in CO2 corrosion. A state-of-the-art appraisal, Materials and Design, 24. 561–575.

Lotz U., van Bodegom L., and Ouwehand C., 1990, The effect of type of oil and gas condensate on carbonic acid corrosion, CORROSION/1990. Paper no. 41, NACE.

Louafi Y., Ladjouzi M., and Taibi K., 2010, Dissolved carbon dioxide effect on the behaviour of carbon steel in a simulated solution at different temperatures and immersion times, Journal of Solid State Electrochemistry, 14. 1499-1508.

Lu Z., Huang C., Huang D., and Yang W., 2006, Effects of a magnetic field on the anodic dissolution, passivation and transpassivation behaviour of iron in weakly alkaline solutions with or without halides, Corrosion Science. 48. 3049-3077.

Lucio-Garcia M., Gonzalez-Rodriguez J., Casales M., Martinez L., Chacon-Nava J., 2009, Effect of heat treatment on H_2S corrosion of a micro-alloyed C–Mn steel, Corrosion Science. 51. 2380-2386.

Lyons W., Plisga G., 2005, Standard handbook of petroleum & natural gas engineering, Elsevier Inc, UK.

Ma H., Li G., Chen S., Quan Z., Zhao S., and Niu L., 2000, The Influence of Hydrogen Sulfide on Corrosion of Iron under Different Conditions, Corrosion Science, 42. 1669-1983.

Ma H., Cheng X., Chen S., Wang C., Zhang J., and Yang H., 1998, An ac impedance study of the anodic dissolution of iron in sulfuric acid solutions containing hydrogen sulfide, Journal of Electrochemical chemistry, 451. 11-17.

Manning F., Thompson R., 1995, Oilfield Processing of Petroleum: Crude oil, PennWell publishing company, USA.

Mao X., Liu X., Revie R., 1994, Pitting corrosion of pipeline steel in dilute bicarbonate solution with chloride ions, Corrosion, 50. 651-657.

Masamura K., HashizumS. , Nunomura K., Sakai J., and Matsushima I., 1984, Corrosion of carbon and alloy steels in aqueous CO_2 environments. CORROSION/1984. Paper no. 14, NACE.

McIntire G., Lippert J., and Yudelson J., 1990, The effect of dissolved CO_2 and O_2 on the corrosion of iron, Corrosion, 46. 91-95.

Mendez C., Duplat S., Hernfindez S., and Vera J., 2001, On the mechanism of corrosion inhibition by crude oils, CORROSION/2001. Paper no.1044, NACE.

Moiseeva L., 2005, Carbon dioxide corrosion of oil and gas field equipment, Protection of Metals. 41. 76-83.

Moiseeva L. and Kuksina O., 2003, On the dependence of steel corrosion in oxygen-free aqueous media on ph and the pressure of CO_2, Protection of metals, 39. 490-498.

Mohorich M., Lamb J., Chandra D., Daemen J., and Rebak R., 2010, Electrochemical studies on silicate and bicarbonate ions for corrosion inhibitors, Metallurgical and materials transactions A, 41. 2563-2574.

Morales J., Perdomo J., Ramirez M., and Viloria A., 2000, Effect of crude oil contaminations on the internal corrosion in gas pipelines, CORROSION/2000. Paper no. 40, NACE.

Mu L., and Zhao W., 2010, Investigation on carbon dioxide corrosion behaviour of HP13Cr110 stainless steel in simulated stratum water, Corrosion Science, 52. 82-89.

Mullins O., 2008, The physics of reservoir fluids: discovery through downhole fluid analysis, Schlumberger, USA.

Murata T., Sato E., and Matsuhashi R., 1986, Factors controlling corrosion of steels in CO_2-saturated environments, CORROSION/1986. Paper no. 7, NACE.

Naiming L., Faqin X., Jun Z., Xiangqing W., Wei T., 2010, Corrosion behaviors of P110 steel and chromium coating in CO_2-saturated simulated oilfield brine, Journal of Wuhan University of Technology--Materials Science Edition, 26. 190-196.

Nazari M., Allahkaram S., and Kerman M., 2010, The effects of temperature and pH on the characteristics of corrosion product in CO_2 corrosion of grade X70 steel, Materials and Design, 31. 3559-3563.

Neshati J., Masiha H., Mahjani M., and Jafarian M., 2007, Study of corrosion of carbon steel API 5L (X60) in $NaHCO_3$/NaCl solutions by electrochemical noise and impedance measurements, Corrosion Engineering, Science and Technology. 42. 371-376.

Nesic S., 2007, Key issues related to modelling of internal corrosion of oil and gas pipelines - A review, Corrosion Science, 49. 4308-4338.

Nesic S., Wang S., Cai J. and Xiao Y., 2004, Integrated CO_2 corrosion - multiphase flow model, CORROSION/04, Paper no. 626, NACE.

Nesic, S., Lee K., 2003, A Mechanistic Model for Carbon Dioxide Corrosion of Mild Steel in the Presence of Protective Iron Carbonate Films - Part 3: Film Growth Model, Corrosion, 59. 616-628.

Nesic S. and Lee K., 2002, The mechanistic model of iron carbonate film growth and the effect on CO_2 corrosion of mild steel, CORROSION/02 Paper no.237, NACE.

Nesic S., Nordsveen M., and Nyborg R., Stangeland A., 2001, A mechanistic model for CO_2 corrosion with protective iron carbonate films, CORROSION/01, Paper no. 40, NACE.

Nesic S., Postlethwaite J., and Olsen S., 1996, An Electrochemical Model for Prediction of Corrosion of Mild Steel in Aqueous Carbon Dioxide Solutions, Corrosion. 52. 280-294.

Niu L., and Cheng Y., 2007, Corrosion behaviour of X-70 pipe steel in near-neutral pH solution, Applied Surface Science, 253. 8626-8631.

Nyborg R., Dugstad A., Dronen P., 1997, Effect of chromium on mesa corrosion attack of carbon steel, Eurocorr 1997. Institute of Materials.

Ogundele G. and White W., 1987, Observations on the influence of dissolved hydrocarbon gases and variable water chemistries on corrosion of an API-L80 steel, Corrosion, 43. 665-673.

Ortega-Toledo D., Gonzalez-Rodriguez J., Casales M., Neri-Florez M., Martinez-Villafa˜ne A., 2010, The CO_2 corrosion inhibition of a high strength pipeline steel by hydroxyethyl imidazoline, Materials Chemistry and Physics, 122. 485- 490.

Palacios C, Shadley J, 1993, CO_2 corrosion of N-80 steel at 71 ^oC in a two-phase flow system. Corrosion, 49. 686 - 693.

Palmer D., Eldik R., 1983, The Chemistry of Metal Carbonato and Carbon Dioxide Complexes, Chemical Reviews, 83, 651-731.

Paolinelli L., Pérez T., and Simiso S., 2008, The effect of pre-corrosion and steel microstructure on inhibitor performance in CO_2 corrosion, Corrosion Science, 50. 2456–2464.

Parkins R., and Zhou S., 1997, The stress corrosion cracking of C-Mn steel in CO_2-HCO_3^--CO_3^{2-} solutions. II. Electrochemical and other data, Corrosion Science, 39. 175-191.

Pourbaix M., 1966, Atlas of Electrochemical Equilibria in Aqueous Solutions, Pergamum Press, New York.

Ren C., Wang X., Liu L., Yang H., and N. Xian, 2010, Lab and field investigations on localized corrosion of casing, Materials and Corrosion, 61. 1-5.

Ren C., Liu D., Bai Z., and Li T., 2005, Corrosion behavior of oil tube steel in simulant solution with hydrogen sulfide and carbon dioxide, Materials Chemistry and Physics, 93. 305-309.

Ruzic, V., Veidt, M., Nesic, S., 2006, Protective iron carbonate films- part 1: mechanical removal in single-phase aqueous flow, Corrosion, 62. 419 - 432.

Saleh M., 2006, Inhibition of mild steel corrosion by hexadecylpyridinium bromide in 0.5M H_2SO_4, Materials Chemistry and Physics, 98. 83–89.

Savoye S., Legrand L., Sagon G., Lecomte S., Chausse A., Messina R., and Toulhoat P., 2001, Experimental investigations on iron corrosion products formed in bicarbonate/carbonate - containing solutions at 90 ^oC, Corrosion Science. 43 (2001) 2049-2064.

Sawyer D., 1995, Electrochemistry for Chemists, John Wiley and Sons Inc, USA.

Schmitt G., Feinen S., 2000, Effect of anions and cations on the pit initiation in CO_2 corrosion of iron and steel, CORROSION/2000, paper no. 1. NACE.

Schmitt G., 1998, Wettability of steel surfaces at CO2 corrosion conditions, I. Effect of surface active compounds in aqueous and hydrocarbon media, CORROSION/2001. Paper no. 28, NACE.

Schmitt G., 1984, Fundamental aspects of CO_2 corrosion, CORROSION/83. Paper no. 3, NACE.

Simard S., Drogowska M., and Menard H., 1997, Electrochemical behaviour of 1024 mild steel in slightly alkaline bicarbonate solutions, Journal of Applied Electrochemistry, 27. 317-324.

Smart J., 1993, Wettability – A major factor in oil and gas system corrosion, CORROSION/1993. Paper no. 70, NACE.

Solmaza R., Kardas G., Culhab M., Yazıcı B., and Erbil M., 2008, Investigation of adsorption and inhibitive effect of 2-mercaptothiazoline on corrosion of mild steel in hydrochloric acid media, Electrochimica Acta, 53. 5941–5952.

Song F., 2010, A comprehensive model for predicting CO_2 corrosion rate in oil and gas production and transportation systems, Electrochimica Acta. 55. 689-700.

Sridharan V., 2009, Measurement of carbon dioxide corrosion on carbon steel using electrochemical frequency modulation, MASc. Thesis, University of Saskatchewan.

Stansbury E., and Buchanan R., 2000, Fundamentals of electrochemical corrosion, ASM International, USA.

Sun Y., George K., and Nesic S., 2003, The Effect of Cl^- and Acetic Acid on Localized CO_2 Corrosion in Wet Gas Flow, CORROSION/2003. Paper no. 327, NACE.

Tang X., Li C., Ayello F., Cai J., and Nesic S., 2007, Effect of oil type on phase wetting transition and corrosion in oil-water flow, CORROSION/2007. Paper no.170. NACE.

Tian B., and Cheng Y., 2008, Electrochemical corrosion behavior of X-65 steel in the simulated oil sand slurry. I: Effects of hydrodynamic condition, Corrosion Science, 50. 773–779.

Tomashov, N., 1966,Theory of Corrosion and Protection of Metals, first ed., The Macmillan Company.

Tong L., Yongjin Y., Kewei G., and Minxu L., 2008, Mechanism of protective film formation during CO_2 corrosion of X65 pipeline steel, Journal of University of Science and Technology. 15, 702-719.

Torres-Islas A., Gonzalez-Rodriguez J., Uruchurtu J., 2008, Stress corrosion cracking study of microalloyed pipeline steels in dilute $NaHCO_3$ solutions, Corrosion Science, 50. 2831-2839.

Vaidya R., 2007, Using electrochemical monitoring to predict metal release in drinking water distribution systems, PhD. Thesis, University of Central Florida.

Veawab A., Aroonwilas A., 2002, Identification of oxidizing agents in aqueous amine–CO_2 systems using a mechanistic corrosion model, Corrosion Science, 44. 967–987.

Videm K., and Koren A., 1993, Corrosion, passivity, and pitting of carbon steel in aqueous solutions of HCO_3^-, CO_2, and Cl^-, Corrosion, 49. 746-754.

Villarreal J., Laverde D., and Fuentes C., 2006, Carbon-steel corrosion in multiphase slug flow and CO_2, Corrosion Science. 48. 2363–2379.

Wang B., Du M., Zhang J., and Gao C., 2011, Electrochemical and surface analysis studies on corrosion inhibition of Q235 steel by imidazoline derivative against CO_2 corrosion, Corrosion Science. 53, 2011. 353-361.

Wang H., 2009, Effect of the environment on near-neutral pH stress corrosion cracking of X-52 pipeline steel, Master of Science Thesis, University of Alberta.

Wang S., George K., and Nesic S., 2004, High pressure CO_2 corrosion electrochemistry and the effect of acetic acid, CORROSION/2004. Paper no. 375, NACE.

Wu S., Cui Z., Zhao G., Yan M., Zhu S., Yang X., 2004 (A), EIS study of the surface film on the surface of carbon steel from supercritical carbon dioxide corrosion, Applied Surface Science. 228. 17–25.

Wu S. ,Cuia Z. ,Heb F., Baic Z. , Zhua S. ,Yang X., 2004 (B), Characterization of the surface film formed from carbon dioxide corrosion on N80 steel. Materials Letters, 58. 1076– 1081.

Xia Z., Chou K., and Smialowska Z., 1989, Pitting corrosion of mild steel in CO_2-containing NaCl brine, Corrosion, 45. 636-642.

Xu L., Dong Z., and Fan H., 1996, Effect of CO_2, HCO_3^- on the corrosion of carbon steel in oil and gas fields productive water, Nut. Gas Znd., 16. 57-69.

Yin Z., Bai Z., Zhou W., and Li B., 2010, Effect of acetic acid on CO2 corrosion of carbon steel in NaCl solution, Surface and interface analysis. 42. 1483-1488.

Yin Z., Zhao W., Lai W., and Zhao X., 2009, Electrochemical behavior of Ni-base alloys exposed under oil/gas field environments, Corrosion Science. 51. 1702-1706.

Zavylov V., 2003, Corrosion of oil-field pipelines, Protection of metals, 39. 274 - 277.

Zhang G., Cheng Y., 2011, Localized corrosion of carbon steel in a CO_2-saturated oilfield formation water, Electrochimica Acta. 56. 1676–1685.

Zhang G., and Cheng Y., 2009 (A), Micro-electrochemical characterization and Mott-Schottky analysis of corrosion of welded X70 pipeline steel in carbonate/bicarbonate solution, Electochimica Acta, 55. 316-324.

Zhang G., Chen C., Lu M., Chai C., Wu Y., 2007, Evaluation of inhibition efficiency of an imidazoline derivative in CO_2-containing aqueous solution, Materials Chemistry and Physics, 105. 331–340.

Zhang G., Lu M., Chai C., and Wu Y., 2006, Effect of HCO_3^- concentration on CO_2 corrosion in oil and gas fields, Materials, 13. 44-49.

Zhang H., Zhao Y., Jiang Z., 2005, Effects of temperature on the corrosion behavior of 13Cr martensitic stainless steel during exposure to CO_2 and Cl^- environment, Materials Letters, 59. 3370-3374.

Zhang X., Wang F., He Y., and Du Y., 2001, Study of the inhibition mechanism of imidazoline amide on CO_2 corrosion of ARMCO iron, Corrosion Science, 43. 1417-1431.

Zheng D., Che D., and Liu Y., 2008, Experimental investigation on gas–liquid two-phase slug flow enhanced carbon dioxide corrosion in vertical upward pipeline, Corrosion Science, 50. 3005-3020.